



THE UNIVERSITY
of ADELAIDE

**A Kinematically Enhanced Constitutive Model for
Progressive Damage Analysis of Unidirectional
Fiber Reinforced Composites**

By

Van D. Vu

B. Eng. (Hons)

A thesis submitted in fulfilment of the requirements for the
degree of **Doctor of Philosophy**

The University of Adelaide

Faculty of Engineering, Computer and Mathematical Sciences

School of Civil, Environmental and Mining Engineering

2018

A Kinematically Enhanced Constitutive Model for Progressive
Damage Analysis of Unidirectional Fiber Reinforced Composite
Structures

By:

Van D. Vu, *B. Eng (Hons)*

Under the guidance of:

Dr. Abdul Hamid Sheikh, *Ph.D, M.E. (Structural), B.E.(Civil), Associate
Professor, School of Civil, Environmental and Mining Engineering, The University
of Adelaide.*

Dr. Giang D. Nguyen, *DPhil, M.E. (Civil), B.E.(Civil), Associate Professor, School
of Civil, Environmental and Mining Engineering, The University of Adelaide.*

A thesis submitted to The University of Adelaide in fulfilment of the requirements
for the degree of Doctor of Philosophy in Civil Engineering.

School of Civil, Environmental and Mining Engineering

Faculty of Engineering, Computer and Mathematical Sciences

The University of Adelaide

North Terrace Campus, Adelaide, SA 5005, Australia

Phone: +61 8 8313 5451

Fax: +61 8 8303 4359

Abstract

The application of fiber reinforced laminated composite structures has been increasing steadily in many engineering disciplines due to their high specific strength and stiffness, corrosion resistance, exceptional durability and many other attractive features over the last few decades. A comprehensive strength and failure assessment of these structures made of composite materials is extremely important for a reliable design of these structures and it has been a major focus of many researchers in this field for a long time. To the best of our knowledge, the majority of the existing studies based on macro based continuum approach are particularly focussed on capturing the effective elastic properties and final failure envelop of the composite material, while the subsequent post-yield inelastic behaviour or the entire nonlinear response is often overlooked. Composite structures with such diverse applications can be subjected to complex loading conditions such as impacts, severe dynamic loads or extreme thermal loads which can lead to a significant damage or complete failure of these structures. It is therefore essential to predict the entire nonlinear response and failure of these structures in many situations for a better design with higher confidence. This problem is quite challenging, specifically with a macro based continuum approach, as the actual failure initiates at the micro scale in the form of matrix cracking, fiber rupture or fiber-matrix interface failure which propagate gradually, accumulate together and finally manifested as macroscale structural failure. Thus tracking the details on the entire failure evolution process from microscale to macroscale is necessary for accurately modelling the structural failure. A detailed micromechanical modelling approach, where all constituents are explicitly modelled, can capture all these microscale failure processes and their evolutions in details but such modelling strategy is not computationally feasible for failure analysis for large structures due to a huge gap between micro/fiber and macro/structural scales. Thus the analysis of these structures requires an innovative modelling approach that can represent and capture the essential features of these microscale failure details, while at the same time, should be computationally efficient like a macro based continuum model for undertaking large scale structural analysis.

In this study, a new three-dimensional kinematically enhanced macro-based constitutive model is developed which is applicable at the lamina/ply scale of these laminated composite structures. A novel analytical technique is developed for upscaling the nonlinear response from the fiber/micro scale to the ply scale which is the key for achieving such precise modelling of composites with feasible computational resources. The proposed approach utilized a strategy of strain field enhancements kinematically to account for different rate of deformations in the local fields within a fiber reinforced composite (FRC) ply. Based on these considerations, closed-form analytical expressions are derived which can be used conveniently to express the average macro strain increments of the entire volume element in terms of strain increments in the local fields and vice versa. This modelling strategy provides an opportunity to incorporate both fiber and matrix constitutive responses as well as their interactions into the overall ply response. To this end, a thermodynamics-based continuum model is developed using damage mechanics and plasticity theory to capture the constitutive response of the matrix. This has incorporated two predominant failure mechanisms in the matrix, which are permanent plastic deformation and loss of stiffness. For the fiber-matrix interface that includes interfacial debonding, an anisotropic damage model is developed to account for the directional dependence of the softening response in FRC ply due to fiber debonding failure. The proposed approach and models are developed in incremental forms, allowing the applications in both linear and nonlinear ranges of behaviour. Their verification with available analytical and numerical approaches together with the validation against a wide range of experimental data show both features and good potentials of the proposed approach.

Declaration

I certify that his work contains no material which has been accepted for the award of any other degree or diploma in my name, in any university or other tertiary institution and, to the best of my knowledge and belief, contains no material previously published or written by another person, except where due reference has been made in the text. In addition, I certify that no part of this work will, in the future, be used in a submission in my name, for any other degree or diploma in any university or other tertiary institution without the prior approval of the University of Adelaide and where applicable, any partner institution responsible for the joint-award of this degree.

I give permission for the digital version of my thesis to be made available on the web, via the University's digital research repository, the Library catalogue and also through web search engines, unless permission has been granted by the University to restrict access for a period of time.

I acknowledge that copyright of published works contained within this thesis resides with the copyright holder(s) of those works.

Name Van Vu Signature _____

Date 18/01/2018

Acknowledgement

I would like to take this opportunity to express my genuine gratitude to all individuals and organisations who have provided me invaluable helps and supports making the completion of this doctoral thesis possible.

First and foremost, I would like to thank to my supervisors, A. Professor Abdul Hamid Sheikh and A. Professor Giang D. Nguyen, for their guidance and continuous academic supports with their in-depth knowledge, for their patience, tolerance and encouragement throughout my research. I also want to thank you for giving me the opportunity to attend conference where I have met many interesting people and was able to visit many exciting places.

Completion of this research would have been much more challenging without the supports and friendship from people who could listen to and understand my concerns. I would like to thank to all my friends and fellow colleagues at the School of Civil, Environmental and Mining Engineering for their inspirations and positive attitudes that helped me overcome difficult times during the course of my study. I also want to thank Dr Mohamed Ali Sadakkathulla for his insightful advices in many aspects of life with his invaluable experience.

I must thank the School of Civil, Environmental and Mining Engineering for providing me the scholarship which allowed me to undertake this research.

Last but not least, I am grateful for my parents, to whom I dedicate this thesis to. Your unconditional supports, encouragements and compassions helped me so much throughout this special and remarkable journey.

Table of Contents

Abstract	i
Declaration	iii
Acknowledgement	v
CHAPTER 1: INTRODUCTION	9
1.1 Background	9
1.2 Mechanical response of FRC	13
1.2.1 Laminated Plate Theories.....	13
1.2.2 Laminated Shell Theories	15
1.2.3 Failure Mechanism of Laminated Unidirectional FRC.....	15
1.3 Constitutive Modelling of Composite Material.....	19
1.3.1 Continuum Constitutive Modelling	19
1.3.2 Micromechanics Modelling.....	22
1.4 Research Objectives	25
1.5 Thesis Overview	27
CHAPTER 2: JOURNAL PAPER 1	31
Statement of Authorship	32
Abstract.....	34
CHAPTER 3: JOURNAL PAPER 2	79
Statement of Authorship	80
Abstract.....	82
CHAPTER 4: MANUSCRIPT 3.....	137
Statement of Authorship	138
Abstract.....	140
CHAPTER 5: CONCLUSIONS AND FUTURE WORK.....	189
5.1 Summary	189
5.2 Research Conclusions.....	191
5.3 Recommended Future Works.....	192
REFERENCES.....	195
APPENDICES	207
Conference Paper 1.....	207
Conference Paper 2.....	226
Conference Paper 3.....	235

CHAPTER 1: INTRODUCTION

1.1 Background

The use of fiber reinforced composite (FRC) materials has been increasing steadily in many engineering disciplines over the last few decades since their attractive features such as high specific strength and stiffness as well as many other properties are preferred over those of conventional materials such as steel or concrete. These superior properties are the direct outcome of composing two or more constituent materials with distinctive properties to form a unique material where certain desirable characteristics can be achieved. In facts, the basic concepts and forms of composite materials are found to be existed for centuries with evidences found in Egypt dated back to 1500 B.C where bamboo shoots glued with laminated wood were used as reinforcement in mud wall [1], or laminated writing materials were made from papyrus plant by ancient Egyptians as early as 4000 B.C [2]. On the other hand, the application of modern composite materials started in early 20th century when fiberglass in polymer matrix were made for manufacturing high-temperature electrical components. Since then scientist and engineering communities around the world have begun to explore the enormous potential of fiber reinforced composite (FRC) materials and by this time, these materials have been radically transforming our everyday lives. For example, athletes' performance can be effectively enhanced with better sport equipment made of composites (racquets, surfing board, bikes, etc.), travelling becomes faster, safer and much more fuel efficient as transport vehicles (cars, boats, airplanes, high speed marine craft, etc.) built from composites are stronger, lighter, easier to manoeuvre and more durable than other traditional materials such as steel or aluminium. A plot of specific strength against specific modulus of various materials including traditional metal materials as well as advanced fibers and composite materials as shown in Figure 1-1 which indicates exceptional characteristics of the new materials.

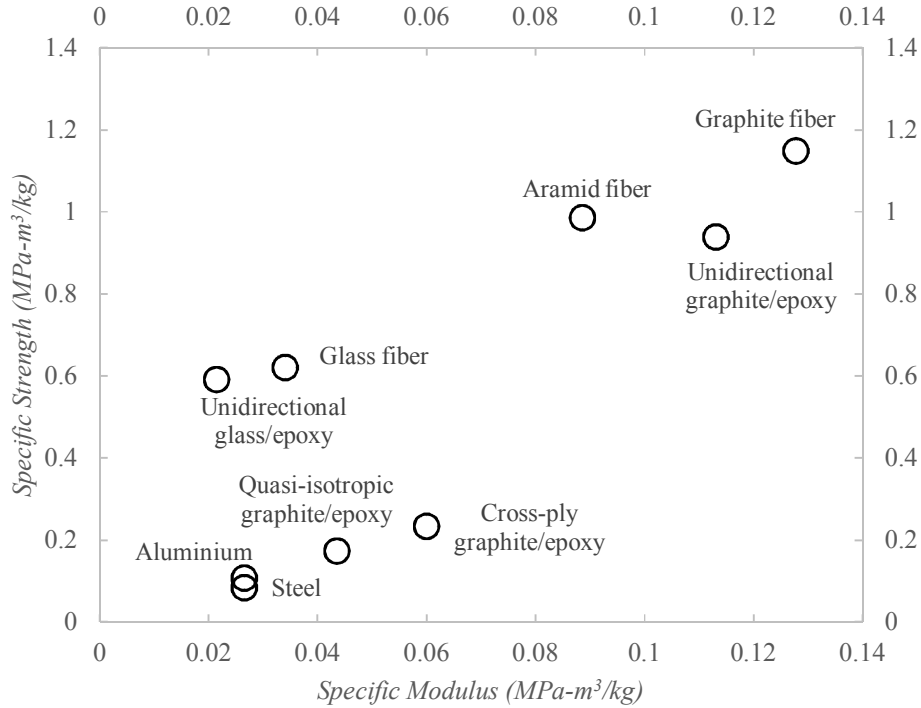


Figure 1-1: Specific Strength and Specific Modulus of fibers, metal and composites (Data obtained from [1])

Advanced composite materials consist of fibers, such as glass, carbon/graphite, aramid or boron, and matrix such as epoxy, polyester or vinyl ester resin systems are also used for building spacecraft, missiles, military aircrafts as well as commercial aircrafts applications. Recent developments in the design and manufacture of new passenger airplanes have made a profound remark on the significance of FRCs in the aviation industry where the material accounts for more than 50% of the entire structural weight of an airplane [3]. Figure 1-2 below shows the rapid increase in usage of composite materials in both commercial and military aircrafts over the period from 1965 until recently. In the transportation industry, the use of composites reduces the self-weight of the vehicles which will improve their fuel efficiency and/or increase their pay load carrying capacity leading to extra revenue over their service life. In the defence sector, the reduction of self-weight will allow for bigger engines having more power which will improve the overall performance such as enhanced operating speed and manoeuvrability of a fighter plane or naval vessel.

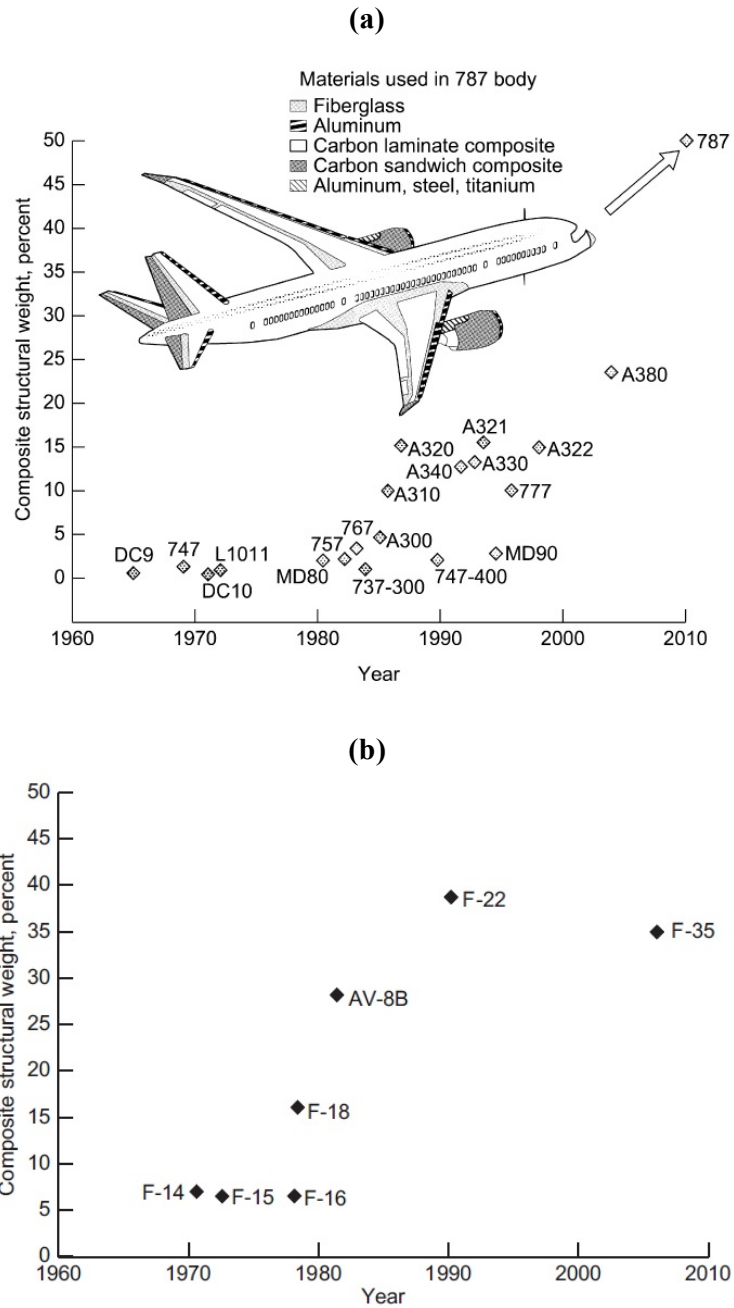


Figure 1-2: Composite material usage by weight in: (a) Commercial aircraft and (b) Military aircraft [4]

Initial applications of composites in construction industry were limited to non-critical components such as cladding, railings or decorations. With the improvement for understanding the material behaviours and reduction in manufacturing costs, the use of FRC materials has been widely spread across the construction industry in the last few decades with more load bearing components such as beams, columns, structural panel for walls or floors, bridge decks, etc. are

made from composite materials. Moreover, with the exceptional stiffness-to-weight ratios and strength-to-weight ratios compared to traditional metals or reinforced concrete materials in the construction industry, shell-shaped structures/roof made of composites are able to span across much greater distances that enable much more flexibility in the design along with remarkable added aesthetic values as well as structural efficiency.

The superior corrosion resistance property of FRC materials are also beneficial for structures located in aggressive environment, e.g. off-shore structures, sub-sea level applications, etc., where traditional metallic materials are susceptible to corrosion and require regular maintenance. Other major use of composite materials in construction industry is retrofitting and rehabilitation of existing infrastructures where repairs are needed for damaged/degraded structures or upgrades are carried out to increase the load bearing capacity of an existing structure [5]. In other specialised fields where weight-reductions play a key role in the overall performance of the structure, such as construction of larger wind turbines and their supporting structure, FRC material has established itself as the most feasible option in the selection of materials [6]. The length of a single blade now can exceed 70m and it is increasing rapidly to achieve a higher energy output per unit cost. The use of composite laminates and some of its other forms such as sandwich laminates has made it possible to design such large blades having sufficient strength and stiffness for their efficient operation. Apart from low maintenance costs, aesthetics and other benefits, the use of these outstanding lightweight materials helps to reduce the transmitted load on the supporting structural components, which has a cumulative advantage in weight or material savings leading to a remarkable overall economic benefit.

With such diverse applications, structural components made of composite materials can be subjected to highly complex stress scenarios produced by different combinations of loading such as extreme thermal loading, severe dynamic loadings or impacts, which may lead to a significant damage or complete failure of these structures. Due to the composite nature of these materials, their failure characteristics are quite complex and an accurate prediction of this process is extremely challenging. Therefore, the analyses of these structures require a reliable material model to correctly predict the strength and inelastic response of laminated

composites. Subsequently, modelling aspects of laminated composite materials receives a vast amount of interests from different research communities with diversified backgrounds and theoretical bases. Various theories and approaches developed for modelling constitutive response of composite materials will be briefly discussed in the following section.

1.2 Mechanical response of FRC

In this section, a review of mechanical response of FRC is present. First, the important aspects of FRC response at structure level are investigated along with the relevant laminated plate and shell theories. It is then followed by literature review of some critical characteristics of damage processes occurred within a laminate. Understandings of these features of FRC structures are essential for the development of a reliable design approach to ensure safety and efficient of these structures.

1.2.1 Laminated Plate Theories

There are different types of plate theories which have been developed since the mid-20th century for modelling flat composite laminates using various kinematic assumptions for representing the variation of displacements and stresses along the laminate thickness. In general, these theories can be categorised into the followings:

- Equivalent single layer theories (ESLT):
 - Classical plate theory (CPT)
 - First order shear deformation theories (FSDT)
 - Higher order shear deformation theories (HSDT)
- Layer wise theories (LWT):
 - Discrete layer theories

The Equivalent Single Layer theories (ESLT) are displacement-based theories where some certain type of variations through the plate thickness are taken for the displacements, which help to express displacements at any point within any layer with respect to displacement parameters at the reference plane (usually plate mid-plane) [7]. Based on this, the heterogeneous laminates are mathematically replaced by a statically equivalent single layer where the stiffness of the laminate is a weighted average of the layer stiffness through the thickness. Most of the early

works employed the Love-Kirchhoff's hypothesis used in classical plate theory for modelling laminated plates. It assumes that a transverse plane normal to the plate mid-plane before bending remains plane and normal/perpendicular to the plate mid-plane after deformation and inextensible [8]. This leads to linear distributions of in-plane displacements along the thickness direction and it does not include any contribution of the transverse shear deformation which may be acceptable for thin plate structures.

On the other hand, the effects of transverse shear deformation are significant in thick plate structures and it is more profound in composite plates as the material is weak in shear. Thus various types of variations for the in-plane displacements have been adopted for developing first order [9, 10], or higher order [7, 9, 11–13] shear deformation theories. In first order shear deformation theory (FSDT), the transverse shear strains are taken as uniform along the plate thickness whereas this variation is parabolic for higher order shear deformation theory (HSDT). In general, HSDTs are more accurate for representations of the transverse shear stress distributions along the thickness of the plate.

In conclusion, the main advantages of ESLT are their inherent simplicity and low computational costs. However, these theories may not be adequate when a more realistic distribution of stresses throughout the plate is needed. For laminated plates, even in the elastic range having no damage, the transverse stresses are continuous and the transverse strains are discontinuous at the interfaces between the layers. Unfortunately, these conditions cannot be satisfied using ESLT as it takes smooth and continuous distributions of the in-plane displacements throughout the plate thickness, which lead to continuous transverse shear strain distributions over the entire plate thickness including the interfaces between the layers.

In certain applications, higher transverse stresses, which are produced at a point in actual scenario, may cause a localised failure at that point of the structure such as delamination between layers, joint separations and matrix cracking [8]. Therefore, a theory that can predict stresses accurately is needed, especially for thick laminate plates/shells. Among several theories/approaches have been developed, the layer wise theories have been found to be the most suitable where the displacements for each layers are modelled explicitly which results in a realistic distribution of

stresses and strain with discontinuities in appropriate locations. Early development of the layer-wise theories includes the works in [14–18] which can adequately predict the deformations of laminated composite structures, however, at the expense of high computational efforts due to a large number of degrees of freedoms in these formulations. Further studies on plate theories [12, 19–23] employed the refinement of the through thickness definition of in-plane displacements follows zigzag functions which gave the desirable strain continuity at the lamina interfaces. These refined theories helped to improve the model accuracy as well as computational efficiency at the same time, however the implementations of these theories are relatively challenging.

1.2.2 Laminated Shell Theories

Besides the architectural aesthetics, the shapes of shell structures are known for their structural efficiency where the majority of applied loads can be transferred in the form of in-plane forces by membrane actions which leads to higher load carrying capacity of the structures. For this reason, applications of composite shell structures can be seen in many fields ranging from military uses, such as aircraft, missiles or submarines, to other engineering applications like construction of liquid-containing vessels or large span dome structures. Many modelling approaches have been developed for the design of these structures where most of the theories of shell structures are extension of plate theories with curved geometrical configurations. Examples of such theory can be found in [24–26] for FSDT, [27] for HSDT or [28–32] for layer-wise theory of multi-layered anisotropic shells. To this end, CPT, FSDT, and HSDT shell theories are applicable for thin shell structures while a thick shell structure needs a discrete layer shell theory or a refined zigzag theory for an accurate prediction of displacements and stresses.

1.2.3 Failure Mechanism of Laminated Unidirectional FRC

The studies on laminated plate and shell theories discussed in the previous sections are primarily restricted to the elastic response of composite structures while their post-yield inelastic behaviour or the entire nonlinear response is often ignored. Nevertheless, composite structures can be subjected to complex loading conditions such as impacts, severe dynamic loads or extreme thermal loads which can lead to a significant damage or complete failure of these structures. For this reason, large volume of attentions has been drawn from the research community worldwide to

investigate the governing failure mechanisms of FRC. To this end, the failure of composites is a complex process which involves several interdependent failures processes which also depends on loading conditions and the constituent properties. In general, there are four common modes of failures observed in composites: matrix cracking (intra-laminar fracture) perpendicular to the loading direction or ply splitting, fiber/matrix debonding, fiber breakage/failure and delamination between two adjacent layers or plies (refer to Figure 1-3).

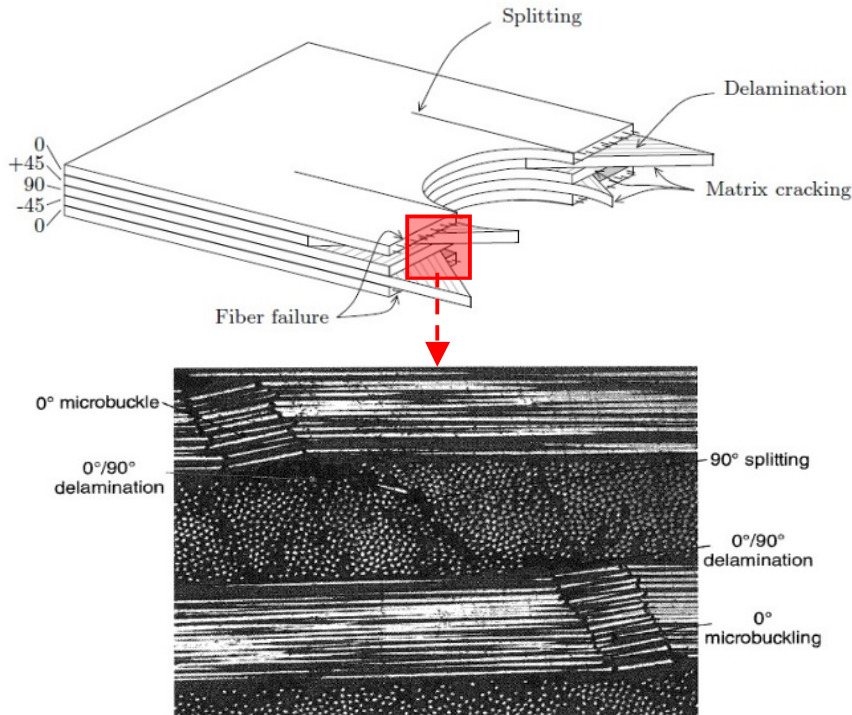


Figure 1-3: Schematic representation of different failure modes in unidirectional laminate under tension [33] and laminate failures at microscopic scale [34]

Amongst these failure mechanisms in FRC, fiber fractures are the least common failure mode as they process very high ultimate stresses which can be as high as 5171 MPa for IM8 carbon fibers [2]. More common types of fibers such as glass or boron fibers also display a high strength of 4585 MPa and 3799 MPa respectively [2]. On the other hand, common matrix materials of advanced composites are epoxy, polyester or urethane [1] which exhibit significant lower strength compared to fibers and are more susceptible to damage. Figure 1-4 shows typical load deflection behaviours of polyester resin where nonlinear behaviours of the matrix material beyond their yielding are clearly observed. The nonlinear post-yield

response of the resin/matrix usually involves two primary nonlinear effects: 1) gradual loss of stiffness (damage) and 2) permanent inelastic (plastic) deformations [8, 9]. These nonlinear responses are caused by the inelastic mechanisms (damage and plasticity) which occur due to progressive micro-structural changes as the material is being loaded. For examples, microscopic processes such as void nucleation, void enlargement, void coalescence and microcracking within the matrix cause stiffness degradations while frictional sliding and dislocations of defects are associated with irreversible plastic deformations [10–12].

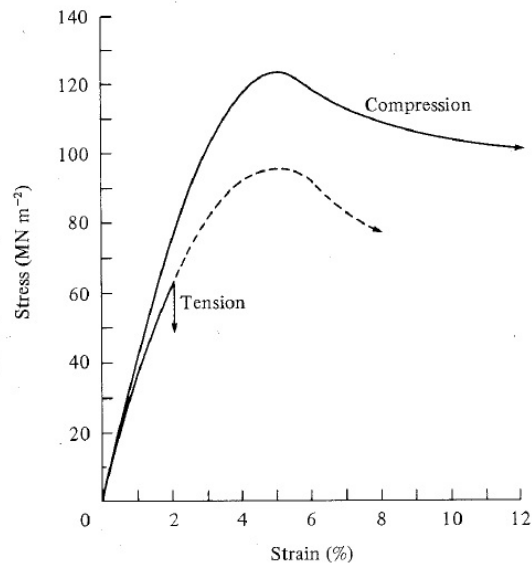


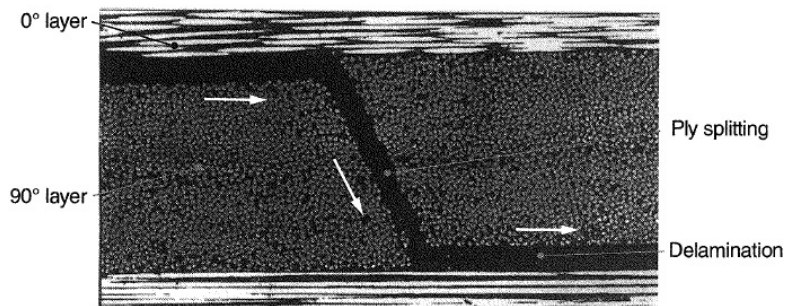
Figure 1-4: Typical Stress-strain relationship of polyester [35]

Furthermore, microcracking in the matrix, under increasing loads, can be accumulated or localised and form macro matrix cracking in the ply and their effects on the macroscopic behaviour of composites are well-documented in many studies [36–41]. In such situations, a sudden change in the stiffness of composites can be observed as a result of the cracking process causing the redistribution of stresses in the local fields.

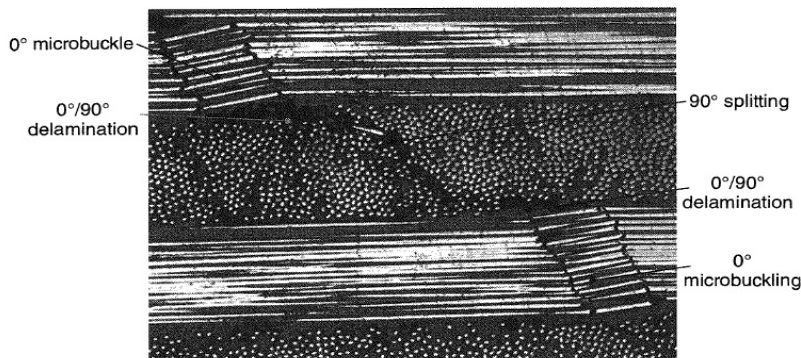
On the other hand, fiber/matrix interface failures (fiber debonding) also play an important role contributing to the loss of stiffness and the ultimate failure of FRCs [34, 42]. Macroscopic responses of composites are primarily influenced by the bonding strength at the fiber/matrix interface [43, 44]. Subsequently, stresses in the local fields of the composites may exceed this bonding strength and lead to a localised separation of the fiber and matrix. Under increasing loads, this will

progressively grow in the fiber direction and simultaneously induce new cracks in the matrix towards a direction normal to the fiber [41]. Further fiber debonding can be initiated from the development of the new matrix cracks and eventually macro transverse cracking or ply delamination can occur in the FRC laminate (Figure 1- 5).

Other mode of failure (relatively less common) includes in-plane/translaminar shear failure, which is extremely rare in unidirectional plies, as longitudinal splits tend to occur before in-plane shear cracks [34]. In addition, fiber kinking/buckling failures can be observed under compression loadings.



(a)



(b)

Figure 1- 5: (a) Matrix cracking (90° splitting) and delamination in a CFRP laminate; (b) Cross-section of a compression failure in a $0^\circ/90^\circ$ laminate [34]

In summary, modelling of unidirectional FRC laminates are quite challenging with complex behaviour of the constituents as well as the macroscopic response in both linear and nonlinear range. In this regard, it is important that several key aspects need to be addressed for a reliable modelling strategy. First, effective elastic properties of the laminates need to be determined from the constituent properties in order to model the laminate response in the elastic range. When inelastic response

of laminate is considered, suitable yielding and failure criteria for the constituents as well as the laminate are needed to accurately depict both constituents' response and the macroscopic behaviour of the laminate under various loading conditions. Furthermore, the prediction of the macroscopic response should be derived on the basis of physical interactions between the material constituents for a better predictive capability of the model rather than based on a curve fitting type approach. More details review on the constitutive modelling of composite materials are provided in the next section.

1.3 Constitutive Modelling of Composite Material

There are a wide range of models available in literature dealing with constitutive modelling of composite laminate. To this end, a brief review of theoretical models available in literature will be presented in this section.

1.3.1 Continuum Constitutive Modelling

Fibre reinforced composite materials have been traditionally modelled as homogeneous materials with orthotropic mechanical properties and based on that, a number of theories have been proposed by various investigators. The developments of these theories rely on phenomenological observations at structure/macro scale in order to obtain and use a suitable failure criterion which will be able to produce results matching with the experimental data. For example, the well-known Tsai-Hill theory [45] belongs to this group, which has been applied to unidirectional FRC using Hill's failures theory for material with low degree of anisotropy [46] and has subsequently been extended to generalise the theory where a second order polynomial in tensor form has been used for the failure surface [47]. Nevertheless, the quadratic nature of this failure criterion implies that it is applicable to materials with identical tensile and compressive strengths only [2]. This limitation has been overcome by Hoffman [48] by adding a linear stress term to Hill's criteria to account for different ultimate stresses in tension and compression for brittle composites [48]. Hashin and Rotem [49] developed a piecewise smooth function at macroscale level which helped to simulate two simple failure modes within a lamina: failures due to fiber breakage under the longitudinal stress, and failures due to matrix cracking under transverse stresses. However, this model [49] is only applicable for plane stress problems. Hashin [50] extended this

approach to model unidirectional laminates under three-dimensional loading conditions considering tensile and compressive failure of both fibers and the matrix. However, the quadratic form of the failure envelop used in these models [49] and [50] has been chosen on the basis of curve fitting and interpretation of the energy density which has a quadratic form in terms of stresses [50]. Thus, it lacks a strong and convincing physical basis. On the other hand, Christensen [51] proposed a 3-D stress-strain relationship for transversely isotropic material and a strain-based failure criterion closely related to Tsai and Tsai-Hill theories. He also derived a stress-based criterion taking into account the effects of hydrostatic pressure on the failure envelop [52]. Again, the explicit representations of the constituent behaviour in the derivation of macroscopic response are absent due to phenomenological nature of the approach. Gosse [53, 54] proposed the well-known Strain Invariant Failure Theory (SIFT) or the Onset theory where the critical values of dilatational volumetric strains and distortional shear strains are used as the criteria for detecting failure initiation of composite lamina, yet the evolutions of failure mechanisms were not considered in these studies.

In the aforementioned works, the focus was to obtain the final failure envelop which is needed for the ultimate strength analysis, whilst the whole nonlinear response after yielding cannot be captured. The post-yield response of fibre reinforced composites usually involves two predominant nonlinear effects: (i) gradual loss of stiffness parameters (damage); and (ii) permanent/irreversible deformations (plasticity) [55, 56]. These nonlinear effects caused by inelastic deformations (damage and plasticity) which occur due to progressive changes in the structural form of materials at microscopic scale as the material is being loaded progressively. For examples, microscopic processes such as void nucleation, void enlargements, void coalescence and micro-cracks within the matrix contribute to the overall material stiffness degradations while frictional sliding and dislocations of defects are associated with permanent deformations [34, 57]. Furthermore, fiber-matrix interface failures (fiber debonding) as well as ply delamination also contribute to loss of stiffness in fiber reinforced laminates [34].

When structures are subjected to extreme loading such as severe dynamic loads, impacts, high temperature, etc., it is crucial to model the progressive failure processes (due to evolutions of damage and plasticity) in order to correctly assess

the safety of a structure. Several attempts have been made to model this nonlinear response with some assumptions where the whole damage and plasticity process is smeared over the entire lamina/ply and the damage parameter and plastic strains, commonly defined as internal variables, are estimated at ply level. The models based on Puck's theory [58, 59] and Pinho's model [60–62] are some representative examples where several failure modes such as fiber failure, matrix failure and inter-fiber fractures are accounted for and they contribute to the overall ply stiffness degradation. The actual physical basis of the inelastic deformations of composites is lacking in these models as they are based on curve fitting technique utilising experimental test data at ply level. This can produce reasonably good results if the loading scenario is not that different from those used to get the data utilised for calibrating these models. However poor results can be produced if the loading scenario is outside this dataset. Some other techniques based on ply level information have also been developed where a plasticity model using Ramberg-Osgood hardening rule [63–66] or a single parameter orthotropic plasticity model [67, 68] have been used. In some of these studies [64–66], the stiffness degradation based on a rational damage model has been combined with the plasticity model. On the other hand, some researchers [69–75] attempted to develop a thermodynamically consistent model where the damage parameter is taken as an internal variable and included in the energy potential (e.g. Helmholtz free energy) of the material. However, the coupling between damage and plasticity is not considered in these models in [69–75]. Schuecker and Pettermann [56] have adopted an ad-hoc approach to enhance their damage model with plasticity to account for shear bands developed in fracture planes, but this approach lacks a strong physical basis for interactions between these two mechanisms. A more thermodynamically rigorous approach has been developed by Barbero and Lonetti [76] but the coupling between damage and plasticity is weak as separate loading surfaces are used for these two processes.

All the above-mentioned models are based on the continuum approach at macro scale which depends on phenomenological observations at macroscopic scale to predict mechanical responses and failures of composites. Although these models are able to produce reasonable results for simple loading scenarios with good computational efficacy, they suffer from the lack of physical basis and therefore

cannot capture well the complex interactions between the constituents (fiber and matrix) found in many abovementioned situations. These physical interactions of the constituents can initiate different localised failure modes at microscopic level such as matrix micro cracks or voids, fiber breakage, fiber-matrix debonding, etc. even at early loading stage [34]. With the increase of loading, these localised failures can accumulate and propagate through the entire laminate leading to possible macro crack formations, ply delamination [71, 75, 77] and eventually a complete collapse of the structure. Therefore, it is essential that these progressively accumulated failure mechanisms and their effects on the overall responses of the composite structure should be captured properly to assess the structural safety and integrity reliably.

1.3.2 Micromechanics Modelling

With the rapid increase of computational resources in recent times and rising demands for a reliable material model for composite materials, approaches involving a detailed micromechanical analysis at fiber scale have quickly gained their momentum in this field of study. These approaches treat composites as non-homogeneous solids where the constituents and their physical interactions are modelled explicitly using finite elements or continuum mechanics based models. Therefore they require the behaviour of constituents in details. In these studies, the stiffness of fibers is found to increase slightly at higher tensile loads [78] and strain rates [79], but this increase is not significant and a linear elastic behaviour of fibers up to their failure is generally acceptable in most cases. In contrast, plastic deformations and stiffness degradations are found as predominant causes of inelastic behaviours of the matrix which need to be correctly captured. Many researchers have used pressure-dependent yield criteria such as Mohr-Coulomb [80, 81] or Drucker-Prager [82] to model epoxy resins as the failure of these matrix materials is sensitive to applied hydrostatic pressure [83]. However, these studies did not consider the effect of damage. Others [86] had taken a different approach by using the strain invariant failure theory (SIFT) [53, 54] in the micromechanical analysis with the use of strain magnification factors to predict the failure behaviour of composites, however, the definition of damage evolution was not included in this work. Canal et al. [84] and Melro et al. [85] have incorporated the effect of stiffness degradation of the matrix in their damage-plasticity coupled models, but

both models did not include strain-hardening behaviours and require two separate dissipation potentials for plasticity and damage. In short, to the best of our knowledge, these available models for matrix are still not adequate yet. In this respect, the modelling of matrix behaviour to capture essential characteristics of matrix failure is therefore an important part in the development and application of micromechanical analysis for FRC.

The micromechanical modelling techniques require explicit modelling of the material constituents and can produce excellent results. Analyses based on a full micromechanical model can capture multiple failure modes of the constituents and simulate their progressions at micro scale with very fine details. However, this requires a huge computational power which is only feasible for small scale applications. In this regards, the concept of multiscale modelling approach is an attractive proposition which attempts to establish a link between the models at the microscopic scale (fiber size) and the macroscopic scale (structure size), where crucial information at one length scale are transferred to the next length scale for simulations [77]. These can be obtained via analytical or computational homogenisation approaches. For composite structures, these approaches can reduce computation costs greatly while at the same time giving reliable predictions as sufficient details of physical interactions of the constituents at microscopic scale are retained within the models. These critical details can subsequently be used for predicting the material response at macroscopic scale utilizing a homogenisation technique. Examples of these (analytical) homogenisation technique can be seen in [87, 88], where inclusions are assumed to be embedded in infinitely extended matrix (Eshelby's assumption) which may not be strictly valid for a composite with large fiber volume fractions. In addition, the prediction of instantaneous compliance tensor based on Mori-Tanaka's model [89] does not satisfy the exact expression related to local and global inelastic effects, therefore it is not suitable for inelastic analyses. Hashin and Rosen [90] develop the well-known concentric cylinder assemblage (CCA) model having hexagonal arrays of identical fiber which is an extension of Hashin's earlier work on concentric sphere model [91]. The model follows the principle of minimum potential energy and complementary energy, which lead to upper and lower bound solutions for the effective elastic modulus of composites. In the same study, the concept of random arrangement of

fibers has been introduced to eliminate these two bounds and obtain a unique value of E_1 , G_{12} and G_{13} . However, this could not be achieved for G_{23} and E_2 which are having two bounds. This concept of Hashin and Rosen [90] has been enhanced by Christensen and Lo [92] using three-phase sphere and cylinder models which helped to produce a unique solution of the effective shear modulus. However, these models are only applicable within the linear elastic range of composite materials [92].

By this time, some efforts have been made to model the nonlinear response of composites based on micro-mechanisms embedded in the macro based continuum descriptions. Sun and Chen [93] have derive a three-phase 2-D representative volume element (RVE) where fibers belong to one phase which is idealised with a square shape and the matrix is divided into two phases which are idealised with two rectangular shapes. A linear elastic behavior is used for fibers whereas a plasticity based model with no damage is used for the matrix. Aboudi [94, 95] has proposed a four-sub-cell RVE, popularly known as method of cells (MOC), which is based on displacement compatibility and traction continuity conditions at the interfaces between sub-cells in order to obtain the links between stresses and strains in each sub-cell and the equivalent homogenised material. Subsequently, the method (MOC) has been extended for modelling composites having irregular fiber configurations and it has been renamed as generalised method of cells (GMC) where a finite element analysis is necessary for modelling a large number of repeating sub-cells within the RVE. This method has been refined further by Pindera and Bednarczyk [96] to improve the model efficiency but the computational cost become very high with the increasing complexity of nonlinear effects in local fields[97]. The GMC has also been used by other researchers to investigate the inelastic response of fibrous composites under off-axis tensile loading [98] or rate-dependent behavior of epoxy composites[99]. On the other hand, Huang [100–102] developed a bridging micromechanics model which has been combined with classical laminate theory to simulate behaviors of multilayered composite laminates. Shokrieh et al. [79] examined the strain-rate effects on mechanical responses of composite laminates under dynamic loadings using Huang's model. Although Huang's model considered the effect of plasticity, it did not include the effect of damage. Santhosh and Ahmad [103] attempted to predict the nonlinear

behaviour of unidirectional fibre reinforced composites made of polymer matrix where the plastic deformation and temperature dependency have been accounted for without having any stiffness degradation due to damage. Tabiei and Aminjikai [104] have considered both damage and plasticity for predicting the response of unidirectional composites under impact loads. They have used Goldberg's viscoplasticity model [105] to account for the rate dependent properties of resin whereas the damage evolutions in fiber and matrix are based on Weibull distribution functions. Although both damage and plasticity have been included in their model, the effects of these two dissipation processes have been included in the model discretely and having no coupling between them.

1.4 Research Objectives

Based on the above observations, it can be concluded that there is a need for development of an efficient constitutive model capable of accurately predicting the inelastic response of unidirectional FRC ply at an affordable computational cost. This is the main aim of the present investigation. In particular, this model should possess the responses and interactions of different constituents (matrix, fiber and interfaces) and should cover a wide range of ply responses under different loading conditions that can lead to the activation of all essential mechanisms of failure at the fibre scale. In addition, the model should have minimal computational demands to ensure that it can be used for large scale structure modelling and at the same time, it can capture sufficient details of the physical interactions between the material constituents (fiber and matrix). In this study, the fiber is assumed to behave elastically while two primary inelastic processes are considered for the matrix: damage and plasticity. Moreover, as the influence of the fiber/matrix interfacial failure process on the response of FRC material is profound, its effects should be properly taken into account in order to capture the ply response accurately. On those basis, three primary objectives are identified in the present investigation which are explained in details as follows:

Objective 1: Development of an analytical model for upscaling the nonlinear response from the fiber/micro scale to the ply scale and vice versa in order to achieve such a high precision modelling tool for fiber reinforced composites with feasible computational resources. In most of the existing models, the micro scale

analysis is carried out with the involvement of a local finite element or other numerical model which poses significant challenges from the computational aspect. In this regard, a micromechanics-based macro constitutive model is an attractive proposition where the behaviour of constituents and their interactions at micro scale are retained within the model which will provide a solid physical basis for the proposed model. The response of these constituents will be homogenised to establish the macro constitutive response of the ply. On the other hand, a model based on continuum damage mechanics and plasticity theory will be used to capture the inelastic response of constituents, particularly matrix, where the effects of the irreversible processes such as permanent plastic deformations and progressive damage mechanism together with the pressure dependent responses cannot be neglected. The development of the coupled damage-plasticity model is linked to the second objective presented below.

Objective 2: The focus of this objective is to develop a coupled damage-plasticity constitutive approach for engineering materials using damage mechanics and plasticity theory, based on the principles of thermodynamics of solids. This model will help to predict the response of the constituent materials in FRC since inelastic response of the matrix/resin involves both permanent deformation and stiffness reduction due to plasticity and damage processes. The coupling technique between damage and plasticity should be sufficiently generic for it to be applicable to a variety of different material behaviour. In particular, it will be shown that these mechanisms and the corresponding proportion of energy dissipations can be controlled or specified to follow the material behaviour observed in experiments. The evolution of the underlying dissipative mechanisms (damage and plasticity) will be controlled with the use of loading functions while the explicit links between these mechanisms are established.

Objective 3: This objective builds on Objectives 1 and 2 where the continuum damage model developed in Objective 2 is incorporated in Objective 1 to capture the response of unidirectional fiber reinforced composite ply in nonlinear range. The combination of all kinematic enrichments to capture the difference in the deformation of different constituents and also their responses in a thermodynamics-based approach will naturally lead to macro homogenised stress and internal equilibrium conditions that governs the behaviour of the FRC. In addition, the

effects of fiber/matrix interfacial imperfection in ply constitutive response, which is essential when the ply nonlinear behaviour is dominated by fiber debonding, will also be accounted for and included in a fiber interface equivalence (FIE) block. Consequently, all three primary failure processes occurred within a FRC ply, which are damage and plasticity in the matrix as well as fiber debonding failure, will be effectively considered in this Objective.

1.5 Thesis Overview

This thesis is broadly divided into five **Chapters**. Apart from the Introduction (**Chapter 1**), the main body of work is included in three **Chapters (Chapter 2 to 4)** where three research articles (two already published and one to be submitted soon for publication) produced by the candidate and his colleges are presented. Minor developments based on these major ones are in the Appendix. The remaining of the thesis is organised as follows:

Chapter 2 (Journal Paper 1): A Kinematically Enhanced Constitutive Model for Elastic and Inelastic Analysis of Unidirectional Fiber Reinforced Composite Materials.

A micromechanics-based constitutive model that relies on the behaviour and interaction of both fiber and matrix components are developed in this paper. Both fiber and matrix are represented by different constitutive responses and their interactions are accounted for through a set of internal equilibrium conditions at their interfaces. The differences in the response of fiber and matrix are represented by the enrichment of strain fields and based on this a novel technique is developed to upscale the inelastic response of the constituents (fiber and matrix) to the macro scale (ply scale). It is noteworthy that the model formulation are conveniently derived in incremental form which helps the proposed model accommodating both linear and nonlinear behaviour of composite material. Subsequently, numerical examples are provided to demonstrate the application of the proposed model for both elastic and inelastic range and the model predictions are validated with experimental data as well as results obtained from some benchmark theories.

Chapter 3 (Journal Paper 2): A Thermodynamics-based Framework for Constitutive Models using Damage Mechanics and Plasticity Theory.

In this paper, a generic framework for coupling damage and plasticity is proposed which focuses on the driving mechanisms behind the coupling of the two processes (damage and plasticity). It will be shown that these mechanisms and their corresponding dissipations can be controlled or specified to follow the material behaviour observed in experiments. In addition, it will be demonstrated that the evolutions of these dissipation processes can be controlled within the proposed framework and different dilative and contractive responses under different loading conditions can be accurately modelled. The detailed formulation of the proposed generic framework for coupling damage and plasticity is provided along with discussions on some of its attractive features. Several aspects of numerical implementation of the proposed framework will also be presented. Finally, the applications of the proposed framework for different material models are also illustrated through a number of examples.

Chapter 4 (Journal Paper 3): A Kinematically Enhanced Constitutive Model for Unidirectional Fiber Reinforced Composite laminae with Imperfect Fiber Interface.

This paper focuses on the fiber/matrix interface failure which plays an important part contributing to the loss of stiffness and ultimate failures of FRCs. To this end, macroscopic responses of composites are significantly influenced by the bonding strength at the fiber/matrix interface while other characteristics such as fracture energy or stiffness of the interface are of less importance. Subsequently, stresses in the composite exceeding this bonding strength can lead to a localised separation of the fiber and matrix which, under increasing loads, continuously grow in the fiber direction and simultaneously induce matrix cracking in the direction normal to the fiber. Further fiber debonding can be initiated from the development of matrix cracking and eventually macro transverse cracking can be formed in a FRC ply. Thus, in this paper the kinematically enhanced constitutive model for predicting the response of unidirectional FRC ply, which is presented in **Chapter 2**, is further enhanced with a thermodynamics-based formulation and extended to include the effects of fiber/matrix interface failure. Applications of the proposed

CHAPTER 1: INTRODUCTION

model are illustrated in a number of examples and its performance is demonstrated by comparing the results to other sources obtained from literature.

Chapter 5: Conclusions and Future Works

This closing chapter provides a summary of important outcomes and contributions of the thesis. Potential applications of the research as well as possible future works are also recommended.

CHAPTER 2: JOURNAL PAPER 1

A Kinematically Enhanced Constitutive Model for Elastic and Inelastic Analysis of Unidirectional Fibre Reinforced Composite Materials

Statement of Authorship

Statement of Authorship	
Title of Paper	A Kinematically Enhanced Constitutive Model for Elastic and Inelastic Analysis of Unidirectional Fibre Reinforced Composite Materials
Publication Status	<input checked="" type="checkbox"/> Published <input type="checkbox"/> Accepted for Publication <input type="checkbox"/> Submitted for Publication <input type="checkbox"/> Unpublished and Unsubmitted work written in manuscript style
Publication Details	Vu, V.D., Sheikh A.D., Nguyen, G.D., Shan, I., 2017. A Kinematically Enhanced Constitutive Model for Elastic and Inelastic Analysis of Unidirectional Fibre Reinforced Composite Materials. <i>International Journal of Mechanical Sciences</i> , 129, pp.171-185.
Principal Author	
Name of Principal Author (Candidate)	Van Duc Vu
Contribution to the Paper	Developed and wrote the formulation and its application and numerical examples. Wrote the manuscript.
Overall percentage (%)	70%
Certification:	This paper reports on original research I conducted during the period of my Higher Degree by Research candidature and is not subject to any obligations or contractual agreements with a third party that would constrain its inclusion in this thesis. I am the primary author of this paper.
Signature	Date 08 / 01 / 2018
Co-Author Contributions	
By signing the Statement of Authorship, each author certifies that:	
i. the candidate's stated contribution to the publication is accurate (as detailed above); ii. permission is granted for the candidate to include the publication in the thesis; and iii. the sum of all co-author contributions is equal to 100% less the candidate's stated contribution.	
Name of Co-Author	Aadu Hamid Sheikh
Contribution to the Paper	Supervision of the technical work, write-up and revision of the manuscript
Signature	Date 15 / 01 / 2018
Name of Co-Author	Giang Dinh Nguyen
Contribution to the Paper	Supervision of the technical work, write-up and revision of the manuscript
Signature	Date 08 / 01 / 2018

CHAPTER 2: JOURNAL PAPER 1

Name of Co-Author	Luming Shen
Contribution to the Paper	Supervision of the technical work, write-up and revision of the manuscript
Signature	
	Date 11/01/2018

End of Document

Abstract

A constitutive model with an enhanced strain field is developed in this study for predicting the behaviour of unidirectional fibre reinforced composite materials. The different deformation modes introduced in the enhanced strain field take into account of both the variation of strains and internal equilibrium conditions across the fibre-matrix interfaces in unidirectional composites. This opens rooms to accommodate the difference in the responses of fibre and matrix and allows both fibre and matrix to be represented separately by their own constitutive responses. The additional deformation modes and internal equilibrium conditions lead to a combination of both upper and lower bound solutions on different components of the stress/strain tensors, resulting a homogenised macro response that compares well with experimental data and sophisticated homogenisation approaches in the literature. In addition, the key feature of the proposed approach is that the macro homogenised behaviour can be written in terms of incremental responses of both constituents and their interactions, facilitating the applications in both linear and nonlinear regimes of behaviour of both fibre and matrix. In parallel with this, a new coupled damage-plasticity model is also developed for the matrix behaviour and validated against experimental data of two resins, before being used in the proposed approach. The performance of the model and its promising features are demonstrated through verification with existing benchmarking models and validation with experimental data in both elastic and inelastic regimes.

Keywords: unidirectional fibre reinforced composite; micromechanics; kinematic enrichment; constitutive modelling; nonlinear behaviour; damage mechanics; plasticity theory.

1. Introduction:

Applications of fibre reinforced composite (FRC) materials are increasing steadily in many engineering disciplines over the last few decades due to their high specific strength and stiffness along with exceptional durability and many other features. Due to the composite nature of these materials, their failure behaviour is quite complex when subjected to extreme loading conditions and an accurate prediction of this process is quite challenging. Therefore, the analyses of these structure require a reliable material model to correctly predict the strengths and responses of fibre reinforced laminated composites. In the literature, the modelling of laminated

composite materials and structures has received a vast amount of interests from different research communities with diversified backgrounds and theoretical bases. For instance, a group of researchers considered FRC as homogeneous materials with orthotropic mechanical properties. From this perspective, several theories have been proposed where phenomenological observations at structure/macroscale are used to obtain a failure criterion which produces results by matching with the experimental data. Some representative samples of these models are found in [1–7] where the focus was to obtain the final failure envelope which is needed for the ultimate strength analysis. However, the entire nonlinear post yielding response of the composite material could not be captured with these models. In the actual loading situation, the post-yield response of composites usually involves two predominant nonlinear effects occurred within the material which are: 1) gradual loss of stiffness (damage) of the constituents and 2) permanent inelastic (plastic) deformations [8, 9]. These nonlinear effects are caused by inelastic mechanisms (damage and plasticity) which occur due to progressive micro-structural changes as the material is being loaded. For examples, microscopic processes such as void nucleation, void enlargement, void coalescence and microcracking within the matrix contribute to overall material stiffness degradations while frictional sliding and dislocations of defects are associated with permanent deformations [10–12]. Furthermore, fibre-matrix interface failures (fibre debonding) and ply delamination also contribute to the loss of stiffness in fibre reinforced composite laminates[11].

By this time, several attempts have been made to model the nonlinear response with an assumption that the entire damage and plasticity process is smeared over the entire lamina/ply and the damage parameter and plastic strains are estimated at ply level. Some important models based on these continuum-based approach can be found in[9, 13–31]. Although these models have good computational efficacy, due to their phenomenological nature (lack of physical insights of the actual failure mechanisms), these models dependence on curve fitting technique utilising experimental data for their calibrations[32, 33]. On the other hand, with a rapid increase of computational resources in recent days, approaches involving a detailed micromechanical analysis at fibre scale have quickly gained their momentum in this field of study. These approaches treat composites as non-homogeneous solids

where the constituents and their physical interactions are modelled explicitly using finite elements and continuum mechanics-based models. Representative examples of such models can be found in [34–40]. To this end, analyses based on a full micromechanical model require explicit modelling of the material constituents and thus they can capture multiple failure modes of the constituents and simulate their progressions at micro scale with very fine details. However, these techniques require a huge computational power which may be feasible for small scale applications only.

In this scenario, the concept of multiscale modelling approaches is an attractive proposition which attempts to establish a link between the models at the microscopic scale (fibre size) and the macroscopic scale (structure size), where crucial information at one length scale is transferred to the next length scale for simulations[32]. For composite materials, these approaches can reduce computation costs greatly while at the same time give reliable predictions as sufficient details of the physical interactions of its constituents at microscopic scale are retained within the models. This can be achieved by considering the composite materials as non-homogeneous solids comprising of fibre and matrix phases and utilizing certain homogenisation techniques to capture the overall behaviour of these materials. Such attempts are made in [41–44] where different approaches are used to determine mechanical properties of composites in elastic range.

By this time, significant efforts have been made to model the nonlinear response of composite materials by embedding micro-mechanisms within a continuum model. Sun and Chen[45] have derive a three-phase 2-D representative volume element (RVE) where fibres belong to one phase which is idealised with a square shaped block or cell and the matrix is divided into two phases which are again idealised with two rectangular shaped cells. In this work, a linear elastic behavior is used for fibres whereas a plasticity based model with no damage is used for the matrix. Aboudi[46, 47] has proposed a RVE consisting of four square and rectangular shaped cells or sub-cells. This is popularly known as method of cells (MOC), which is based on displacement compatibility and traction continuity conditions at the interfaces between these sub-cells in order to establish links between stresses and strains in each sub-cell and the homogenised material. Subsequently, this method (MOC) has been extended for modelling composite materials having irregular fibre

configurations and it has been renamed as generalised method of cells (GMC) which uses a large number of repeating sub-cells within the RVE. This method has been refined further by Pindera and Bednarczyk[48] to improve the model efficiency but the computational cost become very high with the increasing complexity of nonlinear effects in local fields[49]. Further improvements of GMC were introduced in the high fidelity generalised method of cells (HFGMC) proposed by Aboudi and Arnold[50]. The frameworks of GMC and HFGMC have been used extensively to investigate the inelastic response of fibrous composites under off-axis tensile loading[51], rate-dependent behavior of epoxy composites[52], effects of imperfect bonding along fibre/matrix interface[53] or the response of unidirectional composite under large deformation [54]. Huang[55–58] developed another model known as bridging micromechanics model which is combined with classical laminate theory to simulate behaviors of multilayered composite laminates. Shokrieh et al.[59] examined the strain-rate effects on mechanical responses of composite laminates under dynamic loadings using Huang's model. Although Huang's model considered the effects of plasticity, it did not include the effects of damage due to micro-cracking, which is essential in modelling failure. Santhosh and Ahmad[60] also attempted to predict the nonlinear behaviour of unidirectional composites made of polymer matrix where plastic deformation and temperature dependency have been accounted for without any stiffness degradation due to damage. On the other hand, Tabiei and Aminjikai[61] have considered both plasticity and damage mechanisms for predicting the response of unidirectional composites under impact loads. They have used Goldberg's viscoplasticity model[62] to capture the rate dependent properties of resin whereas the damage evolutions of the matrix and fibres are based on Weibull distribution functions. Although both damage and plasticity have been included in this model, the effects of these two dissipation mechanisms have been treated separately without considering any coupling between them.

In this study, a new three-dimensional kinematically enhanced constitutive model for unidirectional FRC capable of simulating the nonlinear response at ply level is proposed. The model relies on the enrichment of strain field with respect to different modes of deformation to take into account the important physical interactions of material constituents at fibre scale. In this sense, the enrichment provides an opportunity to introduce both fibre and matrix constitutive responses

and also their interactions. A novel analytical technique is developed for upscaling the nonlinear response from the fibre/micro scale to the ply scale which is the key to achieving such precise modeling of composites with feasible computational resources. Actually, this specific task encounters significant computational challenges in most of the existing models due to the involvement of a local finite element or numerical model. A thermodynamics-based coupled damage-plasticity model is used for the constituents to account for their plastic deformations and progressive damage mechanism. This has also helped to derive a single dissipative potential capturing all energy dissipation mechanisms which is convenient for implementing the model. It is noted that the proposed formulation is applied to modelling at the constitutive level of the composite materials in the current study and its applications can be extended to full scale finite element model at structural level in future investigations. The structure of this paper is organized as follows. Firstly, mathematical derivations for the proposed constitutive model for unidirectional FRC ply is presented. Secondly, a thermodynamically consistent coupled damage-plasticity formulation is developed to model the constituents' behaviours in the proposed kinematically enriched constitutive model. This is followed by numerical examples to demonstrate the application of the proposed model for both elastic and inelastic range in which the model predictions are validated with experimental data as well as results obtained from some benchmark theories.

2. Mathematical Formulation

Figure 1a shows a typical cross-sectional view of a unidirectional fibre reinforced composite ply having a uniform distribution of fibres or fibre bundles within the matrix. A representative portion of the material (Figure 1a) shown separately in Figure 1b (magnified) is considered for the development of the proposed model. Without changing the fibre volume, a further idealisation of the fibre geometry is made (Figure 1c) to facilitate the formulation.

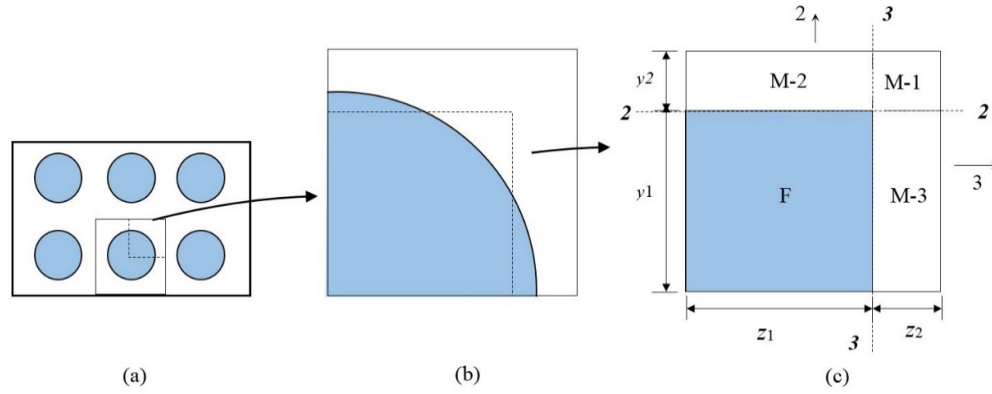


Figure 1: (a) Cross-section of a unidirectional FRC and the UVE; (b) Idealised unit cell; (c) Idealised unit cell element (F: Fibre block; M-1, M-2, M-3: Matrix blocks).

Thus the idealised volume element as shown Figure 1c will finally be used for deriving the present model where the size of this volume element is normalised to unity in all three directions. This unit volume element (Figure 1c) is now divided into four material blocks where one of them represents the fibre (F) and other three blocks for the surrounding matrix (M-1, M-2 and M3). The length of these material blocks along fibres (axis-1 which is perpendicular to both axis-2 and axis-3) is unity where the dimensions of their cross-sections can be calculated with the matrix volume fraction (f) as follows: $y_1 = z_1 = \sqrt{1-f}$ and $y_2 = z_2 = 1 - \sqrt{1-f}$.

The geometric representation of the proposed unit volume element (UVE) may appear similar to that of Aboudi's MOC[46, 63] and few other models (e.g., Robertson and Mall[64]), however their actual model derivations are based on quite distinctive approaches. For example, Aboudi[46, 63] has started with a bilinear variation of the three displacement components within the four individual material blocks which give a non-uniform variation of strain components in any individual material block. However, it should be noted that in Aboudi's model, any increase/decrease in normal stresses of the composite is always accompanied by increase/decrease in shear stresses[64] which is not strictly correct in all cases. On the other hand, Robertson and Mall[64] have started with the strain components having constant values within a material block which is similar to the present approach to have a computationally efficient model. They enforce the traction continuity conditions through normal stresses only at the interface between two adjacent material blocks which is quite different to the current approach and MOC

where the traction continuity across the interfaces of the four materials block is then enforced in a volume average sense of all stress components acting at the interfaces. On the other hand, Robertson and Mall's model upholds a condition of identical transverse shear stresses in all four material blocks and equal to the macroscopic one. Subsequently, the same authors proposed a simple approach to develop their model using viscoplastic theories, but the relationship between stress/strain components of the different material blocks is established using elastic material properties which is not valid in the inelastic loading range

Conversely, Aboudi's method of cells has gradually been enhanced to GMC by Paley and Aboudi[65] and high fidelity generalised method of cells (HFGMC) by Aboudi and Arnold[50] for better accuracy, but these models need a detailed numerical model similar to that of finite element technique for the analysis of the representative volume element . The main difference between the two approaches is that the displacement continuity and traction continuity in GMC or HFGMC are enforced in an average sense at the interfaces whereas FE technique requires displacement continuity to be met at discrete points based on nodal displacements[32]. In addition, the equilibrium condition in FE technique is achieved by using virtual work method while equilibrium condition in Aboudi's approach is satisfied through set of equations which are based on volume average of the subcells. Although GMC is favourable over the standard FE analysis in terms of model efficacy[66], but GMC suffers from the same problem and this is simply its computing cost that has not reached the practical level for its applications in real structures.. The approach in the present study is based on the enrichment strategy proposed in [67–69] for constitutive modelling of localised failure, which is formulated in incremental form and hence can naturally cover both elastic and inelastic ranges of behaviour.

In the present formulation, any variable possessing superscript 1, 2, 3 and 4 corresponds to material blocks $M-1$, $M-2$, $M-3$ and F , respectively. The homogenised or global average strain rate vector $\dot{\boldsymbol{\epsilon}}$ of the UVE (Figure 1c) can be written in terms of strain rate vectors of the four material blocks as:

$$\dot{\boldsymbol{\epsilon}} = \sum_{i=1}^4 f^{(i)} \dot{\boldsymbol{\epsilon}}^{(i)} \quad (1)$$

$$\text{where } \dot{\boldsymbol{\varepsilon}}^{(i)} = \left[\varepsilon_{11}^{(i)}, \varepsilon_{22}^{(i)}, \varepsilon_{33}^{(i)}, \gamma_{12}^{(i)}, \gamma_{23}^{(i)}, \gamma_{13}^{(i)} \right]^T \quad (2)$$

and the volume fractions of the four blocks for a unit volume element $(y_1 + y_2)(z_1 + z_2) = 1$ are:

$$f^{(1)} = y_2 z_2, f^{(2)} = y_2 z_1, f^{(3)} = y_1 z_2, f^{(4)} = y_1 z_1 \quad (3)$$

The constitutive relationship of the material blocks may be expressed in the following generic form:

$$\dot{\boldsymbol{\sigma}}^{(i)} = \mathbf{D}^{(i)} \dot{\boldsymbol{\varepsilon}}^{(i)} \quad (i = 1 \text{ to } 4) \quad (4)$$

where $\mathbf{D}^{(i)}$ is the tangent stiffness of a material block and the incremental stress vector $\dot{\boldsymbol{\sigma}}^{(i)}$ is defined as:

$$\dot{\boldsymbol{\sigma}}^{(i)} = \left[\sigma_{11}^{(i)}, \sigma_{22}^{(i)}, \sigma_{33}^{(i)}, \tau_{12}^{(i)}, \tau_{23}^{(i)}, \tau_{13}^{(i)} \right]^T \quad (5)$$

It should be noted that the behaviour of any material in its inelastic range is nonlinear where the total stresses cannot be obtained from the total strains directly and it needs an incremental approach for solving this problem. In this study, the strains are imposed incrementally on a material and the stresses produced within the material are evaluated iteratively in order to capture the nonlinear behaviour precisely.

At an interfacial plane of two different materials, the in-plane strains (and their rates) are found to be continuous due to displacement compatibility whereas the corresponding stresses are discontinuous due to change of material properties. On the other hand, the out of plane (or transverse) stresses are continuous due to equilibrium of stresses which leads to discontinuous transverse strains. Based on these considerations, an equal axial strain along the fibre direction is taken into account for the four blocks, which leads to unequal axial stresses in these segments. In order to satisfy the equilibrium condition of normal stresses ($\sigma_{22}^{(2)} = \sigma_{22}^{(4)}$; $\sigma_{33}^{(3)} = \sigma_{33}^{(4)}$) in the transverse directions (axis-2 and axis-3 as shown in Figure 1c), the normal strains in the transverse directions should be unequal ($\varepsilon_{22}^{(2)} \neq \varepsilon_{22}^{(4)}$; $\varepsilon_{33}^{(3)} \neq \varepsilon_{33}^{(4)}$) which are imposed by using kinematic enrichments. The shear strains follow the same basis of the normal strains.

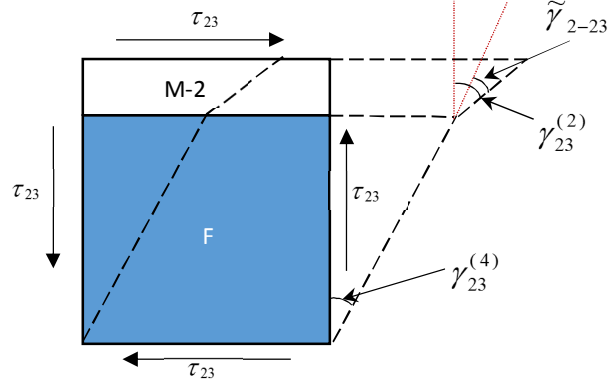


Figure 2: Kinematic strain enhancement of an out-of-plane shear component.

In order to explain the abovementioned interfacial strain discontinuities, the deformation of two material blocks (fibre and matrix block M-2) subjected to an out-of-plane shear stress component (τ_{23}) is taken as a sample case which is illustrated in Figure 2. The deformed shapes of the two blocks due to the applied shear stress are represented by dashed lines. As the matrix is usually having a lower stiffness, it is expected that shear deformation/strain in the matrix block is higher than that of fibre ($\gamma_{23}^{(2)} > \gamma_{23}^{(4)}$). Consequently, the difference between these strains $\tilde{\gamma}_{2-23}$ (Figure 2) is taken as the component of kinematic strain enhancements for this mode of deformation. This will help to derive analytical expressions which can be used to express strain rates of the individual material segments in term of the average strain rates of the entire volume element conveniently.

On this basis, the strain rates of the matrix blocks can be defined in terms of strain rates of the fibre block and the corresponding kinematic strain enhancements as follows:

$$\dot{\boldsymbol{\epsilon}}^{(2)} = \dot{\boldsymbol{\epsilon}}^{(4)} + \mathbf{N}_2 \tilde{\boldsymbol{\epsilon}}_2 \quad (6)$$

$$\dot{\boldsymbol{\epsilon}}^{(3)} = \dot{\boldsymbol{\epsilon}}^{(4)} + \mathbf{N}_3 \tilde{\boldsymbol{\epsilon}}_3 \quad (7)$$

$$\dot{\boldsymbol{\epsilon}}^{(1)} = \dot{\boldsymbol{\epsilon}}^{(4)} + \mathbf{N}_2 \boldsymbol{\mu}_1 \tilde{\boldsymbol{\epsilon}}_2 + \mathbf{N}_3 \boldsymbol{\mu}_2 \tilde{\boldsymbol{\epsilon}}_3 \quad (8)$$

where $\tilde{\boldsymbol{\epsilon}}_2 = [\tilde{\gamma}_{2-12}, \tilde{\boldsymbol{\epsilon}}_{2-22}, \tilde{\gamma}_{2-23}]$ and $\tilde{\boldsymbol{\epsilon}}_3 = [\tilde{\gamma}_{3-13}, \tilde{\gamma}_{3-23}, \tilde{\boldsymbol{\epsilon}}_{3-33}]$ are the rates of kinematic strain enhancements, and \mathbf{N}_2 and \mathbf{N}_3 are dependent on the direction of the interfacial planes 2-2 and 3-3 (Figure 1c) respectively (please see Appendix). In

Equation (8), $\boldsymbol{\mu}_1$ and $\boldsymbol{\mu}_2$ are used to control the proportion of strain enhancements in block M-1, which may be expressed as:

$$\boldsymbol{\mu}_1 = \begin{bmatrix} \alpha & 0 & 0 \\ 0 & \beta & 0 \\ 0 & 0 & 1 \end{bmatrix}; \boldsymbol{\mu}_2 = \begin{bmatrix} \alpha & 0 & 0 \\ 0 & 1 & 0 \\ 0 & 0 & \beta \end{bmatrix} \quad (9)$$

where the default values of parameters α and β are 1.0 but they can be adjusted depending on the material and behaviour. Further explanations and physical implications of α and β can be found in subsequent sections. Using Equations (1)-(6) and (8), the strain rates of the four material blocks can be expressed in term of the homogenised strain rate and enhanced strain rates, as primary variables, as follows:

$$\dot{\boldsymbol{\epsilon}}^{(1)} = \dot{\boldsymbol{\epsilon}} + \mathbf{N}_2 \mathbf{K}_1 \dot{\tilde{\boldsymbol{\epsilon}}}_2 + \mathbf{N}_3 \mathbf{K}_2 \dot{\tilde{\boldsymbol{\epsilon}}}_3 \quad (10)$$

$$\dot{\boldsymbol{\epsilon}}^{(2)} = \dot{\boldsymbol{\epsilon}} + \mathbf{N}_2 \mathbf{K}_1 \dot{\tilde{\boldsymbol{\epsilon}}}_2 - \mathbf{N}_3 \mathbf{K}_3 \dot{\tilde{\boldsymbol{\epsilon}}}_3 \quad (11)$$

$$\dot{\boldsymbol{\epsilon}}^{(3)} = \dot{\boldsymbol{\epsilon}} - \mathbf{N}_2 \mathbf{K}_4 \dot{\tilde{\boldsymbol{\epsilon}}}_2 + \mathbf{N}_3 \mathbf{K}_2 \dot{\tilde{\boldsymbol{\epsilon}}}_3 \quad (12)$$

$$\dot{\boldsymbol{\epsilon}}^{(4)} = \dot{\boldsymbol{\epsilon}} - \mathbf{N}_2 \mathbf{K}_4 \dot{\tilde{\boldsymbol{\epsilon}}}_2 - \mathbf{N}_3 \mathbf{K}_3 \dot{\tilde{\boldsymbol{\epsilon}}}_3 \quad (13)$$

In the above equations, the matrices $\mathbf{K}_1, \mathbf{K}_2, \mathbf{K}_3, \mathbf{K}_4$ contain $\boldsymbol{\mu}_1, \boldsymbol{\mu}_2$ and volume fractions of the different material segments (refer to Appendix for details). Now the vectors corresponding to the kinematic strain enhancements need to be eliminated from the above equations and to achieve this, the Hill-Mandel's condition[41] for virtual works is applied to the unit volume element (Figure 1c) and can be written as:

$$\boldsymbol{\sigma}^T \dot{\boldsymbol{\epsilon}} = \sum_{i=1}^4 f^{(i)} \boldsymbol{\sigma}^{(i)T} \dot{\boldsymbol{\epsilon}}^{(i)} \quad (14)$$

where $\boldsymbol{\sigma}$ is the macro or average stress of the unit volume element.

Substitution of $\dot{\boldsymbol{\epsilon}}^{(i)}$ as given in Equations (10)-(13) in the above Equation (14) and rearranging the obtained expression, we obtain:

$$\begin{aligned} & \left(\boldsymbol{\sigma}^T - f^{(1)} \boldsymbol{\sigma}^{(1)T} - f^{(2)} \boldsymbol{\sigma}^{(2)T} - f^{(3)} \boldsymbol{\sigma}^{(3)T} - f^{(4)} \boldsymbol{\sigma}^{(4)T} \right) \dot{\boldsymbol{\epsilon}} \\ & = \left(f^{(1)} \boldsymbol{\sigma}^{(1)T} \mathbf{N}_2 \mathbf{K}_1 + f^{(2)} \boldsymbol{\sigma}^{(2)T} \mathbf{N}_2 \mathbf{K}_1 - f^{(3)} \boldsymbol{\sigma}^{(3)T} \mathbf{N}_2 \mathbf{K}_4 - f^{(4)} \boldsymbol{\sigma}^{(4)T} \mathbf{N}_2 \mathbf{K}_4 \right) \dot{\tilde{\boldsymbol{\epsilon}}}_2 \\ & + \left(f^{(1)} \boldsymbol{\sigma}^{(1)T} \mathbf{N}_3 \mathbf{K}_2 - f^{(2)} \boldsymbol{\sigma}^{(2)T} \mathbf{N}_3 \mathbf{K}_3 + f^{(3)} \boldsymbol{\sigma}^{(3)T} \mathbf{N}_3 \mathbf{K}_2 - f^{(4)} \boldsymbol{\sigma}^{(4)T} \mathbf{N}_3 \mathbf{K}_3 \right) \dot{\tilde{\boldsymbol{\epsilon}}}_3 \end{aligned} \quad (15)$$

In order to satisfy the above equation for any arbitrary values of the primary variables $\dot{\boldsymbol{\epsilon}}$, $\dot{\boldsymbol{\epsilon}}_2$, and $\dot{\boldsymbol{\epsilon}}_3$, the following conditions are required:

$$\boldsymbol{\sigma} = \sum_{i=1}^4 f^{(i)} \boldsymbol{\sigma}^{(i)} \quad (16)$$

$$f^{(1)} \boldsymbol{\sigma}^{(1)T} \mathbf{N}_2 \mathbf{K}_1 + f^{(2)} \boldsymbol{\sigma}^{(2)T} \mathbf{N}_2 \mathbf{K}_1 - f^{(3)} \boldsymbol{\sigma}^{(3)T} \mathbf{N}_2 \mathbf{K}_4 - f^{(4)} \boldsymbol{\sigma}^{(4)T} \mathbf{N}_2 \mathbf{K}_4 = 0 \quad (17)$$

$$f^{(1)} \boldsymbol{\sigma}^{(1)T} \mathbf{N}_3 \mathbf{K}_2 + f^{(3)} \boldsymbol{\sigma}^{(3)T} \mathbf{N}_3 \mathbf{K}_2 - f^{(2)} \boldsymbol{\sigma}^{(2)T} \mathbf{N}_3 \mathbf{K}_3 - f^{(4)} \boldsymbol{\sigma}^{(4)T} \mathbf{N}_3 \mathbf{K}_3 = 0 \quad (18)$$

The homogenised stresses or macro stresses of the UVE are expressed in terms of local stresses of the individual material blocks and their volume fractions in Equation (16) while the traction continuity across interfaces 2-2 and 3-3 (Figure 1c) is enforced by Equations (17) and (18) respectively. For the implementation of the model in the inelastic range of loading, the above Equations (16) to (18) are expressed in rate forms by replacing the stresses in terms of their rates or increments as follows:

$$\dot{\boldsymbol{\sigma}} = \sum_{i=1}^4 f^{(i)} \dot{\boldsymbol{\sigma}}^{(i)} \quad (19)$$

$$f^{(1)} \dot{\boldsymbol{\sigma}}^{(1)T} \mathbf{N}_2 \mathbf{K}_1 + f^{(2)} \dot{\boldsymbol{\sigma}}^{(2)T} \mathbf{N}_2 \mathbf{K}_1 - f^{(3)} \dot{\boldsymbol{\sigma}}^{(3)T} \mathbf{N}_2 \mathbf{K}_4 - f^{(4)} \dot{\boldsymbol{\sigma}}^{(4)T} \mathbf{N}_2 \mathbf{K}_4 = 0 \quad (20)$$

$$f^{(1)} \dot{\boldsymbol{\sigma}}^{(1)T} \mathbf{N}_3 \mathbf{K}_2 + f^{(3)} \dot{\boldsymbol{\sigma}}^{(3)T} \mathbf{N}_3 \mathbf{K}_2 - f^{(2)} \dot{\boldsymbol{\sigma}}^{(2)T} \mathbf{N}_3 \mathbf{K}_3 - f^{(4)} \dot{\boldsymbol{\sigma}}^{(4)T} \mathbf{N}_3 \mathbf{K}_3 = 0 \quad (21)$$

For a given strain increment, the traction continuity conditions in Equations (20) and (21) will be iteratively utilised to update the strain enhancements, local stresses within individual blocks and eventually the macro stresses of the UVE. A further detail on this process is provided later. Substituting Equations (10) to (13) and (4) into Equations (20) and (21), we can express the strain enhancements in terms of macro strain increments as follows:

$$\begin{bmatrix} \dot{\boldsymbol{\epsilon}}_2 \\ \dot{\boldsymbol{\epsilon}}_3 \end{bmatrix} = \begin{bmatrix} \mathbf{P}_1 \\ \mathbf{P}_2 \end{bmatrix} \dot{\boldsymbol{\epsilon}} \quad (22)$$

where:

$$\begin{bmatrix} \mathbf{P}_1 \\ \mathbf{P}_2 \end{bmatrix} = \begin{bmatrix} \mathbf{A}_{11} & \mathbf{A}_{12} \\ \mathbf{A}_{21} & \mathbf{A}_{22} \end{bmatrix}^{-1} \begin{bmatrix} \mathbf{B}_1 \\ \mathbf{B}_2 \end{bmatrix} \quad (23)$$

In the above equation, the matrices \mathbf{A}_{11} , \mathbf{A}_{12} , \mathbf{A}_{21} , \mathbf{A}_{22} and vectors \mathbf{B}_1 , \mathbf{B}_2 are functions of volume fractions of the material blocks and their material properties (refer to the Appendix for detailed expressions).

Substitution of strain enhancements as given in Equation (22) into Equations (10) to (13), we can express the local strain rates of four material blocks (Figure 1c) exclusively in terms of the macro strain rates of the UVE as follows:

$$\dot{\boldsymbol{\varepsilon}}^{(1)} = (\mathbf{I} + \mathbf{N}_2 \mathbf{K}_1 \mathbf{P}_1 + \mathbf{N}_3 \mathbf{K}_2 \mathbf{P}_2) \dot{\boldsymbol{\varepsilon}} \quad (24)$$

$$\dot{\boldsymbol{\varepsilon}}^{(2)} = (\mathbf{I} + \mathbf{N}_2 \mathbf{K}_1 \mathbf{P}_1 - \mathbf{N}_3 \mathbf{K}_3 \mathbf{P}_2) \dot{\boldsymbol{\varepsilon}} \quad (25)$$

$$\dot{\boldsymbol{\varepsilon}}^{(3)} = (\mathbf{I} - \mathbf{N}_2 \mathbf{K}_4 \mathbf{P}_1 + \mathbf{N}_3 \mathbf{K}_2 \mathbf{P}_2) \dot{\boldsymbol{\varepsilon}} \quad (26)$$

$$\dot{\boldsymbol{\varepsilon}}^{(4)} = (\mathbf{I} - \mathbf{N}_2 \mathbf{K}_4 \mathbf{P}_1 - \mathbf{N}_3 \mathbf{K}_3 \mathbf{P}_2) \dot{\boldsymbol{\varepsilon}} \quad (27)$$

Thus the above equations will help to resolve a macro strain increment imposed on the UVE into local strain increments in four blocks. In fact, this resolves the strain increments at an integration point within a structural element into strain rates of the fibre and surrounding matrix (Figure 1c) when a progressive failure analysis of a structure is carried out incrementally. The matrix blocks on the right-hand side (Equation (24)-(27)) play the role of strain concentration factors and depend on the responses and states of all individual blocks. The local strain increments can be used to update the stresses within individual material blocks using their constitutive relationships (Equation (4)) along with a suitable stress return algorithm [70] due to nonlinear nature of the problem. In the present study, a thermodynamically consistent coupled damage plasticity model is applied for the constitutive modelling of the individual blocks (details will be provided later). Using the stress increments of the individual material blocks, the macro stress increment of the UVE can be obtained using Equation (19). Thus the incremental relation between the macro stresses and macro strains of the composite material can be obtained by substituting Equations (4) and (24) to (27) into Equation (19) and it can be expressed as:

$$\dot{\boldsymbol{\sigma}} = \mathbf{D} \dot{\boldsymbol{\varepsilon}} \quad (28)$$

where the tangent stiffness matrix of the UVE or the composite material is:

$$\mathbf{D} = \sum_{i=1}^4 f^{(i)} \mathbf{D}^{(i)} + f^{(1)} \mathbf{D}^{(1)} \mathbf{N}_2 \mathbf{K}_1 \mathbf{P}_1 + f^{(1)} \mathbf{D}^{(1)} \mathbf{N}_3 \mathbf{K}_2 \mathbf{P}_2 + f^{(2)} \mathbf{D}^{(2)} \mathbf{N}_2 \mathbf{K}_1 \mathbf{P}_1 - f^{(2)} \mathbf{D}^{(2)} \mathbf{N}_3 \mathbf{K}_3 \mathbf{P}_2 - f^{(3)} \mathbf{D}^{(3)} \mathbf{N}_2 \mathbf{K}_4 \mathbf{P}_1 + f^{(3)} \mathbf{D}^{(3)} \mathbf{N}_3 \mathbf{K}_2 \mathbf{P}_2 - f^{(4)} \mathbf{D}^{(4)} \mathbf{N}_2 \mathbf{K}_4 \mathbf{P}_1 - f^{(4)} \mathbf{D}^{(4)} \mathbf{N}_3 \mathbf{K}_3 \mathbf{P}_2 \quad (29)$$

The constitutive relationship of the composite material as presented in Equation (29) is defined explicitly in terms of tangent stiffness matrices of the four constituent material blocks and their volume fractions. The first term in (29) represents the volume averaged stiffness of the four blocks following the rule of mixtures for stiffness components, which is, in fact, the upper bound (Voigt) solution. It is enhanced with the other terms that occur due to the kinematic enrichments of the constitutive structure, resulting in “softer” behaviour that is also closer to the exact solution.

Compared to the HFGMC that needs a detailed numerical model similar to finite element technique to perform analysis on the volume element, the kinematic strain enhancements in the proposed approach can offer a more computationally efficient strategy. In particular, the formulation of HFGMC starts with the definition of three displacement components within the representative volume element, which needs a detailed numerical model (e.g. finite element analysis). The involvement of this numerical analysis at all material or integration point within each iteration of the nonlinear structural analysis will require substantial computational resources, especially in the analysis of large scale structures. On the other hand, the formulation of the proposed approach starts with the definition of strain components of four material blocks where strain components of three matrix blocks are defined in terms strain components of the fibre block and kinematic strain enhancements. This has helped to perform the analysis on the volume element analytically, which is computational much more efficient than the numerical analysis used in HFGMC. Therefore it offers a more computationally efficient strategy in order to achieve a practical level of computing costs for large scale structural applications while adequate level of detail interactions between the constituents are retained within the model. Moreover, in the proposed approach, the homogenization is performed at the constitutive level for all four material blocks, resulting in a macro stress-strain relationship that possesses both responses and volume fractions of the material block and this is valid for both linear and nonlinear behaviour, thanks to the use of rate forms of stress-strain relationships. Thus, the incorporation/implementation of the new approach in a structural scale Finite

Element Analysis will simply involve the integration of the constitutive equation in rate form, like any classical constitutive model, making it straightforward as there is no need to modify the structure of the Finite Element package. In our opinion, compared to HFGMC, these advantages will help to improve the computational efficiency, while not sacrificing much the predictive capability of the model, as demonstrated in the numerical examples. However we also believe that both HFGMC (relatively more accurate, but also more computationally demanding) and the proposed approach (computationally efficient, but relatively less accurate than HFGMC) have their own advantages and disadvantages and their applications depend on the requirements of the problem.

It is also worth mentioning here that level of material nonlinearity such as stiffness degradations due to damage and/or plastic deformations can vary from one material constituent block (Figure 1c) to another block as a result of unequal strain increments. Therefore, tangent stiffness matrices of the constituent matrix blocks are not necessarily identical in the inelastic loading range and they are varied in their own course of deformation or loading. More discussions will be provided in Section 3 dealing with numerical examples on inelastic analyses. Also, it should be noted that Equation (29) cannot be readily used for getting the macro stress increments directly from the macro strain increments as the tangent stiffness matrices $\mathbf{D}^{(i)}$ ($i = 1$ to 4) are progressively changed even within a load increment at the structural level i.e., strain increment at an integration point. This problem is commonly solved iteratively using a stress return algorithm [70] which can be applied to individual material blocks to update their stresses but these updated stresses may not satisfy the traction continuity conditions (Equations (18) and (19)) at the interfaces 2-2 and 3-3 of the UVE (Figure 1c). It needs another level of iterations based on a stress return algorithm applicable to the UVE in order to satisfy these interfacial traction continuity conditions within a tolerable limit. Thus Equations (18) and (19) need to be employed for the derivation of the stress return algorithm applicable to the UVE which is presented in the following section.

2.1 Stress Return Algorithm for the UVE

Due to the nonlinear nature of constituent responses, and the fact that strain increments in numerical analysis are not infinitesimal, the interfacial traction

continuity conditions (Equations (17) and (18)) are not automatically satisfied. Thus the left-hand sides of these equations will produce nonzero values which may be defined as traction residuals and these equations can be rewritten as follows:

$$\mathbf{r}_2 = f^{(1)} \mathbf{K}_1^T \mathbf{N}_2^T \boldsymbol{\sigma}^{(1)} + f^{(2)} \mathbf{K}_1^T \mathbf{N}_2^T \boldsymbol{\sigma}^{(2)} - f^{(3)} \mathbf{K}_4^T \mathbf{N}_2^T \boldsymbol{\sigma}^{(3)} - f^{(4)} \mathbf{K}_4^T \mathbf{N}_2^T \boldsymbol{\sigma}^{(4)} \quad (30)$$

$$\mathbf{r}_3 = f^{(1)} \mathbf{K}_2^T \mathbf{N}_3^T \boldsymbol{\sigma}^{(1)} - f^{(2)} \mathbf{K}_3^T \mathbf{N}_3^T \boldsymbol{\sigma}^{(2)} + f^{(3)} \mathbf{K}_2^T \mathbf{N}_3^T \boldsymbol{\sigma}^{(3)} - f^{(4)} \mathbf{K}_3^T \mathbf{N}_3^T \boldsymbol{\sigma}^{(4)} \quad (31)$$

where \mathbf{r}_2 and \mathbf{r}_3 are the traction residual vectors corresponding to 2-2 and 3-3 interfaces, as shown Figure 1(c).

A Newton-Raphson based iterative scheme is adopted to reduce the value of these residuals to a tolerable limit. For this purpose, a Taylor series expansion of the above equations is performed which may be expressed (neglecting higher order derivatives) as follows:

$$\mathbf{r}_j^{new} = \mathbf{r}_j^{old} + \sum_{i=1}^4 \frac{\partial \mathbf{r}_j}{\partial \boldsymbol{\sigma}^{(i)}} \delta \boldsymbol{\sigma}^{(i)} \quad (32)$$

where $j = 2, 3$. In order to satisfy the interfacial traction continuity, the new value of these residuals should be zero ($\mathbf{r}_i^{new} = 0$) which can be utilised to rewrite the above equation as follows:

$$f^{(1)} \mathbf{K}_1^T \mathbf{N}_2^T \delta \boldsymbol{\sigma}^{(1)} + f^{(2)} \mathbf{K}_1^T \mathbf{N}_2^T \delta \boldsymbol{\sigma}^{(2)} - f^{(3)} \mathbf{K}_4^T \mathbf{N}_2^T \delta \boldsymbol{\sigma}^{(3)} - f^{(4)} \mathbf{K}_4^T \mathbf{N}_2^T \delta \boldsymbol{\sigma}^{(4)} = -\mathbf{r}_2^{old} \quad (33)$$

$$f^{(1)} \mathbf{K}_2^T \mathbf{N}_3^T \delta \boldsymbol{\sigma}^{(1)} - f^{(2)} \mathbf{K}_3^T \mathbf{N}_3^T \delta \boldsymbol{\sigma}^{(2)} + f^{(3)} \mathbf{K}_2^T \mathbf{N}_3^T \delta \boldsymbol{\sigma}^{(3)} - f^{(4)} \mathbf{K}_3^T \mathbf{N}_3^T \delta \boldsymbol{\sigma}^{(4)} = -\mathbf{r}_3^{old} \quad (34)$$

The above stress variations $\delta \boldsymbol{\sigma}^{(i)}$ ($i=1$ to 4) in the material blocks can be expressed in terms of corresponding strain variations $\delta \boldsymbol{\varepsilon}^{(i)}$ using the generic constitutive relationship (Equation (4)) as follows:

$$\delta \boldsymbol{\sigma}^{(i)} = \mathbf{D}^{(i)} \delta \boldsymbol{\varepsilon}^{(i)} \quad (35)$$

Now the strain variations $\delta \boldsymbol{\varepsilon}^{(i)}$ in the above equations can be expressed in terms of iterative strain enhancements $\delta \tilde{\boldsymbol{\varepsilon}}_2$ and $\delta \tilde{\boldsymbol{\varepsilon}}_3$ with the help of Equations (10) to (13) as follows:

$$\delta \boldsymbol{\varepsilon}^{(1)} = \mathbf{N}_2 \mathbf{K}_1 \delta \tilde{\boldsymbol{\varepsilon}}_2 + \mathbf{N}_3 \mathbf{K}_2 \delta \tilde{\boldsymbol{\varepsilon}}_3 \quad (36)$$

$$\delta \boldsymbol{\varepsilon}^{(2)} = \mathbf{N}_2 \mathbf{K}_1 \delta \tilde{\boldsymbol{\varepsilon}}_2 - \mathbf{N}_3 \mathbf{K}_3 \delta \tilde{\boldsymbol{\varepsilon}}_3 \quad (37)$$

$$\delta \boldsymbol{\varepsilon}^{(3)} = -\mathbf{N}_2 \mathbf{K}_4 \delta \tilde{\boldsymbol{\varepsilon}}_2 + \mathbf{N}_3 \mathbf{K}_2 \delta \tilde{\boldsymbol{\varepsilon}}_3 \quad (38)$$

$$\delta \boldsymbol{\varepsilon}^{(4)} = -\mathbf{N}_2 \mathbf{K}_4 \delta \tilde{\boldsymbol{\varepsilon}}_2 - \mathbf{N}_3 \mathbf{K}_3 \delta \tilde{\boldsymbol{\varepsilon}}_3 \quad (39)$$

It should be noted that this iterative process for obtaining $\delta \boldsymbol{\varepsilon}^{(i)}$ ($i = 1$ to 4) starts from the previously converged step (referred to as the “zero” iteration) where $\dot{\boldsymbol{\varepsilon}}^{(i)}$ ($i = 1$ to 4) are obtained with the use of Equations (10) to (13). Therefore, subsequent iterations are required to achieve traction continuity which follow the same operations in the “zero” iteration but without the appearance of $\dot{\boldsymbol{\varepsilon}}$ (Equation (36) - (39)) as it has been expended in the initial (or “zero”) step.

Substituting Equations (35) to (39) into Equations (33) and (34), the iterative strain enhancements can be expressed in terms of traction residuals as follows:

$$\begin{Bmatrix} \delta \tilde{\boldsymbol{\varepsilon}}_2 \\ \delta \tilde{\boldsymbol{\varepsilon}}_3 \end{Bmatrix} = \begin{bmatrix} \mathbf{A}_{11} & \mathbf{A}_{12} \\ \mathbf{A}_{21} & \mathbf{A}_{22} \end{bmatrix}^{-1} \begin{Bmatrix} -\mathbf{r}_2^{old} \\ -\mathbf{r}_3^{old} \end{Bmatrix} \quad (40)$$

where \mathbf{A}_{11} , \mathbf{A}_{12} , \mathbf{A}_{21} and \mathbf{A}_{22} are same as those given in Equation (22).

The iterative stresses of the block are then updated using any classical stress return algorithm followed by the computation of iterative macro stress using Equation (19). By using these updated stresses in the blocks and Equation (33) - (34), the traction residuals are checked against a given limit/tolerance. If traction residuals are not less than this tolerance, the iterative process is repeated until the required tolerance is achieved.

The flowchart in Figure 3 depicts the overall procedure for calculating macro stress increment from a given macro strain increment. In order to have a simple representation of the flowchart, the iterative process is not shown in Figure 3. However, this is explained in the following steps.

1. Resolve the macro strain increments imposed to the material/UVE into local strain increments of the four material blocks using Equations (24) to (27).
2. Use a stress return algorithm to update the stresses within these material blocks due to the strain increments found from step 1.
3. Use the stresses found in step 2 to calculate the traction residuals (Equations (30) to (31)).
 - a. If $\|\mathbf{r}_i\| / \|\mathbf{r}'_i\| < tol^*$ ($i=2,3$), go to step 4. \mathbf{r}'_i are defined as follows:

$$\mathbf{r}'_2 = f^{(3)} \mathbf{K}_4^T \mathbf{N}_2^T \delta \boldsymbol{\sigma}^{(3)} + f^{(4)} \mathbf{K}_4^T \mathbf{N}_2^T \delta \boldsymbol{\sigma}^{(4)}$$

$$\mathbf{r}'_3 = f^{(2)} \mathbf{K}_3^T \mathbf{N}_3^T \delta \boldsymbol{\sigma}^{(2)} + f^{(4)} \mathbf{K}_3^T \mathbf{N}_3^T \delta \boldsymbol{\sigma}^{(4)}$$

- b. If $\|\mathbf{r}_i\| / \|\mathbf{r}'_i\| > tol^*$ ($i=2,3$), perform the following operations:
- Calculate variation of strain enhancements $\delta \bar{\boldsymbol{\epsilon}}_2$ and $\delta \bar{\boldsymbol{\epsilon}}_3$ using Equation (40).
 - Use stress return algorithm to update the stresses within these material blocks due to $\delta \bar{\boldsymbol{\epsilon}}_2$ and $\delta \bar{\boldsymbol{\epsilon}}_3$
 - Go to the beginning of step 3.
4. Update the macro/homogenised stresses of the material. Repeat step 1 to 4 for all the macro strain increments required for an analysis.

* The tolerance used in this study is: $tol = 10^{-4}$.

It should be noted that step 2 and step 3 in the above procedure can be referred to as stress updating scheme at outer level i.e. at the level of the composite block (Figure 3) where an iterative process is implemented to obtain a converged solutions. This process typically requires 10-20 iterations for an imposed macro strain increment with a relatively small size in the order of 10^{-7} . The interfacial traction continuity (Equations (30) - (31)) is satisfied in each iteration and this process also helps to update the enhancement strain rates and adjust the strain increments of the individual material blocks. Subsequently, the stress increments in these material blocks are updated in step 4 which is referred to as the stress return algorithm at the inner level (Figure 3). In addition, the stress return algorithm for the individual blocks is used to ensure the updated stresses of the material blocks are on their updated yield surface in case of inelastic loading. As can be seen, the whole procedure above is written in the incremental form, facilitating the use of any constitutive model for the individual matrix/fibre blocks. This requires a suitable mathematical derivation for a coupled damage-plasticity model to analyse inelastic responses of each individual material block, which are described in details in the following sections.

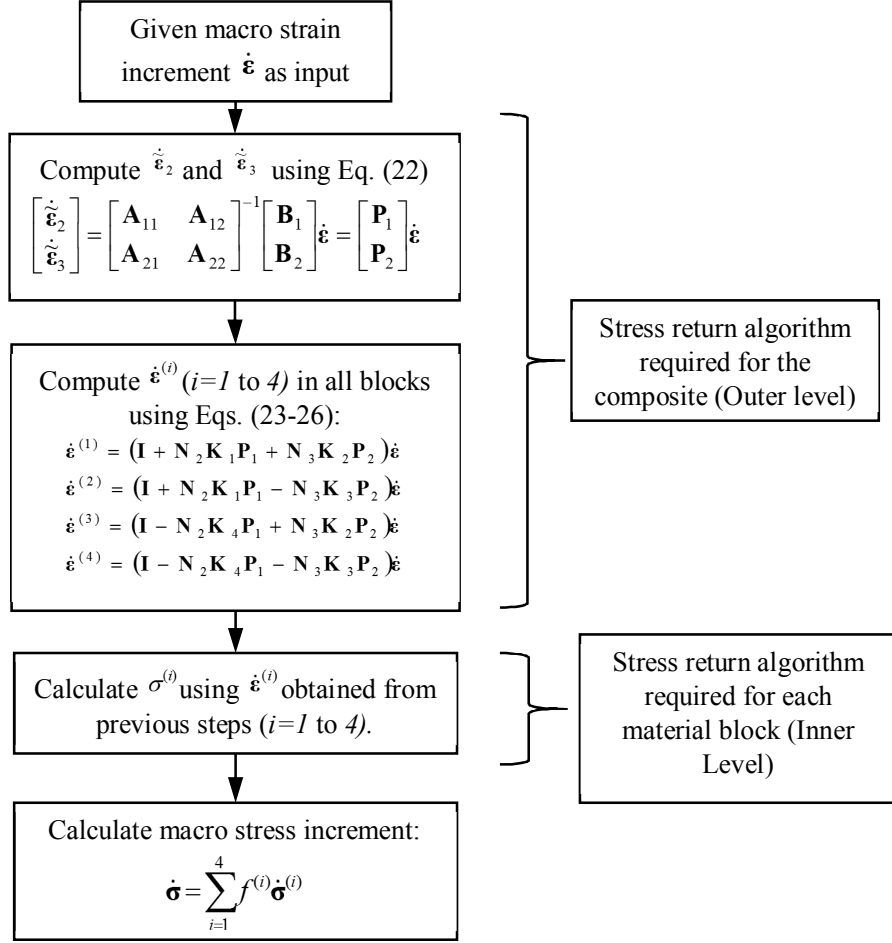


Figure 3: Flowchart for stress return algorithm.

2.2 Modelling Inelastic Response

As discussed in preceding sections, nonlinear responses of unidirectional FRC are caused primarily by the inelastic behaviours of the matrix which are consequences of two major irreversible energy dissipation processes, such as plasticity and damage. As the plastic behaviour of some matrix material including metal matrix such as aluminium are pressure dependent [71], a simple plasticity model such as von Mises plasticity model cannot be used. In this situation, the Drucker Prager plasticity model is a suitable option and its nonlinear (parabolic) form is a good alternative which is adopted in the proposed constitutive model. Since the deformation of matrix and/or fibre material is nonlinear with many coupled processes such as plastic deformation and cracking, the combined use of damage mechanics and plasticity theory for such models is essential. In this sense, a proper

coupling of plastic deformations with damage mechanisms and its numerical implementation in a convenient form is usually a challenging task. This is achieved in the present study by developing an elegant model following the basic concept described in Einav et al [72] and further illustrated in Nguyen et al [73]. The benefit of this approach is that it needs the definition of only two potentials (energy and dissipation potentials) and the model gives a single loading surface which is really convenient for its numerical implementation. The enhancement made in the present formulation will better control the plastic flow directions, including both dilation and compaction that earlier coupled damage-plasticity models under the same thermodynamic framework [72, 73] do not have yet. The general thermodynamic framework of Houlsby and Puzrin [74] is used for the proposed formulation. On the other hand, the inelastic behaviour of fibres is usually not significant and it has negligible contribution to the overall inelastic responses of composite materials. Thus a linear elastic model is often used to simulate fibre response which is also adopted in the present formulation.

As the change of temperature is not considered in the present problem (i.e., the isothermal condition is satisfied), the Helmholtz free energy potential is written in terms of two strain parameters (volumetric and equivalent shear strains) and three internal variables (damage, plastic volumetric and equivalent shear strains) as:

$$\Psi = (1-D) \left[\frac{1}{2} K (\varepsilon_V - \alpha_V)^2 + \frac{3}{2} G (\varepsilon_S - \alpha_S)^2 \right] \quad (41)$$

where D is the damage variable, α_V is the plastic volumetric strain, α_S is the equivalent plastic shear strain, K is the bulk modulus and G is the shear modulus. The total volumetric strain ε_V and the total equivalent shear strain ε_S are defined in terms of strain tensor ε_{ij} and deviatoric strain tensor e_{ij} as:

$$\varepsilon_V = \varepsilon_{ii} ; \varepsilon_S = \sqrt{\frac{2}{3} e_{ij} e_{ij}} ; e_{ij} = \varepsilon_{ij} - \delta_{ij} \varepsilon_V / 3 \quad (42)$$

The Helmholtz free energy can be used to get the pressure p and deviator stress q as follows:

$$p = \frac{\partial \Psi}{\partial \varepsilon_V} = (1-D)K(\varepsilon_V - \alpha_V) \quad (43)$$

$$q = \frac{\partial \Psi}{\partial \varepsilon_S} = (1-D)3G(\varepsilon_S - \alpha_S) \quad (44)$$

Also, the generalised stresses $\bar{\chi}_V$, $\bar{\chi}_S$ and $\bar{\chi}_D$ corresponding to α_V , α_S and D can be obtained from the Helmholtz free energy as follows:

$$\bar{\chi}_V = -\frac{\partial \Psi}{\partial \alpha_V} = (1-D)K(\varepsilon_V - \alpha_V) = p \quad (45)$$

$$\bar{\chi}_S = -\frac{\partial \Psi}{\partial \alpha_S} = (1-D)3G(\varepsilon_S - \alpha_S) = q \quad (46)$$

$$\bar{\chi}_D = \frac{\partial \Psi}{\partial D} = \frac{1}{2}K(\varepsilon_V - \alpha_V)^2 + \frac{3}{2}G(\varepsilon_S - \alpha_S)^2 = \frac{p^2}{2K(1-D)^2} + \frac{q^2}{6G(1-D)^2} \quad (47)$$

The second law of thermodynamics is related to the rate of energy dissipation Φ and the law states that Φ cannot be negative (i.e. $\Phi \geq 0$). For rate-independent behaviour considered in this study, the dissipation Φ is a first order homogeneous function in terms of rates of internal variables. For a tight coupling between different dissipative processes, it can be expressed in the following form:

$$\Phi = \sqrt{\phi_V^2 + \phi_S^2 + \phi_D^2} + f_V \phi_V + f_S \phi_S \quad (48)$$

where ϕ_V , ϕ_S and ϕ_D are components of the dissipation corresponding to plastic volumetric strain, plastic equivalent shear strain and damage but they are different from Φ_V , Φ_S and Φ_D . The dimensionless parameters f_V and f_S used in the above equation are functions of stresses which are expressed along with the dissipation components (ϕ_V , ϕ_S and ϕ_D) in alignment with the parabolic Drucker-Prager yield criterion ($y = q^2 + \beta p - k$) as follows:

$$f_V = \frac{p - a\sqrt{q^2 + \beta p}}{\sqrt{k}} \quad (49)$$

$$f_s = \frac{q - b\sqrt{q^2 + \beta p}}{\sqrt{k}} \quad (50)$$

$$\phi_v = \sqrt{k}\alpha_v \quad (51)$$

$$\phi_s = \sqrt{k}\alpha_s \quad (52)$$

$$\phi_D = \frac{\sqrt{k}\bar{\chi}_D}{r_d\sqrt{q^2 + \beta p}}\dot{D} \quad (53)$$

where β and k are functions of internal variables (please see Section 2.2.1 for more details), a and b are model parameters which are used for adjusting the proportion of dissipations corresponding to plastic volumetric strain and plastic equivalent shear strain respectively which will lead to control the direction of plastic flow as needed. These two parameters may be combined into a single parameter for the entire plastic deformations as:

$$a^2 + b^2 = r_p^2 \quad (54)$$

Similarly, the user-defined parameter r_d in Equation (53) is to adjust the proportion of dissipation corresponding to damage and having a relationship with r_p as:

$$r_p^2 + r_d^2 = 1 \quad (55)$$

The dissipative generalised stresses using the dissipation function (48) are then:

$$\chi_v = \frac{\partial\Phi}{\partial\dot{\alpha}_v} = \frac{\partial\Phi}{\partial\phi_v} \frac{\partial\phi_v}{\partial\dot{\alpha}_v} = \left(\frac{\phi_v}{\sqrt{\phi_v^2 + \phi_s^2 + \phi_D^2}} + f_v \right) \frac{\partial\phi_v}{\partial\dot{\alpha}_v} \quad (56)$$

$$\chi_s = \frac{\partial\Phi}{\partial\dot{\alpha}_s} = \frac{\partial\Phi}{\partial\phi_s} \frac{\partial\phi_s}{\partial\dot{\alpha}_s} = \left(\frac{\phi_s}{\sqrt{\phi_v^2 + \phi_s^2 + \phi_D^2}} + f_s \right) \frac{\partial\phi_s}{\partial\dot{\alpha}_s} \quad (57)$$

$$\chi_D = \frac{\partial\Phi}{\partial\dot{D}} = \frac{\partial\Phi}{\partial\phi_D} \frac{\partial\phi_D}{\partial\dot{D}} = \left(\frac{\phi_D}{\sqrt{\phi_v^2 + \phi_s^2 + \phi_D^2}} \right) \frac{\partial\phi_D}{\partial\dot{D}} \quad (58)$$

The above equations along with the Equations (51) – (53) show that the generalised dissipative stresses are functions of the rate of all internal variables which ensures a strong coupling between the different dissipation mechanisms. Since the

dissipation components (51) – (53) are homogeneous first order functions of the corresponding rate of the internal variable, Equations (56) – (58) can be used to get the loading function in terms of dissipative generalised stresses as:

$$y^* = \left(\frac{\chi_V}{\partial\phi_V/\partial\dot{\alpha}_V} - f_V \right)^2 + \left(\frac{\chi_S}{\partial\phi_S/\partial\dot{\alpha}_S} - f_S \right)^2 + \left(\frac{\chi_D}{\partial\phi_D/\partial\dot{D}} \right)^2 - 1 \leq 0 \quad (59)$$

This is in fact obtained through the Legendre transformation of the dissipation potential (50). The evolution of plastic deformations (plastic flow rules) and damage can be obtained from this loading function by taking its derivatives with respect to the corresponding generalised dissipative stress. These may be expressed with the help of Ziegler's orthogonality condition (i.e., $\chi_V = \bar{\chi}_V$ and $\chi_S = \bar{\chi}_S$) and Equations (45) – (46) as follows:

$$\dot{\alpha}_V = \dot{\lambda} \frac{\partial y^*}{\partial \chi_V} = 2\dot{\lambda} \left(\frac{a\sqrt{q^2 + \beta p}}{k} \right) \quad (60)$$

$$\dot{\alpha}_S = \dot{\lambda} \frac{\partial y^*}{\partial \chi_S} = 2\dot{\lambda} \left(\frac{b\sqrt{q^2 + \beta p}}{k} \right) \quad (61)$$

$$\dot{D} = \dot{\lambda} \frac{\partial y^*}{\partial \chi_D} = 2\dot{\lambda} \frac{r_d^2 (q^2 + \beta p)}{k\chi_D} \quad (62)$$

where $\dot{\lambda}$ is the non-negative common multiplier. It can be noted that the above procedure will give a non-associated plastic flow rule. Finally, using Equation (59) and with the help of Equations (49) – (54) and (45) – (46) along with the Ziegler's orthogonality condition, the parabolic Drucker-Prager yield criterion in true stress space can be described conveniently in terms of pressure p and deviator stress q as:

$$y = q^2 + \beta p - k = 0 \quad (63)$$

The direction of plastic flow can be controlled by adjusting the ratio between plastic volumetric strain and plastic equivalent shear strain which can be obtained with the help of Equations (60) and (61) as:

$$\frac{\dot{\alpha}_V}{\dot{\alpha}_S} = \frac{\partial y^* / \partial \chi_V}{\partial y^* / \partial \chi_S} = \frac{a}{b} \quad (64)$$

In the present study, the yield function (Equation (63)) is utilised to obtain the above ratio for the convenience of numerical implementation as:

$$\frac{a}{b} = c \frac{\partial y / \partial p}{\partial y / \partial q} = c \frac{\beta}{2q} \quad (65)$$

where c is a user defined parameter which will help to get the values of a and b using Equations (54) - (55). When $c = 1$, the direction of plastic flow vector generated by the model is same as that obtained directly from the associated plastic flow rule. In contrasts, non-associated flow rules can be produced by taking $c \neq 1$.

2.2.1 Thermodynamic admissibility of the model

The general condition for thermodynamic admissibility of the proposed technique requires non-negativeness of the dissipation rate function (48). The conditions needed to satisfy $\Phi \geq 0$ can be derived from the general definitions of functions and parameters defined in Section 2.2. Thus, by substituting Equations (49)-(53), (60)-(62) into Equation (48) and makes use of the yield condition (Equation (63)), the dissipation rate function Φ is expressed as:

$$\Phi = 2\dot{\lambda} \left(\sqrt{a^2 + b^2 + r_d^2} + \left(\frac{pa}{\sqrt{k}} + \frac{qb}{\sqrt{k}} \right) - (a^2 + b^2) \right) \geq 0 \quad (66)$$

Recall that $\dot{\lambda} \geq 0$, $a^2 + b^2 = r_p^2$ and $r_p^2 + r_d^2 = 1$, the above expression can be rewritten as:

$$pa + qb + r_d^2 \sqrt{k} \geq 0 \quad (67)$$

It should be noted that in the above expression, qb and $r_d \sqrt{k}$ are always non-negative while the term pa can be negative, e.g. when the material response is governed by dilative behaviour ($a < 0$) under compression ($p > 0$). Thus, Equation (67) can be rewritten as:

$$|pa| \leq qb + r_d^2 \sqrt{k} \quad (67)$$

Furthermore, the ratio between a and b given in Equation (65) can be used to further reduce Equation (67) to:

$$-\frac{2q(qb + r_d^2 \sqrt{k})}{pb\beta} \leq c \leq \frac{2q(qb + r_d^2 \sqrt{k})}{pb\beta} \quad (68)$$

Thus, the above condition implies restrictive bounds for the parameter c which must be met in the selection of c to ensure thermodynamic admissibility of the proposed formulation. Since the proposed damage-plasticity model involves parameter c that controls the dilation behaviour, the restriction (68) on the value of this parameter is needed and this condition is met for the examples in the manuscript.

2.2.2 Tangent Stiffness:

The coupled damage-plasticity formulation presented above is now implemented for its applications. The above formulations produce a nonlinear (parabolic) Drucker-Prager yield surface applicable for a pressure-dependent material as:

$$y = q^2 + \beta p - k = 0 \quad (69)$$

The different terms used in the above equation can be defined as follows:

$$p = \frac{I_1}{3} = \frac{\sigma_{ii}}{3}; \quad q = \sqrt{3J_2} = \sqrt{\frac{3}{2}s_{ij}s_{ij}}; \quad s_{ij} = \sigma_{ij} - \delta_{ij}p; \quad \beta = 3(f_{cy} - f_{ty}); \quad (70)$$

$$k = f_{cy} f_{ty}$$

Where σ_{ij} is the stress tensor, s_{ij} is the deviatoric stress tensor, δ_{ij} is Kronecker delta, I_1 and J_2 are stress invariants, f_{cy} is the uniaxial yield strength in compression and f_{ty} is the uniaxial yield strength in tension. The value of f_{cy} and f_{ty} will be changed progressively with the growth of plastic deformation and damage which are represented using the following functions for their evolutions.

$$f_{cy} = (1-D)(f_{c0} + Q_c (1 - e^{-b_c \varepsilon_p})), \quad f_{ty} = (1-D)(f_{t0} + Q_t (1 - e^{-b_t \varepsilon_p})) \quad (71)$$

where D is the damage variable, ε_p is the accumulated plastic strain with its rate is defined as $\dot{\varepsilon}_p = \sqrt{2/3} \dot{\alpha}_{ij} \dot{\alpha}_{ij}$ ($\dot{\alpha}_{ij}$ is the rate of plastic strain in tensorial form), f_{t0} and f_{c0} are initial yield strengths, and Q_t , Q_c , b_t and b_c are material constants with subscript t and c indicating tension and compression, respectively. The damage variable D admits an initial value of zero and is activated at a certain threshold depending on the plastic deformation. It starts increasing during the failure progression and can have a maximum value of 1 corresponding to a complete failure. The damage growth progressively reduces the values of k and β leading to

contraction of the yield surface (Equation (63)). On the other hand, in pre-peak regime, a strain hardening effect due to plastic deformations is adopted which leads to expansion of the yield surface with the growth of effective plastic strain ε_p .

The plastic flow rule as presented in Equations (60)-(61) provides the plastic strain increment in terms of volumetric and shear components but it is expressed in tensorial form for the convenience of model implementation as:

$$\begin{aligned}\dot{\alpha}_{ij} &= \dot{\lambda} \frac{\partial y^*}{\partial \chi_{ij}} = \dot{\lambda} \left(\frac{\partial y^*}{\partial \chi_v} \frac{\partial \chi_v}{\partial \sigma_{ij}} + \frac{\partial y^*}{\partial \chi_s} \frac{\partial \chi_s}{\partial \sigma_{ij}} \right) \\ &= \dot{\lambda} \left(2 \frac{a \sqrt{q^2 + \beta p}}{k} \frac{\delta_{ij}}{3} + 2 \frac{b \sqrt{q^2 + \beta p}}{k} \frac{3}{2\sqrt{3}J_2} \frac{\partial J_2}{\partial \sigma_{ij}} \right)\end{aligned}\quad (72)$$

On the other hand, damage evolution is given in the following form:

$$\dot{D} = \dot{\lambda} \frac{\partial y^*}{\partial D} = 2 \dot{\lambda} \frac{r_d^2 (q^2 + \beta p)}{k \chi_D} \quad (73)$$

Similarly, the stresses are expressed in tensorial form with the help of Equation (41) as:

$$\sigma_{ij} = \frac{\partial \Psi}{\partial \varepsilon_{ij}} = \frac{\partial \Psi}{\partial \varepsilon_v} \frac{\partial \varepsilon_v}{\partial \varepsilon_{ij}} + \frac{\partial \Psi}{\partial \varepsilon_s} \frac{\partial \varepsilon_s}{\partial \varepsilon_{ij}} = (1-D) (K \varepsilon_r^e \delta_{ij} + 2G e_{ij}^e) = (1-D) C_{ijkl} (\varepsilon_{kl} - \alpha_{kl}) \quad (74)$$

Thus, the incremental stress tensor can be written as:

$$\dot{\sigma}_{ij} = (1-D) C_{ijkl} (\dot{\varepsilon}_{kl} - \dot{\alpha}_{kl}) - \frac{\sigma_{ij}}{(1-D)} \dot{D} \quad (75)$$

The consistency condition for the yield function, $y = y(\sigma_{ij}, \varepsilon_p, D)$, in true stress space, can be written as:

$$\dot{y} = \frac{\partial y}{\partial \sigma_{ij}} \dot{\sigma}_{ij} + \frac{\partial y}{\partial \varepsilon_p} \dot{\varepsilon}_p + \frac{\partial y}{\partial D} \dot{D} = 0 \quad (76)$$

where $\dot{\varepsilon}_p$ is the accumulative plastic strain increment and it is given as:

$$\dot{\varepsilon}_p = \sqrt{\frac{2}{3} \dot{\alpha}_{ij} \dot{\alpha}_{ij}} = \dot{\lambda} \sqrt{\frac{2}{3} \frac{\partial y^*}{\partial \sigma_{ij}} \frac{\partial y^*}{\partial \sigma_{ij}}} \quad (77)$$

Using Equations (72), (73), (75) to (77), the non-negative multiplier $\dot{\lambda}$ can be obtained as:

$$\dot{\lambda} = M_{kl} \dot{\varepsilon}_{kl} \quad (78)$$

where

$$M_{kl} = \frac{(1-D) \frac{\partial y}{\partial \sigma_{ij}} C_{ijkl}}{(1-D) \frac{\partial y}{\partial \sigma_{ij}} C_{ijkl} \frac{\partial y^*}{\partial \sigma_{ij}} + \frac{\partial y}{\partial \sigma_{ij}} \frac{\sigma_{ij}}{1-D} \frac{\partial y^*}{\partial \chi_D} - \frac{\partial y}{\partial \varepsilon_p} \sqrt{\frac{2}{3} \frac{\partial y^*}{\partial \sigma_{ij}} \frac{\partial y^*}{\partial \sigma_{ij}} - \frac{\partial y}{\partial D} \frac{\partial y^*}{\partial \chi_D}}} \quad (79)$$

Finally, the incremental stress-strain relationship can be written as:

$$\dot{\sigma}_{ij} = \left[(1-D) C_{ijkl} - (1-D) C_{ijkl} M_{st} \frac{\partial y^*}{\partial \chi_{kl}} - \frac{\sigma_{ij}}{1-D} M_{st} \frac{\partial y^*}{\partial \chi_D} \right] \dot{\varepsilon}_{kl} = C_{ijkl}^t \dot{\varepsilon}_{kl} \quad (80)$$

In summary, the followings parameters are required by the proposed model: i) for composite model: f_v , α and β ii) for each material constituent (fibre and matrix): E , ν , f_{i0} , f_{c0} , Q_b , Q_c , b_t , b_c , r_d , c , ε_{pc} where ε_{pc} is the critical value of accumulated plastic strain used to activate the damage process (please see Section 2.2.2 and Section 3 for more discussions).

2.2.3 Stress Return Algorithm

If a strain increment is imposed at a point within a structure, the stress state of that point needs to be updated. If the size of strain increments is infinitesimal, these updated stresses can be computed explicitly using the tangent stiffness (Section 2.2.1) following a numerical technique such as forward-Euler scheme. However, the strain increment cannot be restricted to infinitesimal size in actual structural applications and the updated stresses based on above procedure may lie outside the yield surface significantly which can lead to erroneous solutions. Therefore, these stresses need to be corrected so as to return to the new yield surface and this can be achieved by a technique such as backward-Euler scheme. This stress return procedure will not be required unless the updated trial stress based on elastic response lie outside the yield surface (i.e. material is yielding). In the case of

yielding, the new yield surface can be obtained using its Taylor expansion considering it first order terms as:

$$y^{n+1} = y^{trial} + \frac{\partial y}{\partial \sigma_{ij}} \Delta \sigma_{ij}^{re} \Big|^{trial} + \frac{\partial y}{\partial \varepsilon_p} \Delta \varepsilon_p \Big|^{trial} + \frac{\partial y}{\partial D} \Delta D \Big|^{trial} = 0 \quad (81)$$

where $\Delta \sigma_{ij}^{re}$ is the stress return increment which is normal to the trial yield surface. Using Equation (75) and substituting $\Delta \varepsilon_{kl} = 0$, as it has already been used for moving from the current stress point (σ_{ij}^n) to the trial stress point ($\sigma_{ij}^{trial} = \sigma_{ij}^n + \Delta \sigma_{ij}^e$), $\Delta \sigma_{ij}^{re}$ it can be expressed as:

$$\Delta \sigma_{ij}^{re} = \sigma_{ij}^{n+1} - \sigma_{ij}^{trial} = \left[-(1-D) C_{ijkl} \Delta \alpha_{kl} - \frac{\sigma_{ij}}{(1-D)} \Delta D \right] \Big|^{trial} \quad (82)$$

It should be noted that this stress return algorithm is different from the full backward-Euler scheme where $\Delta \sigma_{ij}^{re}$ are recalculated so as make it normal to the new yield surface (y^{n+1}) by applying an iterative scheme (see Crisfield [70] for more detail). By substituting Equations (72), (73), (77) and (82) into (81) and it can be rearranged to get the multiplier $\Delta \lambda$ as follows:

$$\Delta \lambda = \frac{y^{trial}}{\frac{\partial y}{\partial \sigma_{ij}} \left[(1-D) C_{ijkl} \frac{\partial y^*}{\partial \sigma_{kl}} + \frac{\sigma_{ij}}{(1-D)} \frac{\partial y^*}{\partial \chi_D} \right] \Big|^{trial} - \frac{\partial y}{\partial \varepsilon_p} \dot{\lambda} \sqrt{\frac{2 \partial y^*}{3 \partial \chi_{ij}} \frac{\partial y^*}{\partial \chi_{ij}}} \Big|^{trial} - \frac{\partial y}{\partial D} \dot{\lambda} \frac{\partial y^*}{\partial \chi_D} \Big|^{trial}} \quad (83)$$

With these, the final updated stresses can be obtained as:

$$\sigma_{ij}^{n+1} = \sigma_{ij}^{trial} + \Delta \sigma_{ij}^{re} = \sigma_{ij}^{trial} - (1-D) C_{ijkl} \Delta \lambda \frac{\partial y^*}{\partial \sigma_{kl}} - \frac{\sigma_{ij}}{(1-D)} \Delta \lambda \frac{\partial y^*}{\partial \chi_D} \quad (84)$$

Now the coupled damage-plasticity model is ready for its application to the matrix blocks to simulate their inelastic responses. It should be noted that the outer stress return algorithm for the composite UVE (see Section 2.1) is first carried out which gives strain increments in each material blocks. Subsequently, the stresses in the matrix blocks due to these strain increments are updated by employing the stress return scheme described in this section. The coupled damage-plasticity model along with the stress return algorithm are applied to two resin materials (8551-7 and

Epoxy) to model their nonlinear responses which are shown in Figure 4. The model parameters for these materials are provided in Table 1. The stress-strain response of these resins under three different loading configurations (tension, compression, and shear) produced by the proposed model is presented in Figure 4 along with the corresponding experimental data reported by Kaddour and Hinton[20]. The correlation of these results (Figure 4) demonstrates an excellent capability of the present model in capturing the inelastic response of pressure-dependent materials such as epoxy resin. In this example, r_d takes an initial value of zero (damage effect is turned off) until the damage process is activated when the accumulated plastic strain has reached a critical value ($\varepsilon_{pc} = 1.07\%$ and 1.47% for 8551-7 resin and Epoxy resin respectively) then r_d is set to 0.93 in both cases. It should be noted that the rate of softening of the stress-strain curves (Figure 4) can be controlled by specifying the damage parameter r_d . For example, higher values of r_d associated with higher loss of energy due to damage process leads to more abrupt failure (steeper descending curve), whereas lower values of r_d indicate lower energy dissipation due to damage, resulting in gradual loss of stiffness and a lower rate of softening.

Table 1: Model Parameters for 8551-7 Resin and Epoxy Resin

	E (GPa)	ν	f_{t0} (MPa)	f_{c0} (MPa)	Q_t (MPa)	Q_c (MPa)	b_t	b_c	c
8551-7	4.08	0.38	30	40	90	90	100	50	1
Epoxy	3.2	0.35	60	70	25	50	450	350	1

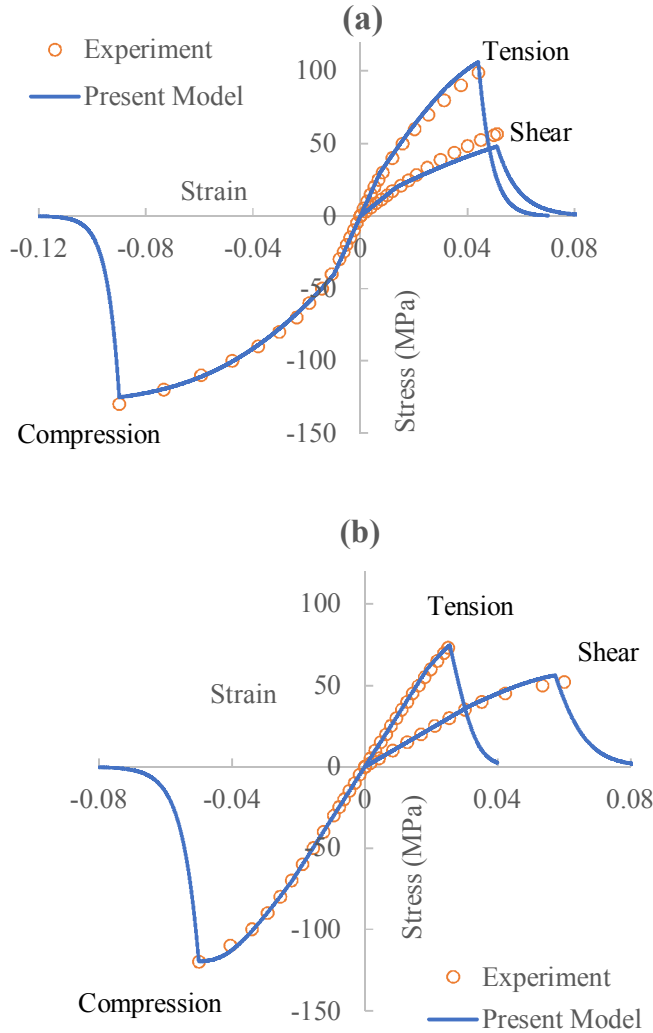


Figure 4: Responses of resins under uniaxial tension, uniaxial compressions, and in-plane shear: (a) 8551-7 Resin; (b) Epoxy Resin. Experimental data is provided in [20].

3. Results and Discussions:

In this section, the capabilities of the proposed model are demonstrated through numerical examples of FRC lamina which include determination of elastic properties in the linear range and inelastic response in the nonlinear range. At first, we will look at how well the model performs in predicting effective elastic properties of unidirectional composites. The results produced by the proposed model are validated against published experimental results as well as theoretical results produced by other reliable techniques. The good performance of the proposed model in the elastic domain will provide confidence in the model's

capability when predicting the inelastic behaviour of unidirectional composite ply which will be discussed in subsequent sections.

3.1 Longitudinal and Transverse Elastic Modulus:

As can be seen in the model formulation, the proposed approach does not take into account the relative sliding between matrix and fibre in the fibre direction. A direct consequence is that the longitudinal modulus E_l predicted by the proposed model follows the upper bound solution (Voigt model), which can be considered as the acceptable behaviour of unidirectional composites under this loading mode. On the other hand, the variations of other effective elastic properties of a unidirectional Glass/epoxy lamina (refer to Table 2 for material properties of its constituents) predicted by the proposed model are plotted against fibre volume fraction and compared with existing solutions for a demonstration of its capabilities.

Table 2: Material Properties of the constituents of a Glass/epoxy lamina[66].

Engineering constant	Epoxy	Glass
E (GPa)	5.35	113.4
ν	0.22	0.35

The transverse modulus of the same FRC predicted by the proposed model for various fibre volume fraction is presented in Figure 5 along with the predictions by some well-regarded classical theories [42, 43, 75, 76]. As shown in Figure 5, the results predicted by the model are in good agreement with these theories. They are in between the upper (Voigt) and lower bound solutions (Reuss), as a consequence of better assumptions and kinematic enhancements of the proposed approach. For instance, the transverse loading in direction 2 will allow to have same transverse normal stress in matrix blocks M-1 and M-2 and the fibre block ($\sigma_{22}^{(1)} = \sigma_{22}^{(2)} = \sigma_{22}^{(4)}$). On the other hand, the transverse normal strain of M-3 is same as that of the fibre block F ($\epsilon_{22}^{(3)} = \epsilon_{22}^{(4)}$) generating different transverse normal stress in M-3 and F due to their different material stiffness values. These phenomenon will lead to deviation of the actual behaviour of the lower bound solution. This is also supported by experimental data which is shown later where

the transverse modulus are found to be slightly higher than the lower bound solution [77].

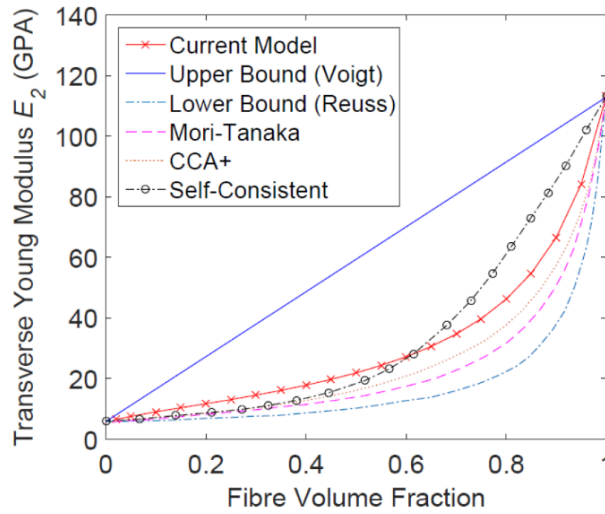


Figure 5: Transverse modulus E_2 – (other results obtained from [66]). Material properties are given in Table 2. Enhancement control parameters $\alpha = \beta = 1$

It should be noted that a default value of the strain enhancement control parameters α and β is taken as 1.0 to produce results given in Figure 6. In order to show the influences of α and β on the prediction of elastic modulus of the same composite, the values of these parameters are varied from 0.8 to 1.4 as illustrated in Figure 6.

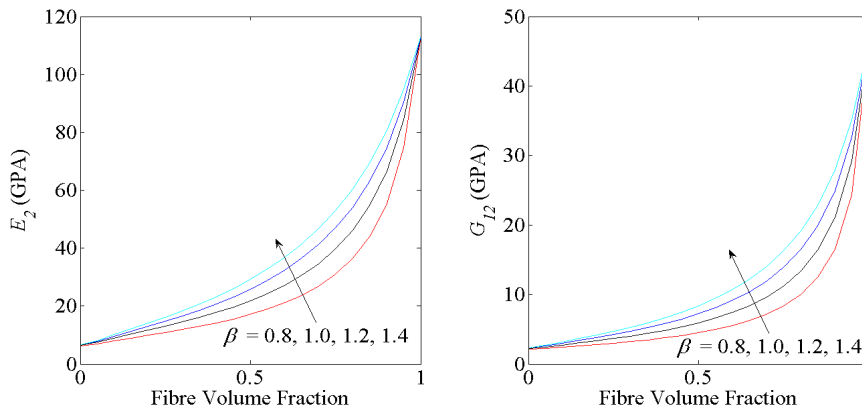


Figure 6: (a) Effects of β on transverse modulus; (b) Effects of α on in-plane shear modulus. Material properties are given in Table 2

Thus α and β can be utilised to control the performance of the model to have a better predictions of the composite elastic modulus. For an example, this is illustrated by adjusting β to improve the predictions of transverse modulus E_2 of a unidirectional

Boron/epoxy lamina (material properties of the constituents are given in Table 3). The results obtained by taking $\beta = 1.0$ (default value) and $\beta = 0.8$ are plotted in Figure 7 along with the experimental data and some commonly used theoretical predictions. Figure 7 shows that the results produced by the proposed model with the use an appropriate value of β is in well agreement in comparisons to test data and other benchmark models.

Table 3: Material Properties obtained from [77].

Engineering constant	Epoxy	Boron
E (GPa)	4.14	414
ν	0.35	0.2

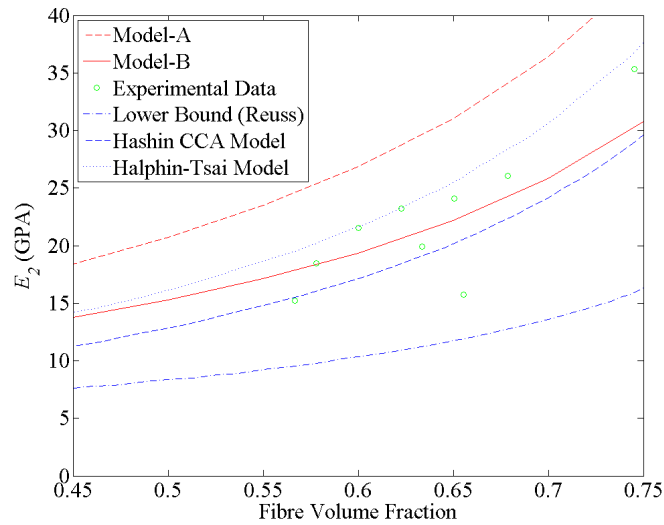


Figure 7: Transverse modulus E_2 (Model-A: $\beta = 1$; Model-B: $\beta = 0.8$) - experimental data and other theoretical results obtained from [77].

3.2 In-plane Shear and Transverse Shear Modulus (G_{12} and G_{23})

The in-plane shear modulus G_{12} (or G_{13}) and the transverse shear modulus G_{23} of the same Glass/epoxy lamina used in Section 3.1 are predicted by the proposed model. These results are presented with numerical results predicted by five benchmark theoretical models in Figure 8 which show a very good predicting capability of the model for both in-plane and transverse shear modulus.

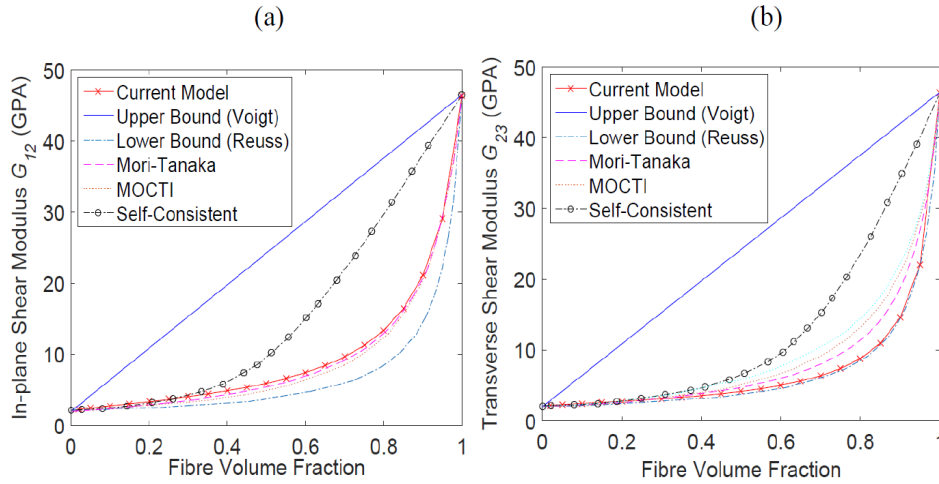


Figure 8: (a) In-plane shear modulus G_{12} ; (b) Transverse shear modulus G_{23} (other results obtained from [66]).

On the other hand, a similar lamina with a slightly different material properties (as given in Table 4) is analysed. The in-plane shear modulus predicted by the proposed model are compared with the experimental results as well as theoretical results in Figure 9. A very good correlation between the present results with the experimental data can be seen.

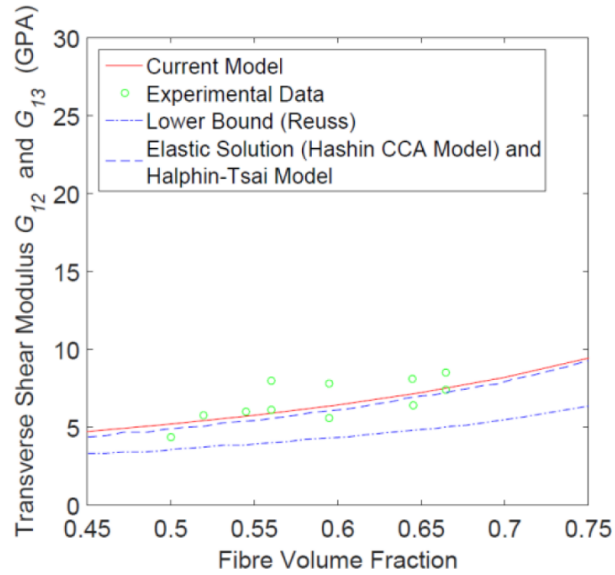


Figure 9: In-plane shear modulus G_{12} (other results obtained from [77]).

Table 4: Material Properties obtained from [77].

Engineering constant	Epoxy	Glass
G (GPa)	1.83	30.19
ν	0.3	0.2

3.3 Inelastic Response

The proposed kinematically enhanced model for unidirectional FRC ply is ready to be extended to inelastic analyses with the use of the coupled damage-plasticity model presented in Section 2.2 for modelling of nonlinear behaviours in matrix blocks. In this study, the nonlinear responses of a composite lamina made of Boron fibres (fibre volume fraction of 0.47) and Aluminium 6061 T0 matrix are examined (refer to Table 5 for their elastic properties). The inelastic stress-strain predictions made by the present model will be verified with those produced by other benchmark models to demonstrate its performance. According to Davidson and Davis [71], mechanical properties of Aluminium 6061 are dependent of hydrostatic pressures (e.g. ultimate stress can be increased up to 60% at higher pressure in certain cases). This pressure-dependent behaviour can be captured by the proposed coupled damage-plasticity model with the use of the parabolic Drucker-Prager yield criterion (see Section 2.2). Model parameters required by the coupled damage-plasticity model for the Aluminium 6061T0 matrix are calibrated from the actual uniaxial tension test data of Aluminium 6061T0 [45] as shown in Figure 10. Based on that, the model parameters estimated for this matrix are: $f_{t0} = 45$ (MPa), $f_{c0} = 47$ (MPa), $Q_t = 41$ (MPa), $Q_c = 44$ (MPa), $b_t = 150$ and $b_c = 155$. These correspond to an excellent correlation of the model results with the experimental test data (see Figure 10).

Table 5: Material Properties.

Engineering constant	Aluminium 6061	Boron
E (GPa)	68.3	379.3
ν	0.3	0.1

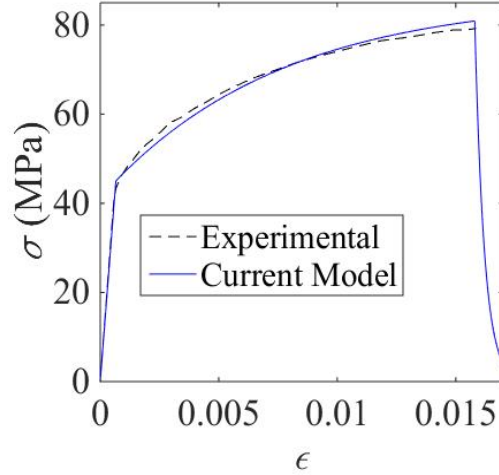


Figure 10: Uniaxial tensile stress-strain curve of Aluminium 6061T0:
Experimental data vs model predictions.

Subsequently, these nonlinear responses within the matrix blocks (responses at the micro scale) can be transferred to a higher scale (macro/ply scale), with the help of the proposed micromechanics based model (Section 2), which can produce overall nonlinear responses of the ply. For this purpose, the nonlinear response of a Boron-Aluminium composite lamina reported by Robertson and Mall[64] is used. It should be noted that information on the plastic volumetric dilation/contracting behaviour of the matrix is not provided by Robertson and Mall[64], and a non-associated flow rule is used in this study where the parameter c (Section 2.2) for controlling the model behaviour is taken as 12.5 to have a good prediction. On the other hand, the fibres are assumed to behave elastically up to the rupture in this study, which is quite common and generally accepted in literature. In addition, it is assumed that the pre-peak response of the composite ply is governed by plastic deformations of the matrix with no damage. The damage is activated while modelling the post-peak behaviour of the composite as its response is dictated by the failure and post-peak behaviour of in matrix. For the damage modelling, the parameter r_d (Section 2.2) controlling the proportion of damage is taken as 0.59 and this is activated when the effective plastic strain ε_p within a matrix block reaches its critical value $\varepsilon_{pc}=0.014$ corresponding to the uniaxial peak stress of the matrix. Based on these assumptions and model parameters, the inelastic response of the composite ply under transverse tensile loading along direction 2 (Figure 1) is simulated by the proposed model and the stress-strain responses are illustrated in Figure 11a.

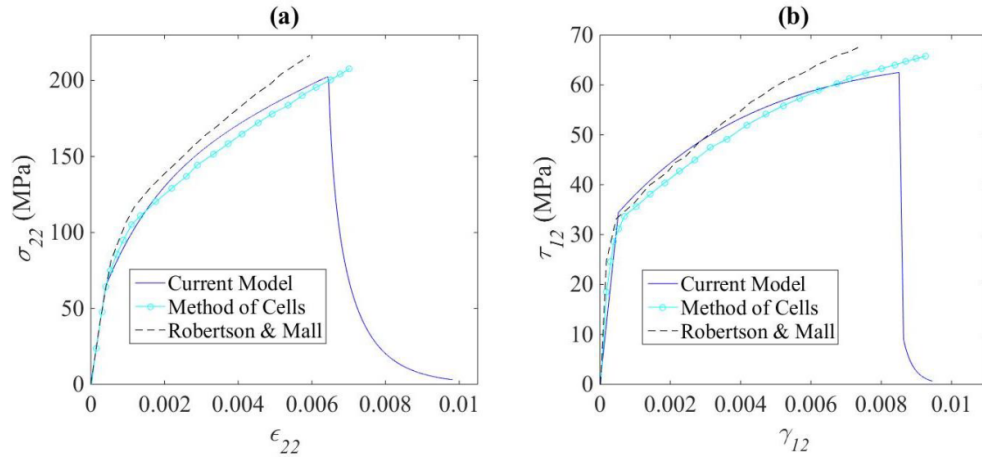


Figure 11: Inelastic responses of Boron/Aluminium 6061 T0 (a) Transverse uniaxial tension (b) In-plane shear.

It can be seen in Figure 11a that the uniaxial tensile response produced by the proposed model agree well with the predictions made by Robertson and Mall[64] as well as MOC[46, 63]. Furthermore, the proposed model has the capability of simulating the strain softening behaviour of the stress-strain curve after its peak stress by activating damage coupled with plastic deformations (Figure 11a). Similarly, the nonlinear response for the in-plane shear of the same composite ply predicted by the proposed model is plotted in Figure 11b along with that of Robertson and Mall[64] as well as MOC[46, 63] which shows a good correlation of the present results with others. These indicate that the proposed models are able to provide reliable and accurate solutions for capturing inelastic responses of unidirectional ply, which properly accounts for the adequate level of coupling between damage and plastic deformations occurred progressively. It should be noted that the effect of fibre debonding is not taken into account yet in the proposed model. Its incorporation requires adding more kinematic enhancements to the current scheme to account for the displacement jumps at the fibre-matrix interface and is a subject of our on-going study.

4. Conclusions

We developed a generic approach for modelling fibre reinforced composites at the ply level. The proposed approach possesses the material and geometric details on the constituents and their interactions, which is applicable in both linear and nonlinear ranges of behaviour. In particular, inhomogeneous stress in the material

due to differences in fibre and matrix material behaviours is represented by different responses of four material blocks characterising fibre and three matrix zones. The interactions between the blocks are taken into account through equilibrium conditions across their boundaries. A homogenisation technique is developed in an incremental form that links the response of the fibre and matrix blocks to produce a macro-mechanical stress-strain relationship. Thanks to the stress inhomogeneity that represents the composite nature of the material behaviour, the resulting effective elastic properties produced by the model agree well with classical models and experimental data in the literature. In addition, the incremental form of the formulation facilitates the application of the proposed approach to inelastic analysis, as it allows the use of any kind of material model for matrix and fibre. In conjunction with the development of the composite model, a thermodynamics-based model that couples damage with plasticity is also developed for its constituents (fibre and matrix). It is shown that the macro failure response of the composite can be captured well due to the use of appropriate models for the constituents and their intrinsic coupled behaviour in the proposed formulation. We acknowledge that the effects of fibre-matrix debonding and fibre distribution on the mechanical responses of unidirectional composites have not been accounted for yet in the proposed approach. These effects will be addressed in our next papers.

Acknowledgements

Giang D. Nguyen would like to thank the Australian Research Council (ARC) for funding support via project FT140100408. The ARC's support to Luming Shen & Giang D. Nguyen through their joint project DP140100945 is also gratefully acknowledged.

5. Appendix

Expression for \mathbf{K}^{-1} :

$$\mathbf{K}_1 = \boldsymbol{\mu}_1 - (f_1 \boldsymbol{\mu}_1 + f_2 \mathbf{I}) \quad (85)$$

$$\mathbf{K}_2 = \boldsymbol{\mu}_2 - (f_1 \boldsymbol{\mu}_2 + f_3 \mathbf{I}) \quad (86)$$

$$\mathbf{K}_3 = f_1 \boldsymbol{\mu}_2 + f_3 \mathbf{I} \quad (87)$$

$$\mathbf{K}_4 = f_1 \boldsymbol{\mu}_1 + f_2 \mathbf{I} \quad (88)$$

Normal matrices in direction 2 and 3:

$$\mathbf{N}_2 = \begin{bmatrix} 0 & 0 & 0 \\ 0 & 1 & 0 \\ 0 & 0 & 0 \\ 1 & 0 & 0 \\ 0 & 0 & 1 \\ 0 & 0 & 0 \end{bmatrix}, \mathbf{N}_3 = \begin{bmatrix} 0 & 0 & 0 \\ 0 & 0 & 0 \\ 0 & 0 & 1 \\ 0 & 0 & 0 \\ 0 & 1 & 0 \\ 1 & 0 & 0 \end{bmatrix} \quad (89)$$

Detailed expressions of matrices in equation (22):

$$\mathbf{A}_{11} = f^{(1)} \mathbf{K}_1^T \mathbf{N}_2^T \mathbf{D}^{(1)} \mathbf{N}_2 \mathbf{K}_1 + f^{(2)} \mathbf{K}_1^T \mathbf{N}_2^T \mathbf{D}^{(2)} \mathbf{N}_2 \mathbf{K}_1 + f^{(3)} \mathbf{K}_4^T \mathbf{N}_2^T \mathbf{D}^{(3)} \mathbf{N}_2 \mathbf{K}_4 + f^{(4)} \mathbf{K}_4^T \mathbf{N}_2^T \mathbf{D}^{(4)} \mathbf{N}_2 \mathbf{K}_4 \quad (90)$$

$$\mathbf{A}_{12} = f^{(1)} \mathbf{K}_1^T \mathbf{N}_2^T \mathbf{D}^{(1)} \mathbf{N}_3 \mathbf{K}_2 - f^{(2)} \mathbf{K}_1^T \mathbf{N}_2^T \mathbf{D}^{(2)} \mathbf{N}_3 \mathbf{K}_3 - f^{(3)} \mathbf{K}_4^T \mathbf{N}_2^T \mathbf{D}^{(3)} \mathbf{N}_3 \mathbf{K}_2 + f^{(4)} \mathbf{K}_4^T \mathbf{N}_2^T \mathbf{D}^{(4)} \mathbf{N}_3 \mathbf{K}_3 \quad (91)$$

$$\mathbf{A}_{21} = f^{(1)} \mathbf{K}_2^T \mathbf{N}_3^T \mathbf{D}^{(1)} \mathbf{N}_2 \mathbf{K}_1 - f^{(2)} \mathbf{K}_3^T \mathbf{N}_3^T \mathbf{D}^{(2)} \mathbf{N}_2 \mathbf{K}_1 - f^{(3)} \mathbf{K}_2^T \mathbf{N}_3^T \mathbf{D}^{(3)} \mathbf{N}_2 \mathbf{K}_4 + f^{(4)} \mathbf{K}_3^T \mathbf{N}_3^T \mathbf{D}^{(4)} \mathbf{N}_2 \mathbf{K}_4 \quad (92)$$

$$\mathbf{A}_{22} = f^{(1)} \mathbf{K}_2^T \mathbf{N}_3^T \mathbf{D}^{(1)} \mathbf{N}_3 \mathbf{K}_2 + f^{(2)} \mathbf{K}_2^T \mathbf{N}_3^T \mathbf{D}^{(2)} \mathbf{N}_3 \mathbf{K}_3 + f^{(3)} \mathbf{K}_2^T \mathbf{N}_3^T \mathbf{D}^{(3)} \mathbf{N}_3 \mathbf{K}_2 + f^{(4)} \mathbf{K}_3^T \mathbf{N}_3^T \mathbf{D}^{(4)} \mathbf{N}_3 \mathbf{K}_3 \quad (93)$$

$$\mathbf{B}_1 = f^{(4)} \mathbf{K}_4^T \mathbf{N}_2^T \mathbf{D}^{(4)} - f^{(1)} \mathbf{K}_1^T \mathbf{N}_2^T \mathbf{D}^{(1)} - f^{(2)} \mathbf{K}_1^T \mathbf{N}_2^T \mathbf{D}^{(2)} + f^{(3)} \mathbf{K}_4^T \mathbf{N}_2^T \mathbf{D}^{(3)} \quad (94)$$

$$\mathbf{B}_2 = f^{(4)} \mathbf{K}_3^T \mathbf{N}_3^T \mathbf{D}^{(4)} - f^{(1)} \mathbf{K}_2^T \mathbf{N}_3^T \mathbf{D}^{(1)} + f^{(2)} \mathbf{K}_3^T \mathbf{N}_3^T \mathbf{D}^{(2)} - f^{(3)} \mathbf{K}_2^T \mathbf{N}_3^T \mathbf{D}^{(3)} \quad (95)$$

6. References

1. Tsai, S.W.: Strength of Theories of Filamentary Structures. Fundamental Aspects of Fibre Reinforced Plastic Composites. John Wiley & Sons, USA (1968).
2. Tsai, S.W., Wu, E.M.: A General Theory of Strength for Anisotropic Materials. J. Compos. Mater. 5, 58–80 (1971).
3. Hoffman, O.: The Brittle Strength of Orthotropic Materials. J. Compos. Mater. 1, (1967).
4. Hashin, Z., Rotem, A.: A Fatigue Failure Criterion for Fibre Reinforced Materials. J. Compos. Mater. 7, 448–464 (1973).
5. Hashin, Z.: Failure Criteria for Unidirectional Fibre Composites. J. Appl. Mech. 47, 329–334 (1980).
6. Christensen, R.M.: Tensor Transformations and Failure Criteria for the Analysis of Fibre Composite Materials. J. Compos. Mater. 22, 874–897

- (1988).
7. Christensen, R.M.: Stress Based Yield/Failure Criteria for Fibre Composites. *Int. J. Solids Struct.* 34, 529–543 (1997).
 8. Van Paepegem, W., De Baere, I., Degrieck, J.: Modelling the nonlinear shear stress-strain response of glass fibre-reinforced composites. Part I: Experimental results. *Compos. Sci. Technol.* 66, 1455–1464 (2006).
 9. Schuecker, C., Pettermann, H.: Combining elastic brittle damage with plasticity to model the non-linear behavior of fibre reinforced laminates. In: Camanho, P.P., Dávila, C.G., Pinho, S.T., and Remmers, J.J.C. (eds.) *Mechanical Response of Composites*. Springer Netherlands (2008).
 10. Lemaitre, J., Desmorat, R.: *Engineering Damage Mechanics*. Springer, The Netherlands (2005).
 11. Greenhalgh, E.S.: *Failure Analysis and Fractography of Polymer Composites*. Woodhead Publishing Limited, USA (2009).
 12. Murakami, S., Kamiya, K.: Constitutive and damage evolution equations of elastic-brittle materials based on irreversible thermodynamics. *Int. J. Mech. Sci.* 39, 473–486 (1997).
 13. Bogetti, T.A., Hoppel, C.P.R., Harik, V.M., Newill, J.F., Burns, B.P.: Predicting the nonlinear response and progressive failure of composite laminates. *Fail. Criteria Fibre-Reinforced-Polymer Compos.* 64, 402–428 (2004).
 14. Sun, C.T., Chen, J.L.: A Simple Flow Rule for Characterizing Nonlinear Behavior of Fibre Composites. *J. Compos. Mater.* 23, 1009–1020 (1989).
 15. Sun, C.T., Yoon, K.J.: Elastic-plastic analysis of AS4/PEEK composite laminate using a one-parameter plasticity model. *J. Compos. Mater.* 26, 293–308 (1990).
 16. Daudeville, L., Allix, O., Ladeveze, P.: Delamination Analysis By Damage Mechanics: Some Applications. *Compos. Part B Eng.* 5, 17–24 (1995).
 17. Schuecker, C., Pettermann, H.E.: A continuum damage model for fibre

- reinforced laminates based on ply failure mechanisms. *Compos. Struct.* 76, 162–173 (2006).
18. Ladeveze, P., Lubineau, G.: On a Damage Mesomodel For Laminates : Micro – Meso Relationships , Possibilities and Limits. *Compos. Sci. Technol.* 61, 2149–2158 (2001).
 19. Ladeveze, P., Lubineau, G., Marsal, D.: Towards a Bridge Between The Micro- and Mesomechanics of Delamination For Laminated Composites. *Compos. Sci. Technol.* 66, 698–712 (2006).
 20. Kaddour, A., Hinton, M.: Input Data for Test Cases Used in Benchmarking Triaxial Failure Theories of Composites. *J. Compos. Mater.* 46, 2295–2312 (2012).
 21. Talreja, R., Yalvac, S., Yats, L.D., Wetters, D.G.: Transverse Cracking and Stiffness Reduction in Cross Ply Laminates of Different Matrix Toughness. *J. Compos. Mater.* 26, 1644–1663 (1992).
 22. Talreja, R.: A Continuum Mechanics Characterization of Damage in Composite Materials. *Proc. R. Soc. London . Ser. A , Math. Phys.* 399, 195–216 (1985).
 23. Puck, A., Schurmann, H.: Failure Analysis of Frp Laminates By Means of Physically Based Phenomenological Models *. *Compos. Sci. Technol.* 58, 1045–1067 (1998).
 24. Deuschle, H.M., Puck, A.: Application of the Puck failure theory for fibre-reinforced composites under three-dimensional stress : Comparison with experimental results. *J. Compos. Mater.* 47, 827–846 (2012).
 25. Pinho, S.T., Darvizeh, R., Robinson, P., Schuecker, C.: Material and structural response of polymer-matrix fibre-reinforced composites. *J. Compos. Mater.* 46, 2313–2341 (2012).
 26. Pinho, S.T., Dávila, C.G., Camanho, P.P., Iannucci, L., Robinson, P.: Failure Models and Criteria for FRP Under In-Plane or Three-Dimensional Stress States Including Shear Non-Linearity. , Hampton (2005).
 27. Pinho, S.T., Iannucci, L., Robinson, P.: Physically-based failure models

- and criteria for laminated fibre-reinforced composites with emphasis on fibre kinking : Part I : Development. *Compos. Part A Appl. Sci. Manuf.* 37, 63–73 (2006).
28. Bogetti, T. a., Staniszewski, J., Burns, B.P., Hoppel, C.P., Gillespie, J.W., Tierney, J.: Predicting the nonlinear response and progressive failure of composite laminates under tri-axial loading. *J. Compos. Mater.* 46, 2443–2459 (2012).
 29. Cuntze, R.G., Freund, A.: The Predictive Capability of Failure Mode Concept-Based Strength Criteria for Multidirectional Laminates. *Compos. Sci. Technol.* 64, 343–377 (2004).
 30. Cuntze, R.: The predictive capability of failure mode concept-based strength conditions for laminates composed of unidirectional laminae under static triaxial stress states. (2012).
 31. Selmi, A., Doghri, I., Adam, L.: Micromechanical simulations of biaxial yield, hardening and plastic flow in short glass fibre reinforced polyamide. *Int. J. Mech. Sci.* 53, 696–706 (2011).
 32. Aboudi, J., Steven, M.A., Brett, A.B.: *Micromechanics of Composite Materials - A Generalized Multiscale Analysis Approach*. Elsevier, US (2013).
 33. Huang, Z.M.: Micromechanical strength formulae of unidirectional composites. *Mater. Lett.* 40, 164–169 (1999).
 34. Vaughan, T.J., McCarthy, C.T.: A combined experimental-numerical approach for generating statistically equivalent fibre distributions for high strength laminated composite materials. *Compos. Sci. Technol.* 70, 291–297 (2010).
 35. Totry, E., Molina-Aldareguia, J.M., Gonzalez, C., LLorca, J.: Effect of fibre, matrix and interface properties on the in-plane shear deformation of carbon-fibre reinforced composites. *Compos. Sci. Technol.* 70, 970–980 (2010).
 36. Romanowicz, M.: A numerical approach for predicting the failure locus of

- fibre reinforced composites under combined transverse compression and axial tension. *Comput. Mater. Sci.* 51, 7–12 (2012).
37. Canal, L.P., González, C., Segurado, J., LLorca, J.: Intraply fracture of fibre-reinforced composites: Microscopic mechanisms and modeling. *Compos. Sci. Technol.* 72, 1223–1232 (2012).
 38. Ladeveze, P., Dantec, E. Le: Damage modelling of the elementary ply for laminated composites. *Compos. Sci. Technol.* 43, 257–267 (1992).
 39. Matsuda, T., Ohno, N., Tanaka, H., Shimizu, T.: Effects of fibre distribution on elastic-viscoplastic behavior of long fibre-reinforced laminates. *Int. J. Mech. Sci.* 45, 1583–1598 (2003).
 40. Ohno, N., Wu, X., Matsuda, T.: Homogenized properties of elastic-viscoplastic composites with periodic internal structures. *Int. J. Mech. Sci.* 42, 1519–1536 (2000).
 41. Hill, R.: Elastic Properties of Reinforced Solids: Some Theoretical Principles. *J. Mech. Phys. Solids.* 11, 357–372 (1963).
 42. Mori, T., Tanaka, K.: Average Stress in Matrix and Average Elastic Energy of Materials with Misfitting Inclusions. *ACTA Metall.* 21, 571–574 (1974).
 43. Hashin, Z., Rosen, B.W.: The Elastic Moduli of Fibre-Reinforced Materials. *J. Appl. Mech.* 223–232 (1964).
 44. Christensen, M.R., Lo, K.H.: Solutions for effective shear properties in three phase sphere and cylinder models. *J. Mech. Phys. Solids.* 27, 315–330 (1979).
 45. Sun, C.T., Chen, J.L.: A Micromechanical Model for Plastic Behavior of Fibrous Composites. *Compos. Sci. Technol.* 40, 115–129 (1991).
 46. Aboudi, J.: Micromechanical Analysis of Composites by the Method of Cells. *Am. Soc. Mech. Eng.* 42, 193–221 (1989).
 47. Aboudi, J.: Journal of Reinforced Plastics and Composites The Nonlinear Behavior of Unidirectional. *J. Reinf. Plast. Compos.* (1990).
 48. Pindera, M.-J., Bednarczyk, B. a: An efficient implementation of the

- generalized method of cells for unidirectional, multi-phased composites with complex microstructures. *Compos. Part B Eng.* 30, 87–105 (1999).
49. Li, H., Zhang, B., Bai, G.: Effects of constructing different unit cells on predicting composite viscoelastic properties. *Compos. Struct.* 125, 459–466 (2015).
 50. Aboudi, J., Arnold, S.M.: *High-Fidelity Generalization Method of Cells for Inelastic Periodic Multiphase Materials.* , Glenn Research Center (2002).
 51. Ogiwara, S., Kobayashi, S.: Characterization of nonlinear behavior of carbon / epoxy unidirectional and angle-ply laminates. *Adv. Compos. Mater.* 11, 239–254 (2003).
 52. Tsai, J.-L., Chen, K.-H.: Characterizing Nonlinear Rate-dependent Behaviors of Graphite/Epoxy Composites using a Micromechanical Approach. *J. Compos. Mater.* 41, 1253–1273 (2007).
 53. Chen, X., Ye, J., Zhai, Z., He, Z.: Micromechanical analysis of off-axis loading of fibre reinforced composites with imperfect interface bonding. *Int. J. Mech. Sci.* 54, 113–120 (2012).
 54. Aboudi, J., Volokh, K.Y.: Failure Prediction of Unidirectional Composites Undergoing Large Deformations. *J. Appl. Mech.* 82, 71004 (2015).
 55. Huang, Z.M.: A Unified Micromechanical Model for the Mechanical Properties of Two Constituents Composite Materials Part II: Plastic Behavior. *J. Thermoplast. Compos. Mater.* 13, 344–362 (2000).
 56. Huang, Z.M.: Simulation of the mechanical properties of fibrous composites by the bridging micromechanics model. *Compos. Part A Appl. Sci. Manuf.* 32, 143–172 (2001).
 57. Huang, Z.M.: Inelastic and Failure Analysis of Laminate Structures by ABAQUS Incorporated with a General Constitutive Relationship. *J. Reinf. Plast. Compos.* 26, 1135–1181 (2007).
 58. Huang, Z., Liu, L.: Predicting strength of fibrous laminates under triaxial loads only upon independently measured constituent properties. *Int. J. Mech. Sci.* 79, 105–129 (2014).

59. Shokrieh, M.M., Mosalmani, R., Omid, M.J.: A strain-rate dependent micromechanical constitutive model for glass/epoxy composites. *Compos. Struct.* 121, 37–45 (2015).
60. Santhosh, U., Ahmad, J.: An approach for nonlinear modeling of polymer matrix composites. *J. Compos. Mater.* 48, 1755–1765 (2014).
61. Tabiei, A., Aminjikai, S.B.: A strain-rate dependent micro-mechanical model with progressive post-failure behavior for predicting impact response of unidirectional composite laminates. *Compos. Struct.* 88, 65–82 (2009).
62. Goldberg, R., Stouffer, D.: Strain rate dependent analysis of a polymer matrix composite utilizing a micromechanics approach. *J. Compos. Mater.* 36, 773–793 (2002).
63. Aboudi, J.: *Mechanics of Composite Materials: A Unified Micromechanical Approach*. Elsevier, Amsterdam (1991).
64. Robertson, D.D., Mall, S.: Micromechanical analysis for thermoviscoplastic behavior of unidirectional fibrous composites. *Compos. Sci. Technol.* 50, 483–496 (1994).
65. Paley, M., Aboudi, J.: Micromechanical Analysis of Composites by the Generalized Cells Model. *Mech. Mater.* 14, 127–139 (1992).
66. Herakovich, C.T.: *Mechanics of Fibrous Composites*. John Wiley & Sons, Inc, New York (1998).
67. Nguyen, G.D., Einav, I., Korsunsky, A. M.: How to Connect Two Scales of Behaviour in Constitutive Modelling of Geomaterials. *Géotechnique Lett.* 2, 129–134 (2012).
68. Nguyen, G.D., Nguyen, C.T., Nguyen, V.P., Bui, H.H., Shen, L.: A size-dependent constitutive modelling framework for localised failure analysis. *Comput. Mech.* 58, 1–24 (2016).
69. Nguyen, G.D., Bui, H.H., Shen, L., Bennett, T., Sheikh, A.H.: Constitutive Modelling of Localized Failure as a Homogenization of Multiphase Materials. In: 10th International Conference on Structural Integrity and

- Failure (SIF-2016): Advances in Materials and Structures. Materials and Structures, Adelaide (2016).
70. Crisfield, M.A.: Non-linear finite element analysis of solids and structures. Volume 1: Essentials. John Wiley & Sons Ltd, Chichester (1991).
 71. Davidson, P., Davis, R.: Mechanical Behavior of 6061 — T651 Aluminum. AIAA J. 13, 1547–1548 (1975).
 72. Einav, I., Houlsby, G.T., Nguyen, G.D.: Coupled Damage and Plasticity Models Derived From Energy and Dissipation Potentials. Int. J. Solids Struct. 44, 2487–2508 (2007).
 73. Nguyen, G.D., Einav, I., Guimatsia, I., 2012, On the partition of fracture energy in constitutive modelling of quasi-brittle materials, Engineering Fracture Mechanics 79, 225-244.
 74. Houlsby, G.T., Puzrin, A.M.: Principles of Hyperplasticity: An Approach to Plasticity Theory Based on Thermodynamic Principles. Springer-Verlag London Limited, London (2006).
 75. Benveniste, Y.: A New Approach to the Application of Mori-Tanaka's Theory in Composite Materials. Mech. Mater. 6, 147–157 (1987).
 76. Hill, R.: Self-Consistent Mechanics of Composite Materials. J. Mech. Phys. Solids. 13, 213–222 (1965).
 77. Kaw, A.K.: Mechanics of Composite Materials. Taylors & Francis Group, New York (2006).

CHAPTER 3: JOURNAL PAPER 2

A Thermodynamics-based Framework for Constitutive Models using Damage Mechanics and Plasticity Theory

Statement of Authorship

Title of Paper	A Thermodynamics-based formulation for constitutive modelling using damage mechanics and plasticity theory
Publication Status	<input checked="" type="checkbox"/> Published <input type="checkbox"/> Accepted for Publication <input type="checkbox"/> Submitted for Publication <input type="checkbox"/> Unpublished and Unsubmitted work written in manuscript style
Publication Details	Vu, V.D., Mir, A., Nguyen, G.D. and Sheikh, A.H., 2017. A thermodynamics-based formulation for constitutive modelling using damage mechanics and plasticity theory. <i>Engineering Structures</i> , 143, pp.22-39.

Principal Author


Name of Principal Author (Candidate)	Van Duc Vu		
Contribution to the Paper	Developed and wrote the generic formulation and its application and numerical examples for concrete and metal.		
Certification:	This paper reports on original research I conducted during the period of my Higher Degree by Research candidature and is not subject to any obligations or contractual agreements with a third party that would constrain its inclusion in this thesis. I am the primary author of this paper.		
Overall percentage (%)	60 %		
Signature		Date	25/05/2017

Co-Author Contributions

By signing the Statement of Authorship, each author certifies that:

- i. the candidate's stated contribution to the publication is accurate (as detailed above);
- ii. permission is granted for the candidate to include the publication in the thesis; and
- iii. the sum of all co-author contributions is equal to 100% less the candidate's stated contribution.

CHAPTER 3: JOURNAL PAPER 2

Name of Co-Author	Arash Mir		
Contribution to the Paper	Developed and wrote the section on the behaviour of geomaterials. Wrote the introduction and actively participated in writing the manuscript		
Signature		Date	25/05/2017

Name of Co-Author	Giang D. Nguyen		
Contribution to the Paper	Supervision of the technical work, write-up and revision of the manuscript		
Signature		Date	25/05/2017

Name of Co-Author	Abdul Hamid Sheikh		
Contribution to the Paper	Supervision of the technical work, write-up and revision of the manuscript		
Signature		Date	25/05/2017

End of document

Abstract

In this study, a generic formulation for constitutive modelling of engineering materials is developed, employing theories of plasticity and continuum damage mechanics. The development of the proposed formulation is carried out within the framework of thermodynamics with internal variables. In this regard, the complete constitutive relations are determined by explicitly defining a free energy potential and a dissipation function. The focus is put on the rigour and consistency of the proposed formulation in accommodating the coupling between damage and plasticity, while keeping its structure sufficiently generic to be applicable to a wide range of engineering materials. In particular, by specifying the coupling between damage and plasticity in the dissipation function, a single generalised loading function that controls the simultaneous evolution of these dissipative mechanisms is obtained. The proposed formulation can be readily used for either enriching existing plasticity models with damage, or for the development of new coupled damage-plasticity models. The promising features and the applications of the proposed formulation for describing the behaviour of different engineering materials are discussed in details.

Keywords: Constitutive modelling; thermodynamics; damage mechanics; plasticity theory; coupled damage-plasticity; concrete; rocks; ductile; brittle

1. Introduction

Computer simulations of the mechanical response of structures, by means of a numerical technique, such as finite element method (FEM), play a key role in many modern civil and mechanical engineering applications. The accuracy of analysis of any numerical simulation, however, depends on a constitutive model, capable of adequately capturing the material behaviour under complex loading scenarios. Theories of plasticity and continuum damage mechanics (CDM) have been widely used for the development of constitutive models in order to describe the inelastic behaviour of materials. At the macroscopic scale, inelastic behaviour can be observed as the reduction in strength and stiffness as well as the occurrence of residual strains. The observable macroscopic behaviour of materials is mainly governed by several underlying microscopic dissipative mechanisms. These dissipative mechanisms are the direct result of progressive, irreversible changes in

the material microstructure. Examples of such changes are closure or expansion of micro-voids, micro-crack initiation and coalescence, frictional sliding between the two surfaces of microcracks, dislocation of defects in the crystal structure of metals and so forth. From a phenomenological perspective, the effects of all underlying mechanisms which cause the occurrence of residual deformations (e.g. frictional sliding, dislocation of defects, etc.) can be represented by a plastic strain tensor as a macroscopic variable. Similarly, the effects of all mechanisms giving rise to strength and stiffness degradation may be accounted for by a damage variable, which can be a scalar or a tensor of higher orders. In general, for any constitutive model, a set of internal variables is required for a complete description of inelastic behaviours of not only the current state but also the previous history of deformations [1-10].

Nomenclature

Ψ	Helmholtz free energy potential
Φ	total dissipation rate function
Φ_v	dissipation rate function corresponding to volumetric plastic deformation
Φ_s	dissipation rate function corresponding to shear plastic deformation
Φ_D	dissipation rate function corresponding to damage
D	scalar damage variable
K	bulk modulus
G	shear modulus
ε_V	total volumetric strain
ε_S	total effective shear strain
α_V	volumetric plastic strain
α_S	effective shear plastic strain
ε_p	accumulative plastic strain
ε_{pc}	critical value of the accumulative plastic strain
σ_{ij}	stress tensor
S_{ij}	deviatoric stress tensor
J_2	second invariant of the deviatoric stress tensor
I_1	first invariant of the stress tensor
ε_{ij}	strain tensor
e_{ij}	deviatoric strain tensor

α_{ij}	plastic strain tensor
λ	non-negative multiplier
δ_{ij}	Kronecker delta
C_{ijkl}	elastic stiffness tensor
C_{ijkl}^t	tangent stiffness tensor
p	mean pressure
q	deviatoric stress
$\bar{\chi}_{ij}$	generalised stress tensor
$\bar{\chi}_V$	generalised mean pressure
$\bar{\chi}_s$	generalised shear stress
$\bar{\chi}_D$	conjugate damage energy
χ_{ij}	generalised dissipative stress tensor
χ_V	generalised dissipative mean pressure
χ_s	generalised dissipative shear stress
χ_D	conjugate dissipative damage energy
y	yield function in true stress space
y^*	yield function in generalised dissipative stress space
ϕ_v	function representing the effect of α_v in total dissipation
ϕ_s	function representing the effect of α_s in total dissipation
ϕ_D	function representing the effect of D in total dissipation
E	function of stresses and internal variables
F	function of stresses and internal variables
f_v	dimensionless function of stresses and internal variables
f_s	dimensionless function of stresses and internal variables
a	dimensionless function of stresses and internal variables
b	dimensionless function of stresses and internal variables
c	dimensionless function of stresses and internal variables
r_d	dimensionless function of stresses and internal variables
r_p	dimensionless function of stresses and internal variables
f_y	dimensionless function of stresses and internal variables
f_{cy}	dimensionless function of stresses and internal variables
f_{ty}	dimensionless function of stresses and internal variables
Q	ultimate stress (Von Mises model)
Q	ultimate stress in tension (parabolic Drucker-Prager model)

Q_c	ultimate stress in compression (parabolic Drucker-Prager model)
H	material parameter determining the rate of expansion of the yield surface
H_t	the value of parameter H in tension
H_c	the value of parameter H in compression
k	material shear strength (Von Mises model)
α	parabolic Drucker-Prager material parameter
β	parabolic Drucker-Prager material parameter
p_c	initial yield pressure under isotropic compression
p_t	initial yield under isotropic decompression (expansion)
ω	material parameter controlling the shape of the yield surface (geomaterials model)
γ	material parameter controlling the shape of the yield surface (geomaterials model)
ρ	back stress (geomaterials model)
M	slope of the final failure envelope (geomaterials model)

During the course of inelastic deformation of engineering materials, plasticity and damage processes normally occur together and one influences the evolution of the other. Hence, constitutive models which take only one of these two mechanisms into account may not adequately represent the observed behaviour of materials. Formulations based merely on plasticity theory [11-19], for instance, generally suffer from limitations in capturing the stiffness reduction due to damage growth [11], although they may be successful in modelling the overall stress-strain response, by explicitly defining some kind of hardening/softening rules for the yield function. Elastic-damage models [20-27], on the other hand, can successfully capture the material stiffness reduction due to damage processes, yet they may be criticised for their inadequacy in properly modelling the residual strains due to plastic deformations, which may only be included into these models by means of some empirical definitions [20]. Hence, a combination of both plasticity theory and CDM is necessary for the development of a realistic and rigorous constitutive model.

Significant efforts have been made during the past few decades to construct coupled damage-plasticity models by specifying the interaction between the two dissipative mechanisms. One of the existing approaches for coupling damage and plasticity is

to employ two separate loading functions pertaining to damage and plasticity. In this approach, the two inelastic mechanisms are linked through the constitutive relations and the plastic yield function is expressed in the effective stress space, associated with the undamaged state of the material [8, 28-51]. In these models, hardening rules are usually introduced to control the evolution of the yield function, while a softening rule controls the evolution of the damage function, and their coupling results in an overall hardening or softening behaviour, owing to the combined effects of both damage and plasticity. Nevertheless, due to the use of two separate loading functions, it is usually difficult to correlate these two surfaces with the experimentally obtained yield envelope and its evolution to failure, especially in multiaxial loading scenarios. In particular, the coupling between damage and plasticity can only take place if the inner loading surface (usually the plastic yield surface) evolves and hits the outer one, after which the two surfaces evolve together.

In another class of coupled damage-plasticity models [9, 52-59], the above-mentioned issues associated with employing two loading surfaces are alleviated by explicitly defining the damage growth as a function of plastic strain. In these models, the role of the damage function is to only determine the onset of the inelastic regime, while the overall inelastic behaviour relies on the yield function and its flow rules. A physical interpretation of these models is that plasticity can be considered as an active mechanism of deformation and energy dissipation followed by damage as a passive mechanism, that is, damage can occur only after some plastic deformation has already taken place. Such models have shown great success in modelling the deformation and failure of a wide range of materials. Nevertheless, the concept of active and passive mechanisms can be used to assess the characteristics of such models for further improvements. For instance, in quasi-brittle materials, such as rocks and concrete under tension, energy dissipation processes usually begin with the development of micro-cracking as an active mechanism, followed by frictional sliding between the newly created crack surfaces (passive mechanism). In compression, on the other hand, experimental observations from geological materials [60-67] suggest that plastic dissipation due to micro-crack closure and the subsequent frictional sliding takes place together with the initiation of new micro-cracks, where the stress condition is favourable.

Another example is grain boundary sliding in metallic materials which can be inferred as an active plasticity mechanism, followed by the stiffness degradation due to debonding process (damage) as a passive mechanism [68]. In our opinion, it is always better to have these features reflected in the constitutive model, in addition to the requirements on its ease of implementation and adequate predictive capability.

Furthermore, it is essential for any constitutive model to conform to the principles of thermodynamics. Although the requirements for the thermodynamic admissibility of a constitutive model can be applied upon completion of its development, a more rigorous and consistent approach is to build a constitutive model within a well-established thermodynamic framework. Keeping all these aspects in view, the development of a generic thermodynamic approach for coupling damage and plasticity by addressing the interaction between these two dissipative mechanisms, as well as controlling the contribution of each of these mechanisms in the total dissipation, is desired. This study is an attempt towards this goal by further developing the results of our previous works [68-70] that are based on a thermodynamic framework proposed earlier by Houlsby and Puzrin [71]. Emphasis is put on the coupling scheme of the proposed formulation so that a single plastic-damage loading function can be obtained to describe both yielding and the ultimate failure of a material. The evolution rules for both damage and plastic strains appear naturally during the derivation of the model from only two scalar thermodynamic functions (i.e. the free energy potential and the dissipation function). In addition, the degree of contribution of each of these dissipative processes can be controlled on the basis of the observed behaviour of materials. This will allow for a more convenient and easier implementation and calibration of models, particularly, under multi-axial loading. In addition, dilative and/or contractive behaviour of engineering materials can be conveniently specified in cases of either enhancing an existing material model or when developing new material models.

The outline of this paper is as follows; in section 2, a complete presentation of the proposed formulation for coupling damage and plasticity along with a detailed discussion on some of its promising features, are provided. In Section 3, the applications of the proposed formulation for enhancing the currently existing

material models as well as constructing new material models are demonstrated through a number of numerical examples.

2. A New Formulation for Coupling Damage and Plasticity

The framework of generalised thermodynamics by Houlsby and Puzrin [71, 72] is adopted in this study to ensure the thermodynamic consistency of the model. A detailed discussion on the development and different features of the proposed formulation is provided in this section. The generic formulation provides a consistent and robust scheme for coupling damage and plasticity and allows for adequately simulating various aspects of material behaviour including dilation, compaction and non-associated flow.

2.1. Thermodynamic-based formulation

In the formulation presented in this section the notation appropriate for triaxial tests is used, with the total volumetric strain being defined as $\varepsilon_V = -\varepsilon_{ii}$ and the total equivalent shear strain as $\varepsilon_S = \sqrt{2/3 e_{ij} e_{ij}}$, where $e_{ij} = \varepsilon_{ij} + \delta_{ij} \varepsilon_V / 3$ and δ_{ij} is the Kronecker delta. Similarly, the plastic volumetric strain is denoted as $\alpha_V = -\alpha_{ii}$ and the equivalent plastic shear strain is represented by $\alpha_S = \sqrt{2/3 e_{ij}^p e_{ij}^p}$, where $e_{ij}^p = \alpha_{ij} + \delta_{ij} \alpha_V / 3$. In addition, the hydrostatic pressure and the deviatoric stress are defined as $p = -I_1 / 3 = -\sigma_{ii} / 3$ and $q = \sqrt{3J_2} = \sqrt{3/2 s_{ij} s_{ij}}$, respectively, where $s_{ij} = \sigma_{ij} + \delta_{ij} p$.

For isothermal processes, the Helmholtz free energy potential is the same as the elastic strain energy and may be written as:

$$\Psi = (1 - D) \left[\frac{1}{2} K (\varepsilon_V - \alpha_V)^2 + \frac{3}{2} G (\varepsilon_S - \alpha_S)^2 \right] \quad (1)$$

where K is the bulk modulus and G is the shear modulus, and D is a scalar damage variable controlling the strength and stiffness degradation of the material [23, 24]. Despite the popularity of this type of isotropic damage formulation used in several well-regarded models [e.g. 8, 26, 46, 47, 57, 58], it has been pointed out [29, 73, 74] that this formulation cannot capture well the change in the Poisson's ratio due

to material deterioration. This is acknowledged as a shortcoming of the proposed approach, and this isotropic damage formulation is adopted here due to the simplicity in both the formulation and the physical interpretation of damage. The resolution of this problem may be the use of tensorial damage [29], or non-linear elasticity coupled with scalar damage [73, 74].

The stresses, p and q can be obtained from the Helmholtz free energy as follows:

$$p = \frac{\partial \Psi}{\partial \varepsilon_V} = (1-D)K(\varepsilon_V - \alpha_V) \quad (2)$$

$$q = \frac{\partial \Psi}{\partial \varepsilon_S} = (1-D)3G(\varepsilon_S - \alpha_S) \quad (3)$$

The generalised stresses $\bar{\chi}_V$, $\bar{\chi}_S$ and $\bar{\chi}_D$, associated with internal variables α_V , α_S and D , can also be obtained as:

$$\bar{\chi}_V = -\frac{\partial \Psi}{\partial \alpha_V} = (1-D)K(\varepsilon_V - \alpha_V) = p \quad (4)$$

$$\bar{\chi}_S = -\frac{\partial \Psi}{\partial \alpha_S} = (1-D)3G(\varepsilon_S - \alpha_S) = q \quad (5)$$

$$\bar{\chi}_D = -\frac{\partial \Psi}{\partial D} = \frac{1}{2}K(\varepsilon_V - \alpha_V)^2 + \frac{3}{2}G(\varepsilon_S - \alpha_S)^2 = \frac{p^2}{2K(1-D)^2} + \frac{q^2}{6G(1-D)^2} \quad (6)$$

In order to specify the coupling between damage and plasticity the following form of the dissipation rate function is proposed:

$$\Phi = \sqrt{\phi_V^2 + \phi_S^2 + \phi_D^2} + f_V \phi_V + f_S \phi_S \geq 0 \quad (7)$$

where ϕ_V , ϕ_S and ϕ_D are homogeneous first order functions in the rates of the internal variables ($\dot{\alpha}_V$, $\dot{\alpha}_S$ and \dot{D}), representing the effect of each dissipative mechanism on the total dissipation rate function, Φ . The dimensionless quantities f_V and f_S are functions of stresses and internal variables, which are responsible for controlling the direction of plastic flow vectors in the true stress space by moving the centre of yield surface in the dissipative stress space (Fig. 1). The physical meaning of these functions will be clearer when the formulation of yield surface will be considered in the dissipative stress space (Equation 17). The generic forms of these functions

along with the dissipation components (ϕ_v , ϕ_s and ϕ_D) used in the above equation are expressed as follows:

$$f_v = \frac{p - a \sqrt{E(p, q, D, \varepsilon_p)}}{F(p, q, D, \varepsilon_p)} \quad (8)$$

$$f_s = \frac{q - b \sqrt{E(p, q, D, \varepsilon_p)}}{F(p, q, D, \varepsilon_p)} \quad (9)$$

$$\phi_v = F(p, q, D, \varepsilon_p) \dot{\alpha}_v \quad (10)$$

$$\phi_s = F(p, q, D, \varepsilon_p) \dot{\alpha}_s \quad (11)$$

$$\phi_D = \frac{F(p, q, D, \varepsilon_p) \bar{\chi}_D}{\sqrt{r_d E(p, q, D, \varepsilon_p)}} \dot{D} \quad (12)$$

where ε_p is the accumulative effective plastic strain the rate of which is given as $\dot{\varepsilon}_p = \sqrt{2\dot{\alpha}_{ij}\dot{\alpha}_{ij}/3}$. In addition, $E(p, q, D, \varepsilon_p)$ and $F(p, q, D, \varepsilon_p)$ are functions of stresses and internal variables and define the form of the yield function in true stress space. Throughout the remainder of this paper, these functions are simply referred to as E and F for notational convenience. Functions a and b are used to control the energy dissipation due to plastic volumetric strain and equivalent shear plastic strain and also to control the direction of the plastic flow vector in the stress space (see Section 2.2 for more details). In addition, the function r_d , in Equation (12), controls the activation and evolution of damage processes. Further discussions on the role of the functions a , b and r_d and their relationship will be provided later when deriving the evolution rules for the internal variables. Considering the definitions given in Equations (8) – (12), the general condition required for thermodynamic admissibility ($\Phi \geq 0$) can be given as (see Appendix A):

$$|pa| \leq qb + r_d F \quad (13)$$

The above condition imposes some restrictions on the selection of model parameters and on the definition of generic functions when their explicit definitions are to be specified for constructing a material model. The further details illustrating the proof of thermodynamic admissibility of the constitutive models used in this study are provided in Appendix A.

The expression of the dissipation rate function as provided in Equation (7) offers some advantages over the existing models which employ similar expressions for the dissipation potential [68-70]. It facilitates to control the direction of plastic flow vector in the stress space for better simulations of dilative and contractive behaviour. Furthermore, the existence of a single generalised yield function which controls the simultaneous evolution of damage and plastic deformations arises as a consequence of expressing the dissipation rate function in the form of Equation (7). Within the framework of generalised thermodynamics, the yield function in generalised dissipative stress space (not true stress space) can be derived by performing a Legendre transformation on the dissipation rate function. Since the dissipation rate function is a homogeneous first order function in rates, this transformation is a degenerate special case of Legendre transformation [71, 72]. Using Equation (7), the generalised dissipative stresses [71] are defined as follows:

$$\chi_v = \frac{\partial \Phi}{\partial \dot{\alpha}_v} = \frac{\partial \Phi}{\partial \phi_v} \frac{\partial \phi_v}{\partial \dot{\alpha}_v} = \left(\frac{\phi_v}{\sqrt{\phi_v^2 + \phi_s^2 + \phi_D^2}} + f_v \right) \frac{\partial \phi_v}{\partial \dot{\alpha}_v} \quad (14)$$

$$\chi_s = \frac{\partial \Phi}{\partial \dot{\alpha}_s} = \frac{\partial \Phi}{\partial \phi_s} \frac{\partial \phi_s}{\partial \dot{\alpha}_s} = \left(\frac{\phi_s}{\sqrt{\phi_v^2 + \phi_s^2 + \phi_D^2}} + f_s \right) \frac{\partial \phi_s}{\partial \dot{\alpha}_s} \quad (15)$$

$$\chi_D = \frac{\partial \Phi}{\partial \dot{D}} = \frac{\partial \Phi}{\partial \phi_D} \frac{\partial \phi_D}{\partial \dot{D}} = \left(\frac{\phi_D}{\sqrt{\phi_v^2 + \phi_s^2 + \phi_D^2}} \right) \frac{\partial \phi_D}{\partial \dot{D}} \quad (16)$$

It is inferred from the above equations and Equations (10) – (12) that the generalised dissipative stresses are functions of the rates of all the internal variables. This is a consequence of expressing the dissipation function in the form of Equation (7), instead of using the usual additive form in earlier studies [8, 9, 46], in which dissipative stresses are dependent on the rate of their associated internal variable only. Material models constructed based on the proposed formulation will benefit from possessing a single loading function, which is obtained from the Legendre transformation of the dissipation function, instead of two separate loading functions corresponding to damage and plasticity, had the additive form of the dissipation potential been used. Equations (14) – (16) can be used to obtain a single generalised loading function as:

$$y^* = \left(\frac{\chi_V}{\partial \phi_V / \partial \dot{\alpha}_V} - f_V \right)^2 + \left(\frac{\chi_S}{\partial \phi_S / \partial \dot{\alpha}_S} - f_S \right)^2 + \left(\frac{\chi_D}{\partial \phi_D / \partial \dot{D}} \right)^2 - 1 \leq 0 \quad (17)$$

As illustrated in Figure 1, the above loading function represents an ellipsoid with its centre at the point $(f_V \frac{\partial \phi_V}{\partial \dot{\alpha}_V}, f_S \frac{\partial \phi_S}{\partial \dot{\alpha}_S}, 0)$ in the generalised dissipative stress space (χ_V, χ_S, χ_D) . The radii of this ellipsoid are also denoted by $l = \partial \phi_V / \partial \dot{\alpha}_V$, $m = \partial \phi_S / \partial \dot{\alpha}_S$ and $n = \partial \phi_D / \partial \dot{D}$ (Fig. 1).

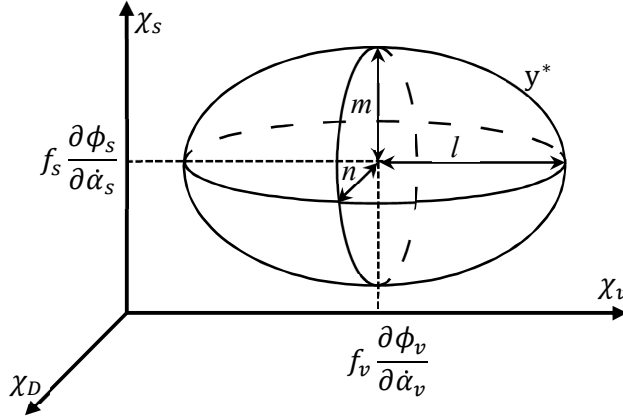


Figure 1: Geometric interpretation of the yield potential in generalised dissipative stress space

With the evolution of internal variables upon yielding, the size of the loading surface and its position in generalised dissipative stress space will vary, however, its centre will always remain in the (χ_V, χ_S) plane (Equation (17)). The evolution of plastic strains and the scalar damage variable can be determined using this loading function and by taking its derivatives with respect to the corresponding generalised dissipative stresses. Therefore, by making use of Equations (4), (5), (8) – (12) and (17), the evolution rules are derived as:

$$\dot{\alpha}_V = \dot{\lambda} \frac{\partial y^*}{\partial \chi_V} = 2 \dot{\lambda} \left(\frac{a \sqrt{E}}{F^2} \right) \quad (18)$$

$$\dot{\alpha}_S = \dot{\lambda} \frac{\partial y^*}{\partial \chi_S} = 2 \dot{\lambda} \left(\frac{b \sqrt{E}}{F^2} \right) \quad (19)$$

$$\dot{D} = \dot{\lambda} \frac{\partial y^*}{\partial \chi_D} = 2 \dot{\lambda} \frac{r_d E}{F^2 \chi_D} \quad (20)$$

where λ is a non-negative multiplier. In deriving the above equations, a constitutive postulate (i.e. $\chi_v = \bar{\chi}_v$ and $\chi_s = \bar{\chi}_s$) equivalent to Ziegler's orthogonality condition [71] is invoked. It is deduced, from Equations (18) - (20), that the plastic flow vector is always normal to the loading surface in the generalised dissipative stress space, regardless of the plastic flow being associated or non-associated in true stress space. Furthermore, by making use of Equations (4) – (6) and substitution of Equations (8) – (12) into Equation (17), the general form of the yield function in true stress space can be given as:

$$y = (a^2 + b^2 + r_d)E - F^2 = 0 \quad (21)$$

As can be seen in Equation (21) for the yield function, a , b and r_d will affect the initial shape and size of the yield surface. As these functions a , b and r_d are also involved in the evolution rules for plastic strains and the scalar damage variable (Equations (18) – (20)), they will have effects on the evolution of the yield surface. It should be noted that the evolution of the yield surface in a damage-plasticity model is governed by both damage and plastic strains. In this sense, the functions a , b and r_d will have both direct (Equation (21)) and indirect (Equations (18) – (20)) influence on the evolution of the yield surface. In order to simplify the calibration procedure of the initial yield surface against experimental data, the effects of model parameters on the initial the yield surface, and its evolution need to be separated. In other words, the calibration of the initial yield can be independent from its evolution. For this purpose, the following conditions are imposed to eliminate the direct effects of a , b and r_d on the initial size and shape of the yield function in true stress space:

$$a^2 + b^2 = r_p \quad \text{and} \quad r_d + r_p = 1 \quad (22)$$

By imposing the above conditions, the functions a , b and r_d will only control the evolution of the yield surface and not its initial size and shape in true stress space. Accordingly, a user input with $r_d = 1$ implies that damage is the only active dissipative mechanism and no plastic deformation will take place, whereas the reverse is true when $r_p = 1$. For all other cases ($0 < r_d < 1$ and $0 < r_p < 1$), damage and plasticity occur together, while $r_d > r_p$ (or $r_p > r_d$) indicates that damage (or plasticity) is the dominant mechanism. Therefore, in order to control the coupling between damage and plasticity, the model requires only one input parameter r_d (or

r_p). Similarly, for controlling the direction of plastic flow vector in stress space, only one parameter a (or b) is needed. Finally, by imposing the condition of Equation (22) on Equation (21), the general form of the yield in true stress space is expressed as:

$$y = E - F^2 = 0 \quad (23)$$

The explicit form of the yield function can be determined by specifying the functions E and F which in turn are defined on the basis of the specific application and the problem to be solved. Further discussion on the various forms of these functions E and F is provided in Section 3. In addition, it is important to examine the proportion of energy dissipation due to damage and plasticity relative to the total dissipation rate (defined as R_D and R_P , respectively). Since for rate independent material behaviour, the dissipation potential is a homogeneous first-order function in terms of the rates of internal variables [71], by making use of Euler's theorem for homogeneous functions, the dissipation function can be written as:

$$\Phi = \frac{\partial \Phi}{\partial \dot{\alpha}_V} \dot{\alpha}_V + \frac{\partial \Phi}{\partial \dot{\alpha}_S} \dot{\alpha}_S + \frac{\partial \Phi}{\partial \dot{D}} \dot{D} = \chi_V \dot{\alpha}_V + \chi_S \dot{\alpha}_S + \chi_D \dot{\alpha}_D = \Phi_V + \Phi_S + \Phi_D \geq 0 \quad (24)$$

where Φ_V , Φ_S and Φ_D are the dissipation rate functions corresponding to plastic volumetric deformation, plastic shear deformation and damage, respectively (note that they are different form functions ϕ_V , ϕ_S and ϕ_D in Equation (7)). As the functions Φ_V , Φ_S and Φ_D can be written explicitly in term of stresses (see Appendix B), the ratios between the dissipation rate due to plasticity or damage and the total dissipation rate can be obtained as follows:

$$\frac{\Phi_D}{\Phi} = \frac{r_d \sqrt{E}}{r_d \sqrt{E} + pa + qb} \quad (25)$$

$$\frac{\Phi_V + \Phi_S}{\Phi} = \frac{pa + qb}{r_d \sqrt{E} + pa + qb} \quad (26)$$

Also, the expressions of Φ_V and Φ_S (Appendix B) can be used to obtain the ratio between the dissipation rates associated with volumetric and shear components of the plastic deformations (\bar{R}_P) as:

$$\frac{\Phi_V}{\Phi_S} = \frac{pa}{qb} \quad (27)$$

In order to facilitate the calibration of model parameters, the total dissipated energy during the entire course of deformation are calculated and compared with the experimentally measured total dissipation. This can be achieved if the total dissipation rate function can be expressed as an integrable function in terms of the rate of one internal variable. For instance, the total dissipation rate function can be expressed as a homogeneous first order function in term of $\dot{\alpha}_s$ as (see Appendix B):

$$\Phi = \left(\frac{r_d \sqrt{E}}{b} + \frac{pa}{b} + q \right) \dot{\alpha}_s = \Gamma(\alpha_s) \dot{\alpha}_s \quad (28)$$

The final form of $\Gamma(\alpha_s)$ is determined by specifying the function E . The above discussion is further clarified through an example, given in Section 3.1, for a one-dimensional Von Mises model, where an explicit form of the total energy dissipation (fracture energy) is obtained by integrating the dissipation rate function.

2.2. Controlling the direction of plastic flow vector

As discussed previously, the evolutions of plastic strains (Equations (18) – (19)) can be controlled by functions a (or b) and r_d (or r_p), where the relationship between these functions is given through the conditions of Equation (22). In this regard, Equations (18) and (19) can be used to give the ratio between the rates of plastic volumetric strain and equivalent shear plastic strain as:

$$\frac{\dot{\alpha}_v}{\dot{\alpha}_s} = \frac{a}{b} \quad (29)$$

As mentioned earlier, the plastic flow vector is always normal to the loading surface y^* in the generalised dissipative stress space. However, it is normal to the yield surface y in p - q stress space only if the flow rule is associated, where it will satisfy the following condition:

$$\frac{a}{b} = \frac{\partial y / \partial p}{\partial y / \partial q} \quad (30)$$

In order to control the ratio between the plastic volumetric strain and the equivalent shear plastic strain rates for simulating non-associated flow, a dimensionless function c can be introduced as:

$$\frac{a}{b} = c \frac{\partial y / \partial p}{\partial y / \partial q} \quad (31)$$

where the flow rule is associated if $c = 1$, and it is non-associated if $c \neq 1$. By making use of the conditions of Equation (22) functions, a and b can be expressed in term of c as follows:

$$a = \pm \sqrt{\frac{c^2 r_p}{c^2 + \left(\frac{\partial y / \partial q}{\partial y / \partial p}\right)^2}} \quad (32)$$

$$b = \sqrt{\frac{r_p}{1 + c^2 \left(\frac{\partial y / \partial p}{\partial y / \partial q}\right)^2}} \quad (33)$$

Thus, a and b can, in general, be determined indirectly by defining the function c . Following the sign convention adopted in this study (compression is positive), positive values of a ($a > 0$) correspond to plastic compaction, whereas negative values of a ($a < 0$) indicate plastic dilation (see Equations (18) and (19)). Furthermore, $a = 0$ implies pure plastic shear deformations (no plastic volumetric deformation), which is commonly observed in metals. The role of the function c in modelling the material behaviour and its influences on the plastic flow direction is illustrated by providing an example in Section 3.

2.3. Tangent stiffness tensor

In this section, the formulation of the tangent stiffness tensor C_{ijkl}^t is presented as it may be necessary for integration of the rate equations if an explicit integration scheme is used. The stress tensor can be given, by making use of Equation (1) as:

$$\sigma_{ij} = \frac{\partial \Psi}{\partial \varepsilon_{ij}} = \frac{\partial \Psi}{\partial \varepsilon_V} \frac{\partial \varepsilon_V}{\partial \varepsilon_{ij}} + \frac{\partial \Psi}{\partial \varepsilon_S} \frac{\partial \varepsilon_S}{\partial \varepsilon_{ij}} = (1-D) (K \varepsilon_V^e \delta_{ij} + 2G e_{ij}^e) = (1-D) C_{ijkl} (\varepsilon_{kl} - \alpha_{kl}) \quad (34)$$

From the above equation, the incremental stress tensor can be determined as:

$$\dot{\sigma}_{ij} = (1-D) C_{ijkl} (\dot{\varepsilon}_{kl} - \dot{\alpha}_{kl}) - \frac{\sigma_{ij}}{(1-D)} \dot{D} \quad (35)$$

Furthermore, Equations (18) and (19) can be used to obtain the incremental plastic strain tensor $\dot{\alpha}_{ij}$, which can be written as:

$$\dot{\alpha}_{ij} = \dot{\lambda} \frac{\partial y^*}{\partial \chi_{ij}} = \dot{\lambda} \left(\frac{\partial y^*}{\partial \chi_V} \frac{\partial \chi_V}{\partial \sigma_{ij}} + \frac{\partial y^*}{\partial \chi_S} \frac{\partial \chi_S}{\partial \sigma_{ij}} \right) \quad (36)$$

The consistency condition can now be written by utilising the yield function of Equation (23) as:

$$\dot{y} = \frac{\partial y}{\partial \sigma_{ij}} \dot{\sigma}_{ij} + \frac{\partial y}{\partial \varepsilon_p} \dot{\varepsilon}_p + \frac{\partial y}{\partial D} \dot{D} = 0 \quad (37)$$

where the rate of effective plastic strain $\dot{\varepsilon}_p$ can be obtained using Equation (36) as:

$$\dot{\varepsilon}_p = \sqrt{\frac{2}{3} \dot{\alpha}_{ij} \dot{\alpha}_{ij}} = \dot{\lambda} \sqrt{\frac{2}{3} \frac{\partial y^*}{\partial \chi_{ij}} \frac{\partial y^*}{\partial \chi_{ij}}} \quad (38)$$

Therefore, the non-negative multiplier $\dot{\lambda}$ is obtained, by making use of Equations (20) and (35) – (38), as:

$$\dot{\lambda} = M_{kl} \dot{\varepsilon}_{kl} \quad (39)$$

where

$$M_{kl} = \frac{(1-D) \frac{\partial y}{\partial \sigma_{ij}} C_{ijkl}}{(1-D) \frac{\partial y}{\partial \sigma_{ij}} C_{ijkl} \frac{\partial y^*}{\partial \chi_{kl}} + \frac{\partial y}{\partial \sigma_{ij}} \frac{\sigma_{ij}}{1-D} \frac{\partial y^*}{\partial \chi_D} - \frac{\partial y}{\partial \varepsilon_p} \sqrt{\frac{2}{3} \frac{\partial y^*}{\partial \chi_{ij}} \frac{\partial y^*}{\partial \chi_{ij}} - \frac{\partial y}{\partial D} \frac{\partial y^*}{\partial \chi_D}}} \quad (40)$$

Finally, the incremental stress-strain relationship is expressed as:

$$\dot{\sigma}_{ij} = \left[(1-D) C_{ijkl} - (1-D) C_{ijst} \frac{\partial y^*}{\partial \chi_{st}} M_{kl} - \frac{\sigma_{ij}}{1-D} M_{kl} \frac{\partial y^*}{\partial \chi_D} \right] \dot{\varepsilon}_{kl} = C_{ijkl}^t \dot{\varepsilon}_{kl} \quad (41)$$

where C_{ijkl}^t represents the tangent stiffness tensor.

2.4. Stress Return Algorithm

Numerical implementations require the stress state be updated for a given strain increment. For infinitesimal increments in strains, stresses can be updated explicitly using the tangent stiffness or a forward-Euler scheme. However, in practical applications, the strain field within a structure is not uniform and hence, strain increments at material points (e.g. Gauss points in FEM) may not be infinitesimal throughout the body and consequently, the updated stresses may lie outside the yield surface. Unless the stresses are corrected and returned onto the yield surface, the forward-Euler scheme may give rise to erroneous values for stresses at the material point which in turn may result in a divergence in numerical scheme applied

for satisfying equilibrium equations at the structural level. Hence, a form of backward-Euler scheme is adopted here to return the stresses to the yield surface following an elastic trial predictor. Returning procedures, which involve returning the trial stresses onto a new yield surface (in cases of hardening or softening), are activated only if the trial stresses lie outside the yield surface. To this end, the new yield surface is approximated at the trial stress values using a first order Taylor expansion as follows:

$$y^{n+1} = y^{trial} + \frac{\partial y}{\partial \sigma_{ij}} \Delta \sigma_{ij}^{re} \Big|^{trial} + \frac{\partial y}{\partial \varepsilon_p} \Delta \varepsilon_p \Big|^{trial} + \frac{\partial y}{\partial D} \Delta D \Big|^{trial} = 0 \quad (42)$$

As the strain increment has been utilised to move to trial stress values, the return stress increments, $\Delta \sigma_{ij}^{re}$, in the above equation can be obtained as:

$$\Delta \sigma_{ij}^{re} = \sigma_{ij}^{n+1} - \sigma_{ij}^{trial} = \left[-(1-D) C_{ijkl} \Delta \alpha_{kl} - \frac{\sigma_{ij}}{(1-D)} \Delta D \right] \Big|^{trial} \quad (43)$$

This stress return algorithm is slightly different from a full backward-Euler scheme in which $\Delta \sigma_{ij}^{re}$ are calculated as normal to the new yield surface (y^{n+1}) by applying an iterative scheme. By substituting Equations (20), (36), (38) and (43) into Equation (42), the non-negative multiplier $\Delta \lambda$ can be obtained as follows:

$$\Delta \lambda = \frac{y^{trial}}{\frac{\partial y}{\partial \sigma_{ij}} \left[(1-D) C_{ijkl} \frac{\partial y^*}{\partial \sigma_{kl}} + \frac{\sigma_{ij}}{(1-D)} \frac{\partial y^*}{\partial \chi_D} \right] \Big|^{trial} - \frac{\partial y}{\partial \varepsilon_p} \dot{\lambda} \sqrt{\frac{2}{3}} \frac{\partial y^*}{\partial \chi_{ij}} \frac{\partial y^*}{\partial \chi_{ij}} \Big|^{trial} - \frac{\partial y}{\partial D} \dot{\lambda} \frac{\partial y^*}{\partial \chi_D} \Big|^{trial}} \quad (44)$$

Therefore, the final updated stresses can be obtained as:

$$\sigma_{ij}^{n+1} = \sigma_{ij}^{trial} + \Delta \sigma_{ij}^{re} = \sigma_{ij}^{trial} - (1-D) C_{ijkl} \Delta \lambda \frac{\partial y^*}{\partial \sigma_{kl}} - \frac{\sigma_{ij}}{(1-D)} \Delta \lambda \frac{\partial y^*}{\partial \chi_D} \quad (45)$$

3. Applications

In this section, the applicability of the proposed formulation for modelling the inelastic behaviour of a wide range of materials is discussed and its promising features are demonstrated through some numerical examples. In each case, the model predictions are validated against experimental data available in the literature. In what follows, firstly, the features of the proposed formulation are illustrated

through coupling damage with the Von Mises plasticity model, which is widely utilised for modelling the behaviour of pressure independent materials. Secondly, the influence of the plastic flow direction on the material response is investigated through the development of a coupled damage plasticity model for pressure dependent materials based on the parabolic Drucker-Prager yield function. Finally, through constructing a new model for cohesive frictional geomaterials, it is demonstrated that the proposed formulation can also facilitate the development of new elastoplastic damage models.

On the other hand, it should be noted that the focus of this paper is on the development of a thermodynamic-based formulation at the constitutive level and the issues related to material stability of the model in solving Boundary Value Problems are not considered in this study. The enhancements of the proposed models using nonlocal theory or viscous regularization for effectively dealing with the issues related to solution of boundary value problems will be the next step of developments. Our experience with these kinds of regularisation [8, 9, 32, 70, 81, 82] showed that these techniques can be readily added to obtain discretisation-independent numerical solutions.

3.1. Coupling damage with the Von Mises plasticity model

The yield function of the classical Von Mises model in the $(p - q)$ stress space can be written in the following form:

$$y = \sqrt{3J_2} - k(D, \varepsilon_p) = q - k(D, \varepsilon_p) = 0 \quad (46)$$

The exclusion of pressure (or the first invariant of stresses I_1) in the above expression indicates its pressure independency. In order to incorporate the effects of plastic deformations and damage in the model the shear strength, k is defined as a function of two internal variables, namely, the scalar damage variable, D and accumulated plastic strain, ε_p as:

$$k = (1 - D) \left(f_y + Q \left(1 - e^{-H\varepsilon_p} \right) \right) \quad (47)$$

where f_y and Q are the initial yield and the ultimate stresses, respectively, and H is a material parameter which determines the rate of expansion/contraction of the yield surface. It can be seen from Equations (46) and (47) that the evolution of the yield surface is governed by evolutions of damage D and equivalent plastic strain

ε_p , where the evolution of ε_p is defined by Equation (38). Comparing Equation (46) with the generic form of yield function as stated by Equation (23), it can be inferred that $E = q$ and $F^2 = k$ for von Mises yield function. Therefore, the flow rules can be obtained by making use of Equations (18) – (20) as follows:

$$\dot{\alpha}_V = 2\dot{\lambda} \frac{a\sqrt{q}}{k} \quad (48)$$

$$\dot{\alpha}_S = 2\dot{\lambda} \frac{b\sqrt{q}}{k} \quad (49)$$

$$\dot{D} = 2\dot{\lambda} \frac{r_d q}{k \bar{\chi}_D} \quad (50)$$

In addition, the plastic flow rule in the tensorial form can be derived using Equation (36) as:

$$\dot{\alpha}_{ij} = \dot{\lambda} \frac{\partial y^*}{\partial \chi_{ij}} = \dot{\lambda} \left(2 \frac{a\sqrt{q}}{k} \frac{\delta_{ij}}{3} + 2 \frac{b\sqrt{q}}{k} \frac{3}{2\sqrt{3}J_2} \frac{\partial J_2}{\partial \sigma_{ij}} \right) \quad (51)$$

The stress-strain response produced by the above model definitions is illustrated in Figure 2. The effect of different levels of damage activity, for different values of r_d , can also be observed in Figure 2. Also, the model parameters used are: Young's modulus = 200000 MPa, Poisson's ratio (ν) = 0.3, $f_y = 250$ MPa, $Q = 50$ MPa and $H = 1000$. It should be noted that the incompressibility condition ($\dot{\alpha}_V = 0$) of the Von Mises model can be accounted for by setting $a = 0$. In Figure 2, the curve associated with $r_d = 0$ indicates a pure plastic deformation of the material without having any damage, while for other cases, where the damage and plastic deformations evolve together ($0 < r_d < 1$), the effect of damage is observed as reduction in the ultimate stress and the softening behaviour (Figure 2).

In general, the strain hardening behaviour of ductile metals (e.g. steel) under uniaxial tensile loading is accompanied by an insignificant reduction in stiffness immediately after the initial yielding. For these materials, softening behaviour is observed after the ultimate stress is reached followed by complete failure of the material. This behaviour can be replicated by making use of the enhanced Von Mises model, introduced here, by controlling the degree of activation of damage and plasticity. For instance, damage can be switched off during the strain hardening

process, where no considerable stiffness reduction is observed (Figure 3(a)), by setting $r_d = 0$ (see Equations (48) – (50)).

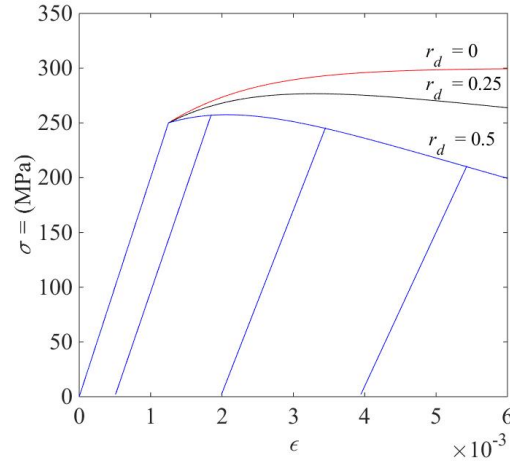


Figure 2: Stress-strain response of a coupled damage-plasticity model based on Von Mises model under uniaxial stress condition for various values of r_d .

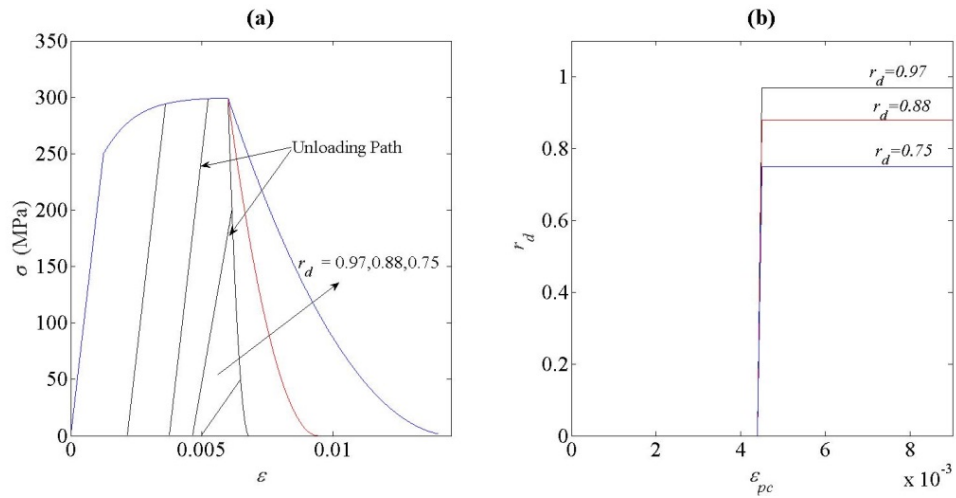


Figure 3: (a) Effects of different values of r_d on the stress-strain response of steel under uniaxial tension (b) Corresponding values of r_d for activation of damage mechanism at a critical value of plastic strain $\epsilon_{pc} = 4.5 \times 10^{-3}$.

The softening behaviour, however, can be modelled through activation of damage by using a value of r_d greater than 0, once the accumulated plastic strain reaches a critical value ϵ_{pc} (Figure 3(b)). As illustrated in Figure 3 (a), higher values of r_d correspond to more brittle behaviour with steeper slopes in the post-peak response. Furthermore, the stress-strain response of Aluminium Alloy 6082 under uniaxial tension [75] can be adequately captured by the proposed model as illustrated in

Figure 4. The model parameters used for this analysis are: Young's modulus = 30000 MPa, Poisson's ratio (ν) = 0.3, $f_y = 40$ MPa, $Q = 85$ MPa, $H = 50$, and $\varepsilon_{pc} = 0.48$ and $r_d = 0.97$.

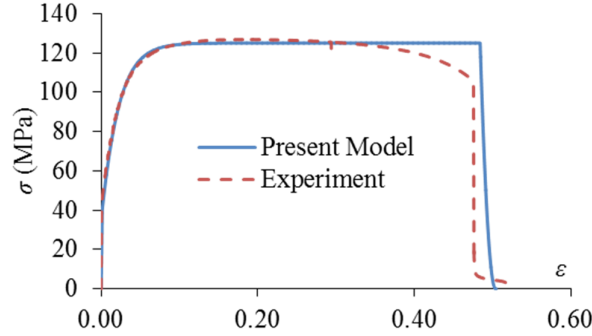


Figure 4: Stress-strain response of Aluminium Alloy 6082 under uniaxial tension. Damage is activated at a critical value of the plastic strain $\varepsilon_{pc} = 0.48$ and $r_d = 0.97$.

As discussed earlier in Section 2, the calibration of model parameters can be facilitated by calculating the total energy dissipation during the course of inelastic deformation and also by comparing the calculated and experimentally measured total dissipated energy. The explicit analytical expression of the total dissipation for the enhanced Von Mises model under uniaxial stress condition is provided in Appendix C.

3.2. Coupling damage with the parabolic Drucker-Prager plasticity model

Figure 5 illustrates a typical yield surface of plain epoxy resin which has a parabolic shape in its initial and final yielding states [76]. In this section, based on the coupling scheme of the generic formulation, the parabolic Drucker-Prager model is enhanced by coupling this pressure-dependent plasticity model with damage. In addition, the non-associated flow and inelastic volumetric deformations (dilation and compaction) are successfully modelled thanks to the coupling scheme of the proposed generic formulation.

The parabolic Drucker-Prager yield function can be expressed in terms of pressure p and deviatoric stress q as:

$$y = 3J_2 + \frac{\alpha}{3}I_1 - \beta(D, \varepsilon_p) = q^2 - \alpha p - \beta(D, \varepsilon_p) = 0 \quad (52)$$

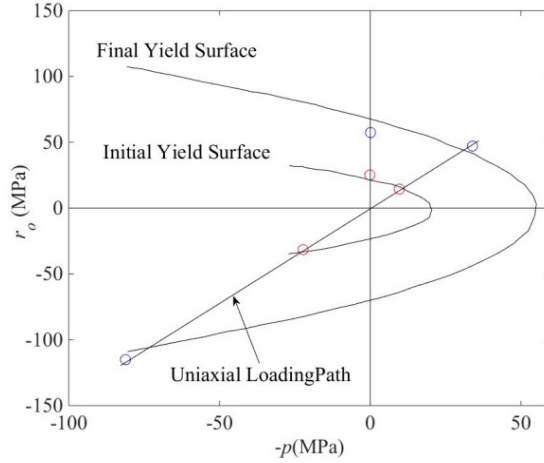


Figure 5: Parabolic Drucker-Prager yield function applied to plain epoxy resin [76] where $\tau_o = \pm\sqrt{\frac{9}{2}}q$ is the octahedral shear stress (Circles indicate experimental data points).

The parameters α and β in the above expression are given as:

$$\beta = f_{cy}f_{ty} \text{ and } \alpha = 3(f_{cy} - f_{ty}) \quad (53)$$

where f_{cy} and f_{ty} are the uniaxial yield stress in compression and tension, respectively. It is assumed that, f_{cy} and f_{ty} will vary progressively with the evolution of plastic deformation and therefore their dependency on the damage variable and accumulated plastic strain can be defined as:

$$f_{cy} = (1 - D)(f_{c0} + Q_c(1 - e^{-H_c \epsilon_p})); \text{ and } f_{ty} = (1 - D)(f_{t0} + Q_t(1 - e^{-H_t \epsilon_p})) \quad (54)$$

where f_{t0} and f_{c0} are initial yield stresses, and Q_t , Q_c , H_t , H_c are material constants with subscript t and c corresponding to tension and compression, respectively. The growth of damage will progressively reduce the values of α and β leading to the contraction of the yield surface (Equation (54)). On the other hand, the growth the effective plastic strain ϵ_p will give rise to the expansion of the yield surface. By comparing Equation (52) with Equation (23), it is deduced that E and F can be defined as: $E = q^2 - \alpha p$ and $F^2 = \beta$. With these expressions of E and F , the flow rules can be obtained using Equations (18) – (20) as follows:

$$\dot{\alpha}_v = 2\lambda \frac{a\sqrt{q^2 - \alpha p}}{k} \quad (55)$$

$$\dot{\alpha}_s = 2\lambda \frac{b\sqrt{q^2 - \alpha p}}{k} \quad (56)$$

$$\dot{D} = 2\lambda \frac{r_d(q^2 - \alpha p)}{\beta \chi_D} \quad (57)$$

Furthermore, by making use of Equation (34), the plastic flow rule is obtained in its tensorial form as:

$$\dot{\alpha}_{ij} = \lambda \frac{\partial y^*}{\partial \sigma_{ij}} = \lambda \left(2 \frac{a\sqrt{q^2 - \alpha p}}{\beta} \frac{(-\delta_{ij})}{3} + 2 \frac{b\sqrt{q^2 - \alpha p}}{\beta} \frac{3}{2\sqrt{3}J_2} \frac{\partial J_2}{\partial \sigma_{ij}} \right) \quad (58)$$

3.2.1. The effect of r_d and c on the model response

The stress-strain response of the coupled damage-plasticity model based on the parabolic Drucker-Prager yield function, for uniaxial loading, is illustrated in Figure 6. The parameters used for this analysis are: young's modulus = 35000 MPa, Poisson's ratio (ν) = 0.18, $f_{t0} = 5$ MPa, $f_{c0} = 10$ MPa, $Q_t = 15$ MPa, $Q_c = 30$ MPa, $H_t = 2000$, $H_c = 2000$. The effect of r_d on the material behaviour is also shown in Figure 6, where r_d varies from 0 (no damage activation) to 0.18. As can be observed in Figure 6 a higher value of r_d leads to a higher level of damage activity gives rise to a lower ultimate stress with a more significant softening behaviour.

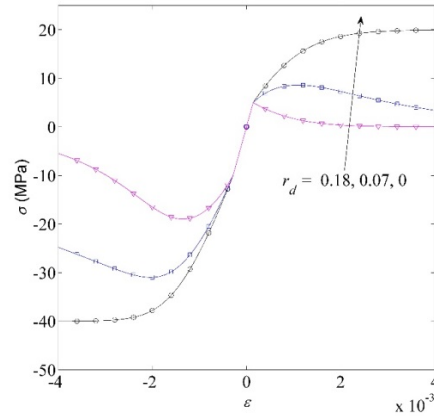


Figure 6: Effect of r_d on the stress-strain response of a material under uniaxial loading based on the associated flow rule.

The direction of the plastic flow vector in stress space is indicative of the level of contribution of the volumetric and the shear plastic strains to the total plastic dissipation. In addition, dilational and/or contractive modes of deformation give rise to different directions of the plastic flow vector in stress space. The reverse scenario is, however, pursuit here as the model response is controlled by the

direction of the plastic flow vector in stress space. The variation in the model behaviour due to changes in the direction of plastic flow vector (different values of the parameter c) is illustrated in Figure 7. Cases with $c > 1$ correspond to larger plastic volumetric strain rates, with the plastic flow vector being more inclined towards the p axis in the $(p - q)$ stress space, compared to that in the case of associated flow ($c = 1$), and the reverse is true for cases with $c < 1$. In addition, a higher value of c gives rise to more dilational behaviour, as illustrated in Figure 7 (b).

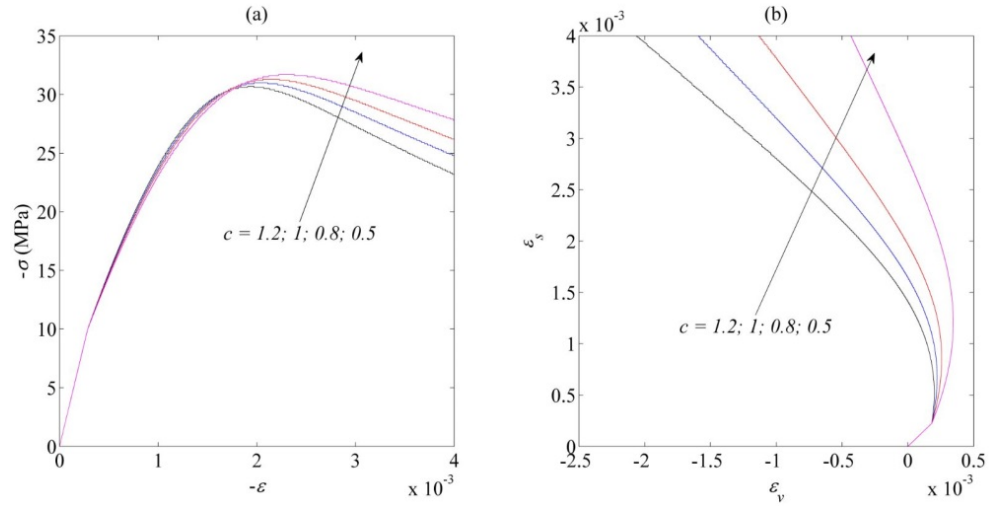


Figure 7: (a) Effect of c on the stress-strain response of a material under uniaxial compression ($r_d = 0.07$), (b) Effect of c on the total volumetric strain and equivalent shear strain under uniaxial compression ($r_d = 0.07$).

3.2.2. Behaviour of concrete under uniaxial cyclic loading

The nonlinear responses of concrete materials under cyclic tensile and compressive loading [77] are predicted by the proposed model and the results obtained are presented in Figure 8. The model parameters used for the tensile loading are: young's modulus = 31700 MPa, Poisson's ratio (ν) = 0.18, $f'_t = 3.48$ MPa, $f_{t0} = 3.48$ MPa, $f_{c0} = 10$ MPa, $Q_t = 0$ MPa, $Q_c = 15$ MPa, $H_t = 0$, $H_c = 1000$ and $r_d = 0.14$. Figure 8 (a) shows a reasonable agreement between the model prediction and the experimental data.

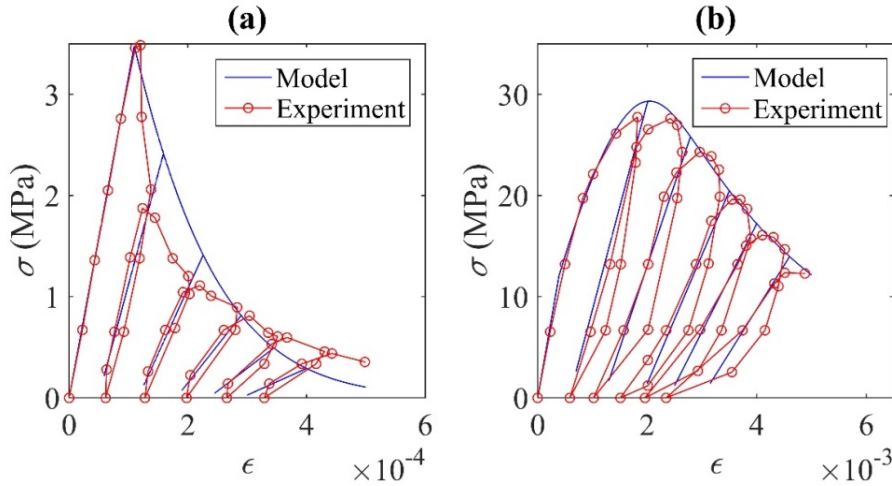


Figure 8: Behaviour of concrete under cyclic loading: (a) uniaxial tension (experimental data obtained from [77]); (b) uniaxial compression (experimental data obtained from [78])

In addition, Figure 8 (b) compares the model prediction with the experimental data from cyclic compressive loading on concrete [78]. In this case, the model parameters used are: young's modulus = 31000 MPa, Poisson's ratio (ν) = 0.18, $f'_c = 27.6$ MPa, $f_{t0} = 3.48$ MPa, $f_{c0} = 12$ MPa, $Q_t = 0$ MPa, $Q_c = 38$ MPa, $H_t = 0$, $H_c = 1600$ and $r_d = 0.28$. Figure 8(b) also shows a very good agreement between the model predictions and the experimental data which indicates a successful performance of the proposed model.

3.2.3. Dilation of unconfined concrete under uniaxial compression

The dilative or contractive behaviour of material models constructed following the proposed generic formulation can be controlled by appropriately defining the parameter c (or functions a and b (see Section 3.3)). The experimental results of an unconfined concrete specimen under uniaxial compression [79] is used to determine the variation of parameter c with respect to the equivalent shear strain ϵ_s , as illustrated in Figure 9.

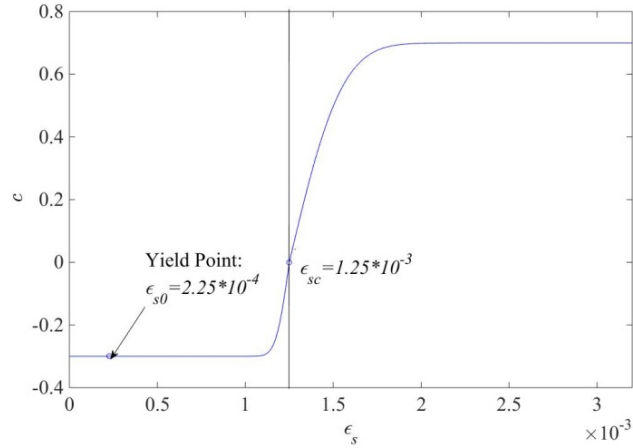


Figure 9: Evolution of c for unconfined concrete under uniaxial compression.

The nonlinear response of the concrete specimen is predicted by the proposed model using material properties as; young's modulus = 35000 MPa, Poisson's ratio (ν) = 0.18, $f'_t = 2.4$ MPa, and $f'_c = 32$ MPa [78]. The model parameters used are: $f_{t0} = 2.4$ MPa, $f_{c0} = 10$ MPa, $Q_t = 0$ MPa, $Q_c = 29$ MPa, $H_t = 0$, $H_c = 2600$ and $r_d = 0.17$ along with the values of c as indicated in Figure 9. The comparison between the model prediction and experimental data, as illustrated in Figure 10, highlights the capability of the proposed model.

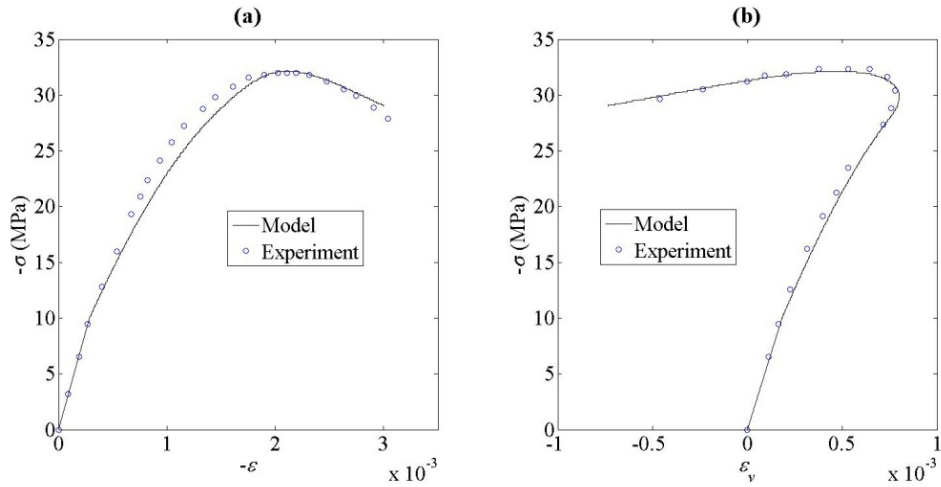


Figure 10: (a) Stress-strain response of concrete under uniaxial compressive loading; (b) Variation of volumetric strain (experimental validation).

3.3. Development of an elastoplastic damage model for cohesive-frictional geomaterials

In laboratory experiments, inelastic deformation of cohesive-frictional geomaterials such as rocks, hard clays, etc., is observed as a reduction in stiffness and strength as well as the occurrence of residual strains. The failure process begins with a relatively uniform distribution of micro-cracks throughout the material followed by localisation of microcracks within a band which finally leads to the formation of a macro-crack and then shear sliding of the two faces of the macroscopic fracture. A common strategy for modelling such failure process is to employ a yield function or a plastic potential, which controls the evolution of dissipative processes (damage and plasticity), for the states before the formation of the final macro-fracture, and a separate failure function to describe the shear sliding between the two faces of the macro-fracture [36]. In this section, specific definitions of the functions E and F , in the generic formulation, are given so that a single-surface yield function in true stress space is obtained. This yield surface is then transformed to a final failure function as the scalar damage variable grows from zero to one. This is a promising feature of this model which facilitates capturing the brittle and ductile responses as well as the brittle-ductile transition, without any need for separately introducing hardening/softening rules. It is also demonstrated briefly that the features of proposed generic formulation facilitate the modelling of dilative and contractive responses of cohesive geomaterials.

3.3.1. The yield function

In order for the model to be capable of capturing the inelastic volumetric deformation of the material under isotropic compression (or expansion), it is required that the yield function have a closed envelope in the principal stress space. Hence, a single-surface yield function with a tear-drop shape in true stress space [4] is derived following the structure of the proposed generic formulation. In this regard, the damage is incorporated in the model formulation in such a way that the initial yield function is transformed gradually into a linear frictional failure function as the damage variable grows from zero to unity. To this end, the functions E and F in Equations (8) – (12) are defined as follows:

$$E = \left[\frac{(1-D)(p-\rho) \left(p - \sqrt{(1-D)} \omega (p-\rho) \right)}{\left(\frac{(1-\gamma)p_c - p_t}{p_c + p_t} \right) p + \frac{1}{2}(1-D)\gamma p_c} \right]^2 + \left[\frac{q}{M} \right]^2 \quad (59)$$

$$F = p - \sqrt{(1-D)} \omega (p-\rho) \quad (60)$$

In the above expressions, $0 \leq \omega \leq 1$ and $0 \leq \gamma \leq 1$ are materials parameters while p_c and p_t represent pressures at initial yield under isotropic compression and expansion, respectively. The parameter M represents the slope of the final failure envelope in true stress space. By making use of the above definitions and the general form of the yield function, given by Equation (23), the yield function in true stress space is obtained as:

$$y = \left(\frac{(1-D)(p-\rho)}{\left(\frac{(1-\gamma)p_c - p_t}{p_c + p_t} \right) p + \frac{1}{2}(1-D)\gamma p_c} \right)^2 + \left(\frac{q}{M(p - \sqrt{(1-D)} \omega (p-\rho))} \right)^2 - 1 = 0 \quad (61)$$

In the above expressions, parameter ρ represents the pressure at the intersection of the final failure envelope and the initial yield surface and it can be calculated by considering the yield condition under isotropic compression as:

$$\rho = \frac{(4-\gamma)p_c p_t + \gamma p_c^2}{2(p_c + p_t)} \quad (62)$$

In addition, for $\gamma = \omega = 1$ and $p_t = 0$ the yield function of Equation (61) is the same as the modified Cam-Clay. Figure 11 illustrates the evolution of the yield surface with damage growth and the transformation of the initial yield surface to the final failure surface when the damage variable is one.

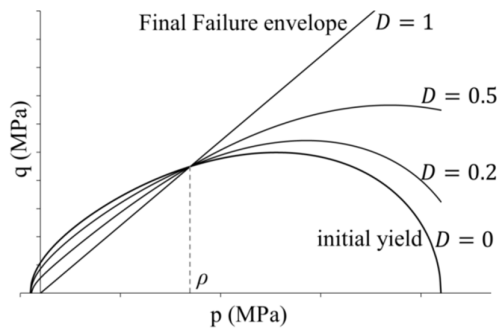


Figure 11: Evolution of the yield surface with damage growth.

3.3.2. Dilative and contractive responses with non-associated flow rules

For any point (stress state) on the initial yield surface y in true stress space p - q , there exists an elliptical loading surface y^* in generalised dissipative stress space $\chi_V - \chi_S$ which can be expressed by making use of Equation (17) as:

$$y^* = \left[\chi_V - (p - a\sqrt{E}) \right]^2 + \left[\chi_S - (q - b\sqrt{E}) \right]^2 - F^2 - r_d E = 0 \quad (63)$$

These loading functions in dissipative stress space are analogous to the concept of plastic potential in conventional plasticity. As illustrated in Figure 12, the flow vectors in true stress space are defined as normal to the corresponding elliptical loading function in dissipative stress space. Furthermore, functions a and b , appeared in Equation (63), can be defined in terms of true stresses which helps to predict the directions of flow vectors in true stress space. Possible definitions of these functions are proposed as follows:

$$a = \pm \sqrt{r_p \left[1 - \frac{q^2}{M^2 F^2} \right]} \quad (64)$$

$$b = \sqrt{r_p \frac{q^2}{M^2 F^2}} \quad (65)$$

Following the sign convention of compression positive, the plus and minus signs used in Equation (64) correspond to plastic volumetric contraction and dilation, respectively. Hence, a dilative or contractive response at any point on the yield surface can be simulated by choosing the appropriate sign of parameter a . For instance, Figure 12 (a) – (c) illustrates the directions of flow vectors on the initial yield surface of Bentheim sandstone corresponding to confining pressures (σ_r) of 30 MPa, 120 MPa and 300 MPa. For any positive value of parameter a , the model behaviour is contractive, whereas the model exhibits dilational behaviour if a negative value of a is chosen (Figure 12).

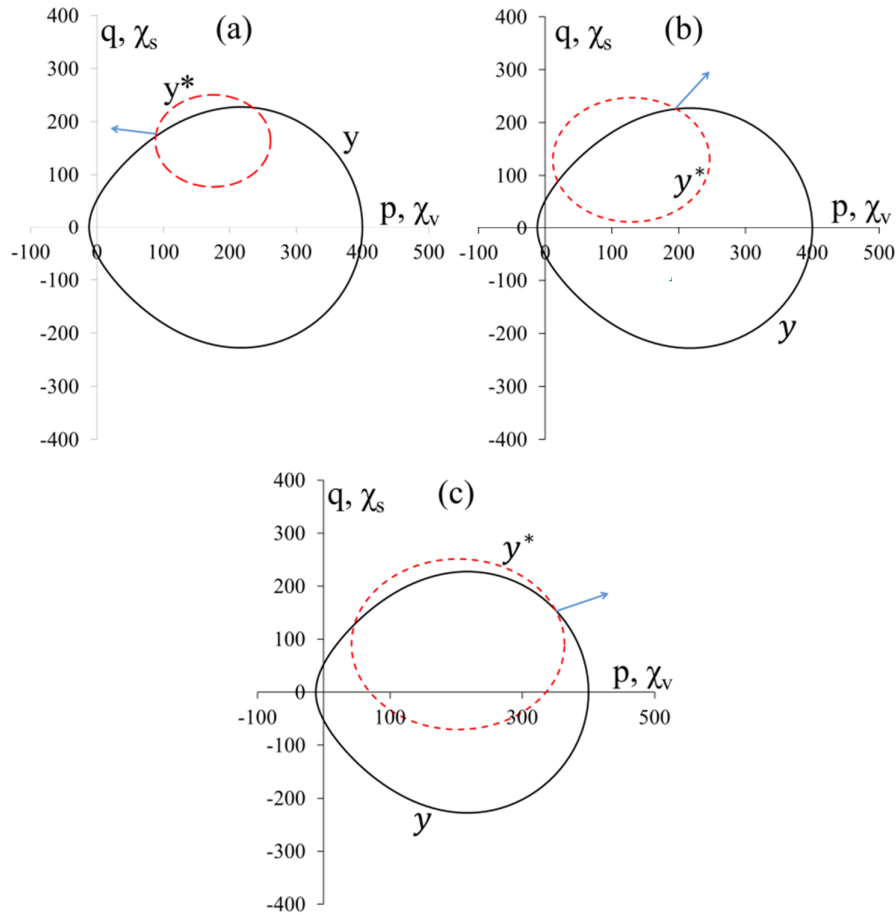


Figure 12: Initial yield loci in dissipative stress space (y^*) and in true stress space (y), with directions of flow vectors for Bentheim sandstone at the onset of yielding under triaxial loading at (a) 30 MPa, (b) 120 MPa and (c) 300 MPa confinement

In order to set a criterion for appropriately choosing the sign of parameter a , the pressure at the intersection of the final failure line and the initial yield locus, i.e. ρ (Equation (62)), is defined as the critical pressure. Any point on the yield surface with a pressure below the critical pressure ($p < \rho$) corresponds to dilative response and softening behaviour, where the parameter a is negative. If, on the other hand, this pressure exceeds the critical pressure ($p > \rho$), the model exhibits compaction and hardening or ductile behaviour where parameter a will be positive. The model behaviour at the intersection of the initial yield surface and the final failure line ($p = \rho$) is perfectly plastic (brittle-ductile transition), as shown in Figure 13. It is also important to note that regardless of the sign of a , the dissipation rate function, as given in Equation (7), is always positive (see Appendix C).

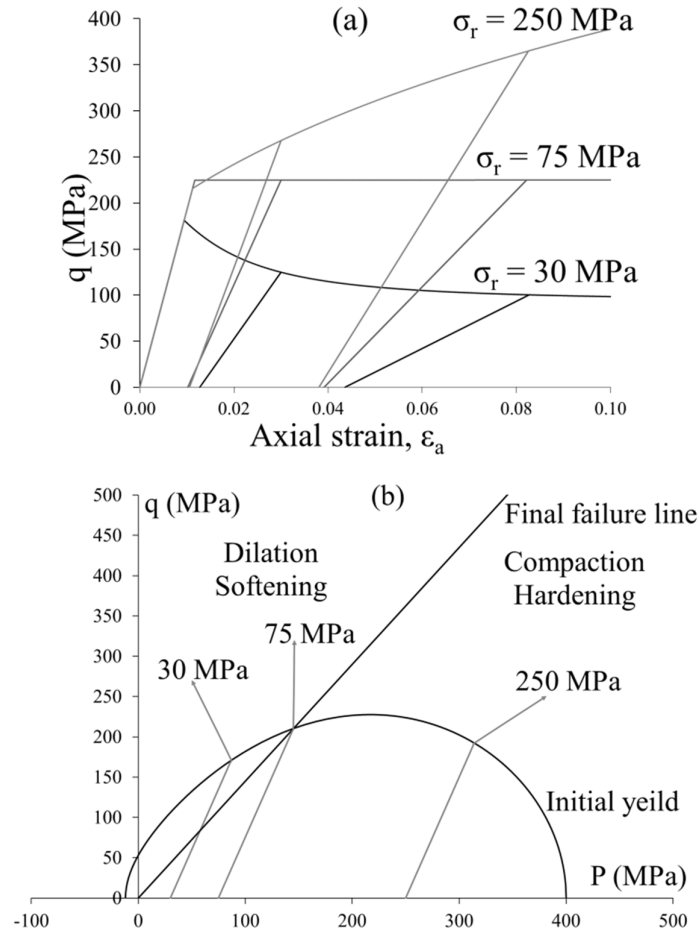


Figure 12: (a) Brittle, brittle-ductile transition and ductile responses and (b) Dilation/softening and compaction/hardening regions with their transition for Bentheim sandstone ($p_c=400$ MPa, $p_t = 10$ MPa, $M=1.45$, $\omega = 0.6$ and $\gamma = 0.8$)

4.1.1 Behaviour and validation of the proposed model

A series of experimental data of Bentheim sandstone [80] is used to assess the performance of the model. A number of yield points (Figure 14) corresponding to different confining pressures are used for the calibration of initial yield parameters, i.e. p_c , p_t , M , ω and γ .

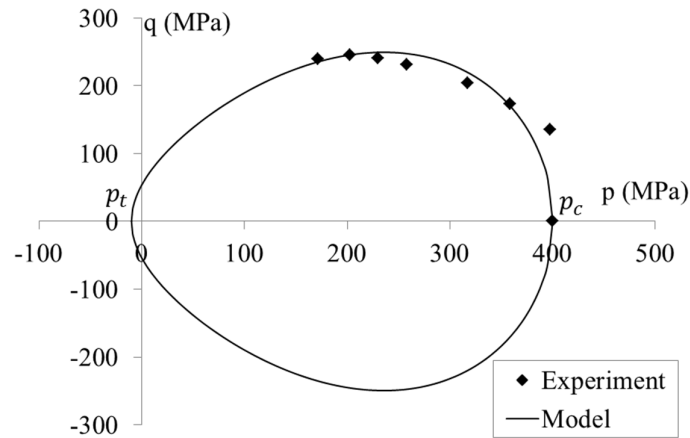


Figure 14: Calibration of the model parameters ($p_c=400$ MPa, $p_t = 10$ MPa, $M = 1.45$, $\omega = 0.6$ and $\gamma = 0.8$)

Figure 15 illustrates the performance of the model with the same level of activity for damage and plasticity processes, i.e. $r_d = r_p = 0.5$. It is expected, however, that the contributions of damage and plasticity in energy dissipation vary for different levels of confining pressure. In the dilation/softening region (see Figure 13 (b)), under low confining pressures, damage is the dominant mechanism of the inelastic deformation, while at medium to relatively high confining pressure, the dominant mechanism of deformation and energy dissipation is plasticity. At significantly high confining pressures, however, damage is envisaged to be the dominant mechanism again. The dominance of the damage dissipation at significantly high pressures in granular materials can be attributed to phenomena like grain crushing [5, 6, 81, 82]. Model predictions, in general, show a reasonable agreement with the experimental data (Figure 15). However, as can be seen in Figure 15 (b), the model prediction does not closely follow the experimental data in the brittle/softening region. The main reason for this deviation is that the material behaviour, produced by the model, is compared with that of the specimen without considering the size effect of the specimen used for recording the experimental data. The size effect of a structure (or a specimen) on the nominal strength and post-peak behaviour is a well-known issue and it is more profound when the material undergoes softening [see e.g. 83]. The issues of localised failure and size effects can be resolved by using a regularisation technique which is not considered in this study as this is not the primary focus of this investigation.

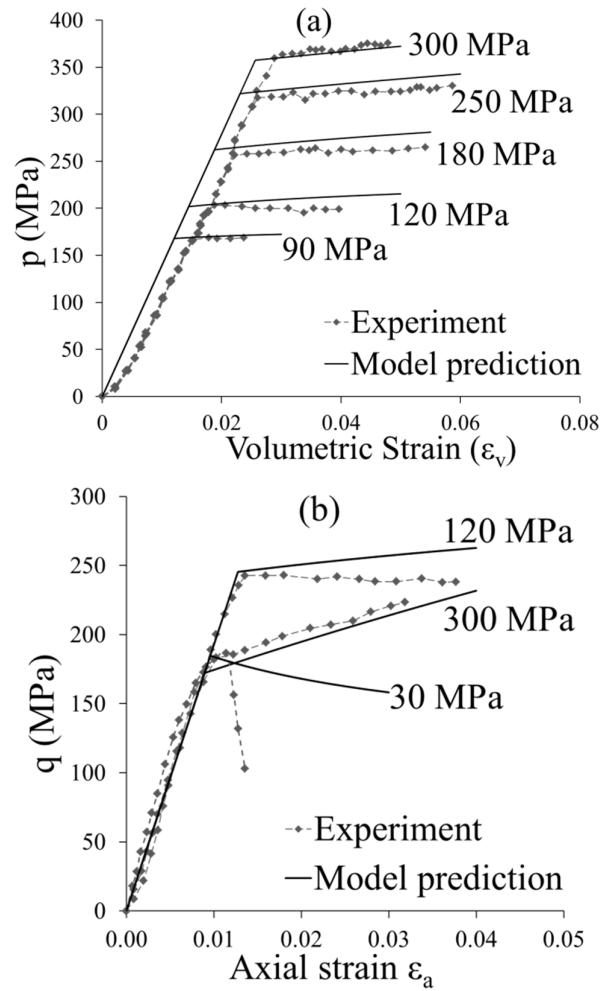


Figure 15: Model validation against experimental data of Bentheim sandstone [79], (a) pressure-volumetric strain (b) differential stress-axial strain with $r_d = r_p = 0.5$

4. Discussions and Conclusions

A thermodynamically consistent generic formulation for constructing constitutive models for engineering materials is proposed in this study. The focus of the study is to obtain a rigorous and consistent method for coupling damage and plasticity for a range of engineering materials. As a result, a general form of the total dissipation rate function is developed which can be conveniently transformed to get a single generalised loading surface for both yield and failure states. This single loading surface governs the simultaneous evolutions of both damage and plasticity where the coupling between these two mechanisms is effectively specified through a model parameter without imposing any restrictions to the model. In addition, the

inherent features of the generic formulation also facilitate the modelling of the inelastic dilative and contractive behaviour of materials.

It is shown that the proposed generic formulation possesses good potentials in enhancing existing as well as developing new constitutive models. Despite the impression that a large number of parameters is needed for the model, it should be noted that the majority of these parameters are in fact used for defining the yielding behaviour of three different types of materials in a generic form utilising functions E and F . Since the yield points in stress space are usually obtained from experiments (see the example of porous rocks in Section 3.3), these parameters can be readily calibrated. It is to be noted that these parameters are independent from the remaining small number of parameters used for defining the failure evolutions, which facilitates the calibration of the remaining parameters for the inelastic behaviour. For defining the inelastic response, besides the elastic modulus and the Poisson's ratio, the proposed formulation requires two mandatory parameters which are r_d (or r_p) to specify the proportion of energy dissipation due to damage (or plasticity), and a (or b) to control the direction of the plastic flow vector. Besides these mandatory parameters, an additional set of 3 to 4 parameters are needed to control the hardening and softening processes of metal (Figure 4) and concrete (Figure 8) while the failure of porous rock (Figure 13) does not need any additional parameters. We also acknowledge that all models used in this work are relatively simple, as they are just used for the purpose of illustrating the applicability of the proposed generic approach. In this sense, future focus on a particular material and/or behaviour may help to identify shortcomings of the approach for further developments and improvements.

Acknowledgements

This research was supported by the Australian Government through Australian Government Research Training Program Scholarship (Van D. Vu). Funding support from the Australian Research Council via projects DP110102645 and FT140100408 (Giang D. Nguyen) is also gratefully acknowledged.

References

1. R. Alessi, J.-J. Marigo, and S. Vidoli, "Gradient damage models coupled with plasticity: Variational formulation and main properties," *Mechanics of Materials*, vol. 80, pp. 351-367, 2015.
2. B. Bourdin, J.-J. Marigo, C. Maurini, and P. Sicsic, "Morphogenesis and propagation of complex cracks induced by thermal shocks," *Physical review letters*, vol. 112, p. 014301, 2014.
3. I. Collins and P. Kelly, "A thermomechanical analysis of a family of soil models," *Geotechnique*, vol. 52, pp. 507-518, 2002.
4. I. F. Collins and T. Hilder, "A theoretical framework for constructing elastic/plastic constitutive models of triaxial tests," *International Journal for Numerical and Analytical Methods in Geomechanics*, vol. 26, pp. 1313-1347, 2002.
5. I. Einav, "Breakage mechanics—part I: theory," *Journal of the Mechanics and Physics of Solids*, vol. 55, pp. 1274-1297, 2007.
6. I. Einav, "Breakage mechanics—Part II: Modelling granular materials," *Journal of the Mechanics and Physics of Solids*, vol. 55, pp. 1298-1320, 2007.
7. N. Mozaffari and G. Z. Voyiadjis, "Phase field based nonlocal anisotropic damage mechanics model," *Physica D: Nonlinear Phenomena*, vol. 308, pp. 11-25, 7/15/ 2015.
8. G. D. Nguyen and A. M. Korsunsky, "Development of an approach to constitutive modelling of concrete: isotropic damage coupled with plasticity," *International Journal of Solids and Structures*, vol. 45, pp. 5483-5501, 2008.
9. G. D. Nguyen, A. M. Korsunsky, and J. P.-H. Belnoue, "A nonlocal coupled damage-plasticity model for the analysis of ductile failure," *International Journal of Plasticity*, vol. 64, pp. 56-75, 2015.

10. G. Z. Voyiadjis and N. Mozaffari, "Nonlocal damage model using the phase field method: Theory and applications," *International Journal of Solids and Structures*, vol. 50, pp. 3136-3151, 10/1/ 2013.
11. P. H. Feenstra and R. De Borst, "A composite plasticity model for concrete," *International Journal of Solids and Structures*, vol. 33, pp. 707-730, 2// 1996.
12. P. Grassl, K. Lundgren, and K. Gylltoft, "Concrete in compression: a plasticity theory with a novel hardening law," *International Journal of Solids and Structures*, vol. 39, pp. 5205-5223, 10// 2002.
13. H. Park and J.-Y. Kim, "Plasticity model using multiple failure criteria for concrete in compression," *International Journal of Solids and Structures*, vol. 42, pp. 2303-2322, 4// 2005.
14. P. Folino and G. Etse, "Performance dependent model for normal and high strength concretes," *International Journal of Solids and Structures*, vol. 49, pp. 701-719, 2012.
15. Y. Chi, L. Xu, and H.-s. Yu, "Constitutive modeling of steel-polypropylene hybrid fiber reinforced concrete using a non-associated plasticity and its numerical implementation," *Composite Structures*, vol. 111, pp. 497-509, 2014.
16. D. Lu, X. Du, G. Wang, A. Zhou, and A. Li, "A three-dimensional elastoplastic constitutive model for concrete," *Computers & Structures*, vol. 163, pp. 41-55, 2016.
17. T. D. Dinh, A. Rezaei, L. De Laet, M. Mollaert, D. Van Hemelrijck, W. Van Paepegem, "A new elasto-plastic material model for coated fabric," *Engineering Structures*, vol. 71, p. 12, 2014.
18. N. Kumar, A. Rajagopal, and M. Pandey, "Plasticity based approach for failure modelling of unreinforced masonry," *Engineering Structures*, vol. 80, p. 13, 2014.

19. R. Carrazedo, A. Mirmiran, and J. B. d. Hanai, "Plasticity based stress–strain model for concrete confinement," *Engineering Structures*, vol. 48, p. 13, 2013.
20. C. Comi and U. Perego, "Fracture energy based bi-dissipative damage model for concrete," *International Journal of Solids and Structures*, vol. 38, pp. 6427-6454, 9// 2001.
21. Z. Guangming, X. Lixiang, and M. Xiangrui, "A damage-based constitutive model for rock under impacting load," *International Journal of Mining Science and Technology*, vol. 24, p. 7, 2014.
22. A. Khan, A. Al-Gadhib, and M. Baluch, "Elasto-damage model for high strength concrete subjected to multiaxial loading," *International Journal of Damage Mechanics*, 2007.
23. J. Lemaitre, *A course on damage mechanics*: Springer Verlag, 1992.
24. J. Lemaitre, and J.L. Chaboche, *Mechanics of solid materials*, Cambridge University Press, Cambridge, 1990.
25. J. Mazars, "A description of micro- and macroscale damage of concrete structures," *Engineering Fracture Mechanics*, vol. 25, pp. 729-737, 1986/01/01 1986.
26. J. Mazars and G. Pijaudier-Cabot, "Continuum damage theory-application to concrete," *Journal of Engineering Mechanics*, vol. 115, pp. 345-365, 1989.
27. J. Pituba and G. Fernandes, "Anisotropic damage model for concrete," *Journal of Engineering Mechanics*, vol. 137, pp. 610-624, 2011.
28. S. Yazdani and H. Schreyer, "Combined plasticity and damage mechanics model for plain concrete," *Journal of engineering mechanics*, 1990.
29. N. Hansen and H. Schreyer, " A thermodynamically consistent framework for theories of elasticity coupled with damage", *Int. J. Solids Struct.*, 31, 359–389.

30. J. Lee and G. L. Fenves, "Plastic-damage model for cyclic loading of concrete structures," *Journal of engineering mechanics*, vol. 124, pp. 892-900, 1998.
31. A. Jefferson, "Craft—a plastic-damage-contact model for concrete. I. Model theory and thermodynamic considerations," *International journal of solids and structures*, vol. 40, pp. 5973-5999, 2003.
32. G. Nguyen and G. Houlsby, "A coupled damage–plasticity model for concrete based on thermodynamic principles: Part II: nonlocal regularization and numerical implementation," *International Journal for Numerical and Analytical Methods in Geomechanics* 32(4), 353-389..
33. M. Salari, S. Saeb, K. Willam, S. Patchet, and R. Carrasco, "A coupled elastoplastic damage model for geomaterials," *Computer methods in applied mechanics and engineering*, vol. 193, pp. 2625-2643, 2004.
34. L. Contrafatto and M. Cuomo, "A framework of elastic–plastic damaging model for concrete under multiaxial stress states," *International Journal of Plasticity*, vol. 22, pp. 2272-2300, 2006.
35. L. Jason, A. Huerta, G. Pijaudier-Cabot, and S. Ghavamian, "An elastic plastic damage formulation for concrete: Application to elementary tests and comparison with an isotropic damage model," *Computer methods in applied mechanics and engineering*, vol. 195, pp. 7077-7092, 2006.
36. J.-F. Shao, Y. Jia, D. Kondo, and A.-S. Chiarelli, "A coupled elastoplastic damage model for semi-brittle materials and extension to unsaturated conditions," *Mechanics of materials*, vol. 38, pp. 218-232, 2006.
37. U. Cicekli, G. Z. Voyiadjis, and R. K. A. Al-Rub, "A plasticity and anisotropic damage model for plain concrete," *International Journal of plasticity*, vol. 23, pp. 1874-1900, 2007.
38. G. Z. Voyiadjis, Z. N. Taqieddin, and P. I. Kattan, "Anisotropic damage–plasticity model for concrete," *International Journal of Plasticity*, vol. 24, pp. 1946-1965, 2008.

39. F. Parisio, S. Samat, and L. Laloui, "Constitutive analysis of shale: a coupled damage plasticity approach," *International Journal of Solids and Structures*, vol. 75, pp. 88-98, 2015.
40. A. Pouya and P. B. Yazdi, "A damage-plasticity model for cohesive fractures," *International Journal of Rock Mechanics and Mining Sciences*, vol. 73, pp. 194-202, 2015.
41. D. Kim, G. F. Dargush, and C. Basaran, "A cyclic two-surface thermoplastic damage model with application to metallic plate dampers," *Engineering Structures*, vol. 53, pp. 608-620, 2013.
42. B. Valentini, Y. Theiner, M. Aschaber, H. Lehar, and G. Hofstetter, "Single-phase and multi-phase modeling of concrete structures," *Engineering Structures*, vol. 47, p. 10, 2013.
43. B. Ayhan, P. Jehel, D. Brancherie, and A. Ibrahimbegovic, "Coupled damage–plasticity model for cyclic loading: Theoretical formulation and numerical implementation," *Engineering Structures*, vol. 50, p. 13, 2013.
44. L. Chen, J. Shao, and H. Huang, "Coupled elastoplastic damage modeling of anisotropic rocks," *Computers and Geotechnics*, p. 8, 2010.
45. A. Chiarelli, J. Shao, and N. Hoteit, "Modeling of elastoplastic damage behavior of a claystone " *International Journal of Plasticity*, p. 23, 2003.
46. G. Nguyen and G. Houlsby, "A coupled damage–plasticity model for concrete based on thermodynamic principles: Part I: model formulation and parameter identification," *International Journal For Numerical And Analytical Methods In Geomechanics*, vol. 32, p. 37, 2008.
47. B. Luccioni and V. Rougier, "A plastic damage approach for confined concrete," *Computers and Structures*, p. 19, 2005.
48. J. Zhang, W. Xu, H. Wang, R. Wang, Q. Meng, and S. Du, "A coupled elastoplastic damage model for brittle rocks and its application in

- modelling underground excavation," *International Journal of Rock Mechanics & Mining Sciences & Geomechanical Abstracts*, p. 12, 2016.
49. C. Zhou and F. Zhu, "An elasto-plastic damage constitutive model with double yield surfaces for saturated soft rock," *International Journal of Rock Mechanics & Mining Sciences*, p. 11, 2010.
50. A. Karrech, K. Regenauer-Lieb, and T. Poulet, "A damaged viscoplasticity model for pressure and temperature sensitive geomaterials," *International Journal of Engineering Science*, vol. 49, p. 10, 2011.
51. A. Karrech, K. Regenauer-Lieb, and T. Poulet, "Continuum damage mechanics for the lithosphere," *Journal Of Geophysical Research*, vol. 116, p. 14, 2011.
52. W. B. Krätzig and R. Pölling, "An elasto-plastic damage model for reinforced concrete with minimum number of material parameters," *Computers & Structures*, vol. 82, pp. 1201-1215, 6// 2004.
53. S. Liu, J. G. Ning, Y. L. Tan, and Q. H. Gu, "Damage constitutive model based on energy dissipation for intact rock subjected to cyclic loading," *International Journal of Rock Mechanics & Mining Sciences*, vol. 85, p. 6, 2016.
54. J. Lubliner, J. Oliver, S. Oller, and E. Onate, "A plastic-damage model for concrete," *International Journal of solids and structures*, vol. 25, pp. 299-326, 1989.
55. N. Mozaffari and Z. V. George, "Coupled gradient damage–Viscoplasticity model for ductile materials: Phase field approach," *International Journal of Plasticity*, vol. 83, p. 19, 2016.
56. G. Z. Voyiadjis and T. M. Abu-Lebdeh, "Damage model for concrete using bounding surface concept," *Journal of engineering mechanics*, vol. 119, pp. 1865-1885, 1993.

57. D. Xenos and P. Grassl, "Modelling the failure of reinforced concrete with nonlocal and crack band approaches using the damage-plasticity model CDPM2," *Finite Elements in Analysis and Design*, vol. 117-118, p. 10, 2016.
58. P. Grassl, D. Xenos, U. Nyström, R. Rempling, and K. Gylltoft, "CDPM2: A damage-plasticity approach to modelling the failure of concrete," *International Journal of Solids and Structures*, vol. 50, pp. 3805-3816, 2013.
59. D. Unteregger, B. Fuchs, and G. Hofstetter, "A damage plasticity model for different types of intact rock," *International Journal of Rock Mechanics & Mining Sciences*, vol. 80, p. 12, 2015.
60. P. Tapponnier and W. Brace, "Development of stress-induced microcracks in Westerly granite," in *International Journal of Rock Mechanics and Mining Sciences & Geomechanics Abstracts*, 1976, pp. 103-112.
61. M. L. Batzle, G. Simmons, and R. W. Siegfried, "Microcrack closure in rocks under stress: direct observation," *Journal of Geophysical Research: Solid Earth*, vol. 85, pp. 7072-7090, 1980.
62. R. L. Kranz, "Microcracks in rocks: a review," *Tectonophysics*, vol. 100, pp. 449-480, 1983.
63. E. Eberhardt, D. Stead, B. Stimpson, and R. Read, "Identifying crack initiation and propagation thresholds in brittle rock," *Canadian Geotechnical Journal*, vol. 35, pp. 222-233, 1998.
64. H. Xie and F. Gao, "The mechanics of cracks and a statistical strength theory for rocks," *International Journal of Rock Mechanics and Mining Sciences*, vol. 37, pp. 477-488, 2000.
65. Y. Seo, G. Jeong, J. Kim, and Y. Ichikawa, "Microscopic observation and contact stress analysis of granite under compression," *Engineering Geology*, vol. 63, pp. 259-275, 2002.

66. V. Vajdova, W. Zhu, T.-M. N. Chen, and T.-f. Wong, "Micromechanics of brittle faulting and cataclastic flow in Tavel limestone," *Journal of Structural Geology*, vol. 32, pp. 1158-1169, 2010.
67. E. Hoek and C. Martin, "Fracture initiation and propagation in intact rock—a review," *Journal of Rock Mechanics and Geotechnical Engineering*, vol. 6, pp. 287-300, 2014.
68. G. Nguyen, I. Einav, I. Guiamatsia, and A. M. Korsunsky, "From Diffuse to Localised Damage: the Role of Friction," presented at the The International Conference on Advances in Computational Mechanics, Ho Chi Minh City, Vietnam, 2012.
69. I. Einav, G. Houlsby, and G. Nguyen, "Coupled damage and plasticity models derived from energy and dissipation potentials," *International Journal of Solids and Structures*, vol. 44, pp. 2487-2508, 2007.
70. G. D. Nguyen and I. Einav, "Nonlocal regularisation of a model based on breakage mechanics for granular materials," *International Journal of Solids and Structures*, vol. 47, pp. 1350-1360, 2010.
71. G. Houlsby and A. Puzrin, "A thermomechanical framework for constitutive models for rate-independent dissipative materials," *International Journal of Plasticity*, vol. 16, pp. 1017-1047, 2000.
72. G. T. Houlsby and A. M. Puzrin, *Principles of hyperplasticity: an approach to plasticity theory based on thermodynamic principles*: Springer Science & Business Media, 2007.
73. Lyakhovsky, V., Ben-Zion, Y., & Agnon, A., 1997a. Distributed damage, faulting, and friction, *J. geophys. Res.*, 102, 27 635–27 649.
74. Lyakhovsky, V., Reches, Z., Weinberger., R. & Scott, T.E., 1997b. Nonlinear elastic behavior of damaged rocks, *Geophys. J. Int.*, 130, 157–166.

75. A. M. Korsunsky, G. D. Nguyen, and K. Kim, "The analysis of deformation size effects using multiple gauge length extensometry and the essential work of rupture concept," *Materials Science and Engineering A*, vol. 423, p. 7, 2006.
76. B. Fiedler, M. Hojo, S. Ochiai, K. Schulte, and M. Ando, "Failure behavior of an epoxy matrix under different kinds of static loading," *Composites Science and Technology*, vol. 61, p. 10, 2001.
77. V. S. Gopalaratnam and S. P. Shah, "Softening response of plain concrete in direct tension," *ACI Materials Journal*, vol. 82, p. 14, 1985.
78. I. D. Karsan and J. O. Jirsa, "Behavior of concrete under compressive loadings," *ASCE journal of Structural engineering*, vol. 95, 1969.
79. H. Kupfer, K. Hilsdorf, and H. Rusch, "Behavior of concrete under biaxial stresses," *Journal of American Concrete Institute*, vol. 66, p. 11, 1969.
80. T. f. Wong, P. Baud, and E. Klein, "Localized failure modes in a compactant porous rock," *Geophysical Research Letters*, vol. 28, pp. 2521-2524, 2001.
81. A. Das, G. D. Nguyen, and I. Einav, "The propagation of compaction bands in porous rocks based on breakage mechanics," *Journal of Geophysical Research: Solid Earth*, vol. 118, pp. 2049-2066, 2013.
82. A. Das, A. Tengattini, G. D. Nguyen, G. Viggiani, S. A. Hall, and I. Einav, "A thermomechanical constitutive model for cemented granular materials with quantifiable internal variables. Part II—validation and localization analysis," *Journal of the Mechanics and Physics of Solids*, vol. 70, pp. 382-405, 2014.
83. Z. P. Bažant and L. Cedolin, *Stability of structures: elastic, inelastic, fracture and damage theories*: World Scientific, 2010.

Appendix A: The general condition for thermodynamic admissibility

The general condition for thermodynamic admissibility is derived from the premise of strictly non-negativeness of the dissipation rate function, given by Equation (7). This condition can be derived by making use of the general definition of functions and parameters appearing in Equation (7), and defined through Equations (8) – (12) as well as the flow rules of Equations (18) – (20) and the yield condition, as given by Equation (23). For convenience these Equations and definitions are also repeated here:

The dissipation potential

$$\Phi = \sqrt{\phi_V^2 + \phi_S^2 + \phi_D^2} + f_V \phi_V + f_S \phi_S \geq 0 \quad (\text{A-1})$$

Definition of functions

$$f_V = \frac{p - a\sqrt{E(p, q, D, \varepsilon_p)}}{F(p, q, D, \varepsilon_p)} \quad (\text{A-2})$$

$$f_S = \frac{q - b\sqrt{E(p, q, D, \varepsilon_p)}}{F(p, q, D, \varepsilon_p)} \quad (\text{A-3})$$

$$\phi_V = F(p, q, D, \varepsilon_p) \dot{\alpha}_V \quad (\text{A-4})$$

$$\phi_S = F(p, q, D, \varepsilon_p) \dot{\alpha}_S \quad (\text{A-5})$$

$$\phi_D = \frac{F(p, q, D, \varepsilon_p) \bar{\chi}_D \dot{D}}{\sqrt{r_d E(p, q, D, \varepsilon_p)}} \quad (\text{A-6})$$

Flow rules

$$\dot{\alpha}_V = \dot{\lambda} \frac{\partial y^*}{\partial \chi_V} = 2 \dot{\lambda} \left(\frac{a\sqrt{E}}{F^2} \right) \quad (\text{A-7})$$

$$\dot{\alpha}_S = \dot{\lambda} \frac{\partial y^*}{\partial \chi_S} = 2 \dot{\lambda} \left(\frac{b\sqrt{E}}{F^2} \right) \quad (\text{A-8})$$

$$\dot{D} = \dot{\lambda} \frac{\partial y^*}{\partial \chi_D} = 2 \dot{\lambda} \frac{r_d E}{F^2 \chi_D} \quad (\text{A-9})$$

The yield function in true stress space

$$y = E - F^2 = 0 \quad (\text{A-10})$$

Substitution of Equations (A-2) – (A-9) into Equation (A-1) and making use of Equation (A-10), results in:

$$\Phi = 2\lambda \left(\sqrt{a^2 + b^2 + r_d} + \left(\frac{pa}{F} + \frac{qb}{F} \right) - (a^2 + b^2) \right) \geq 0 \quad (\text{A-11})$$

Since $\lambda \geq 0$ the non-negativeness of the term in the parentheses is required, i.e.

$$\sqrt{a^2 + b^2 + r_d} + \left(\frac{pa}{F} + \frac{qb}{F} \right) - (a^2 + b^2) \geq 0 \quad (\text{A-12})$$

Since $F \geq 0$, recalling the condition of Equation (22) ($a^2 + b^2 = r_p$ and $r_p + r_d = 1$) and, the above expression is reduced to:

$$pa + qb + r_d F \geq 0 \quad (\text{A-13})$$

In the above expression, the second and the third terms are always non-negative. The first term, however, can be negative when the model behaviour is dilative ($a < 0$) under compression ($p > 0$). The following general condition is therefore required to be satisfied for thermodynamic admissibility:

$$|pa| \leq qb + r_d F \quad (\text{A-14})$$

It should be noted that the expression at the right-hand side of the inequality in the above condition is always non-negative.

In the case of the Von Mises model, due to incompressibility constraint, i.e. $\alpha_v = a = 0$, the condition of Equation (A-14) is always satisfied. For the case of the enhanced Drucker-Prager model, in which an additional parameter c is used to control the direction of the plastic flow vector in stress space, no general proof can be given for thermodynamic admissibility. However, by making use of the general condition of Equation (A-14), some restriction is put on selecting the parameter c for modelling the dilational behaviour under compression. In this regards, parameter a in (A-14) can be substituted for form Equation (31) to give the following restrictive condition on c :

$$c \leq \frac{qb + r_d F}{\left| pb \frac{\partial y / \partial p}{\partial y / \partial q} \right|} \quad (\text{A-15})$$

Considering the Drucker-Prager yield function, as stated by Equation (52) the above condition can be rewritten as:

$$-\frac{2q(qb + r_d \sqrt{\beta})}{pba} \leq c \leq \frac{2q(qb + r_d \sqrt{\beta})}{pba} \quad (\text{A-16})$$

This condition imposes a restriction on the direction of the flow vector and is met for the example presented in the manuscript.

In the case of the new geomaterial model it is required to demonstrate that the model conforms to the condition of Equation (A-14) for modelling the dilative behaviour under compression. To this end, parameters a and b in (A-14) are substituted for from Equations (64) and (65) to give:

$$\left| p \sqrt{r_p \left(1 - \frac{q^2}{M^2 F^2} \right)} \right| \leq q \sqrt{r_p \frac{q^2}{M^2 F^2}} + r_d F \quad (\text{A-17})$$

Comparing the above expression with the yield function of Equation (61), the above expression can be rewritten as:

$$\left| p \sqrt{r_p \left(\frac{(1-D)(p-\rho)}{A} \right)^2} \right| \leq q \sqrt{r_p \left(1 - \left(\frac{(1-D)(p-\rho)}{A} \right)^2 \right)} + r_d F \quad (\text{A-18})$$

where

$$A = \frac{(1-\gamma)p_c - p_t}{p_c + p_t} p + \frac{1}{2}(1-D)\gamma p_c \quad (\text{A-19})$$

Functions F and A are always positive or non-negative, therefore, (A-18) can be rearranged to give:

$$p - \rho \leq \frac{A \left(q \sqrt{r_p \left(1 - \left(\frac{(1-D)(p-\rho)}{A} \right)^2 \right)} + Fr_d \right)}{(1-D)p \sqrt{r_p}} \quad (\text{A-20})$$

In the dilation regime the term $(p - \rho)$ is always negative See Figure A1, while the right-hand side of the above expression is always positive. Therefore, it is deduced that the model follows the general condition for thermodynamic admissibility as stated by Equation (A-14).

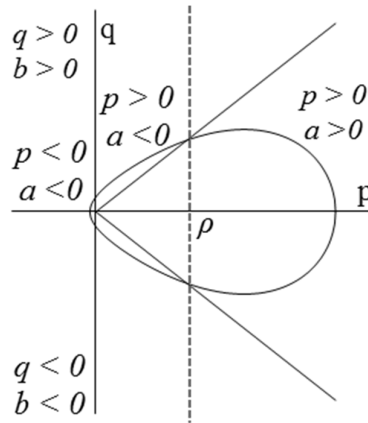


Figure A1: Sign determination diagram for volumetric and shear dissipation rate functions

APPENDIX B: Energy dissipation potential as a function of stresses and $\dot{\alpha}_s$

Using the definition of χ_V , χ_S and χ_D , Equation (24) can be rewritten as:

$$\Phi = \chi_V \dot{\alpha}_V + \chi_S \dot{\alpha}_S + \chi_D \dot{D} \geq 0 \quad (\text{B-1})$$

Substitutions of Equations (18) – (20) into Equation (B-1), gives:

$$\Phi = \chi_V 2\lambda \frac{a\sqrt{E}}{F^2} + \chi_S 2\lambda \frac{b\sqrt{E}}{F^2} + 2\lambda \frac{r_d E}{F^2} \quad (\text{B-2})$$

Recalling the constitutive postulate of $\bar{\chi}_V = \chi_V$ and $\bar{\chi}_S = \chi_S$ and using Equations (4) and (5), the above expression can be rewritten as:

$$\Phi = p 2\lambda \frac{a\sqrt{E}}{F^2} + q 2\lambda \frac{b\sqrt{E}}{F^2} + 2\lambda \frac{r_d E}{F^2} \quad (\text{B-3})$$

Therefore, the following expressions for the dissipation rate functions corresponding to each internal variable can be obtained, using Equation (B-3), as:

$$\Phi_V = p 2\lambda \frac{a\sqrt{E}}{F^2} \quad (\text{B-4})$$

$$\Phi_S = q 2\lambda \frac{b\sqrt{E}}{F^2} \quad (\text{B-5})$$

$$\Phi_D = 2\lambda \frac{r_d E}{F^2} \quad (\text{B-6})$$

From the above equations, the following ratios are defined:

$$\frac{\Phi_S}{\Phi_D} = \frac{qb}{r_d \sqrt{E}} \quad (\text{B-7})$$

$$\frac{\Phi_V}{\Phi_S} = \frac{pa}{qb} \quad (\text{B-8})$$

Substituting the above ratios into Equation (24), the total dissipation rate function Φ can be expressed in terms of Φ_S and stresses as:

$$\Phi = \frac{pa}{qb}\Phi_S + \Phi_S + \frac{r_d \sqrt{E}}{qb}\Phi_S = \left(\frac{pa}{qb} + 1 + \frac{r_d \sqrt{E}}{qb} \right) \Phi_S \quad (\text{B-9})$$

Since $\Phi_S = \chi_S \dot{\alpha}_S$ and $\chi_S = \bar{\chi}_S = q$, it follows that:

$$\Phi_S = q \dot{\alpha}_S \quad (\text{B-10})$$

Thus, substitution of Equation (B-10) into Equation (B-9), the expression of the total dissipation rate function, Φ , in terms of $\dot{\alpha}_S$ and stresses are obtained as:

$$\Phi = \left(\frac{pa}{b} + q + \frac{r_d \sqrt{E}}{b} \right) \dot{\alpha}_S \quad (\text{B-11})$$

APPENDIX C: Energy dissipation aspects of Von-Mises materials under uniaxial loading

As $\alpha_V = 0$ in the Von-Mises material model, $e_{ij}^p = \alpha_{ij} - \frac{\alpha_V}{3} = \alpha_{ij}$ and thus $\dot{\alpha}_S$ can be written as:

$$\dot{\alpha}_S = \sqrt{\frac{2}{3} \dot{e}_{ij}^p \dot{e}_{ij}^p} = \sqrt{\frac{2}{3} \dot{\alpha}_{ij} \dot{\alpha}_{ij}} = \dot{\epsilon}_p \quad (C-1)$$

Furthermore, using Equations (47) and (48), the relationship between \dot{D} and $\dot{\epsilon}_p$ is expressed as:

$$\frac{\dot{D}}{\dot{\epsilon}_p} = \frac{\dot{D}}{\dot{\alpha}_S} = \frac{r_d \sqrt{q}}{b \bar{\chi}_D} \quad (C-2)$$

For the case of uniaxial stress, the pressure p and the deviatoric stress q are given as follows:

$$p = -\frac{\sigma}{3}, \{s\} = \left\{ \frac{2}{3}\sigma \quad -\frac{1}{3}\sigma \quad -\frac{1}{3}\sigma \quad 0 \quad 0 \quad 0 \right\}, \quad (C-3)$$

$$q = \sqrt{\frac{3}{2} \{s\}^T [T] \{s\}} = \sqrt{\frac{3}{2} \left(\frac{4}{9} + \frac{1}{9} + \frac{1}{9} \right) \sigma^2} = \sigma \quad (C-4)$$

Using Equation (7) and Equations (C-3) and (C-4), χ_D can be expressed as:

$$\chi_D = T \frac{q^2}{(1-D)^2} \quad \text{where} \quad T = \frac{G+3K}{18KG} \quad (C-5)$$

Substitution of Equation (C-5) into Equation (C-2) gives the following relationship:

$$\frac{\dot{D}}{\dot{\epsilon}_p} = \frac{r_d \sqrt{q}}{bT \frac{q^2}{(1-D)^2}} \quad (C-6)$$

From the yield function, given by Equation (46), q can be obtained as:

$$q = k = (1 - D) \left(f_y + Q \left(1 - e^{-H\epsilon_p} \right) \right) \quad (C-7)$$

Thus, the following expression can be derived by making use of Equations (C-6) and (C-7):

$$\frac{1}{\sqrt{(1-D)}} \dot{D} = \frac{r_d}{bT} \frac{1}{\left(f_y + Q \left(1 - e^{-H\epsilon_p} \right) \right)^{3/2}} \dot{\epsilon}_p \quad (C-8)$$

Integrating both sides of Equation (C-8) with results in the following expression:

$$2\sqrt{(1-D)} = \frac{r_d}{bT} \left(f_y + Q \left(1 - e^{-H\epsilon_p} \right) \right)^{-1/2} \frac{1}{-0.5QH e^{-H\epsilon_p}} + C \quad (C-9)$$

The integration constant C is calculated for the following cases:

Case 1: *Evolution of damage and plasticity together at yielding (see Figure 1 for $r_d = 0.5$ and 0.25)*

For the case of damage being initiated at the onset of yielding together with plastic strains, the expression of C can be obtained by using $\epsilon_p = 0$, $D = 0$ as the initial conditions which are substituted into Equation (C-9) to give the following expression for the constant C :

$$C = 2 - \frac{r_d}{bT} (f_y)^{-1/2} \frac{1}{-0.5QH} \quad (C-10)$$

Case 2: *Only plasticity occurs at yielding and damage initiates when $\epsilon_p > \epsilon_{pc}$ (see Figure 2(a))*

In the example provided in Section 3.1, damage is not initiated ($r_d = 0$) until $\epsilon_p > \epsilon_{pc}$ ($= 4.5 \times 10^{-3}$). Hence, the initial conditions are: $D = 0$, $\epsilon_p = 4.5 \times 10^{-3}$ which are substituted into Equation (C-9) to obtain the integration constant C as follows:

$$C = 2 - \frac{r_d}{bT} \left(f_y + Q \left(1 - e^{-H\epsilon_{pc}} \right) \right)^{-1/2} \frac{1}{-0.5QH e^{-H\epsilon_{pc}}} \quad (C-11)$$

In order to obtain the explicit expression of D in term of the accumulated plastic strain, ϵ_p , Equation (C-9) is rearranged to give:

$$D = 1 - 0.25 \left[\frac{r_d}{bT} \left(f_y + Q \left(1 - e^{-H\epsilon_p} \right) \right)^{-1/2} \frac{1}{-0.5QHe^{-H\epsilon_p} + C} + C \right]^2 = 1 - M \quad (\text{C-12})$$

$$\text{where: } M = 0.25 \left[\frac{r_d}{bT} \left(f_y + Q \left(1 - e^{-H\epsilon_p} \right) \right)^{-1/2} \frac{1}{-0.5QHe^{-H\epsilon_p} + C} + C \right]^2$$

It is critical to note that the expression of D in Equation (C-12) is defined only for $\epsilon_p \in (\epsilon_{pc}, \epsilon_{pf})$ where ϵ_{pc} is the effective plastic strain at the onset of damage initiation, and ϵ_{pf} is the effective plastic strain at failure. By substituting Equation (C-12) into Equation (C-8), \dot{D} can be expressed explicitly in term of $\dot{\epsilon}_p$ as:

$$\dot{D} = \frac{r_d}{bT} \frac{\sqrt{1-D}}{\left(f_y + Q \left(1 - e^{-H\epsilon_p} \right) \right)^{3/2}} \dot{\epsilon}_p = \frac{r_d}{bT} \frac{\sqrt{M}}{\left(f_y + Q \left(1 - e^{-H\epsilon_p} \right) \right)^{3/2}} \dot{\epsilon}_p = N \dot{\epsilon}_p \quad (\text{C-13})$$

$$\text{where: } N = \frac{r_d}{bT} \frac{\sqrt{M}}{\left(f_y + Q \left(1 - e^{-H\epsilon_p} \right) \right)^{3/2}}$$

Now the total dissipation rate function can be expressed as:

$$\dot{\Phi} = \chi_D \dot{D} + \chi_S \dot{\alpha}_S \quad (\text{no volumetric plastic strain}) \quad (\text{C-14})$$

Substituting (C-5), (C-7), (C-12) and (C-13) into the above equation, gives:

$$\begin{aligned} \dot{\Phi} &= \chi_D \dot{D} + q \dot{\epsilon}_p = [\chi_D N + q] \dot{\epsilon}_p = \left[T \frac{q^2}{M^2} N + q \right] \dot{\epsilon}_p \\ &= \left[T \frac{\left(M \left(f_y + Q \left(1 - e^{-H\epsilon_p} \right) \right) \right)^2}{M^2} N + M \left(f_y + Q \left(1 - e^{-H\epsilon_p} \right) \right) \right] \dot{\epsilon}_p \quad (\text{C-15}) \\ &= \left[T \left(f_y + Q \left(1 - e^{-H\epsilon_p} \right) \right)^2 N + M \left(f_y + Q \left(1 - e^{-H\epsilon_p} \right) \right) \right] \dot{\epsilon}_p \end{aligned}$$

Thus, the total energy dissipated during the entire deformation process (or the total fracture energy) can be calculated by integrating both sides of Equation (C-15) with respect to ϵ_p . In addition, the damage dissipation rate ratio R_D , given in Equation (25), can also be defined as a function of ϵ_p by making use of Equation (C-7) as:

$$R_D = \frac{r_d}{\sqrt{r_p M \left(f_y + Q \left(1 - e^{-H \epsilon_p} \right) \right)}} \quad (C-16)$$

The above equation provides the explicit link between the proportion of energy dissipation due to damage and plasticity. With the expressions given in Equations (C-12) and (C-16), the variation of R_D and D with respect to ϵ_p are plotted for different values of r_d in Figure B1 (Case 1) and Figure B2 (Case 2).

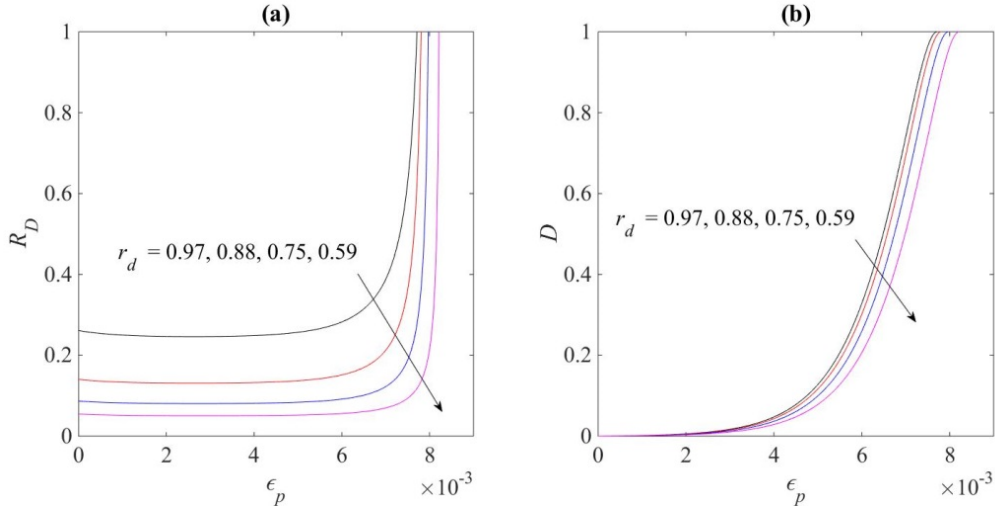


Figure B1: Von Mises material model under uniaxial tension (Case 1: damage is activated simultaneously with plasticity)

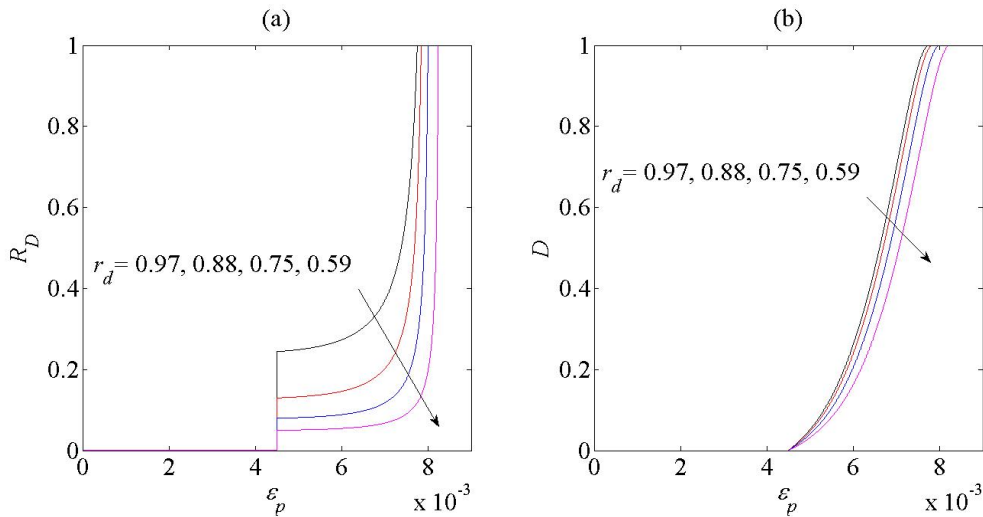


Figure B2: Von Mises material model under uniaxial tension (Case 2: damage is activated at $\epsilon_p = 4.5 \times 10^{-3}$).

As illustrated in Figures B1 and B2, a higher level of damage activation (by assigning a larger r_d) associates with a higher proportion of damage dissipation rate R_D and a faster damage growth compared to a lower level of damage activity (lower r_d). Furthermore, Figures B1(a) and B2(a) show a sharp increase in damage dissipation rate at sufficiently high plastic strain which indicates a complete disintegration of material towards the end of loading procedure where damage is the dominant mechanism of energy dissipation.

CHAPTER 4: MANUSCRIPT 3

A Thermodynamics-based Formulation for Kinematically Enhanced Constitutive Modelling of Unidirectional Fiber Reinforced Composite laminae with Imperfect Fiber Interface

Statement of Authorship

Title of Paper	A Thermodynamics-based Formulation for Kinematically Enhanced Constitutive Modelling of Unidirectional Fiber Reinforced Composite laminae with Imperfect Fiber Interface
Publication Status	<input checked="" type="checkbox"/> Published <input type="checkbox"/> Accepted for Publication <input type="checkbox"/> Submitted for Publication <input type="checkbox"/> Unpublished and Unsubmitted work written in manuscript style
Publication Details	Vu, V.D., Nguyen, G.D. and Sheikh, A.H., 2018. A Thermodynamics-based Formulation for Kinematically Enhanced Constitutive Modelling of Unidirectional Fiber Reinforced Composite laminae with Imperfect Fiber Interface, to be submitted.

Principal Author

Name of Principal Author (Candidate)	Van Duc Vu		
Contribution to the Paper	Developed and wrote the generic formulation, its applications and numerical examples.		
Overall percentage (%)	60 %		
Certification	This paper reports on original research I conducted during the period of my Higher Degree by Research candidature and is not subject to any obligations or contractual agreements with a third party that would constrain its inclusion in this thesis. I am the primary author of this paper.		
Signature	_____	Date	15/01/2018

Co-Author Contributions

By signing the Statement of Authorship, each author certifies that:

- i. the candidate’s stated contribution to the publication is accurate (as detailed above);
- ii. permission is granted for the candidate to include the publication in the thesis; and
- iii. the sum of all co-author contributions is equal to 100% less the candidate’s stated contribution.

Name of Co-Author	Giang D. Nguyen		
Contribution to the Paper	Developed the thermodynamics enhancements for the generic formulation. Supervision of the technical work, write-up and revision of the manuscript.		
Signature	_____	Date	15/01/2018

CHAPTER 4: MANUSCRIPT 3

Name of Co-Author	Abdul Hamid Sheikh		
Contribution to the Paper	Supervision of the technical work, write-up and revision of the manuscript		
Signature		Date	15/01/2018

End of document

Abstract

In this study, the evolution of fiber debonding, degradation of matrix modulus and failure of fibers in unidirectional fiber reinforced composite (FRC) ply is analysed using a thermodynamics- and micromechanics-based constitutive model possessing the mechanical responses and interaction of different constituents. The combination of all kinematic enrichments to capture the difference in the deformation of different constituents and also their responses in a thermodynamics-based approach naturally leads to macro homogenised stress and internal equilibrium conditions that governs the behaviour of the FRC. As a consequence, the overall ply constitutive behaviour consists of four material blocks: one is used to represent the fiber constituent and other three are for matrix. In addition, the effects of fiber/matrix interfacial imperfection in ply constitutive response, which is essential when the ply nonlinear behaviour is dominated by fiber debonding, is also accounted for and included in the fiber block. This overcomes a vital drawback of many existing constitutive models where a perfect bonding condition at the interface of fiber and matrix is assumed. The performance of the proposed model is demonstrated through several examples using experimental data available in literature as well as numerical results obtained from other studies using detailed micromechanical analyses or homogenisation techniques.

Keywords: fibre reinforced composite, unidirectional, constitutive modelling, nonlinear behaviour, damage, plasticity, fiber debonding.

1. Introduction:

The use of unidirectional fiber reinforced composite (FRC) has become increasingly common in many engineering disciplines and distinctive fields such as aircraft/aerospace, defence or construction industries. Its superior properties in term of strength, stiffness and lightweight are favoured over many conventional materials such as steel or aluminium. However, failure behaviour of FRC is quite complex and highly nonlinear which has imposed serious challenges for the material to be used as the primary components and structures. To overcome this difficulty, significant volume of research has been dedicated to gain the understanding of the fundamental mechanisms behind the nonlinear response of composite materials.

Extensive literature survey suggests clear attributions of material properties of the composite constituents (i.e. fiber and matrix) as well as their bonding characteristics at the interfaces to the macroscopic behaviour of composite ply [1–6]. Due the immense difference in stiffness between fiber and matrix, the latter may exhibit extremely large deformations before the ultimate fracture while the response of the former one usually is much stiffer and more brittle in nature. To this end, the macroscopic response of FRCs is characterised by the governing source of deformation that is whether it is controlled by either fiber or matrix [7]. In facts, the deformations in fiber and matrix in a FRC ply are varied significantly under different loading direction which explains highly anisotropic behaviour observed in FRCs. For example, deformations of FRCs loaded longitudinally in fiber direction are controlled by fiber properties whereas matrix and the interface deformations prevail under transverse tension/compression. In this regard, linear-elastic behaviour of fiber [8, 9] leads to linear elastic response of FRC ply in fiber direction under the dominance of fiber response. On the other hand, nonlinear behaviour of FRC plies in transverse direction is a direct result of nonlinear deformations due to the inelastic processes taking place within the matrix as well as due to fiber debonding failure mechanism occurs at the interface of fiber and matrix. These two primary sources of nonlinearity are widely recognised by many researchers as the essential elements in any modelling approaches/theories dealing with nonlinear response of FRC. To this end, matrix constituents are manufactured primarily from aluminium, ceramic or polymer resin and for such materials, loading beyond elastic domain leads to the activation of two irreversible energy dissipation mechanisms: (i) the gradual loss of stiffness (damage) and (ii) permanent inelastic deformation (plasticity) [6, 10, 11]. In facts, closer examinations of microstructural changes in various materials reveal that irreversible deformation mechanisms such as void nucleation, void growths and coalescence along with microcracking are responsible the stiffness degradations [12–14] while dislocations of defects, frictional sliding and twinning are associated with plastic deformations [6, 15–17]. At macroscopic scale, the impacts of matrix cracking on the macroscopic behaviour of composites are well-documented in many studies [4, 18–22] where sudden change in stiffness of the composite can be observed as a result of cracking process causing the redistribution of stresses in the local fields. Furthermore, experimental evidence also suggests that the progression of these microscopic mechanisms can

be profoundly influenced by the nature of deformations induced under different loading conditions. For examples, Aps et al [23] explored the effects of yielding and failures of polymer composite due to cavitation-inducing cracking in matrix where an interesting link between the initiation of cavitation and dilatational behaviour was presented. On the other hand, crack-closure effects in matrix under hydrostatic compression were examined in [24, 25]. In addition, the rate-dependent characteristic of polymer matrix, commonly observed when the material is subjected to dynamic or impact loadings, was also investigated numerically and experimentally in several studies such as those found in [26–33].

On the other hand, fiber/matrix interface failures (fiber debonding) also play an important part contributing to the loss of stiffness and ultimate failures of FRCs [2, 13]. Macroscopic responses of composites are primarily influenced by the bonding strength at the fiber/matrix interface [34, 35] while other characteristics such as fracture energy or stiffness of the interface are of less importance [36]. Subsequently, stresses in the local fields of the composite may exceed this bonding strength and lead to a localised separation of the fiber and matrix which, under increasing loads, will progressively grow in the fiber direction and simultaneously induce new cracks in the matrix towards the direction normal to the fiber [4]. Further fiber debonding can be initiated from the development of the new matrix cracks and eventually macro transverse cracking can be formed in the FRC ply. Numbers of investigators have devoted to investigate the aspect that influences the debonding process as well as its development in FRCs. For instance, the effects of fiber spatial distribution on the sensitivity of interfacial failure which is more likely to occur in region with higher fiber density due to higher local stresses compared to that in region having less fibers [37]. Furthermore, numbers of studies [38, 39], both analytical and experimental, also reported more profound impacts of interfacial damage on the macroscopic behaviour of composite materials, are associated with higher fiber volume fractions. In such cases, the debonding behaviour is magnified by larger area of debonded interface which proportionates with the fiber volume, i.e. larger contact area between fiber and matrix.. In addition, the connections between the fiber size as well as its shape and the failure behaviour of composite were also examined in numbers of studies [37, 40–43].

Complexity in modelling of constituent behaviours and progressive failure mechanism in composite materials pose a great challenge in predicting the response of composites. Many experts have attempted to tackle this problem and the majority of them have very distinctive research background and disciplines with very specific needs and agendas. As a result, there are large numbers of different approaches used to solve this problem which involves vast variation of length scales at which the material descriptions are given. For instance, a detailed micromechanical analysis of FRC failures can be carried out at fiber length scale (microscopic scale) [44–47]. The behaviours of each fiber, the surrounding matrix as well as the fiber/matrix interface are modelled explicitly based on continuum mechanics and the overall characteristics of the composites can be obtained using finite element technique. The result is a rigorous analysis of failure mechanisms and their progression along with detailed insights of the stress/strain fields in the composite. In addition, important information such as fibers size, shape and the distribution of fibers, which can affect the macroscopic behaviour of composite, can be included in the micromechanical analysis for more realistic representation of the homogenised material response. However, the shortfall of such approach is that it cannot be implemented in large structures due to the huge computational costs involved.

On the other hand, some researchers have attempted to capture the behaviour of FRC using material descriptions and properties observed at macroscopic scale. Examples of models based on such approach can be found in [11, 48–65] where composites were considered as homogeneous anisotropic materials. Nonlinear response of composites is subsequently captured by using continuum models in which damage or plastic strains variables are characterised at ply level. In this sense, macromechanics models have an advantage over a full micromechanics analysis in terms of computational efficacy, however they are generally perceived as lack of strong physical basis for the development failure mechanisms, subsequently lead to their dependency on experiment data and curve fitting technique for model calibrations [8, 66].

To that end, multiscale approach is an appealing alternative concept which utilises detail descriptions of the materials in both microscopic and macroscopic scales [8, 67, 68] to offer a balance between computing powers and model details. The

strategy here is to perform detailed micromechanical analyses only at integration points within a structural element, the resulted material responses are then used to comprise the overall structural response accordingly with the help of finite element analyses. Despite several promising features and improvements in modelling efficiency, enormous amount of computational power is still needed for the simulation and the approach is ineffective for failure analyses of large structure. Alternatively by utilising this concept, however, the full micromechanics analyses at integration points are replaced by more efficient homogenisation technique where only the most important failure mechanisms at fiber scale are retained [69–84]. Therefore, adequate level of details can be obtained in the model for accurate predictions of material behaviour without the need of a detail finite element analysis.

Recently, an analytical technique is developed by Vu et al [85] for upscaling the nonlinear response from the fiber/micro scale to the ply scale in order to capture the inelastic response of unidirectional FRCs. In this model, the physical interactions between fiber and matrix are accounted for by incorporating the kinematic strain enhancements into the analytical expressions of the strain fields in fiber and matrix, thus, the relationship between local/micro and homogenized/macro stress and strain fields were established. The inelastic behaviours of the material constituents, particularly matrix, are modelled by using a coupled damage-plasticity formulation in order to capture plastic deformations and progressive damage mechanism within the matrix. In this paper, the kinematically enhanced constitutive model for predicting the response of unidirectional FRC ply is extended to include the effects of fiber/matrix interface failure. First, mathematical formulations of the proposed constitutive model are introduced with a new thermodynamics-based approach. This is then followed by illustrations of model applications to number of examples and the results are compared to other sources obtained from literature to demonstrate its performance.

2. Kinematically Enhanced Multi-phase Constitutive Model for Unidirectional FRC Ply

2.1 Basis of kinematic enrichments

The constitutive model for unidirectional FRC adopted in this study is developed in a generic form based on thermodynamics principles and the procedures for plasticity-based models in [86]. The multi-phase nature of the approach, which include fibre and different matrix phases corresponding to different stress states in the matrix, together with the incremental form allow the employment of the approach in both elastic and inelastic stages of behaviour. While the basis, in terms of kinematic enrichments and idealised configuration of a unit volume element (UVE), is similar to and based on our previous works [85], the thermodynamic formulation in this paper allows connecting all these ingredients in a rigorous and consistent way. In addition, improvements in modelling fibre-matrix interfacial debonding is also included to cover a wide range of loading conditions in which interface failure plays a key role in the behaviour of the material. All these were missing or not addressed at length in our previous work [85].

Before the assembly of all ingredients in a thermodynamic formulation for constitutive models of unidirectional FRCs, a basis on the kinematic enrichments to represent the difference in strain distributions and mechanical responses in both matrix and fibre is needed here, following our earlier work [85]. For this purpose, a typical cross-section of a unidirectional FRC ply with a uniform distribution of the fibers or fiber bundles within the matrix, as shown in Figure 1a, is analysed and a magnified portion of the material is also shown separately in Figure 1b. Subsequently, this unit volume element (UVE) is further idealised and partitioned into four rectangular material blocks where the fiber is represented by one block (F) and other three blocks (M-1, M-2 and M3) are used for the matrix Figure 1c). The dimensions of these material blocks are normalised to unity in all three directions (axis-1, axis-2 and axis-3 as seen in Figure 1c), thus from the given matrix volume fraction (f), volume fractions of these blocks can be computed as:

$$f^{(1)} = y_2 z_2, f^{(2)} = y_2 z_1, f^{(3)} = y_1 z_2, f^{(4)} = y_1 z_1 \quad (1)$$

where $\dot{\boldsymbol{\epsilon}}^{(i)}$ and $\dot{\boldsymbol{\gamma}}^{(i)}$. The strain rate (or increment) vectors of the four material blocks can be used to obtain an expression for the average (homogenised) strain rate vector $\dot{\boldsymbol{\epsilon}}$ of the UVE (Figure 1c) as:

$$\dot{\boldsymbol{\epsilon}} = \sum_{i=1}^4 f^{(i)} \dot{\boldsymbol{\epsilon}}^{(i)} \quad (2)$$

$$\text{where } \dot{\boldsymbol{\epsilon}}^{(i)} = [\boldsymbol{\epsilon}_{11}^{(i)}, \boldsymbol{\epsilon}_{22}^{(i)}, \boldsymbol{\epsilon}_{33}^{(i)}, \boldsymbol{\gamma}_{12}^{(i)}, \boldsymbol{\gamma}_{23}^{(i)}, \boldsymbol{\gamma}_{13}^{(i)}]^T \quad (3)$$

In the above expression and throughout this article, any variables having the superscript (i) with $i = 1, 2, 3$ and 4 are corresponding to material blocks M-1, M-2, M-3 and F, respectively.

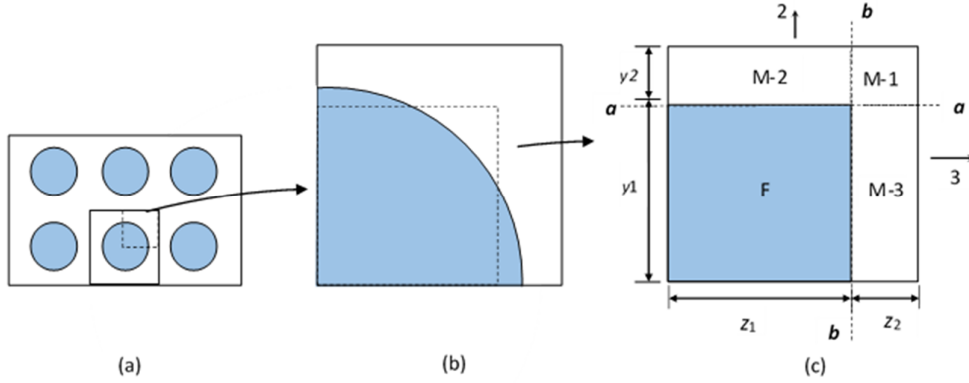


Figure 1: (a) Cross-section of a unidirectional FRC and the UVE; (b) Idealised unit cell; (c) Idealised unit cell element (F: Fiber block; M-1, M-2, M-3: Matrix blocks), after [85].

The strain rates of the matrix blocks are defined in terms of strain rates of the fiber block as well as the corresponding kinematic strain enhancements as follows:

$$\dot{\boldsymbol{\epsilon}}^{(1)} = \dot{\boldsymbol{\epsilon}}^{(4)} + \mathbf{N}_2 \boldsymbol{\mu}_1 \tilde{\boldsymbol{\epsilon}}_2 + \mathbf{N}_3 \boldsymbol{\mu}_2 \tilde{\boldsymbol{\epsilon}}_3 \quad (4)$$

$$\dot{\boldsymbol{\epsilon}}^{(2)} = \dot{\boldsymbol{\epsilon}}^{(4)} + \mathbf{N}_2 \tilde{\boldsymbol{\epsilon}}_2 \quad (5)$$

$$\dot{\boldsymbol{\epsilon}}^{(3)} = \dot{\boldsymbol{\epsilon}}^{(4)} + \mathbf{N}_3 \tilde{\boldsymbol{\epsilon}}_3 \quad (6)$$

where $\tilde{\boldsymbol{\epsilon}}_2 = [\tilde{\boldsymbol{\gamma}}_{2-12}, \tilde{\boldsymbol{\epsilon}}_{2-22}, \tilde{\boldsymbol{\gamma}}_{2-23}]$ and $\tilde{\boldsymbol{\epsilon}}_3 = [\tilde{\boldsymbol{\gamma}}_{3-13}, \tilde{\boldsymbol{\gamma}}_{3-23}, \tilde{\boldsymbol{\epsilon}}_{3-33}]$ are the kinematic strain enhancements defined in rate form, \mathbf{N}_2 and \mathbf{N}_3 are operational matrices correspond to $\tilde{\boldsymbol{\epsilon}}_2$ and $\tilde{\boldsymbol{\epsilon}}_3$, $\boldsymbol{\mu}_1$ and $\boldsymbol{\mu}_2$ are used to specify the proportion of $\tilde{\boldsymbol{\epsilon}}_2$ and $\tilde{\boldsymbol{\epsilon}}_3$ allocated to the strain rates of material block M-1. The readers may refer to [85] for more

detailed descriptions and explanations on these model parameters. To this end, the generic form of the constitutive relationship for the material blocks is given as:

$$\dot{\boldsymbol{\sigma}}^{(i)} = \mathbf{D}^{(i)} \dot{\boldsymbol{\varepsilon}}^{(i)} \quad (i = 1 \text{ to } 4) \quad (7)$$

where $\mathbf{D}^{(i)}$ is the tangent stiffness of a material block, and $\dot{\boldsymbol{\sigma}}^{(i)}$ is the stress increment vector.

2.2 A thermodynamics-based formulation

Due to the multi-phase nature of the model that includes four different material blocks representing fibre and three matrix phases under different deformation, the Helmholtz free energy for isothermal process can be written as volume-averaged energy, in the following form:

$$\Psi = \sum_{i=1}^4 f^{(i)} \Psi^{(i)} + \mathbf{C}_1^T \boldsymbol{\Lambda}_1 + \mathbf{C}_2^T \boldsymbol{\Lambda}_2 + \mathbf{C}_3^T \boldsymbol{\Lambda}_3 + \mathbf{C}_4^T \boldsymbol{\Lambda}_4 \quad (8)$$

where $f^{(i)}$ represents the volume fraction of block (i) (see details in the preceding section), and $\Psi^{(i)}$ is the corresponding Helmholtz free energy potential of that block. The first three constraints in (8) are related to the three strain enrichments (4-6) described in the preceding section:

$$\mathbf{C}_1 = \boldsymbol{\varepsilon}^{(1)} - \left(\boldsymbol{\varepsilon}^{(4)} + \mathbf{N}_2 \boldsymbol{\mu}_1 \tilde{\boldsymbol{\varepsilon}}_2 + \mathbf{N}_3 \boldsymbol{\mu}_2 \tilde{\boldsymbol{\varepsilon}}_3 \right) = \mathbf{0} \quad (9)$$

$$\mathbf{C}_2 = \boldsymbol{\varepsilon}^{(2)} - \left(\boldsymbol{\varepsilon}^{(4)} + \mathbf{N}_2 \tilde{\boldsymbol{\varepsilon}}_2 \right) = \mathbf{0} \quad (10)$$

$$\mathbf{C}_3 = \boldsymbol{\varepsilon}^{(3)} - \left(\boldsymbol{\varepsilon}^{(4)} + \mathbf{N}_3 \tilde{\boldsymbol{\varepsilon}}_3 \right) = \mathbf{0} \quad (11)$$

while the last constraint \mathbf{C}_4 links the strains in the four blocks with the macrostrain $\boldsymbol{\varepsilon}$:

$$\mathbf{C}_4 = \boldsymbol{\varepsilon} - \sum_{i=1}^4 f^{(i)} \boldsymbol{\varepsilon}^{(i)} = \mathbf{0} \quad (12)$$

In this sense, the strains in the four blocks and the enrichment strains $\tilde{\boldsymbol{\varepsilon}}_2$ and $\tilde{\boldsymbol{\varepsilon}}_3$ are considered as internal variables of the macro model represented by the relationship between macro strain $\boldsymbol{\varepsilon}$ and macro stress $\boldsymbol{\sigma}$. In a similar way, the macro dissipation potential takes the following form:

$$\Phi = \sum_{i=1}^4 f^{(i)} \Phi^{(i)} \quad (13)$$

where $\Phi^{(i)}$ are the dissipation potential of the individual block (i).

Following the procedures established beforehand in [106] for the derivation of a model from the Helmholtz and dissipation potentials, from the Helmholtz free energy, the true stresses and generalised stresses associated with corresponding internal variables, which as mentioned are strains in the four blocks and enrichment strains, are:

$$\boldsymbol{\sigma} = \frac{\partial \Psi}{\partial \boldsymbol{\varepsilon}} = \boldsymbol{\Lambda}_4 \quad (14)$$

$$\bar{\boldsymbol{\chi}}_{\boldsymbol{\varepsilon}^{(1)}} = -\frac{\partial \Psi}{\partial \boldsymbol{\varepsilon}^{(1)}} = -f^{(1)} \frac{\partial \Psi^{(1)}}{\partial \boldsymbol{\varepsilon}^{(1)}} - \boldsymbol{\Lambda}_1 + f^{(1)} \boldsymbol{\Lambda}_4 \quad (15)$$

$$\bar{\boldsymbol{\chi}}_{\boldsymbol{\varepsilon}^{(2)}} = -\frac{\partial \Psi}{\partial \boldsymbol{\varepsilon}^{(2)}} = -f^{(2)} \frac{\partial \Psi^{(2)}}{\partial \boldsymbol{\varepsilon}^{(2)}} - \boldsymbol{\Lambda}_2 + f^{(2)} \boldsymbol{\Lambda}_4 \quad (16)$$

$$\bar{\boldsymbol{\chi}}_{\boldsymbol{\varepsilon}^{(3)}} = -\frac{\partial \Psi}{\partial \boldsymbol{\varepsilon}^{(3)}} = -f^{(3)} \frac{\partial \Psi^{(3)}}{\partial \boldsymbol{\varepsilon}^{(3)}} - \boldsymbol{\Lambda}_3 + f^{(3)} \boldsymbol{\Lambda}_4 \quad (17)$$

$$\bar{\boldsymbol{\chi}}_{\boldsymbol{\varepsilon}^{(4)}} = -\frac{\partial \Psi}{\partial \boldsymbol{\varepsilon}^{(4)}} = -f^{(4)} \frac{\partial \Psi^{(4)}}{\partial \boldsymbol{\varepsilon}^{(4)}} + \boldsymbol{\Lambda}_1 + \boldsymbol{\Lambda}_2 + \boldsymbol{\Lambda}_3 + f^{(4)} \boldsymbol{\Lambda}_4 \quad (18)$$

$$\bar{\boldsymbol{\chi}}_{\tilde{\boldsymbol{\varepsilon}}_2} = -\frac{\partial \Psi}{\partial \tilde{\boldsymbol{\varepsilon}}_2} = (\mathbf{N}_2 \boldsymbol{\mu}_1)^T \boldsymbol{\Lambda}_1 + \mathbf{N}_2^T \boldsymbol{\Lambda}_2 \quad (19)$$

$$\bar{\boldsymbol{\chi}}_{\tilde{\boldsymbol{\varepsilon}}_3} = -\frac{\partial \Psi}{\partial \tilde{\boldsymbol{\varepsilon}}_3} = (\mathbf{N}_3 \boldsymbol{\mu}_2)^T \boldsymbol{\Lambda}_1 + \mathbf{N}_3^T \boldsymbol{\Lambda}_3 \quad (20)$$

From the dissipation potential (13), we obtain the following dissipative generalised stresses associated with their corresponding rates of internal variables, which in fact do not appear in the dissipation potential. As a consequence, we have:

$$\boldsymbol{\chi}_{\dot{\boldsymbol{\varepsilon}}^{(1)}} = \frac{\partial \Phi}{\partial \dot{\boldsymbol{\varepsilon}}^{(1)}} = \mathbf{0} \quad (21)$$

$$\boldsymbol{\chi}_{\dot{\boldsymbol{\varepsilon}}^{(2)}} = \frac{\partial \Phi}{\partial \dot{\boldsymbol{\varepsilon}}^{(2)}} = \mathbf{0} \quad (22)$$

$$\boldsymbol{\chi}_{\dot{\boldsymbol{\varepsilon}}^{(3)}} = \frac{\partial \Phi}{\partial \dot{\boldsymbol{\varepsilon}}^{(3)}} = \mathbf{0} \quad (23)$$

$$\boldsymbol{\chi}_{\boldsymbol{\varepsilon}^{(4)}} = \frac{\partial \Phi}{\partial \dot{\boldsymbol{\varepsilon}}^{(4)}} = \mathbf{0} \quad (24)$$

$$\boldsymbol{\chi}_{\dot{\boldsymbol{\varepsilon}}_2} = \frac{\partial \Phi}{\partial \dot{\boldsymbol{\varepsilon}}_2} = \mathbf{0} \quad (25)$$

$$\boldsymbol{\chi}_{\dot{\boldsymbol{\varepsilon}}_3} = \frac{\partial \Phi}{\partial \dot{\boldsymbol{\varepsilon}}_3} = \mathbf{0} \quad (26)$$

The Ziegler's orthogonality conditions [106] in the forms, $\bar{\boldsymbol{\chi}}_{\boldsymbol{\varepsilon}^{(1)}} = \boldsymbol{\chi}_{\boldsymbol{\varepsilon}^{(1)}}$,

$\bar{\boldsymbol{\chi}}_{\boldsymbol{\varepsilon}^{(2)}} = \boldsymbol{\chi}_{\boldsymbol{\varepsilon}^{(2)}}$, $\bar{\boldsymbol{\chi}}_{\boldsymbol{\varepsilon}^{(3)}} = \boldsymbol{\chi}_{\boldsymbol{\varepsilon}^{(3)}}$, $\bar{\boldsymbol{\chi}}_{\boldsymbol{\varepsilon}^{(4)}} = \boldsymbol{\chi}_{\boldsymbol{\varepsilon}^{(4)}}$, $\bar{\boldsymbol{\chi}}_{\dot{\boldsymbol{\varepsilon}}_2} = \boldsymbol{\chi}_{\dot{\boldsymbol{\varepsilon}}_2}$, and $\bar{\boldsymbol{\chi}}_{\dot{\boldsymbol{\varepsilon}}_3} = \boldsymbol{\chi}_{\dot{\boldsymbol{\varepsilon}}_3}$ lead to:

$$\boldsymbol{\Lambda}_1 = f^{(1)} \boldsymbol{\sigma} - f^{(1)} \boldsymbol{\sigma}^{(1)} \quad (27)$$

$$\boldsymbol{\Lambda}_2 = f^{(2)} \boldsymbol{\sigma} - f^{(2)} \boldsymbol{\sigma}^{(2)} \quad (28)$$

$$\boldsymbol{\Lambda}_3 = f^{(3)} \boldsymbol{\sigma} - f^{(3)} \boldsymbol{\sigma}^{(3)} \quad (29)$$

$$f^{(4)} \boldsymbol{\sigma}^{(4)} = f^{(4)} \frac{\partial \Psi^{(4)}}{\partial \boldsymbol{\varepsilon}^{(4)}} = f^{(1)} \boldsymbol{\sigma} - f^{(1)} \boldsymbol{\sigma}^{(1)} + f^{(2)} \boldsymbol{\sigma} - f^{(2)} \boldsymbol{\sigma}^{(2)} + f^{(3)} \boldsymbol{\sigma} - f^{(3)} \boldsymbol{\sigma}^{(3)} + f^{(4)} \boldsymbol{\sigma} \quad (30)$$

$$(\mathbf{N}_2 \boldsymbol{\mu}_1)^T \boldsymbol{\Lambda}_1 = -\mathbf{N}_2^T \boldsymbol{\Lambda}_2 \quad (31)$$

$$(\mathbf{N}_3 \boldsymbol{\mu}_2)^T \boldsymbol{\Lambda}_1 = -\mathbf{N}_3^T \boldsymbol{\Lambda}_3 \quad (32)$$

From Eq. (30), we obtain the volume-averaged form of macro stress $\boldsymbol{\sigma}$:

$$f^{(1)} \boldsymbol{\sigma}^{(1)} + f^{(2)} \boldsymbol{\sigma}^{(2)} + f^{(3)} \boldsymbol{\sigma}^{(3)} + f^{(4)} \boldsymbol{\sigma}^{(4)} = (f^{(1)} + f^{(2)} + f^{(3)} + f^{(4)}) \boldsymbol{\sigma} = \boldsymbol{\sigma} \quad (33)$$

Using Eqs. (27) to (29), (31) to (32) we obtain the following conditions:

$$\boldsymbol{\mu}_1^T \mathbf{N}_2^T (f^{(1)} \boldsymbol{\sigma} - f^{(1)} \boldsymbol{\sigma}^{(1)}) = -\mathbf{N}_2^T (f^{(2)} \boldsymbol{\sigma} - f^{(2)} \boldsymbol{\sigma}^{(2)}) \quad (34)$$

$$\boldsymbol{\mu}_2^T \mathbf{N}_3^T (f^{(1)} \boldsymbol{\sigma} - f^{(1)} \boldsymbol{\sigma}^{(1)}) = -\mathbf{N}_3^T (f^{(3)} \boldsymbol{\sigma} - f^{(3)} \boldsymbol{\sigma}^{(3)}) \quad (35)$$

These equations (34) and (35) can be combined with the one expressing the macro stress (33) as volume-averaged stress to obtain the following internal equilibrium conditions across the boundaries of the blocks. In particular, (33) and (34) lead to the traction continuity in averaged form between blocks (1, 2) and (3, 4), e.g. the interface indicated by line **a-a** in Figure 1c:

$$\begin{aligned}
 & f^{(1)} \boldsymbol{\sigma}^{(1)T} \mathbf{N}_2 \left[\boldsymbol{\mu}_1 - \left(f^{(1)} \boldsymbol{\mu}_1 + f^{(2)} \mathbf{I} \right) \right] + f^{(2)} \boldsymbol{\sigma}^{(2)T} \mathbf{N}_2 \left[\mathbf{I} - \left(f^{(1)} \boldsymbol{\mu}_1 + f^{(2)} \mathbf{I} \right) \right] \\
 & - f^{(3)} \boldsymbol{\sigma}^{(3)T} \mathbf{N}_2 \left(f^{(1)} \boldsymbol{\mu}_1 + f^{(2)} \mathbf{I} \right) - f^{(4)} \boldsymbol{\sigma}^{(4)T} \mathbf{N}_2 \left(f^{(1)} \boldsymbol{\mu}_1 + f^{(2)} \mathbf{I} \right) = 0
 \end{aligned} \tag{36}$$

And in a similar way, (33) and (35) lead to the internal equilibrium condition between blocks (1, 3) and (2, 4), e.g. the interface indicated by line **b-b** in Figure 1c:

$$\begin{aligned}
 & f^{(1)} \boldsymbol{\sigma}^{(1)T} \mathbf{N}_3 \left[\boldsymbol{\mu}_2 - \left(f^{(1)} \boldsymbol{\mu}_2 + f^{(3)} \mathbf{I} \right) \right] + f^{(3)} \boldsymbol{\sigma}^{(3)T} \mathbf{N}_3 \left[\mathbf{I} - \left(f^{(1)} \boldsymbol{\mu}_2 + f^{(3)} \mathbf{I} \right) \right] \\
 & - f^{(2)} \boldsymbol{\sigma}^{(2)T} \mathbf{N}_3 \left(f^{(1)} \boldsymbol{\mu}_2 + f^{(3)} \mathbf{I} \right) - f^{(4)} \boldsymbol{\sigma}^{(4)T} \mathbf{N}_3 \left(f^{(1)} \boldsymbol{\mu}_2 + f^{(3)} \mathbf{I} \right) = 0
 \end{aligned} \tag{37}$$

In summary, Eq. (33) provides the relationship between the homogenised (macro) stress increments of the UVE and the local stress increments in the four material blocks. On the other hand, Eqs (36) and (37) specify the conditions required for fulfilling traction continuity across the interfaces **a-a** and **b-b** (Figure 1c). This traction continuity condition, however, is not automatically achieved for any arbitrary stress/strain increment due to nonlinear nature of the constituent behaviour, in which case an iterative scheme is needed to correctly update the strain enhancements and the stresses in the UVE. Such computational scheme has been developed and implemented in the works of [107] and hence is not presented here.

In this regard, by utilising Equations (1), (4) to (4), (36) and (37) along with a series of mathematical operations, the local strain rates of four material blocks (Figure 1c) can be determined completely from the macro strain rates as follows:

$$\dot{\boldsymbol{\epsilon}}^{(1)} = (\mathbf{I} + \mathbf{N}_2 \mathbf{K}_1 \mathbf{P}_1 + \mathbf{N}_3 \mathbf{K}_2 \mathbf{P}_2) \dot{\boldsymbol{\epsilon}} \tag{38}$$

$$\dot{\boldsymbol{\epsilon}}^{(2)} = (\mathbf{I} + \mathbf{N}_2 \mathbf{K}_3 \mathbf{P}_1 - \mathbf{N}_3 \mathbf{K}_4 \mathbf{P}_2) \dot{\boldsymbol{\epsilon}} \tag{39}$$

$$\dot{\boldsymbol{\epsilon}}^{(3)} = (\mathbf{I} - \mathbf{N}_2 \mathbf{K}_5 \mathbf{P}_1 + \mathbf{N}_3 \mathbf{K}_6 \mathbf{P}_2) \dot{\boldsymbol{\epsilon}} \tag{40}$$

$$\dot{\boldsymbol{\epsilon}}^{(4)} = (\mathbf{I} - \mathbf{N}_2 \mathbf{K}_4 \mathbf{P}_1 - \mathbf{N}_3 \mathbf{K}_3 \mathbf{P}_2) \dot{\boldsymbol{\epsilon}} \tag{41}$$

where matrices \mathbf{P}_1 and \mathbf{P}_2 can be obtained from the properties of the four material blocks and their volume fractions (please see detailed expression given in Appendix. Essentially, when nonlinear analyses are performed on a structure, the strain increments in the local fields (material blocks) are obtained from a given macro strain increment (Eqs (38)-(41)) at each integration points within a structural element. The corresponding stresses in the material blocks are subsequently

updated using the constitutive relationship specified for each block (Equation (4)), and the macro stress of the UVE can also be determined through volume averaging stresses in all four material blocks (Eq. (33)). Based on these considerations, the macro stress increment can be related to the macro strain increment by substituting Equations (4), (38)-(41) into Eq. (33) and the following expression for macro stress increment can be obtain:

$$\dot{\boldsymbol{\sigma}} = \mathbf{D} \dot{\boldsymbol{\varepsilon}} \quad (42)$$

where the tangent stiffness matrix of the UVE or the composite material is given as:

$$\begin{aligned} \mathbf{D} = & \sum_{i=1}^4 f^{(i)} \mathbf{D}^{(i)} + f^{(1)} \mathbf{D}^{(1)} \mathbf{N}_2 \mathbf{K}_1 \mathbf{P}_1 + f^{(1)} \mathbf{D}^{(1)} \mathbf{N}_3 \mathbf{K}_2 \mathbf{P}_2 + f^{(2)} \mathbf{D}^{(2)} \mathbf{N}_2 \mathbf{K}_3 \mathbf{P}_1 - f^{(2)} \mathbf{D}^{(2)} \mathbf{N}_3 \mathbf{K}_4 \mathbf{P}_2 \\ & - f^{(3)} \mathbf{D}^{(3)} \mathbf{N}_2 \mathbf{K}_5 \mathbf{P}_1 + f^{(3)} \mathbf{D}^{(3)} \mathbf{N}_3 \mathbf{K}_6 \mathbf{P}_2 - f^{(4)} \mathbf{D}^{(4)} \mathbf{N}_2 \mathbf{K}_4 \mathbf{P}_1 - f^{(4)} \mathbf{D}^{(4)} \mathbf{N}_3 \mathbf{K}_3 \mathbf{P}_2 \end{aligned} \quad (43)$$

The constitutive relationship of the composite material as presented in Equation (43) requires the descriptions of the tangent stiffness matrices for all four material blocks and their volume fractions. In addition, the proposed tangent stiffness formulation is described in an incremental form which facilitates the model application in both elastic and inelastic ranges of response of the material. To this end, the main sources of nonlinearity in the behaviour of composite material are matrix inelastic response, due to damage coupled with plasticity process, and fiber debonding mechanism, caused by failure of the cohesive layer between fiber and matrix. Thus, these two distinctive failure processes need separate approaches to capture the constitutive response of composite materials under their influences. As a result, two different damage models will be used to describe the evolution of the tangent stiffness for the four material blocks which will be presented in the subsequent sections for a complete mathematical formulation of the proposed model.

3. Anisotropic Damage Model for Fiber Interfacial Debonding:

3.1 Fiber and Fiber Interface Failure Behaviour:

The response of fiber and failure behaviour due to debonding mechanism that takes place at the fiber/matrix interface is an important factor that influences the aggregate behaviour of the FRC plies, and consequently their effects need adequate understanding. To this end, experimental results indicate the properties of fiber

remain linear elastic until final fracture occurs [2, 77], which is immediately followed by its brittle failure behaviour. In addition, recent study [79] reported a variation of fiber elastic modulus along with changing strain rates (or rate of loading). However, under assumption of quasi-static loading condition, it is generally sufficient to assume a constant elastic modulus of fiber throughout loading prior to fiber fracture. This presumption is also widely adopted in many other studies such as those found in [79, 81, 93, 108–110]. On the other hand, the behaviour of fiber interfacial failure is much more complex which has considerable effects on the macroscopic performance of FRCs. Experimental findings [111–113] documented direct relations between nonlinear behaviour of FRCs and fiber debonding mechanism along with frictional sliding at the end of the debonding process. These investigations are commonly carried out using fiber/rod pull out test where the reported load-displacement curves clearly show nonlinear portion of the curve characterised by interface debonding. It is worth mentioning that under increasing loads, excessive fiber debonding is followed by a completed separation of fiber from matrix and the specimen enters a stage where only frictional forces remained acting at the interface. This fiber interface failure process usually initiates from matrix cracks or defects in the matrix that develop towards fiber/matrix interface where a region of stress concentration is formed. Subsequently, if the bonding between the two constituents is strong enough, the fiber and matrix are compatible at the interface since there will be no sliding or debonding and there is no loss of stiffness in the overall ply response due to interfacial failure. On the contrary, fiber fracture can occur instead of fiber debonding as a result of matrix cracks penetrating through the fiber and this process usually happens when the toughness of the fiber/matrix interface is much greater than the fiber toughness [114, 115]. In this situation, the energy is dissipated mainly via fiber fracture. Furthermore, it is noted failure mode due to the fiber debonding is much more common than fiber fracture since modern fibers usually possess excellent toughness that helps to deflect the progression of matrix cracking and prevent premature failure of fiber. Thus, with weaker interfacial bonding strength, separation of fiber from the surrounding matrix occurs and subsequently results in progressive sliding at the fiber/matrix interface and the degradation of bonding strength between the two surfaces [115]. As fiber/matrix interfacial failure progresses, a gradual loss of overall stiffness of the composite is noted which is

most profound in the transverse direction perpendicular to the fiber [81]. The aggregate stiffness of the composite in the longitudinal direction, on the other hand, is also affected by fiber debonding process, however to a much lesser extent [116], since the deformations occur in this direction are not severely influenced by the conditions of the interface but rather being mainly controlled by fiber characteristics [81].

Based on the above considerations, the intention of this study is to incorporate the nonlinear effects due to fiber/matrix interfacial debonding mechanism into the proposed micromechanical model. Among all four material blocks that constitute the homogenised ply response, only fiber behaves in a linear-elastic manner until its final fracture while matrix blocks process inelastic properties beyond their elastic domain. In this study, it is proposed that the inelastic effects of debonding failure on the ply response to be encapsulated in the response of a modified fiber block, namely Fiber-Interface Equivalence (FIE) block which is shown in Figure 1. The response of FIE block will be specified in such a way that it has the combined characteristics of both linear-elastic behaviour of fiber and inelastic behaviour of the interface. This actually reflects changes of stress fields in the fiber due to softening interface that weakens the load carrying capability of the whole composite system. In this sense, fiber is not able to fully utilise its outstanding stiffness and excellent load carrying capacity but its performance is rather dictated by the bonding properties of the interface. Thus, a new constitutive model is needed to effectively convey the nonlinear effects of interfacial failure in the FIE block (Figure 2) which will be described in the next section.

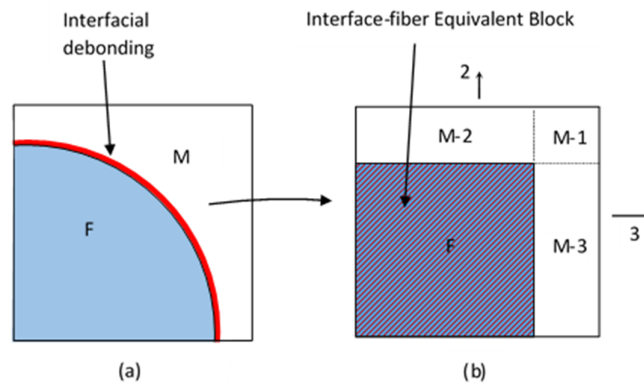


Figure 2: (a) Idealised unit cell with fiber/matrix interface debonding (b) Idealised unit cell element takes into account the effects of interface debonding in the Fiber-Interface Equivalent (FIE) block

3.2 Anisotropic Damage Model for Fiber Interface Failures:

Fiber interfacial failure is highly anisotropic in nature and therefore capturing its response requires anisotropic damage model accordingly. It is also noted that the development of fiber/matrix interface failure is restricted to pre-defined planes parallel to the fiber direction and the direction perpendicular to this surface will be referred to as the direction of fiber decohesion/debonding from here onwards. As discussed previously, ply stiffness reductions due to fiber interface failure are the most profound in the direction of debonding, whereas its softening effects also can be observed in the other transverse direction (perpendicular to fiber direction), however, to a lesser extent. For example, Figure 3 depicts the fiber debonding failure in direction 3 due to the applied tensile stress σ_3 and compressive stress σ_2 in direction 3 and 2 respectively. In this case, it can be expected that the stiffness reductions of the homogenised material are much more severe in the direction 3 compared to that of direction 2. On this basis, an isotropic damage model with the use of a scalar damage variable deems to be inadequate to capture the varying effects of damage in different directions. Therefore an anisotropic model is essential.

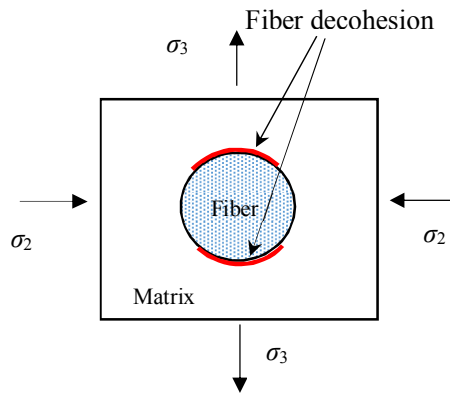


Figure 3: Illustration of Fiber/matrix interface failure due to tensile loading in direction 2 and compressive loading in direction 3.

On the other hand, the proposed micromechanics model enables explicit modelling of stresses and strains in the constituent blocks which can be used conveniently to control the initiation and progressions of debonding failure in the FIE block. Furthermore, strains in principal stress directions normal to the fiber of FIE block are compared against a critical debonding threshold ε_c and the debonding failure

process is activated only when this threshold is exceeded. This can be illustrated in Figure 4 which shows the limit of strains in the principal direction 2 and 3 where values of strain lying inside these limits ($\varepsilon_2^{(4)} < \varepsilon_c$ and $\varepsilon_3^{(4)} < \varepsilon_c$) imply perfect bonds between fiber and matrix (no debonding failure takes place). On the other hand, debonding failure is in effects if $\varepsilon_2^{(4)} > \varepsilon_c$ or $\varepsilon_3^{(4)} > \varepsilon_c$.

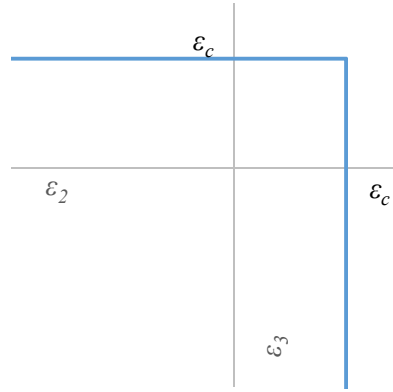


Figure 4: Limits of strains for fiber debonding failure

On this basis, the damage evolution rule is proposed in the following form:

$$\omega_{(i)} = 1 - e^{-\gamma \varepsilon_i^d} \quad (44)$$

($i = 2, 3$ represents the principal stress directions normal to the fiber)

where $\omega_{(i)}$ is damage variable associated with debonding failure, parameter γ governs rate of damage growth, and ε_i^d is the portion of strain in the principal stress direction that exceeds the debonding threshold and its expression is given as:

$$\varepsilon_i^d = \langle \varepsilon_i^{(4)} - \varepsilon_c \rangle \quad (45)$$

where $\langle \rangle$ is Macaulay bracket, ε_c is the debonding failure threshold that evolves with deformation and keeps its maximum previously reached value of $\varepsilon_i^{(4)}$, where $\varepsilon_i^{(4)}$ is the strain in FIE block in principal stress direction i^{th} (Equation (45)). From the above equation, it can be inferred that for $\varepsilon_i^{(4)} < \varepsilon_c$, ε_i^d takes a value of zero and damage is inactive as $\omega_{(i)} = 0$ (Equations (44)). In contrast, if $\varepsilon_i^{(4)} > \varepsilon_c$, the debonding mechanism is activated since $\omega_{(i)}$ now takes a nonzero and increasing value and the damage effects are incorporated into the elastic stiffness matrix of fiber in the total form as follow:

$$D_{damaged}^{(4)} = \begin{bmatrix} D_{11} & \Gamma_{12}D_{12} & \Gamma_{13}D_{13} & 0 & 0 & 0 \\ \Gamma_{21}D_{21} & \Gamma_{22}D_{22} & \Gamma_{23}D_{23} & 0 & 0 & 0 \\ \Gamma_{31}D_{31} & \Gamma_{32}D_{32} & \Gamma_{33}D_{33} & 0 & 0 & 0 \\ 0 & 0 & 0 & D_{44} & 0 & 0 \\ 0 & 0 & 0 & 0 & D_{55} & 0 \\ 0 & 0 & 0 & 0 & 0 & D_{66} \end{bmatrix} \quad (46)$$

where D_{ij} are the elastic constants of the elastic stiffness matrix of fiber while Γ_{11} , Γ_{22} and Γ_{33} are given as follows:

$$\Gamma_{22} = (1 - \omega_{(2)})(1 - \omega_{(3)})^{1/n} \quad (47)$$

$$\Gamma_{33} = (1 - \omega_{(3)})(1 - \omega_{(2)})^{1/n} \quad (48)$$

$$\Gamma_{12} = \Gamma_{21} = (1 - \omega_{(2)}) \quad (49)$$

$$\Gamma_{13} = \Gamma_{31} = (1 - \omega_{(3)}) \quad (50)$$

$$\Gamma_{23} = \Gamma_{32} = (1 - \omega_{(2)})(1 - \omega_{(3)}) \quad (51)$$

The parameter n in the above expressions is used to account for the unequal effects of debonding failure in different directions. For instance, $n > 1$ indicates that the effects of damage are lesser in the principal direction where debonding failure does not occur. In contrast, for $n = 1$, the stiffness reductions due to debonding failure are of the same order of magnitude in both directions ($\Gamma_{22} = \Gamma_{33}$). More detail analyses on the influence of n are provided in subsequent sections. On this basis, the principal stresses in the FIE block is calculated using the following expression:

$$\sigma_p^{(4)} = D_{damaged}^{(4)} \mathcal{E}_p^{(4)} \quad (52)$$

Thus, the proposed debonding criterion leads to the establishment of a failure surface in the principal stress space for the FIE block. The envelop is obtained by producing a uniaxial/biaxial stress state with a constant ratio between σ_2 and σ_3 and both stress values are recorded when debonding failure is activated (see Equations (44) and (45)). These stresses at the onset of debonding under various ratios between σ_2 and σ_3 are subsequently used to form the initial debonding envelop which can be illustrated in Figure 5 along with the corresponding stress-strain responses under (a) uniaxial tension; (b) uniaxial compression and (c) biaxial loading (tension along direction 3 and compression along direction 2). It can be seen in Figure 5 that stress state of the material falling inside this envelop implies there is no debonding while stress state outside this initial surface is an indication

of debonding failure between fiber and matrix. Furthermore, it can be seen in Figure 5 that the softening effects of varied magnitude are seen in all transverse directions which is characterised by the anisotropic nature of fiber debonding problems.

Furthermore, it is worthy of attention that the evolution of damage is a function of the tensile strains in the corresponding principal direction (see Equation (44)). The rate of deformation (or strain increment), on the other hand, effectively depends on the characteristics of applied loads in the material block. The effects of different loading condition on the growth of damage can also be illustrated in Figure 5 where identical strain rate is imposed on both loading case (a) and (b) and fiber is debonded from the surrounding matrix in the principal direction 3. In loading case (b), debonding failure is activated by tensile strain in the principal direction 3 developed under Poisson effects. Thus, this tensile strain increment is only a fraction of strain rate in the loading direction 3 and it is much less than that of loading case (a). As a result, the damage effects are developed at a slower rate in loading case (b) compared to the other case which eventually manifest in much more profound nonlinearity observed in loading case (a).

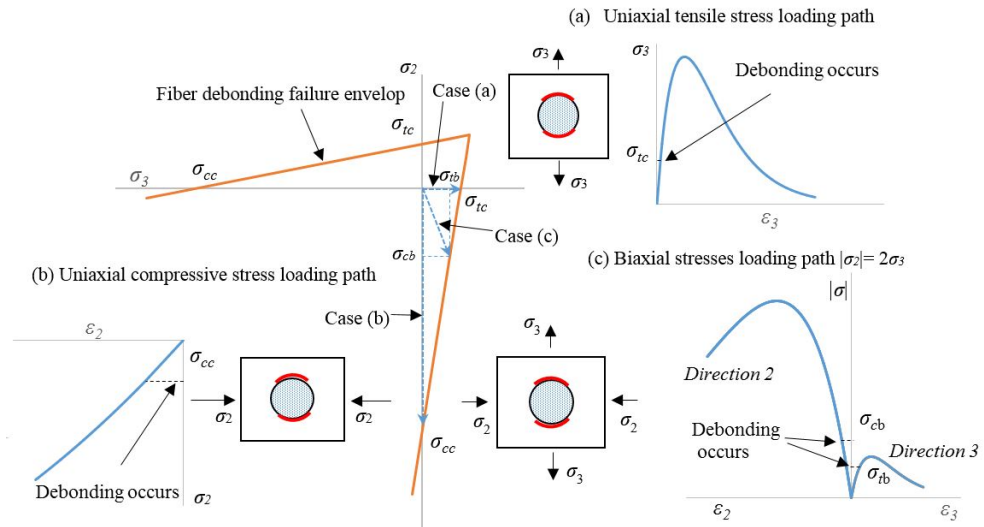


Figure 5: Illustration of debonding failure envelop in biaxial stress space and typical stress-strain responses of the FIE block in three loading cases (a) uniaxial tension; (b) uniaxial compression and (c) biaxial loading.

3.3 Parametric Study:

The rate of damage evolution in the proposed model is influenced by strain increment (Equation (44)) in the principal direction as well as anisotropic characteristics of the debonding failure. To this end, the proposed model utilises a parameter n (Equations (47) - (48)) to specify the anisotropic effects of fiber debonding on the constitutive response of the material. This can be illustrated in Figure 6 which shows the stress-strain response of the FIE block under loading case (c) for different parameter $n = 1, 3, 4, 5$ and 100 and the material parameters used in the proposed constitutive model are $E = 74000$ (MPa), $\nu = 0.15$, $\gamma = 1400$, $\varepsilon_c = 0.0001$. The material specimen is subjected to tension along principal direction 2 ($\varepsilon_2 > 0$) and compression in direction 3 ($\varepsilon_3 < 0$) while the ratio between ε_2 and ε_3 is maintained at $\varepsilon_2/\varepsilon_3 = -2$ throughout the entire loading domain. It should be noted that $n = 1$ implies that damage effects are identical in both directions which is in contrast with the case where $n = 100$ ($n \rightarrow \infty$) indicates that debonding failure in direction 2 does not have any impacts on the stress-strain response in direction 3 and the reverse is also hold.

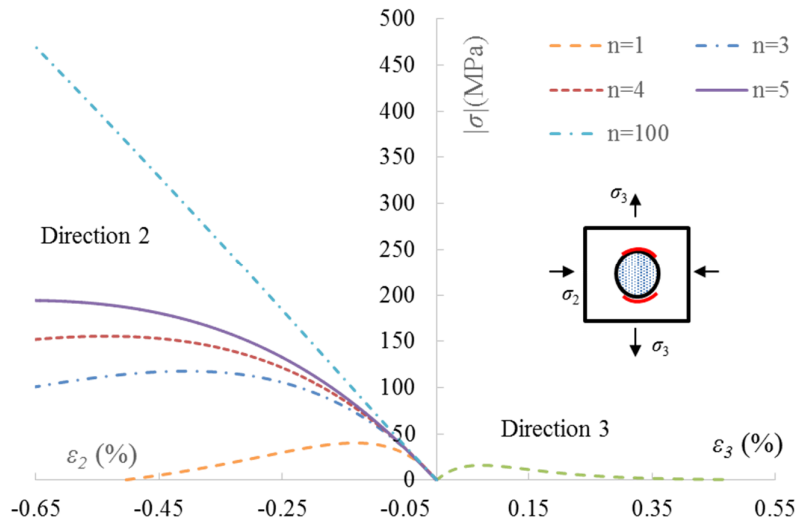


Figure 6: Stress-strain response in biaxial loading case for various values of n .

On the other hand, the evolution of damage due to debonding is governed by parameter γ which is coupled with the strain increment in the corresponding principal direction (Equation (44)). Examples of using γ in the proposed model to capture effects of debonding with various magnitudes are shown in Figure 7 where the constitutive responses with damage of the FIE block are illustrated for the

following cases: uniaxial tension (Figure 7a) and uniaxial compression (Figure 7b). The material parameters used in this example are $E = 74000$ (MPa), $\nu = 0.15$, $n = 2$, $\varepsilon_c = 0.0001$. It can be seen in Figure 7 that the rate of softening is increased with increasing values of γ in both uniaxial tension and uniaxial compression cases where much more abrupt drop in stiffness are observed in the former case for the same value of γ . This is due to the fact that debonding failure strain ε_d (Equation (45)) is developed in the same direction as loading in uniaxial tension case (Figure 7a) and therefore its magnitude is much higher to that of uniaxial compression case (Figure 7b) where fiber is debonded in transverse direction of loading. This debonding failure strain ε_d is subsequently magnified by the parameter γ which eventually either intensify or lessen the effects of fiber debonding depending on the chosen value of parameter γ . Thus, the use of γ within the proposed model helps to properly capture the effects of debonding on the constitutive response of the material which will be present in more realistic applications in subsequent sections.

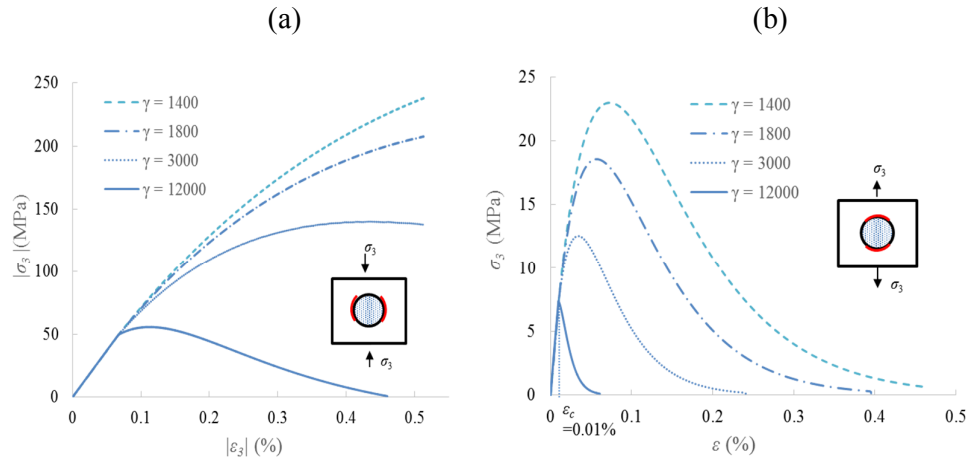


Figure 7: Effects of changing γ in (a) uniaxial tensile stress and (b) uniaxial compressive stress

4. A coupled Damage-Plasticity Constitutive Model for Matrix:

4.1 Mathematical Formulation:

The evolutions of plasticity and damage processes are dependent on one another, thus, their coupling effects should be appropriately reflected in the development of a constitutive model for matrix. In this study, the inelastic response of each matrix block (Figure 1c) is modelled based on the coupled damage-plasticity formulation

proposed by [117] where failures in the matrix is accounted for using an isotropic damage model. The stress-strain-damage relationship is of the following form:

$$\sigma_{ij} = (1-D) C_{ijkl} (\varepsilon_{kl} - \alpha_{kl}) \quad (53)$$

where σ_{ij} is the stress tensor, D is the scalar damage variable C_{ijkl} is the tangent stiffness tensor, ε_{kl} is the strain tensor, α_{kl} is the plastic strain tensor. The model utilises a Drucker-Prager yield criterion given the pressure-dependent behaviour commonly observed in polymer composite [83] and even in metals such as Aluminium [118]. Furthermore, the experimental evidence [83, 119] reveals that the yield surface of polymer matrix takes a parabolic shape in the $(p-q)$ stress space, where p is the hydrostatic pressure and q is the deviatoric stress. Based on these considerations, the yield function for matrix can be expressed in the following form:

$$y = q^2 + \beta p - k \quad (54)$$

The different terms used in the above equation can be defined as follows [120]:

$$p = \frac{I_1}{3} = \frac{\sigma_{ii}}{3}; \quad q = \sqrt{3J_2} = \sqrt{\frac{3}{2}s_{ij}s_{ij}}; \quad s_{ij} = \sigma_{ij} - \delta_{ij} p; \quad (55)$$

$$\beta = 3(f_{cy} - f_{ty}); \quad k = f_{cy} f_{ty}$$

where s_{ij} is the deviatoric stress tensor, δ_{ij} is Kronecker delta, I_1 and J_2 are stress invariants, f_{cy} is the uniaxial yield strength in compression and f_{ty} is the uniaxial yield strength in tension. The value of f_{cy} and f_{ty} are defined using the following functions:

$$f_{cy} = (1-D)(f_{c0} + Q_c (1 - e^{-b_c \varepsilon_p})), \quad f_{ty} = (1-D)(f_{t0} + Q_t (1 - e^{-b_t \varepsilon_p})) \quad (56)$$

where ε_p is the effective/accumulative plastic strain (where its rate is defined in Equation (57)), f_{t0} and f_{c0} are initial yield strengths, and Q_t , Q_c , b_t and b_c are material constants with subscript t and c indicating tensile and compressive states, respectively. The rate of accumulative plastic strain $\dot{\varepsilon}_p$ is given as:

$$\dot{\varepsilon}_p = \sqrt{\frac{2}{3} \dot{\alpha}_{ij} \dot{\alpha}_{ij}} \quad (57)$$

On the other hand, the evolutions of plastic strain tensor $\dot{\alpha}_{ij}$ and damage variable D are obtained from a unique loading function [117] and they are given as follows:

$$\dot{\alpha}_{ij} = \dot{\lambda} \left(2 \frac{a \sqrt{q^2 + \beta p}}{k} \frac{\delta_{ij}}{3} + 2 \frac{b \sqrt{q^2 + \beta p}}{k} \frac{3}{2\sqrt{3}J_2} \frac{\partial J_2}{\partial \sigma_{ij}} \right) \quad (58)$$

$$\dot{D} = 2 \dot{\lambda} \frac{r_d^2 (q^2 + \beta p)}{k \chi_D} \quad (59)$$

where a and b in the above equations are related to the growths of volumetric and deviatoric components, respectively, of the total plastic strain and they can be combined into a single parameter r_p ($0 \leq r_p \leq 1$) representing the energy dissipation due to plasticity. On the other hand, the parameter r_d represents the energy dissipated due to damage process and it is calculated as $r_d = 1 - r_p$. For more comprehensive model derivations and definitions, the readers may refer to [117]. In their works, the direction of plastic flow can be controlled by specifying the ratio between parameters a and b in Equation (58) and for associated flow rules (plastic flow vector normal to the yield surface), which will be used throughout this paper, the parameters a and b are given as follows:

$$a = \pm \sqrt{\frac{r_p}{1 + \left(\frac{\partial y / \partial q}{\partial y / \partial p} \right)^2}} \quad (60)$$

$$b = \sqrt{\frac{r_p}{1 + \left(\frac{\partial y / \partial p}{\partial y / \partial q} \right)^2}} \quad (61)$$

The coupled damage-plasticity model described above along with a stress return algorithm [107] are then implemented in a Matlab program to produce the nonlinear behaviour of several polymer resins. Figure 8 shows the responses of four epoxies under uniaxial tension obtained from experiments (data collected by Asp [121]) along with the plot of results produced by the proposed model. The model parameters used to capture the response of the four epoxies are given in Table 1. The Young's Modulus E were given in [121] by averaging the data obtained in several studies. The Poisson ratio is assumed to be 0.35 as this is a standard value assigned to epoxy in the range 0.32 – 0.35 [121]. It can be seen from Figure 8 that the coupled damage-plasticity capture very well the response of polymer resin in uniaxial tension.

Table 1: Model Parameters for *Epoxy Resins*

	E	ν	f_{t0}	f_{c0}	Q_t	Q_c	b_t	b_c	r_d
	GPa		MPa	MPa	MPa	MPa			
TGDDM/DDS	3.77	0.35	35	70	40	50	600	600	0
DGEBA/MHPA	2.92	0.35	40	70	50	50	250	350	0.008
DGEBA/APTA	2.93	0.35	40	70	40	50	350	350	0.07
DGEBA/DETA	2.07	0.35	25	70	50	50	150	350	0

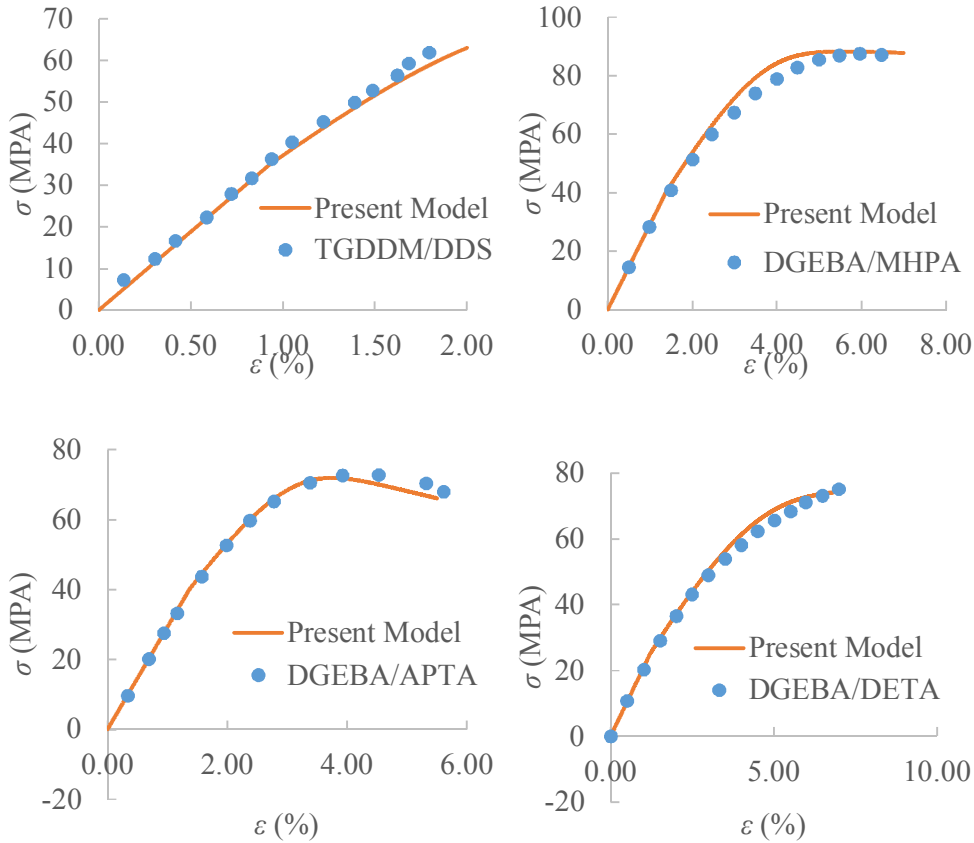


Figure 8: Responses epoxies under uniaxial tension (Experimental Data obtained from Aps 1995).

In addition, the response of other epoxy is also measured experimentally in [83] under uniaxial tension, uniaxial compression and pure in-plane shear. The experimental results are plotted in Figure 9 along with results obtained from [109]. Figure 9 also shows the results produced by the proposed model using the following model parameters: $E = 3.76$ (GPa), $\nu = 0.39$, $f_{t0} = 45$ (MPa), $f_{c0} = 70$ (MPa), $Q_t = 48$ (MPa), $Q_c = 55$ (MPa), $b_t = 200$, $b_c = 200$, $r_d = 0$. It can be seen that the present results are in good agreement with both experimental measurement and results

provided by others. It should be noted that post-peak response of the specimen was not obtained from experiment for all three loading scenarios, thus in the current study it is assumed that the stress response of the epoxy will exhibit a perfect plasticity behaviour once the ultimate values of stresses have been reached. This results in plateau responses in the stress-strain curve of the epoxy under all three loading cases as seen in Figure 9.

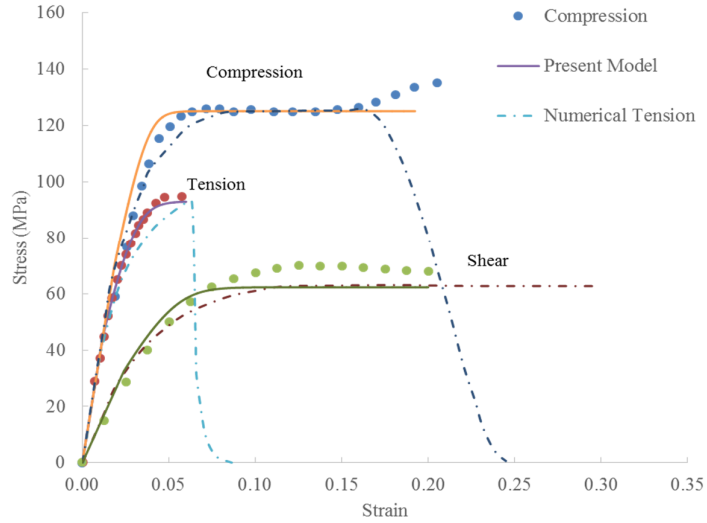


Figure 9: Responses of epoxy under uniaxial tension, uniaxial compression and pure in-plane shear: Comparisons between experimental measurements, numerical results and results produced by the proposed model.

5. Inelastic Response of FRC Ply

The proposed kinematically enhanced constitutive model for FRCs described in Section 2.1 requires separate constitutive models for its constituent blocks (fiber and matrix – Figure 1c). Thus, Section 2.2 provides a constitutive model for the modified fiber block, so-called FIE block (Figure 2), which accounts the response of fiber as well as the effects of fiber/matrix interface failure. On the other hand, a coupled damage-plasticity model, which can capture the effects of nonlinear mechanisms such as damage and plasticity on the response of matrix, is presented in Section 2.3. Subsequently, the two constitutive relationships for the fiber-interface and the matrix are incorporated into the overall constitutive model for unidirectional FRC ply in a Matlab programme. In this section, the inelastic

behaviours of FRCs are generated by the model for three different loading conditions: uniaxial longitudinal tension, uniaxial transverse tension and uniaxial transverse compression. To demonstrate the performance of the proposed model, for each loading condition the homogenised stress-strain response are plotted and compared to experimental measurements obtained from literature as well as predictions made by other existing models.

5.1 Uniaxial tension along fiber direction

In this example, the composite ply is made of silicon carbide (*SCS6*) fibers and titanium-based-alloy (*Ti-β21S*) resin with fiber volume fraction of 0.343 and it is subjected to uniaxial tension along fiber directions. The responses of the ply produced by the model are plotted in Figure 10. The model parameters used for the FIE block are: $E = 400$ (GPa), $\nu = 0.25$, $\varepsilon_c = 0.01\%$, $n = 2$ and $\gamma = 140$ whereas model parameters for the matrix blocks are: $E = 100$ (GPa), $\nu = 0.35$, $f_{i0} = 200$ (MPa), $f_{c0} = 250$ (MPa), $Q_t = 280$ (MPa), $Q_c = 400$ (MPa), $b_t = 100$, $b_c = 100$, $r_d = 0$. It should be noted that due to the nature of loading condition, fiber debonding does not occur and hence an assumption on perfect fibre-matrix interface can be taken [107]. Figure 10 shows that the results produced by the proposed model are in good agreement with both experimentally measured values and numerical results provided by Robertson & Mall [110].

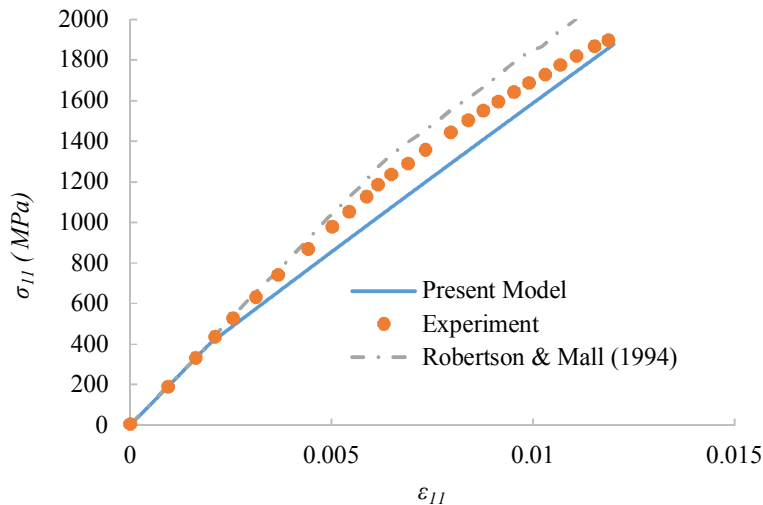


Figure 10: Responses of 0°-lamina for *SCS6/Ti-β21S* under uniaxial tension.

It can be seen from Figure 10 that the model is able to properly capture the high stress state exhibited in the composite owing to its inherent high stiffness and high load carrying capacity of fiber in tension. The homogenised response is dictated by the elastic behaviour of fiber with only low degree of nonlinearity is observed due to inelastic response of matrix in high strains for both present model and other results.

5.2 Uniaxial tension in transverse direction

The same composite ply *SCS6/Ti-β21S* (Section 5.1) is now examined for its response under uniaxial transverse tension in the directional normal to the fiber. Figure 11 shows the good agreement between the results produced by the proposed model and experimental measurements as well as numerical results provided by Robertson & Mall [110]. It should be underlined that the observed nonlinearity in the homogenised response of the composite ply under transverse tension is due to the combination of fiber debonding (in the direction of loading) and matrix yielding, both mechanisms are effectively taken into account by the proposed model. The softening effects of fiber debonding are manifested in the nonlinear response of FIE block as seen in Figure 12. This is further confirmed in a numerical study carried out by Melro et al [85] where the influences of fiber/matrix interface failure and inelastic behaviour of matrix on the response of the E-glass/epoxy unidirectional ply are investigated. The ply has a fiber volume fraction of 0.6 and is subjected to transverse tension. In their study, the same epoxy behaviour described in *Section 2.4.1* is used for the response of matrix constituent in a detailed finite element analysis with and without the consideration of fiber debonding mechanism. The numerical results obtained from their study [85] are plotted in Figure 13 which indicates strong influence of fiber/matrix interface failure on the homogenised response. The results produced by the proposed model are also plotted in Figure 13. For the current analysis involved fiber debonding failure, the model parameters taken for the FIE block are: $E = 40$ (GPa), $\nu = 0.2$, $\varepsilon_c = 0.001\%$, $n = 1.3$ and $\gamma = 250$, for the matrix block the model parameters are: $E = 3.76$ (GPa), $\nu = 0.39$, $f_{t0} = 25$ (MPa), $f_{c0} = 40$ (MPa), $Q_t = 48$ (MPa), $Q_c = 80$ (MPa), $b_t = 350$, $b_c = 350$, $r_d = 0$. In other case where interface failure is neglected, ε_c is set to a large value so fiber debonding is inactive through the entire loading curve. Although the proposed model requires much less computational demand, thanks to the embedded

responses of different matrix, fibre and interfaces, the results produced by the proposed model are comparable to the numerical results given by [85] where a detailed finite element analysis is needed. Again, it can be seen in Figure 14 that the softening response due to fiber debonding process is captured in the proposed model thanks to the nonlinear responses of both the FIE block and other matrix blocks.

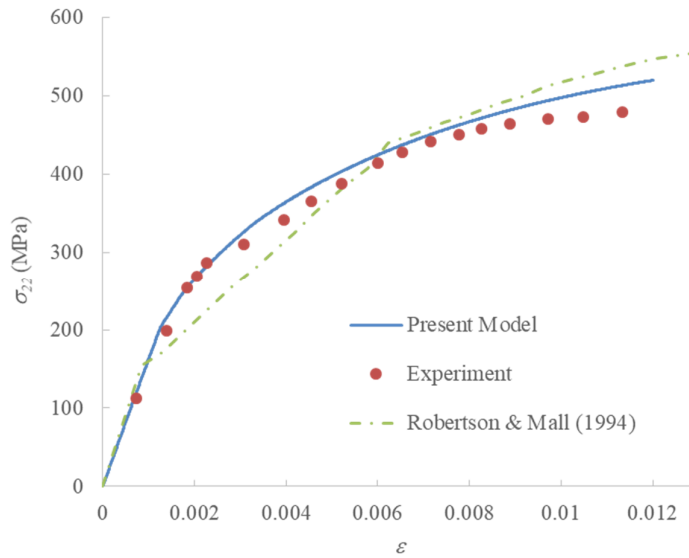


Figure 11: Responses of *SCS6/Ti-β21S* under uniaxial tension in transverse direction.

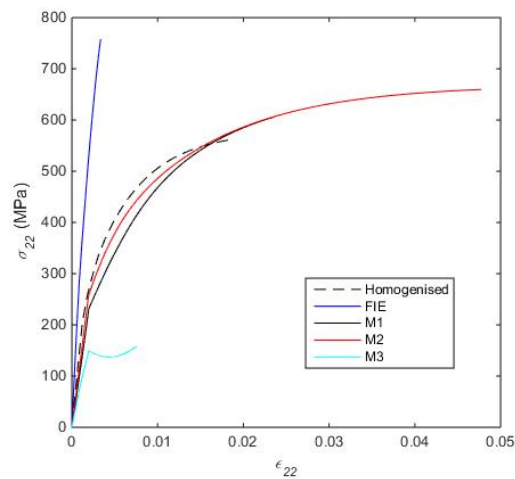


Figure 12: Responses of each material block *FIE*, *M1*, *M2*, *M3* and the homogenised response *SCS6/Ti-β21S* lamina under transverse tension

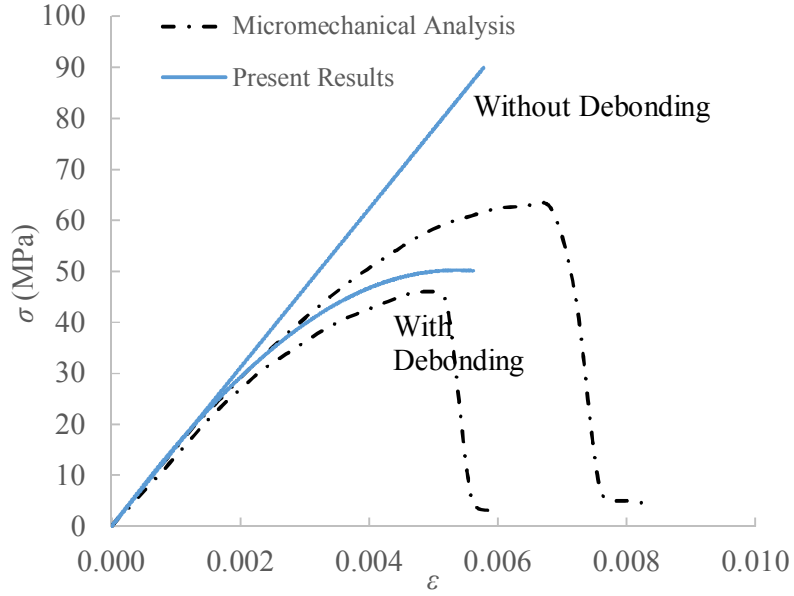


Figure 13: Responses of *E-Glass/Epoxy* under uniaxial tension in transverse direction. Micromechanical results are from [85]

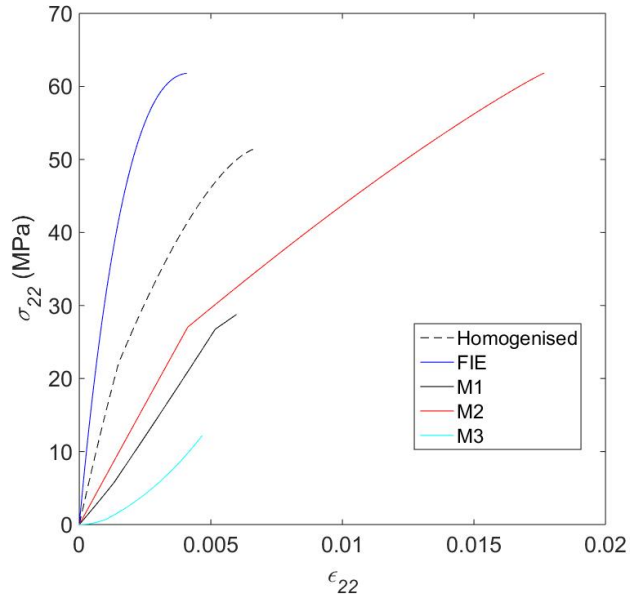


Figure 14: Responses of each material block *FIE*, *M1*, *M2*, *M3* and the homogenised response of *E-Glass/Epoxy* lamina under transverse tension

5.3 Uniaxial compression in transverse direction

The stress-strain responses of five different laminas which are subjected to transverse uniaxial compression are examined. All five laminas were tested by

Kaddour and Hinton as part of the Second World-wide Failure Exercise and the results are provided in [73]. These experimental results will be used to evaluate the performance of the proposed model by comparing these test data to the results produced by the model. The material constituents of these lamina are summarised in Table 2. On the other hand, the model parameters used for matrix blocks in Lamina 1, 2 and 5 are calibrated from their uniaxial responses obtained from experiment [73]. These experimental results are plotted in Figure 15 along with the model predictions which show good alignments between test data and model outputs. Thus, the corresponding model parameters obtained are given in Table 3 which are subsequently used to produce the overall stress-strain response of the laminas. It should be noted that the behaviour of *Epoxy 1* and *PR319* is assumed to be elastic up to failure point [73] where their elastic properties are also provided in Table 3.

Table 2: Lamina subjected to transverse uniaxial compression

	<i>Fiber Volume Fraction</i>	<i>Fiber</i>	<i>Matrix</i>	α	β
Lamina 1	0.6	<i>E-Glass</i>	<i>MY750</i>	1	0.85
Lamina 2	0.6	<i>S-Glass</i>	<i>Epoxy 2</i>	1	1.5
Lamina 3	0.6	<i>AS - Carbon</i>	<i>Epoxy 1</i>	1	2.6
Lamina 4	0.6	<i>T300</i>	<i>PR319</i>	1	3.0
Lamina 5	0.6	<i>IM7</i>	<i>8551</i>	1	0.01

Table 3: Model Parameters for matrix blocks

	E (GPa)	ν	f_{t0} (MPa)	f_{c0} (MPa)	Q_t (MPa)	Q_c (MPa)	b_t	b_c
<i>MY750</i>	3.35	0.35	65	70	35	50	450	350
<i>Epoxy 2</i>	3.2	0.35	60	70	25	50	450	350
<i>8551-7</i>	4.08	0.38	30	40	90	90	100	50
<i>Epoxy 1</i>	3.2	0.35	N/A	N/A	N/A	N/A	N/A	N/A
<i>PR319</i>	0.95	0.35	N/A	N/A	N/A	N/A	N/A	N/A

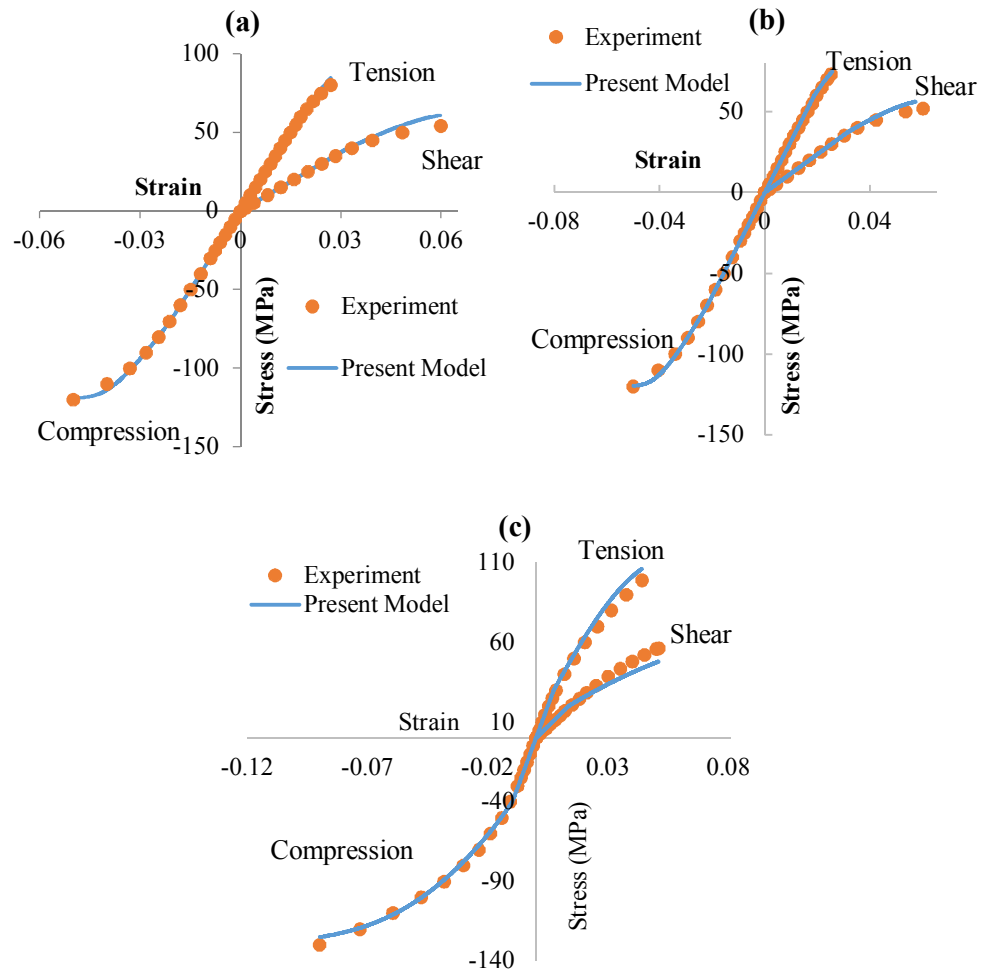


Figure 15: Responses of resins under uniaxial tension, uniaxial compression in transverse direction and in-plane shear: (a) *MY750* Resin; (b) *Epoxy 2* Resin; (c) *8551-7* Resin. Experimental data is provided in [73].

In other tests, as all five laminas are compressed in transverse direction (e.g. direction 2 – Figure 1c), it is expected that tensile stresses/strains will occur at the interface between fiber and matrix in direction 3 due to Poisson effects which will lead to fiber debonding failure. Thus, these debonding failure can cause the reductions in the overall stiffness of the composite which subsequently manifest in the nonlinear response of the lamina as seen in Figure 16. The parameters used for fiber models are given in Table 4. Figure 16 shows that there are high correlations between the model and experimental results which indicates very good performance of the proposed model. The inelastic characteristics of the stress-strain response observed in Figure 16 are the results of the proposed formulation taking into accounts of fiber debonding mechanisms introduced in the previous sections.

These nonlinear effects can be observed in the stress-strain curves of all four material block for the five laminas as illustrated in Figure 17 to Figure 21. We note that our previous model in [107] neglects the effects of interface debonding and hence cannot capture these responses. The responses of individual blocks constitute the overall ply behaviour, demonstrating both the effectiveness and predictive capability of the proposed approach.

Table 4: Model Parameters used to model the behaviour of FIE block

Fiber	E_1 (GPa)	E_2 (GPa)	ν_{12}	ν_{23}	ϵ_c (%)	n	γ
<i>E-Glass</i>	74	74	0.2	0.2	0.005	2	850
<i>S-Glass</i>	87	87	0.2	0.2	0.01	1.4	750
<i>AS-Carbon</i>	231	15	0.2	0.071	0.06	7	300
<i>T300</i>	231	15	0.2	0.071	0.009	3	600
<i>IM7</i>	276	19	0.2	0.357	0.01	2	130

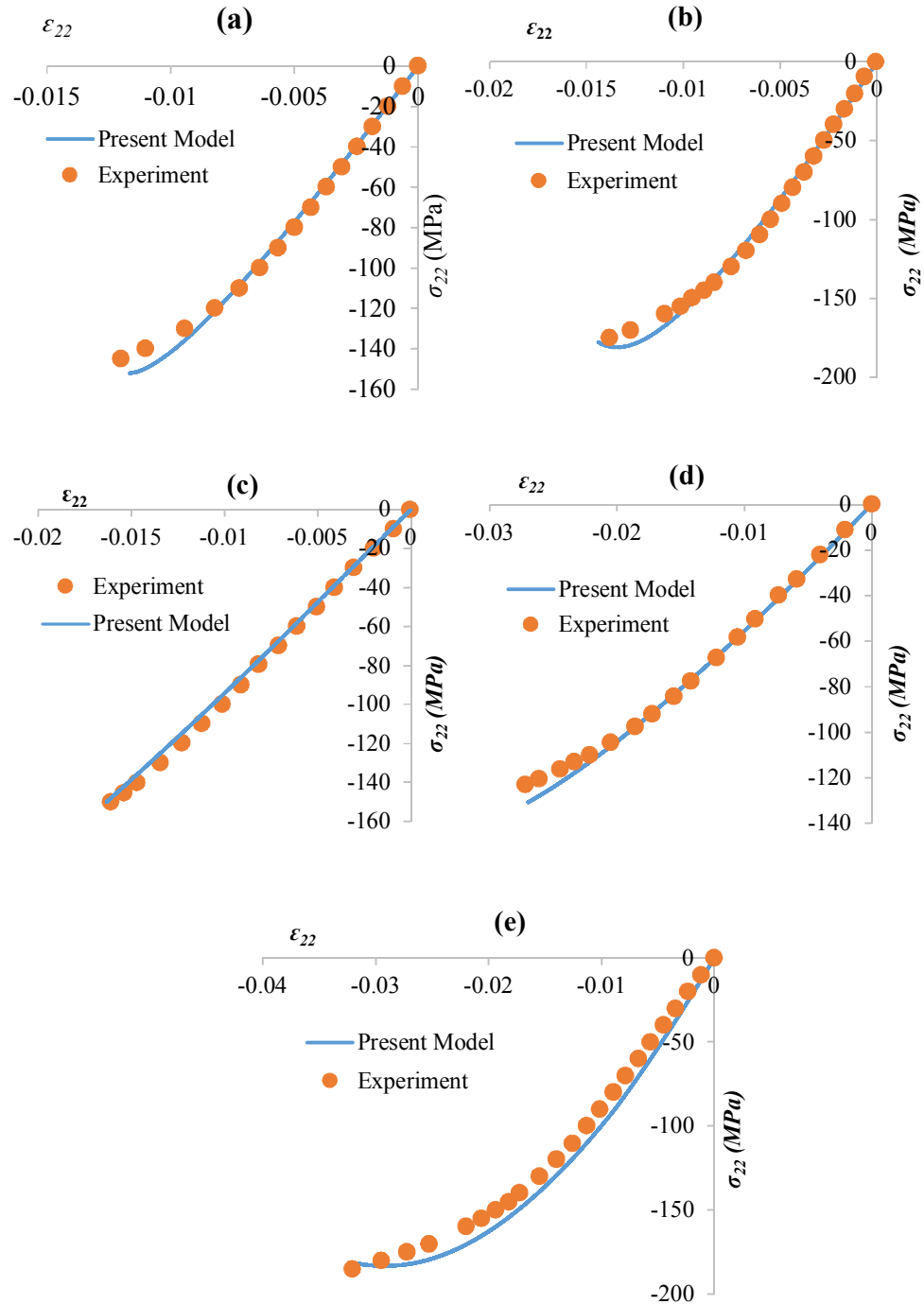


Figure 16: Responses composite under uniaxial compression in transverse direction: (a) Lamina 1: *E-Glass/MY750*; (b) Lamina 2: *S-Glass/Epoxy 2*; (c) Lamina 3: *AS-Carbon/Epoxy 1*; (d) Lamina 4: *T300/PR319*; (e) Lamina 5: *IM7/8551*.

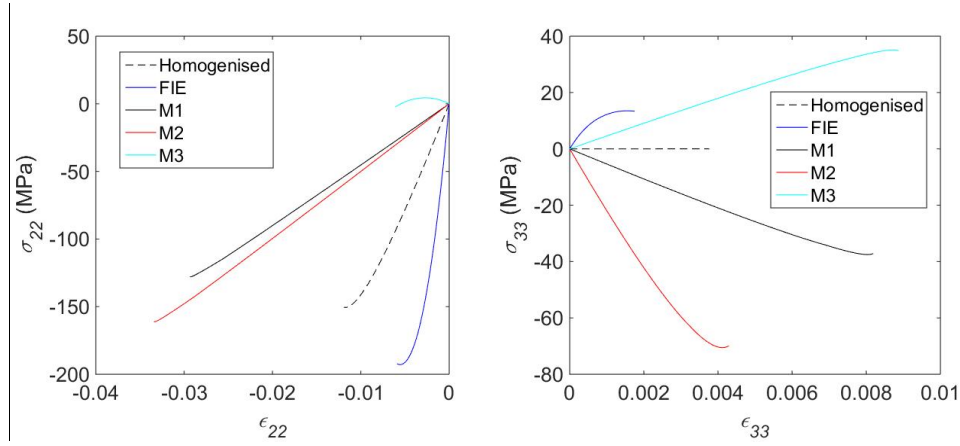


Figure 17: Lamina 1: *E-Glass/MY750* – Response of *FIE*, *M1*, *M2*, *M3* and the homogenised response

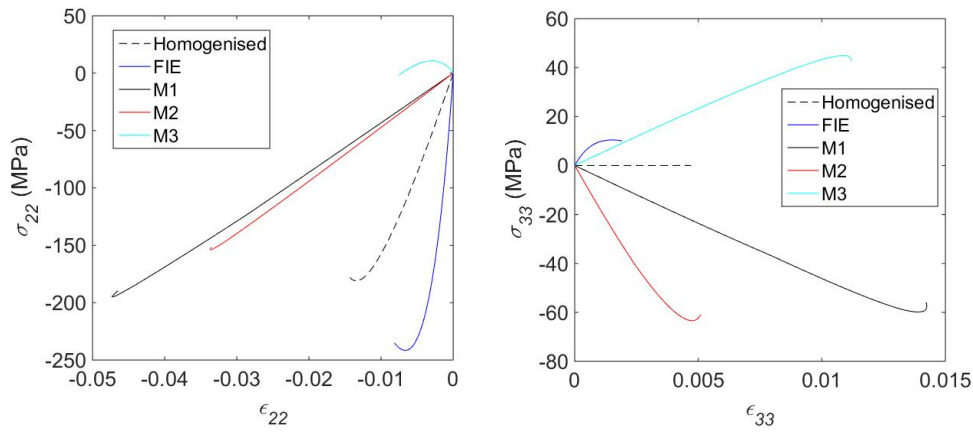


Figure 18: Lamina 2: *S-Glass/Epoxy 2* – Response of *FIE*, *M1*, *M2*, *M3* and the homogenised response

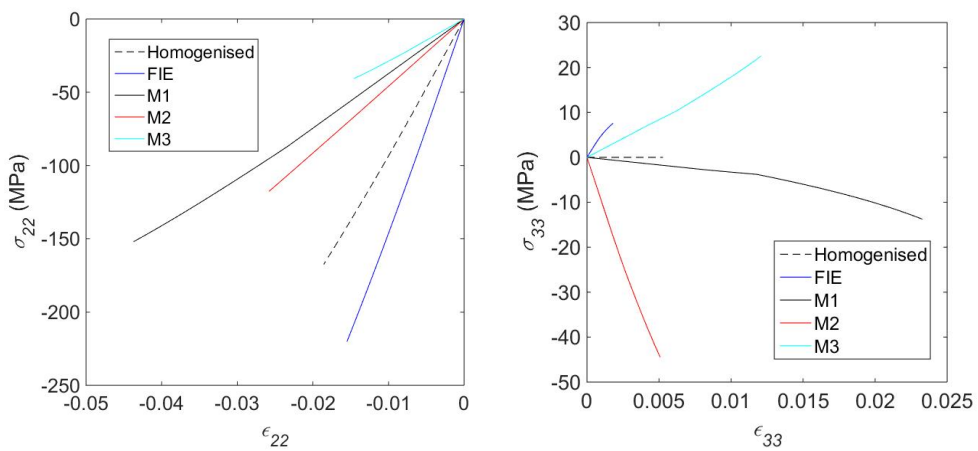


Figure 19: Lamina 3: *AS-Carbon/Epoxy 1* – Response of *FIE*, *M1*, *M2*, *M3* and the homogenised response.

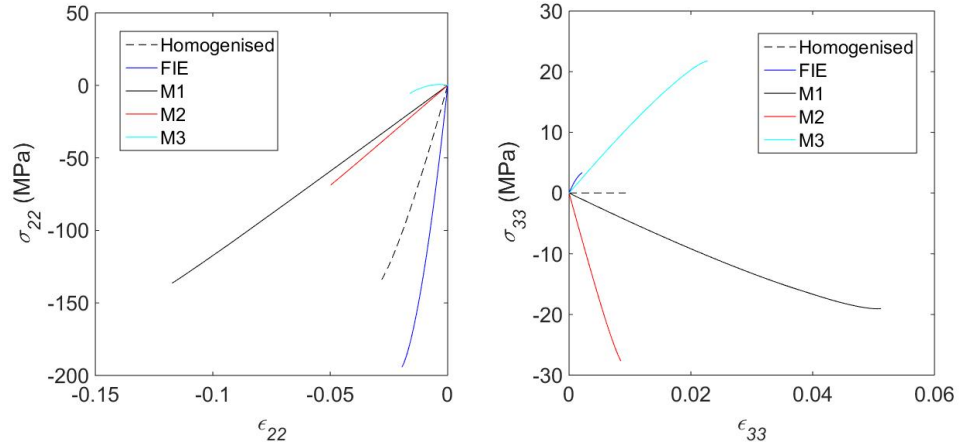


Figure 20: Lamina 4: *T300/PR319* – Response of *FIE*, *M1*, *M2*, *M3* and the homogenised response

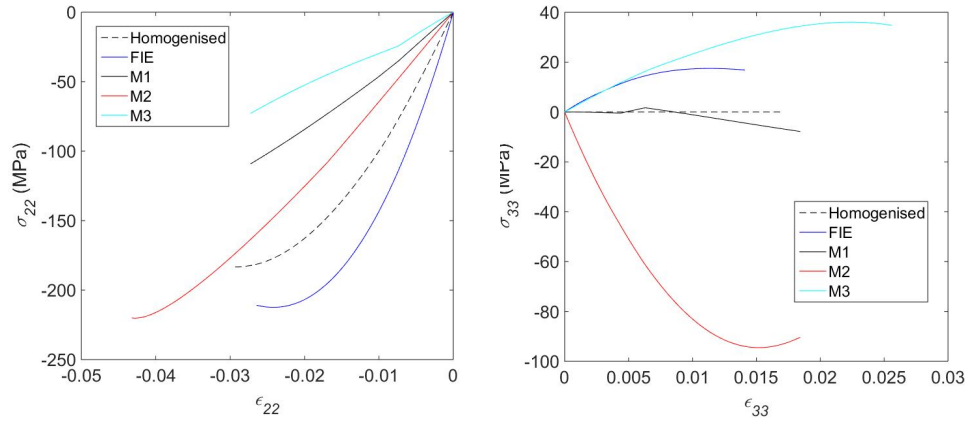


Figure 21: Lamina 5: *IM7/8551* – Response of *FIE*, *M1*, *M2*, *M3* and the homogenised response

Furthermore, the performance of the proposed model under this loading mode is also evaluated by comparing the results predicted by the present model with numerical results provided in [85] for the response of *E-glass/epoxy* ply under transverse uniaxial compression. The model parameters for matrix are given in Section 2.3.2 and model parameters used for the FIE block are in Section 3.2. The results are plotted in Figure 22 which shows that the present results for ply response are predominantly linear in the case interface failure is neglected whereas a slight nonlinearity is observed in other case considering debonding effects. This indicates the present model is capable of successfully capturing the debonding mechanism at the interface of fiber and matrix. The results are in good correlations with the

numerical predictions in small to medium strain, however in large strain region more non-linear behaviour is observed in the latter model. It is noted that the softening curves are provided in the micromechanical analysis which are not produced by the present model. This is due to the assumption made in [85] where total failure of matrix in compression occurs at high strain (Figure 9) whereas in the present model the stress-strain response of matrix is assumed to follow a perfectly plastic response once the ultimate strength has been reached. The issue with identifying the ultimate failure point for epoxy material under uniaxial compression is commonly encountered where special settings for the experiment are usually required for the failure to occur. It is also worth mentioning that the failure characteristics of the specimen are size-dependent due to the effects of localised failures which can be addressed through regularisation techniques. However, this is not a focus of this study and therefore it is not considered in this paper. Further investigations on the performance of the proposed model in relations to this matter may be carried out in future studies.

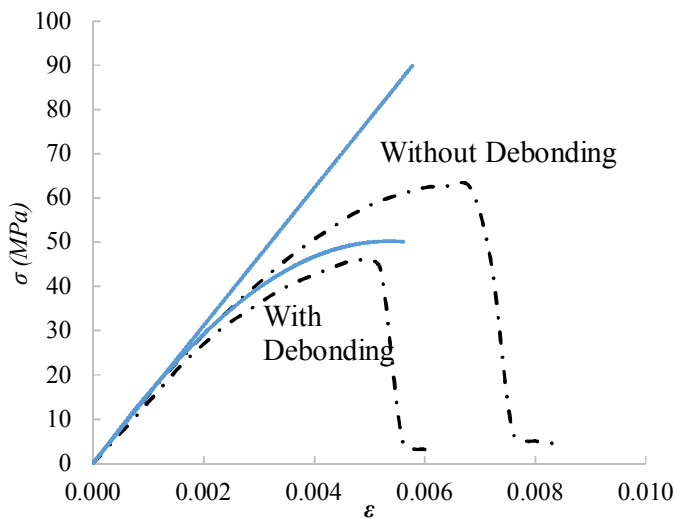


Figure 22: Comparisons between finite element results by Melro et al [85] and the present model for uniaxial compression in transverse direction.

4. Conclusions

The kinematically enhanced constitutive model developed in [107] to predict the behaviour of unidirectional FRC ply is used in this study where a RVE is considered for which fiber and matrix can be characterised by four material blocks, one is used for fiber and the other three are for matrix. Furthermore, a new thermodynamics-based formulation is employed to assemble all essential ingredients of the previously proposed micromechanics-based model. The internal equilibrium conditions between the four material blocks and the homogenised stresses are obtained as a results of the proposed thermodynamics formulations. This leads to the establishment of a complete homogenisation procedure where the responses of the four material blocks comprise the overall macro constitutive relationship of the composite ply.

On the other hand, the inelastic behaviour of composite ply beyond elastic range due to matrix yielding/softening and fiber delamination are also captured in this study. A coupled damage-plasticity constitutive model [107, 117] is used to capture the inelastic effects in the matrix constituent while the nonlinear effects of interfacial debonding are taken into account by using a newly proposed anisotropic damage model in a combined fiber-interface-equivalence (FIE) block. In facts, this damage model helps to characterise the directional dependence of the softening response in FRC ply due to fiber debonding failure. Applications of the proposed model are carried out on a number of examples and the produced results compare very well to other existing numerical models as well as experimental measurements which indicates good performance of the proposed model.

5. Acknowledgements

Giang D. Nguyen would like to thank the Australian Research Council for funding support via project FT140100408.

6. Appendices

Expressions for \mathbf{A}_{11} , \mathbf{A}_{12} , \mathbf{A}_{21} , \mathbf{A}_{22} are:

$$\begin{aligned} \mathbf{A}_{11} = & f^{(1)}\mathbf{K}_1^T \mathbf{N}_2^T \mathbf{D}^{(1)}\mathbf{N}_2 \mathbf{K}_1 + f^{(2)}\mathbf{K}_3^T \mathbf{N}_2^T \mathbf{D}^{(2)}\mathbf{N}_2 \mathbf{K}_3 + f^{(3)}\mathbf{K}_5^T \mathbf{N}_2^T \mathbf{D}^{(3)}\mathbf{N}_2 \mathbf{K}_5 \\ & + f^{(4)}\mathbf{K}_4^T \mathbf{N}_2^T \mathbf{D}^{(4)}\mathbf{N}_2 \mathbf{K}_4 \end{aligned} \quad (62)$$

$$\begin{aligned} \mathbf{A}_{12} = & f^{(1)}\mathbf{K}_1^T \mathbf{N}_2^T \mathbf{D}^{(1)}\mathbf{N}_3 \mathbf{K}_2 - f^{(2)}\mathbf{K}_3^T \mathbf{N}_2^T \mathbf{D}^{(2)}\mathbf{N}_3 \mathbf{K}_4 - f^{(3)}\mathbf{K}_5^T \mathbf{N}_2^T \mathbf{D}^{(3)}\mathbf{N}_3 \mathbf{K}_6 \\ & + f^{(4)}\mathbf{K}_4^T \mathbf{N}_2^T \mathbf{D}^{(4)}\mathbf{N}_3 \mathbf{K}_3 \end{aligned} \quad (63)$$

$$\begin{aligned} \mathbf{A}_{21} = & f^{(1)}\mathbf{K}_2^T \mathbf{N}_3^T \mathbf{D}^{(1)}\mathbf{N}_2 \mathbf{K}_1 - f^{(2)}\mathbf{K}_4^T \mathbf{N}_3^T \mathbf{D}^{(2)}\mathbf{N}_2 \mathbf{K}_3 - f^{(3)}\mathbf{K}_6^T \mathbf{N}_3^T \mathbf{D}^{(3)}\mathbf{N}_2 \mathbf{K}_5 \\ & + f^{(4)}\mathbf{K}_3^T \mathbf{N}_3^T \mathbf{D}^{(4)}\mathbf{N}_2 \mathbf{K}_4 \end{aligned} \quad (64)$$

$$\begin{aligned} \mathbf{A}_{22} = & f^{(1)}\mathbf{K}_2^T \mathbf{N}_3^T \mathbf{D}^{(1)}\mathbf{N}_3 \mathbf{K}_2 + f^{(2)}\mathbf{K}_4^T \mathbf{N}_3^T \mathbf{D}^{(2)}\mathbf{N}_3 \mathbf{K}_4 + f^{(3)}\mathbf{K}_6^T \mathbf{N}_3^T \mathbf{D}^{(3)}\mathbf{N}_3 \mathbf{K}_6 \\ & + f^{(4)}\mathbf{K}_3^T \mathbf{N}_3^T \mathbf{D}^{(4)}\mathbf{N}_3 \mathbf{K}_3 \end{aligned} \quad (65)$$

Expressions for \mathbf{P}_1 and \mathbf{P}_2 are:

$$\begin{bmatrix} \mathbf{P}_1 \\ \mathbf{P}_2 \end{bmatrix} = \begin{bmatrix} \mathbf{A}_{11} & \mathbf{A}_{12} \\ \mathbf{A}_{21} & \mathbf{A}_{22} \end{bmatrix}^{-1} \begin{bmatrix} \mathbf{B}_1 \\ \mathbf{B}_2 \end{bmatrix} \quad (66)$$

Where:

$$\mathbf{B}_1 = f^{(4)}\mathbf{K}_4^T \mathbf{N}_2^T \mathbf{D}^{(4)} - f^{(1)}\mathbf{K}_1^T \mathbf{N}_2^T \mathbf{D}^{(1)} - f^{(2)}\mathbf{K}_3^T \mathbf{N}_2^T \mathbf{D}^{(2)} + f^{(3)}\mathbf{K}_5^T \mathbf{N}_2^T \mathbf{D}^{(3)} \quad (67)$$

$$\mathbf{B}_2 = f^{(4)}\mathbf{K}_3^T \mathbf{N}_3^T \mathbf{D}^{(4)} - f^{(1)}\mathbf{K}_2^T \mathbf{N}_3^T \mathbf{D}^{(1)} + f^{(2)}\mathbf{K}_4^T \mathbf{N}_3^T \mathbf{D}^{(2)} - f^{(3)}\mathbf{K}_6^T \mathbf{N}_3^T \mathbf{D}^{(3)} \quad (68)$$

Expressions for \mathbf{K}_s are:

$$\mathbf{K}_1 = \boldsymbol{\mu}_1 - (f_1\boldsymbol{\mu}_1 + f_2\mathbf{I}) \quad (69)$$

$$\mathbf{K}_2 = \boldsymbol{\mu}_2 - (f_1\boldsymbol{\mu}_2 + f_3\mathbf{I}) \quad (70)$$

$$\mathbf{K}_3 = \mathbf{I} - (f_1\boldsymbol{\mu}_1 + f_2\mathbf{I}) \quad (71)$$

$$\mathbf{K}_4 = f_1\boldsymbol{\mu}_2 + f_3\mathbf{I} \quad (72)$$

$$\mathbf{K}_5 = f_1\boldsymbol{\mu}_1 + f_2\mathbf{I} \quad (73)$$

$$\mathbf{K}_6 = \mathbf{I} - (f_1\boldsymbol{\mu}_2 + f_3\mathbf{I}) \quad (74)$$

7. References

1. Kaw, A.K.: Mechanics of Composite Materials. Taylors & Francis Group, New York (2006)
2. Herakovich, C.T.: Mechanics of Fibrous Composites. John Wiley & Sons, Inc, New York (1998)
3. Chady, T.: Airbus Versus Boeing—Composite Materials : The sky's the limit... , <http://www.lemauricien.com/article/airbus-versus-boeing-composite-materials-sky-s-limit>, (2013)
4. Harris, C.E., Starnes, J.H., Shuart, M.J.: An Assessment the Design Composite Vehicles of the State-of-the-Art in and Manufacturing of Large Structures for Aerospace. , Hampton (2001)
5. Arvind, N., Samantha, A., Singha Roy, D., Thanikal, J.: Retrofitting of Reinforced Concrete Beams using Fibre Reinforced Polymer (FRP) Composites – A Review. J. Urban Environ. Eng. 1, 164–175 (2013)
6. Thomsen, O.: Sandwich Materials for Wind Turbine Blades – Present and Future. J. Sandw. Struct. Mater. 7–26 (2009)
7. Reddy, J.N.: A Simple Higher-Order Theory for Laminated Composite Plates. J. Appl. Mech. 51, 745–752 (1984)
8. Reddy, J.N.: Mechanics of Laminated Composite Plates and Shells – Theory and Analysis. CRC Press LLC, USA (1997)
9. Lo, K.H., Christensen, R.M., Wu, E.M.: A High-Order Theory of Plate Deformation - Part 2: Laminated Plates. J. Appl. Mech. 669–676 (1977)
10. Yang, P.C., Norris, C.H., Stavskys, Y.: Elastic Wave Propagation in Heterogeneous Plates. Int. J. Solids Struct. 2, 665–684 (1966)
11. Kant, T., Owen, D.R.J., Zienkiewicz, O.C.: A Refined Higher-Order C0 Plate Bending Element. 15, 177–183 (1982)
12. Toledano, A., Murakami, H.: A Composite Plate Theory for Arbitrary Laminate Configurations. J. Appl. Mech. 54, 181–189 (1987)
13. Khdeir, A.A., Reddy, J.N.: Free Vibrations of Laminated Composite Plates

- Using Second-Order Shear Deformation Theory. *Comput. Struct.* 71, 617–626 (1999)
14. Ambartsumyan, S.A.: *Theory of Anisotropic Plates* [In Russian]. Izdat. Nauka, Moskva (1969)
 15. Whitney, J.M.: The Effect of Transverse Shear Deformation on the Bending of Laminated Plates. *J. Compos. Mater.* 3, 534 (1969). doi:10.1177/002199836900300316
 16. Pryor, C.W., Barker, R.M.: A Finite-Element Analysis Including Transverse Shear Effects for Applications to Laminated Plates. *AIAA J.* 9, 912–917 (1971)
 17. Reissner, E.: A Consistent Treatment of Transverse Shear Deformation in Laminated Anisotropic Plates. *AIAA J.* 10, 716–718 (1972)
 18. Srinivas, S.: A Refined Analysis of Composite Laminates. 30, 495–507 (1973)
 19. Murakami, H.: Laminated Composite Plate Theory With Improved In-Plane Responses. *J. Appl. Mech.* 53, 661–666 (1986)
 20. Reissner, E.: On A Certain Mixed Variational Theorem and A Proposed Application. *Int. J. Numer. Methods Eng.* 20, 1366–1368 (1984)
 21. Reddy, J.N.: A Generalization of Two-Dimensional Theories of Laminated Composite Plates. *Commun. Appl. Numer. Methods.* 3, 173–180 (1987)
 22. Cho, K.N., Bert, C.W., Striz, A.G.: Free Vibrations of Laminated Rectangular Plates Analyzed by Higher Order Individual-Layer Theory. *J. Sound Vib.* 145, 429–442 (1991)
 23. Li, X., Liu, D.: Zigzag Theory for Composite Laminates. *AIAA J.* 33, 1163–1165 (1994)
 24. Dong, S.B., Tso, F.K.W.: On a Laminated Orthotropic Shell Theory Including Transverse Shear Deformation. *J. Appl. Mech.* 1091–1097 (1972)
 25. Whitney, J.M., Sun, C.T.: A Refined Theory for Laminated Anisotropic ,

- Cylindrical Shells. *J. Appl. Mech.* 471–476 (1974)
26. Whitney, J.M., Sun, C.T.: A Higher Order Theory for Extensional Motion of Laminated Composites. *J. Sound Vib.* 30, 85–97 (1973)
 27. Bhimaraddi, A.: Higher Order Theory for Free Vibration Analysis of Circular Cylindrical Shells. *Int. J. Solids Struct.* 20, 623–630 (1984)
 28. Zukas, J.A., Vinson, J.R.: Laminated Transversely Isotropic Cylindrical Shells. *J. Appl. Mech.* 400–407 (1971)
 29. Barbero, E.J., Reddy, J.N.: Modeling of Delamination In Composite Laminates Using A Layer-wise Plate Theory. *Int. J. Solids Struct.* 28, 373–388 (1991)
 30. Carrera, E.: Single- vs Multilayer Plate Modelings on the Basis of Reissner’s Mixed Theorem. *AIAA J.* 38, 342–352 (2000)
 31. Carrera, E., Demasi, L.: Classical and Advanced Multilayered Plate Elements Based Upon PVD and RMVT . Part 1 : Derivation of Finite Element Matrices. *Int. J. Numer. Methods Eng.* 55, 191–231 (2002). doi:10.1002/nme.492
 32. Carrera, E., Demasi, L.: Classical and Advanced Multilayered Plate Elements Based Upon PVD and RMVT . Part 2 : Numerical Implementations. *Int. J. Numer. Methods Eng.* 55, 253–291 (2002). doi:10.1002/nme.493
 33. Van Der Meer, F.P.: Computational Modeling of Failure in Composite Laminates, (2010)
 34. Greenhalgh, E.S.: Failure Analysis and Fractography of Polymer Composites. Woodhead Publishing Limited, USA (2009)
 35. Hull, D.: An Introduction to Composite Materials. Cambridge University Press, Cambridge (1981)
 36. Curtin, W.A.: Multiple Matrix Cracking in Brittle Matrix Composites. *Acta Metall. Mater.* 41, 1369–1377 (1993)
 37. Ye, J., Lam, D., Zhang, D.: Initiation and Propagation of Transverse

- Cracking in Composite Laminates. *Comput. Mater. Sci.* 47, 1031–1039 (2010)
38. Spearing, S.M., Zok, F.W.: Stochastic Aspects of Matrix Cracking in Brittle Matrix Composites. *J. Eng. Mater. Technol.* 115, 314–318 (1993)
39. McCartney, L.N.: Energy-based prediction of progressive ply cracking and strength of general symmetric laminates using an homogenisation method. *Compos. Part A Appl. Sci. Manuf.* 36, 119–128 (2005).
doi:10.1016/j.compositesa.2004.06.003
40. Zhang, Y., Xia, Z., Ellyin, F.: Nonlinear viscoelastic micromechanical analysis of fibre-reinforced polymer laminates with damage evolution. *Int. J. Solids Struct.* 42, 591–604 (2005). doi:10.1016/j.ijsolstr.2004.06.021
41. Budiansky, B., Hutchinson, J.W., Evans, A.G.: Matrix Fracture in Fiber-Reinforced Ceramics. *J. Mech. Phys. Solids.* 34, 167–189 (1986)
42. Meng, Q., Wang, Z.: Theoretical model of fiber debonding and pull-out in unidirectional composites. *J. Compos. Mater.* 49, 1739–1751 (2015).
doi:10.1177/0021998314540191
43. Jeng, S.M., Yang, C.J.: Fracture mechanisms of fiber-reinforced titanium alloy matrix composites Part I: Interfacial behavior. *Mater. Sci. Eng.* 138, 155–167 (1991)
44. Koyanagi, J., Ogihara, S., Nakatani, H., Okabe, T.: Mechanical properties of fiber/matrix interface in polymer matrix composites. *Adv. Compos. Mater.* 23, 551–570 (2014)
45. Tsai, S.W.: Strength of Theories of Filamentary Structures. *Fundamental Aspects of Fiber Reinforced Plastic Composites.* John Wiley & Sons, USA (1968)
46. Stabb, G.H.: *Laminar Composites.* Butterworth-Heinemann, USA (1999)
47. Tsai, S.W., Wu, E.M.: A General Theory of Strength for Anisotropic Materials. *J. Compos. Mater.* 5, 58–80 (1971).
doi:10.1177/002199837100500106

48. Hoffman, O.: The Brittle Strength of Orthotropic Materials. *J. Compos. Mater.* 1, (1967). doi:10.1177/002199836700100210
49. Hashin, Z., Rotem, A.: A Fatigue Failure Criterion for Fiber Reinforced Materials. *J. Compos. Mater.* 7, 448–464 (1973). doi:10.1177/002199837300700404
50. Hashin, Z.: Failure Criteria for Unidirectional Fiber Composites. *J. Appl. Mech.* 47, 329–334 (1980)
51. Christensen, R.M.: Tensor Transformations and Failure Criteria for the Analysis of Fiber Composite Materials. *J. Compos. Mater.* 22, 874–897 (1988). doi:10.1177/002199838802200906
52. Christensen, R.M.: Stress Based Yield/Failure Criteria for Fiber Composites. *Int. J. Solids Struct.* 34, 529–543 (1997)
53. Gosse, J.H., Christensen, S.: Strain Invariant Failure Criteria for Polymers in Composite Materials. *AIAA J.* 1184 (2011)
54. Gosse, J.H.: Failure Criteria in Fibre-Reinforced-Polymer Composites. In: Thirteen ICCM Conference. p. Paper ID 1687. , Beijing (2001)
55. Van Paepegem, W., De Baere, I., Degrieck, J.: Modelling the nonlinear shear stress-strain response of glass fibre-reinforced composites. Part I: Experimental results. *Compos. Sci. Technol.* 66, 1455–1464 (2006). doi:10.1016/j.compscitech.2005.04.014
56. Schuecker, C., Pettermann, H.: Combining elastic brittle damage with plasticity to model the non-linear behavior of fiber reinforced laminates. In: Camanho, P.P., Dávila, C.G., Pinho, S.T., and Remmers, J.J.C. (eds.) *Mechanical Response of Composites*. Springer Netherlands (2008)
57. Lemaitre, J., Desmorat, R.: *Engineering Damage Mechanics*. Springer, The Netherlands (2005)
58. Puck, A., Schurmann, H.: Failure Analysis of Frp Laminates By Means of Physically Based Phenomenological Models *. *Compos. Sci. Technol.* 58, 1045–1067 (1998)

59. Deuschle, H.M., Puck, A.: Application of the Puck failure theory for fibre-reinforced composites under three-dimensional stress : Comparison with experimental results. *J. Compos. Mater.* 47, 827–846 (2012).
doi:10.1177/0021998312462158
60. Pinho, S.T., Darvizeh, R., Robinson, P., Schuecker, C.: Material and structural response of polymer-matrix fibre-reinforced composites. *J. Compos. Mater.* 46, 2313–2341 (2012). doi:10.1177/0021998312454478
61. Pinho, S.T., Dávila, C.G., Camanho, P.P., Iannucci, L., Robinson, P.: Failure Models and Criteria for FRP Under In-Plane or Three-Dimensional Stress States Including Shear Non-Linearity. , Hampton (2005)
62. Pinho, S.T., Iannucci, L., Robinson, P.: Physically-based failure models and criteria for laminated fibre-reinforced composites with emphasis on fibre kinking : Part I: Development. *Compos. Part A Appl. Sci. Manuf.* 37, 63–73 (2006). doi:10.1016/j.compositesa.2005.04.016
63. Bogetti, T.A., Hoppel, C.P.R., Harik, V.M., Newill, J.F., Burns, B.P.: Predicting the nonlinear response and progressive failure of composite laminates. *Fail. Criteria Fibre-Reinforced-Polymer Compos.* 64, 402–428 (2004). doi:10.1016/B978-008044475-8/50017-2
64. Bogetti, T. a., Staniszewski, J., Burns, B.P., Hoppel, C.P., Gillespie, J.W., Tierney, J.: Predicting the nonlinear response and progressive failure of composite laminates under tri-axial loading. *J. Compos. Mater.* 46, 2443–2459 (2012). doi:10.1177/0021998312449889
65. Cuntze, R.G., Freund, A.: The Predictive Capability of Failure Mode Concept-Based Strength Criteria for Multidirectional Laminates. *Compos. Sci. Technol.* 64, 343–377 (2004). doi:10.1016/S0266-3538(03)00218-5
66. Cuntze, R.: The predictive capability of failure mode concept-based strength conditions for laminates composed of unidirectional laminae under static triaxial stress states. (2012)
67. Sun, C.T., Chen, J.L.: A Simple Flow Rule for Characterizing Nonlinear Behavior of Fiber Composites. *J. Compos. Mater.* 23, 1009–1020 (1989).

doi:10.1177/002199838902301004

68. Sun, C.T., Yoon, K.J.: Elastic-plastic analysis of AS4/PEEK composite laminate using a one-parameter plasticity model. *J. Compos. Mater.* 26, 293–308 (1990)
69. Daudeville, L., Allix, O., Ladeveze, P.: Delamination Analysis By Damage Mechanics: Some Applications. *Compos. Part B Eng.* 5, 17–24 (1995). doi:10.1016/0961-9526(95)93976-3
70. Schuecker, C., Pettermann, H.E.: A continuum damage model for fiber reinforced laminates based on ply failure mechanisms. *Compos. Struct.* 76, 162–173 (2006). doi:10.1016/j.compstruct.2006.06.023
71. Ladeveze, P., Lubineau, G.: On a Damage Mesomodel For Laminates : Micro – Meso Relationships , Possibilities and Limits. *Compos. Sci. Technol.* 61, 2149–2158 (2001)
72. Ladeveze, P., Lubineau, G., Marsal, D.: Towards a Bridge Between The Micro- and Mesomechanics of Delamination For Laminated Composites. *Compos. Sci. Technol.* 66, 698–712 (2006). doi:10.1016/j.compscitech.2004.12.026
73. Kaddour, A., Hinton, M.: Input Data for Test Cases Used in Benchmarking Triaxial Failure Theories of Composites. *J. Compos. Mater.* 46, 2295–2312 (2012). doi:10.1177/0021998312449886
74. Talreja, R., Yalvac, S., Yats, L.D., Wetters, D.G.: Transverse Cracking and Stiffness Reduction in Cross Ply Laminates of Different Matrix Toughness. *J. Compos. Mater.* 26, 1644–1663 (1992). doi:10.1177/002199839202601105
75. Talreja, R.: A Continuum Mechanics Characterization of Damage in Composite Materials. *Proc. R. Soc. London . Ser. A , Math. Phys.* 399, 195–216 (1985)
76. Barbero, E.J., Lonetti, P.: An Inelastic Damage Model for Fiber Reinforced Laminates. *J. Compos. Mater.* 36, 941–962 (2002). doi:10.1106/002199802023549

77. Aboudi, J., Steven, M.A., Brett, A.B.: *Mircomechanics of Composite Materials - A Generalized Multiscale Analysis Approach*. Elsevier, US (2013)
78. Curtis, G.J., Milne, J.M., Reynolds, W.N.: Non-Hookean Behaviour of Strong Carbon Fibres. *Nature*. 20, 1968 (1968)
79. Shokrieh, M.M., Mosalmani, R., Omid, M.J.: A strain-rate dependent micromechanical constitutive model for glass/epoxy composites. *Compos. Struct.* 121, 37–45 (2015). doi:10.1016/j.compstruct.2014.10.035
80. Vaughan, T.J., McCarthy, C.T.: A combined experimental-numerical approach for generating statistically equivalent fibre distributions for high strength laminated composite materials. *Compos. Sci. Technol.* 70, 291–297 (2010). doi:10.1016/j.compscitech.2009.10.020
81. Totry, E., Molina-Aldareguia, J.M., Gonzalez, C., LLorca, J.: Effect of fiber, matrix and interface properties on the in-plane shear deformation of carbon-fiber reinforced composites. *Compos. Sci. Technol.* 70, 970–980 (2010). doi:10.1016/j.compscitech.2010.02.014
82. Romanowicz, M.: A numerical approach for predicting the failure locus of fiber reinforced composites under combined transverse compression and axial tension. *Comput. Mater. Sci.* 51, 7–12 (2012). doi:10.1016/j.commatsci.2011.07.039
83. Fiedler, B., Hojo, M., Ochiai, S., Schulte, K., Ando, M.: Failure behavior of an epoxy matrix under different kinds of static loading. 61, 1615–1624 (2001)
84. Canal, L.P., González, C., Segurado, J., LLorca, J.: Intraply fracture of fiber-reinforced composites: Microscopic mechanisms and modeling. *Compos. Sci. Technol.* 72, 1223–1232 (2012). doi:10.1016/j.compscitech.2012.04.008
85. Melro, A.R., Camanho, P.P., Andrade Pires, F.M., Pinho, S.T.: Micromechanical analysis of polymer composites reinforced by unidirectional fibres: Part II – Micromechanical analyses. *Int. J. Solids*

- Struct. 50, 1906–1915 (2013). doi:10.1016/j.ijsolstr.2013.02.007
86. Tay, T.E., Tan, S.H.N., Tan, V.B.C., Gosse, J.H.: Damage progression by the element-failure method (EFM) and strain invariant failure theory (SIFT). *Compos. Sci. Technol.* 65, 935–944 (2005). doi:10.1016/j.compscitech.2004.10.022
87. Hill, R.: Elastic Properties of Reinforced Solids: Some Theoretical Principles. *J. Mech. Phys. Solids.* 11, 357–372 (1963)
88. Mori, T., Tanaka, K.: Average Stress in Matrix and Average Elastic Energy of Materials with Misfitting Inclusions. *ACTA Metall.* 21, 571–574 (1974)
89. Dvorak, G.J.: Transformation Field Analysis of Inelastic Composite Materials. *Proc. R. Soc. A Math. Phys. Eng. Sci.* 437, 311–327 (1992). doi:10.1007/BF00370073
90. Hashin, Z., Rosen, B.W.: The Elastic Moduli of Fiber-Reinforced Materials. *J. Appl. Mech.* 223–232 (1964)
91. Hashin, Z.: The Elastic Moduli of Heterogeneous Materials. *J. Appl. Mech.* 29, 143–150 (1962)
92. Christensen, M.R., Lo, K.H.: Solutions for effective shear properties in three phase sphere and cylinder models. *J. Mech. Phys. Solids.* 27, 315–330 (1979)
93. Sun, C.T., Chen, J.L.: A Micromechanical Model for Plastic Behavior of Fibrous Composites. *Compos. Sci. Technol.* 40, 115–129 (1991). doi:10.1016/0266-3538(91)90092-4
94. Aboudi, J.: Micromechanical Analysis of Composites by the Method of Cells. *Am. Soc. Mech. Eng.* 42, 193–221 (1989)
95. Aboudi, J.: Journal of Reinforced Plastics and Composites The Nonlinear Behavior of Unidirectional. *J. Reinf. Plast. Compos.* (1990). doi:10.1177/073168449000900102
96. Pindera, M.-J., Bednarczyk, B. a: An efficient implementation of the generalized method of cells for unidirectional, multi-phased composites

- with complex microstructures. *Compos. Part B Eng.* 30, 87–105 (1999).
doi:10.1016/S1359-8368(98)00040-7
97. Li, H., Zhang, B., Bai, G.: Effects of constructing different unit cells on predicting composite viscoelastic properties. *Compos. Struct.* 125, 459–466 (2015). doi:10.1016/j.compstruct.2015.02.028
98. Ogihara, S., Kobayashi, S.: Characterization of nonlinear behavior of carbon / epoxy unidirectional and angle-ply laminates. *Adv. Compos. Mater.* 11, 239–254 (2003)
99. Tsai, J.-L., Chen, K.-H.: Characterizing Nonlinear Rate-dependent Behaviors of Graphite/Epoxy Composites using a Micromechanical Approach. *J. Compos. Mater.* 41, 1253–1273 (2007).
doi:10.1177/0021998306067307
100. Huang, Z.M.: A Unified Micromechanical Model for the Mechanical Properties of Two Constituents Composite Materials Part II: Plastic Behavior. *J. Thermoplast. Compos. Mater.* 13, 344–362 (2000).
doi:0803973233
101. Huang, Z.M.: Simulation of the mechanical properties of fibrous composites by the bridging micromechanics model. *Compos. Part A Appl. Sci. Manuf.* 32, 143–172 (2001). doi:10.1016/S1359-835X(00)00142-1
102. Huang, Z.M.: Inelastic and Failure Analysis of Laminate Structures by ABAQUS Incorporated with a General Constitutive Relationship. *J. Reinf. Plast. Compos.* 26, 1135–1181 (2007). doi:10.1177/0731684407079753
103. Santhosh, U., Ahmad, J.: An approach for nonlinear modeling of polymer matrix composites. *J. Compos. Mater.* 48, 1755–1765 (2014).
doi:10.1177/0021998313490581
104. Tabiei, A., Aminjikai, S.B.: A strain-rate dependent micro-mechanical model with progressive post-failure behavior for predicting impact response of unidirectional composite laminates. *Compos. Struct.* 88, 65–82 (2009). doi:10.1016/j.compstruct.2008.02.017
105. Goldberg, R., Stouffer, D.: Strain rate dependent analysis of a polymer

- matrix composite utilizing a micromechanics approach. *J. Compos. Mater.* 36, 773–793 (2002). doi:10.1106/002199802024613
106. Houlsby, G.T., Puzrin, a. M.: Thermomechanical Framework for Constitutive Models for Rate-independent Dissipative Materials. *Int. J. Plast.* 16, 1017–1047 (2000). doi:10.1016/S0749-6419(99)00073-X
107. Vu, V.D., Sheikh, A.H., Nguyen, G.D., Shen, L.: A kinematically enhanced constitutive model for elastic and inelastic analysis of unidirectional fibre reinforced composite materials. *Int. J. Mech. Sci.* 126, 171–185 (2017). doi:10.1016/j.ijmecsci.2017.03.027
108. Aboudi, J.: *Mechanics of Composite Materials: A Unified Micromechanical Approach*. Elsevier, Amsterdam (1991)
109. Melro, A.R., Camanho, P.P., Andrade Pires, F.M., Pinho, S.T.: Micromechanical analysis of polymer composites reinforced by unidirectional fibres: Part I - Constitutive modelling. *Int. J. Solids Struct.* 50, 1897–1905 (2013). doi:10.1016/j.ijsolstr.2013.02.009
110. Robertson, D.D., Mall, S.: Micromechanical analysis for thermoviscoplastic behavior of unidirectional fibrous composites. *Compos. Sci. Technol.* 50, 483–496 (1994). doi:10.1016/0266-3538(94)90057-4
111. Lin, G., Geubelle, P.H., Sottos, N.R.: Simulation of fiber debonding with friction in a model composite pushout test. *Int. J. Solids Struct.* 38, 8547–8562 (2001). doi:10.1016/S0020-7683(01)00085-3
112. Bowling, J., Groves, G.W.: The debonding and pull-out of ductile wires from a brittle matrix. *J. Mater. Sci.* 14, 431–442 (1979). doi:10.1007/BF00589836
113. Atkinson, C., Avila, J., Betz, E., Smelser, R.E.: The Rod Pull Out Problem, Theory and Experiment. *J. Mech. Phys. Solids.* 30, 97–120 (1982)
114. Hutchinson, J.W., Mear, M.E., Rice, J.R.: Crack Paralleling an Interface Between Dissimilar Materials. *J. Appl. Mech.* 54, 9 (1987)
115. Hutchinson, J.W., Jensen, H.M.: Models of fiber debonding and pullout in brittle composites with friction. *Mech. Mater.* 9, 139–163 (1990).

doi:10.1016/0167-6636(90)90037-G

116. Wriggers P, Zavarise G, Zohdi T I: A computational study of interfacial debonding damage in brous composite materials. *Comput. Mater. Sci.* 12, 39–56 (1998)
117. Vu, V.D., Mir, A., Nguyen, G.D., Sheikh, A.H.: A thermodynamics-based formulation for constitutive modelling using damage mechanics and plasticity theory. *Eng. Struct.* 143, 22–39 (2017)
118. Davidson, P., Davis, R.: Mechanical Behavior of 6061 — T651 Aluminum. *AIAA J.* 13, 1547–1548 (1975)
119. Ghorbel, E.: A viscoplastic constitutive model for polymeric materials. *Int. J. Plast.* 24, 2032–2058 (2008). doi:10.1016/j.ijplas.2008.01.003
120. Wood, D.: Soil Behaviour and Critical State Soil Mechanics, http://books.google.pt/books/about/Soil_Behaviour_and_Critical_State_Soil_M.html?id=CBVVG1zzjjEC&redir_esc=y, (1990)
121. Asp, L.E., Berglund, L.A., Gudmundson, P.: Effects of a composite-like stress state on the fracture of epoxies. *Compos. Sci. Technol.* 53, 27–37 (1995). doi:10.1016/0266-3538(94)00075-1
122. Puck, A.: Calculating The Strength of Glass Fibre/Plastic Laminates Under Combined Load. *Kunststoffe, Gennan Plast.* 55, 18–19 [German] (1969)
123. Crisfield, M.A.: Non-linear finite element analysis of solids and structures. Volume 1: Essentials. John Wiley & Sons Ltd, Chichester (1991)
124. Vu, V.: A MICROMECHANICS BASED FINITE ELEMENT MODEL FOR PROGRESSIVE DAMAGE ANALYSIS OF COMPOSITE PLATE / SHELL. , Adelaide (2015)
125. Hill, R.: Self-Consistent Mechanics of Composite Materials. *J. Mech. Phys. Solids.* 13, 213–222 (1965)

CHAPTER 5: CONCLUSIONS AND FUTURE WORK

5.1 Summary

A micromechanics-based constitutive model for predicting progressive failures in unidirectional FRC ply has been proposed in the previous Chapters. Along with the development of the model and other related components, several key research contributions have been made which are outlined as follows:

1. A generic kinematically enhanced and thermodynamically based approach for developing micromechanics-based models for FRC ply has been developed. The fiber and matrix constituents are represented by four idealised material blocks one of which is used for fiber and other three are for matrix. The interactions between the blocks are taken into account through equilibrium conditions across their boundaries. This strategy allows for the ply response of the FRC to be explicitly derived from the constitutive behaviours of fiber and matrix, and their interactions. Therefore the homogenised constitutive relationship can be obtained conveniently in a concise analytical expression. The incremental form of the formulation facilitates the use of the model in both elastic and inelastic domains. The effective elastic properties obtained from this homogenisation scheme are in good agreement with both sophisticated analytical solutions in the literature and available experimental data. It is addressed here that the incremental form of the homogenised response is a great advantage compared to these sophisticated techniques as this facilitate the inelastic analysis without having to make any further assumptions. The constitutive response of matrix in the inelastic range is captured using a coupled damage-plasticity model based on continuum damage mechanics. The damage-plasticity model and a new way to couple damage with plasticity are developed within a generic framework proposed by Houlsby and Puzrin [106] to ensure its thermodynamic consistency.
2. A new thermodynamic consistent framework, employing theories of plasticity and continuum damage mechanics, is developed to model a wide range of material behaviour, including both pressure-independent and pressure-dependent materials. The proposed formulation is derived within

the framework of thermodynamics with internal variables. In this regard, the complete constitutive relations are determined by explicitly defining a free energy potential and a special form of dissipation function which can be transformed to obtain a unique loading surface for both yield and failure states. This single loading surface governs the simultaneous evolutions of both damage and plasticity where the coupling between these two mechanisms is effectively specified through a model parameter without imposing any restrictions to the model. Direction of plastic flow vector can be conveniently controlled which facilitates the modelling of the inelastic dilative and contractive behaviour of materials. This development facilitates the modelling of matrix failure, which has been shown to be pressure-sensitive. In addition it is also generic enough to cover a wide range of models and responses and can be used either for the development of new models, or for enhancing existing models. The examples in Chapter 3 and in the Appendix show the versatility of the proposed framework.

3. The development of a new anisotropic damage model for the proposed Fiber-Interface Equivalence (FIE) block to effectively capture the effects fibre-matrix debonding failures. The interactions between the FIE block and the other three matrix blocks are then combined in a thermodynamics based approach naturally leads to macro homogenised stress and internal equilibrium conditions that governs the behaviour of the FRC ply. To this end, the proposed model for FRC ply is able to simultaneously incorporate the three primary inelastic mechanisms, which are plasticity and damage mechanisms of matrix as well as fiber debonding. All these have profound impacts on the response of FRC ply in order to produce the most reliable and realistic predictions with regards to FRC ply behaviour at a fraction of computational cost compared to sophisticated and detailed micromechanical modelling of FRC. To the best of our knowledge, this offers a good balance between accuracy, predictive capability, and computational expense. This is an advantage that can facilitate the applications of the proposed model in structural analysis.

5.2 Research Conclusions

The reliability and performance of the proposed model have been verified in number of numerical examples. Based on these investigations, the main conclusions are drawn as follows:

1. It is always possible to extend the existing approaches to modelling FRC for large scale applications. Within the scope of this thesis, the limitations of these existing approach in our opinion are the imbalance between several factors which are the accuracy and also predictive capability in both elastic and inelastic ranges of behaviour as well as simplicity in implementation and low computational demanding. In this respect, the framework for modelling unidirectional FRC ply developed in this thesis is believed to be able to strike a balance between the above-mentioned aspects. In particular, the proposed model possesses links between the macro ply response and its individual constituents (fibre, matrix and interface) and hence is capable of effectively capture the mechanical response of unidirectional FRC ply in both elastic and inelastic ranges, including plies consisting of isotropic or anisotropic fibers embedded in polymer or metal matrices. The proposed homogenisation technique using the kinematic strain enhancements significantly improves the computational effectiveness of the model as well as maintains a reasonable level of details on the physical interactions between the constituents.
2. The newly developed thermodynamic consistent framework is able to properly model diversified material behaviour ranging from pressure independent materials such as steel to pressure dependent materials such as concrete or other geotechnical materials. It can be used to enhance existing models or to develop new ones with many desired characteristics reflecting the experimental observations. Dilative and contractive behaviours of distinctive materials beyond elastic domain can be effectively modelled and controlled by adjusting the plastic flow direction via a few parameters. Furthermore, only a single loading (or yield) function is obtained from the Legendre transformation of the dissipation, instead of having two separate loading functions corresponding to damage and plastic when the additive form of dissipation potential is used. To this end, the use of a single loading

surface is very helpful in the implementation stage as it helps eliminating the risks of numerical instabilities caused by complex numerical algorithm which is required for combining multiple loading surfaces. Thus, the evolution rules for both damage variable and plastic strains can be derived directly from the same loading function. The proportions of energy dissipation due to plasticity and damage can be specified through a user-defined parameter r_d which is introduced as part of the model derivations without imposing any restrictions to the formulation.

3. The softening effects of interfacial debonding are successfully considered with the use of an anisotropic damage model in a combined FIE block. In addition, the proposed damage model helps to properly characterise the directional dependence of the softening response in FRC ply due to fiber debonding failure. This helps to overcome a vital drawbacks of many existing constitutive models where a perfect bonding condition at the interface of fiber and matrix is assumed.

5.3 Recommended Future Works

In the present study, we developed an efficient constitutive model to predict the behaviour of FRC ply in inelastic range. The followings are some of the possible areas of research where the present study can be extended in future:

1. The present investigation is based on the assumption of quasi-static loading where the strain-rate has no effects on the material response. Further investigations on viscoplastic behaviour of composite materials is a potential area of research since some applications of composite materials can induce extremely high strain-rates. Under such loading scenario, the actual material response cannot be captured accurately if viscoplastic behaviour of the material are not properly addressed.
2. Due to limited amount of suitable test data at the time of conducting this research, the model analyses were carried out for uniaxial loading cases. It is recommended that future works may include undertaking biaxial as well as off-axis loading tests to obtain suitable data for model validation purposes.

3. Stiffness reduction due to fatigue loading in composite structures is one of the critical issues that needs to be taken care of by designers and engineers, especially when these structures/components are subjected to cyclic loadings over a long period of time. Fatigue-induced damage usually involves extensive matrix cracking throughout the structural volume and over the long period, it can lead to the formation of ply cracking, interfacial debonding or delamination. As a result, this may cause significant degradation of the structure integrity (reduced strength and stiffness) and eventually leads to structural failures. It is possible to extend the present study to include the effects of fatigue damage on the response of FRC ply by incorporating a fatigue damage model into the constitutive response of the individual material blocks including FIE. It is expected that the prediction of fatigue at the ply level can be obtained as a result of the combined responses and interactions of fatigue response of these individual blocks.
4. In the present study, the proposed model used for predicting the constitutive response of FRC is limited at the ply level. To perform a progressive damage analysis of a full structure, the current constitutive model for ply failure need to be implemented within a finite element framework for modelling composite plates/shells having multilayered configurations. To this end, the present constitutive model can be integrated into a laminated plate/shell element or a 3-D element at their integration points. By doing this, the characteristics of multilayered composite laminates can be determined which helps to construct the overall structural stiffness matrix that is required in a finite element analysis of a large structure.

REFERENCES

1. Kaw, A.K.: Mechanics of Composite Materials. Taylors & Francis Group, New York (2006)
2. Herakovich, C.T.: Mechanics of Fibrous Composites. John Wiley & Sons, Inc, New York (1998)
3. Chady, T.: Airbus Versus Boeing—Composite Materials : The sky’s the limit... , <http://www.lemauricien.com/article/airbus-versus-boeing-composite-materials-sky-s-limit>, (2013)
4. Harris, C.E., Starnes, J.H., Shuart, M.J.: An Assessment the Design Composite Vehicles of the State-of-the-Art in and Manufacturing of Large Structures for Aerospace. , Hampton (2001)
5. Arvind, N., Samantha, A., Singha Roy, D., Thanikal, J.: Retrofitting of Reinforced Concrete Beams using Fibre Reinforced Polymer (FRP) Composites – A Review. *J. Urban Environ. Eng.* 1, 164–175 (2013)
6. Thomsen, O.: Sandwich Materials for Wind Turbine Blades – Present and Future. *J. Sandw. Struct. Mater.* 7–26 (2009)
7. Reddy, J.N.: A Simple Higher-Order Theory for Laminated Composite Plates. *J. Appl. Mech.* 51, 745–752 (1984)
8. Reddy, J.N.: Mechanics of Laminated Composite Plates and Shells – Theory and Analysis. CRC Press LLC, USA (1997)
9. Lo, K.H., Christensen, R.M., Wu, E.M.: A High-Order Theory of Plate Deformation - Part 2: Laminated Plates. *J. Appl. Mech.* 669–676 (1977)
10. Yang, P.C., Norris, C.H., Stavskys, Y.: Elastic Wave Propagation in Heterogeneous Plates. *Int. J. Solids Struct.* 2, 665–684 (1966)
11. Kant, T., Owen, D.R.J., Zienkiewicz, O.C.: A Refined Higher-Order C0 Plate Bending Element. 15, 177–183 (1982)
12. Toledano, A., Murakami, H.: A Composite Plate Theory for Arbitrary Laminate Configurations. *J. Appl. Mech.* 54, 181–189 (1987)

REFERENCES

13. Khdeir, A.A., Reddy, J.N.: Free Vibrations of Laminated Composite Plates Using Second-Order Shear Deformation Theory. *Comput. Struct.* 71, 617–626 (1999)
14. Ambartsumyan, S.A.: *Theory of Anisotropic Plates* [In Russian]. Izdat. Nauka, Moskva (1969)
15. Whitney, J.M.: The Effect of Transverse Shear Deformation on the Bending of Laminated Plates. *J. Compos. Mater.* 3, 534 (1969).
doi:10.1177/002199836900300316
16. Pryor, C.W., Barker, R.M.: A Finite-Element Analysis Including Transverse Shear Effects for Applications to Laminated Plates. *AIAA J.* 9, 912–917 (1971)
17. Reissner, E.: A Consistent Treatment of Transverse Shear Deformation in Laminated Anisotropic Plates. *AIAA J.* 10, 716–718 (1972)
18. Srinivas, S.: A Refined Analysis of Composite Laminates. 30, 495–507 (1973)
19. Murakami, H.: Laminated Composite Plate Theory With Improved In-Plane Responses. *J. Appl. Mech.* 53, 661–666 (1986)
20. Reissner, E.: On A Certain Mixed Variational Theorem and A Proposed Application. *Int. J. Numer. Methods Eng.* 20, 1366–1368 (1984)
21. Reddy, J.N.: A Generalization of Two-Dimensional Theories of Laminated Composite Plates. *Commun. Appl. Numer. Methods.* 3, 173–180 (1987)
22. Cho, K.N., Bert, C.W., Striz, A.G.: Free Vibrations of Laminated Rectangular Plates Analyzed by Higher Order Individual-Layer Theory. *J. Sound Vib.* 145, 429–442 (1991)
23. Li, X., Liu, D.: Zigzag Theory for Composite Laminates. *AIAA J.* 33, 1163–1165 (1994)
24. Dong, S.B., Tso, F.K.W.: On a Laminated Orthotropic Shell Theory Including Transverse Shear Deformation. *J. Appl. Mech.* 1091–1097 (1972)

REFERENCES

25. Whitney, J.M., Sun, C.T.: A Refined Theory for Laminated Anisotropic , Cylindrical Shells. *J. Appl. Mech.* 471–476 (1974)
26. Whitney, J.M., Sun, C.T.: A Higher Order Theory for Extensional Motion of Laminated Composites. *J. Sound Vib.* 30, 85–97 (1973)
27. Bhimaraddi, A.: Higher Order Theory for Free Vibration Analysis of Circular Cylindrical Shells. *Int. J. Solids Struct.* 20, 623–630 (1984)
28. Zukas, J.A., Vinson, J.R.: Laminated Transversely Isotropic Cylindrical Shells. *J. Appl. Mech.* 400–407 (1971)
29. Barbero, E.J., Reddy, J.N.: Modeling of Delamination In Composite Laminates Using A Layer-wise Plate Theory. *Int. J. Solids Struct.* 28, 373–388 (1991)
30. Carrera, E.: Single- vs Multilayer Plate Modelings on the Basis of Reissner’s Mixed Theorem. *AIAA J.* 38, 342–352 (2000)
31. Carrera, E., Demasi, L.: Classical and Advanced Multilayered Plate Elements Based Upon PVD and RMVT . Part 1 : Derivation of Finite Element Matrices. *Int. J. Numer. Methods Eng.* 55, 191–231 (2002). doi:10.1002/nme.492
32. Carrera, E., Demasi, L.: Classical and Advanced Multilayered Plate Elements Based Upon PVD and RMVT . Part 2 : Numerical Implementations. *Int. J. Numer. Methods Eng.* 55, 253–291 (2002). doi:10.1002/nme.493
33. Van Der Meer, F.P.: Computational Modeling of Failure in Composite Laminates, (2010)
34. Greenhalgh, E.S.: Failure Analysis and Fractography of Polymer Composites. Woodhead Publishing Limited, USA (2009)
35. Hull, D.: An Introduction to Composite Materials. Cambridge University Press, Cambridge (1981)
36. Curtin, W.A.: Multiple Matrix Cracking in Brittle Matrix Composites. *Acta Metall. Mater.* 41, 1369–1377 (1993)

REFERENCES

37. Ye, J., Lam, D., Zhang, D.: Initiation and Propagation of Transverse Cracking in Composite Laminates. *Comput. Mater. Sci.* 47, 1031–1039 (2010)
38. Spearing, S.M., Zok, F.W.: Stochastic Aspects of Matrix Cracking in Brittle Matrix Composites. *J. Eng. Mater. Technol.* 115, 314–318 (1993)
39. McCartney, L.N.: Energy-based prediction of progressive ply cracking and strength of general symmetric laminates using an homogenisation method. *Compos. Part A Appl. Sci. Manuf.* 36, 119–128 (2005).
doi:10.1016/j.compositesa.2004.06.003
40. Zhang, Y., Xia, Z., Ellyin, F.: Nonlinear viscoelastic micromechanical analysis of fibre-reinforced polymer laminates with damage evolution. *Int. J. Solids Struct.* 42, 591–604 (2005). doi:10.1016/j.ijsolstr.2004.06.021
41. Budiansky, B., Hutchinson, J.W., Evans, A.G.: Matrix Fracture in Fiber-Reinforced Ceramics. *J. Mech. Phys. Solids.* 34, 167–189 (1986)
42. Meng, Q., Wang, Z.: Theoretical model of fiber debonding and pull-out in unidirectional composites. *J. Compos. Mater.* 49, 1739–1751 (2015).
doi:10.1177/0021998314540191
43. Jeng, S.M., Yang, C.J.: Fracture mechanisms of fiber-reinforced titanium alloy matrix composites Part I: Interfacial behavior. *Mater. Sci. Eng.* 138, 155–167 (1991)
44. Koyanagi, J., Ogihara, S., Nakatani, H., Okabe, T.: Mechanical properties of fiber/matrix interface in polymer matrix composites. *Adv. Compos. Mater.* 23, 551–570 (2014)
45. Tsai, S.W.: Strength of Theories of Filamentary Structures. *Fundamental Aspects of Fiber Reinforced Plastic Composites.* John Wiley & Sons, USA (1968)
46. Stabb, G.H.: *Laminar Composites.* Butterworth-Heinemann, USA (1999)
47. Tsai, S.W., Wu, E.M.: A General Theory of Strength for Anisotropic Materials. *J. Compos. Mater.* 5, 58–80 (1971).
doi:10.1177/002199837100500106

REFERENCES

48. Hoffman, O.: The Brittle Strength of Orthotropic Materials. *J. Compos. Mater.* 1, (1967). doi:10.1177/002199836700100210
49. Hashin, Z., Rotem, A.: A Fatigue Failure Criterion for Fiber Reinforced Materials. *J. Compos. Mater.* 7, 448–464 (1973). doi:10.1177/002199837300700404
50. Hashin, Z.: Failure Criteria for Unidirectional Fiber Composites. *J. Appl. Mech.* 47, 329–334 (1980)
51. Christensen, R.M.: Tensor Transformations and Failure Criteria for the Analysis of Fiber Composite Materials. *J. Compos. Mater.* 22, 874–897 (1988). doi:10.1177/002199838802200906
52. Christensen, R.M.: Stress Based Yield/Failure Criteria for Fiber Composites. *Int. J. Solids Struct.* 34, 529–543 (1997)
53. Gosse, J.H., Christensen, S.: Strain Invariant Failure Criteria for Polymers in Composite Materials. *AIAA J.* 1184 (2011)
54. Gosse, J.H.: Failure Criteria in Fibre-Reinforced-Polymer Composites. In: Thirteen ICCM Conference. p. Paper ID 1687. , Beijing (2001)
55. Van Paepegem, W., De Baere, I., Degrieck, J.: Modelling the nonlinear shear stress-strain response of glass fibre-reinforced composites. Part I: Experimental results. *Compos. Sci. Technol.* 66, 1455–1464 (2006). doi:10.1016/j.compscitech.2005.04.014
56. Schuecker, C., Pettermann, H.: Combining elastic brittle damage with plasticity to model the non-linear behavior of fiber reinforced laminates. In: Camanho, P.P., Dávila, C.G., Pinho, S.T., and Remmers, J.J.C. (eds.) *Mechanical Response of Composites*. Springer Netherlands (2008)
57. Lemaitre, J., Desmorat, R.: *Engineering Damage Mechanics*. Springer, The Netherlands (2005)
58. Puck, A., Schurmann, H.: Failure Analysis of Frp Laminates By Means of Physically Based Phenomenological Models *. *Compos. Sci. Technol.* 58, 1045–1067 (1998)

REFERENCES

59. Deuschle, H.M., Puck, A.: Application of the Puck failure theory for fibre-reinforced composites under three-dimensional stress : Comparison with experimental results. *J. Compos. Mater.* 47, 827–846 (2012). doi:10.1177/0021998312462158
60. Pinho, S.T., Darvizeh, R., Robinson, P., Schuecker, C.: Material and structural response of polymer-matrix fibre-reinforced composites. *J. Compos. Mater.* 46, 2313–2341 (2012). doi:10.1177/0021998312454478
61. Pinho, S.T., Dávila, C.G., Camanho, P.P., Iannucci, L., Robinson, P.: Failure Models and Criteria for FRP Under In-Plane or Three-Dimensional Stress States Including Shear Non-Linearity. , Hampton (2005)
62. Pinho, S.T., Iannucci, L., Robinson, P.: Physically-based failure models and criteria for laminated fibre-reinforced composites with emphasis on fibre kinking : Part I: Development. *Compos. Part A Appl. Sci. Manuf.* 37, 63–73 (2006). doi:10.1016/j.compositesa.2005.04.016
63. Bogetti, T.A., Hoppel, C.P.R., Harik, V.M., Newill, J.F., Burns, B.P.: Predicting the nonlinear response and progressive failure of composite laminates. *Fail. Criteria Fibre-Reinforced-Polymer Compos.* 64, 402–428 (2004). doi:10.1016/B978-008044475-8/50017-2
64. Bogetti, T. a., Staniszewski, J., Burns, B.P., Hoppel, C.P., Gillespie, J.W., Tierney, J.: Predicting the nonlinear response and progressive failure of composite laminates under tri-axial loading. *J. Compos. Mater.* 46, 2443–2459 (2012). doi:10.1177/0021998312449889
65. Cuntze, R.G., Freund, A.: The Predictive Capability of Failure Mode Concept-Based Strength Criteria for Multidirectional Laminates. *Compos. Sci. Technol.* 64, 343–377 (2004). doi:10.1016/S0266-3538(03)00218-5
66. Cuntze, R.: The predictive capability of failure mode concept-based strength conditions for laminates composed of unidirectional laminae under static triaxial stress states. (2012)
67. Sun, C.T., Chen, J.L.: A Simple Flow Rule for Characterizing Nonlinear Behavior of Fiber Composites. *J. Compos. Mater.* 23, 1009–1020 (1989).

REFERENCES

- doi:10.1177/002199838902301004
68. Sun, C.T., Yoon, K.J.: Elastic-plastic analysis of AS4/PEEK composite laminate using a one-parameter plasticity model. *J. Compos. Mater.* 26, 293–308 (1990)
69. Daudeville, L., Allix, O., Ladeveze, P.: Delamination Analysis By Damage Mechanics: Some Applications. *Compos. Part B Eng.* 5, 17–24 (1995). doi:10.1016/0961-9526(95)93976-3
70. Schuecker, C., Pettermann, H.E.: A continuum damage model for fiber reinforced laminates based on ply failure mechanisms. *Compos. Struct.* 76, 162–173 (2006). doi:10.1016/j.compstruct.2006.06.023
71. Ladeveze, P., Lubineau, G.: On a Damage Mesomodel For Laminates : Micro – Meso Relationships , Possibilities and Limits. *Compos. Sci. Technol.* 61, 2149–2158 (2001)
72. Ladeveze, P., Lubineau, G., Marsal, D.: Towards a Bridge Between The Micro- and Mesomechanics of Delamination For Laminated Composites. *Compos. Sci. Technol.* 66, 698–712 (2006). doi:10.1016/j.compscitech.2004.12.026
73. Kaddour, A., Hinton, M.: Input Data for Test Cases Used in Benchmarking Triaxial Failure Theories of Composites. *J. Compos. Mater.* 46, 2295–2312 (2012). doi:10.1177/0021998312449886
74. Talreja, R., Yalvac, S., Yats, L.D., Wetters, D.G.: Transverse Cracking and Stiffness Reduction in Cross Ply Laminates of Different Matrix Toughness. *J. Compos. Mater.* 26, 1644–1663 (1992). doi:10.1177/002199839202601105
75. Talreja, R.: A Continuum Mechanics Characterization of Damage in Composite Materials. *Proc. R. Soc. London . Ser. A , Math. Phys.* 399, 195–216 (1985)
76. Barbero, E.J., Lonetti, P.: An Inelastic Damage Model for Fiber Reinforced Laminates. *J. Compos. Mater.* 36, 941–962 (2002). doi:10.1106/002199802023549

REFERENCES

77. Aboudi, J., Steven, M.A., Brett, A.B.: *Micromechanics of Composite Materials - A Generalized Multiscale Analysis Approach*. Elsevier, US (2013)
78. Curtis, G.J., Milne, J.M., Reynolds, W.N.: Non-Hookean Behaviour of Strong Carbon Fibres. *Nature*. 20, 1968 (1968)
79. Shokrieh, M.M., Mosalmani, R., Omid, M.J.: A strain-rate dependent micromechanical constitutive model for glass/epoxy composites. *Compos. Struct.* 121, 37–45 (2015). doi:10.1016/j.compstruct.2014.10.035
80. Vaughan, T.J., McCarthy, C.T.: A combined experimental-numerical approach for generating statistically equivalent fibre distributions for high strength laminated composite materials. *Compos. Sci. Technol.* 70, 291–297 (2010). doi:10.1016/j.compscitech.2009.10.020
81. Totry, E., Molina-Aldareguia, J.M., Gonzalez, C., LLorca, J.: Effect of fiber, matrix and interface properties on the in-plane shear deformation of carbon-fiber reinforced composites. *Compos. Sci. Technol.* 70, 970–980 (2010). doi:10.1016/j.compscitech.2010.02.014
82. Romanowicz, M.: A numerical approach for predicting the failure locus of fiber reinforced composites under combined transverse compression and axial tension. *Comput. Mater. Sci.* 51, 7–12 (2012). doi:10.1016/j.commatsci.2011.07.039
83. Fiedler, B., Hojo, M., Ochiai, S., Schulte, K., Ando, M.: Failure behavior of an epoxy matrix under different kinds of static loading. 61, 1615–1624 (2001)
84. Canal, L.P., González, C., Segurado, J., LLorca, J.: Intraply fracture of fiber-reinforced composites: Microscopic mechanisms and modeling. *Compos. Sci. Technol.* 72, 1223–1232 (2012). doi:10.1016/j.compscitech.2012.04.008
85. Melro, A.R., Camanho, P.P., Andrade Pires, F.M., Pinho, S.T.: Micromechanical analysis of polymer composites reinforced by unidirectional fibres: Part II – Micromechanical analyses. *Int. J. Solids*

REFERENCES

- Struct. 50, 1906–1915 (2013). doi:10.1016/j.ijsolstr.2013.02.007
86. Tay, T.E., Tan, S.H.N., Tan, V.B.C., Gosse, J.H.: Damage progression by the element-failure method (EFM) and strain invariant failure theory (SIFT). *Compos. Sci. Technol.* 65, 935–944 (2005). doi:10.1016/j.compscitech.2004.10.022
87. Hill, R.: Elastic Properties of Reinforced Solids: Some Theoretical Principles. *J. Mech. Phys. Solids.* 11, 357–372 (1963)
88. Mori, T., Tanaka, K.: Average Stress in Matrix and Average Elastic Energy of Materials with Misfitting Inclusions. *ACTA Metall.* 21, 571–574 (1974)
89. Dvorak, G.J.: Transformation Field Analysis of Inelastic Composite Materials. *Proc. R. Soc. A Math. Phys. Eng. Sci.* 437, 311–327 (1992). doi:10.1007/BF00370073
90. Hashin, Z., Rosen, B.W.: The Elastic Moduli of Fiber-Reinforced Materials. *J. Appl. Mech.* 223–232 (1964)
91. Hashin, Z.: The Elastic Moduli of Heterogeneous Materials. *J. Appl. Mech.* 29, 143–150 (1962)
92. Christensen, M.R., Lo, K.H.: Solutions for effective shear properties in three phase sphere and cylinder models. *J. Mech. Phys. Solids.* 27, 315–330 (1979)
93. Sun, C.T., Chen, J.L.: A Micromechanical Model for Plastic Behavior of Fibrous Composites. *Compos. Sci. Technol.* 40, 115–129 (1991). doi:10.1016/0266-3538(91)90092-4
94. Aboudi, J.: Micromechanical Analysis of Composites by the Method of Cells. *Am. Soc. Mech. Eng.* 42, 193–221 (1989)
95. Aboudi, J.: Journal of Reinforced Plastics and Composites The Nonlinear Behavior of Unidirectional. *J. Reinf. Plast. Compos.* (1990). doi:10.1177/073168449000900102
96. Pindera, M.-J., Bednarczyk, B. a: An efficient implementation of the generalized method of cells for unidirectional, multi-phased composites

REFERENCES

- with complex microstructures. *Compos. Part B Eng.* 30, 87–105 (1999).
doi:10.1016/S1359-8368(98)00040-7
97. Li, H., Zhang, B., Bai, G.: Effects of constructing different unit cells on predicting composite viscoelastic properties. *Compos. Struct.* 125, 459–466 (2015). doi:10.1016/j.compstruct.2015.02.028
98. Ogihara, S., Kobayashi, S.: Characterization of nonlinear behavior of carbon / epoxy unidirectional and angle-ply laminates. *Adv. Compos. Mater.* 11, 239–254 (2003)
99. Tsai, J.-L., Chen, K.-H.: Characterizing Nonlinear Rate-dependent Behaviors of Graphite/Epoxy Composites using a Micromechanical Approach. *J. Compos. Mater.* 41, 1253–1273 (2007).
doi:10.1177/0021998306067307
100. Huang, Z.M.: A Unified Micromechanical Model for the Mechanical Properties of Two Constituents Composite Materials Part II: Plastic Behavior. *J. Thermoplast. Compos. Mater.* 13, 344–362 (2000).
doi:0803973233
101. Huang, Z.M.: Simulation of the mechanical properties of fibrous composites by the bridging micromechanics model. *Compos. Part A Appl. Sci. Manuf.* 32, 143–172 (2001). doi:10.1016/S1359-835X(00)00142-1
102. Huang, Z.M.: Inelastic and Failure Analysis of Laminate Structures by ABAQUS Incorporated with a General Constitutive Relationship. *J. Reinf. Plast. Compos.* 26, 1135–1181 (2007). doi:10.1177/0731684407079753
103. Santhosh, U., Ahmad, J.: An approach for nonlinear modeling of polymer matrix composites. *J. Compos. Mater.* 48, 1755–1765 (2014).
doi:10.1177/0021998313490581
104. Tabiei, A., Aminjikai, S.B.: A strain-rate dependent micro-mechanical model with progressive post-failure behavior for predicting impact response of unidirectional composite laminates. *Compos. Struct.* 88, 65–82 (2009). doi:10.1016/j.compstruct.2008.02.017
105. Goldberg, R., Stouffer, D.: Strain rate dependent analysis of a polymer

REFERENCES

- matrix composite utilizing a micromechanics approach. *J. Compos. Mater.* 36, 773–793 (2002). doi:10.1106/002199802024613
106. Houlsby, G.T., Puzrin, a. M.: Thermomechanical Framework for Constitutive Models for Rate-independent Dissipative Materials. *Int. J. Plast.* 16, 1017–1047 (2000). doi:10.1016/S0749-6419(99)00073-X
107. Vu, V.D., Sheikh, A.H., Nguyen, G.D., Shen, L.: A kinematically enhanced constitutive model for elastic and inelastic analysis of unidirectional fibre reinforced composite materials. *Int. J. Mech. Sci.* 126, 171–185 (2017). doi:10.1016/j.ijmecsci.2017.03.027
108. Aboudi, J.: *Mechanics of Composite Materials: A Unified Micromechanical Approach*. Elsevier, Amsterdam (1991)
109. Melro, A.R., Camanho, P.P., Andrade Pires, F.M., Pinho, S.T.: Micromechanical analysis of polymer composites reinforced by unidirectional fibres: Part I - Constitutive modelling. *Int. J. Solids Struct.* 50, 1897–1905 (2013). doi:10.1016/j.ijsolstr.2013.02.009
110. Robertson, D.D., Mall, S.: Micromechanical analysis for thermoviscoplastic behavior of unidirectional fibrous composites. *Compos. Sci. Technol.* 50, 483–496 (1994). doi:10.1016/0266-3538(94)90057-4
111. Lin, G., Geubelle, P.H., Sottos, N.R.: Simulation of fiber debonding with friction in a model composite pushout test. *Int. J. Solids Struct.* 38, 8547–8562 (2001). doi:10.1016/S0020-7683(01)00085-3
112. Bowling, J., Groves, G.W.: The debonding and pull-out of ductile wires from a brittle matrix. *J. Mater. Sci.* 14, 431–442 (1979). doi:10.1007/BF00589836
113. Atkinson, C., Avila, J., Betz, E., Smelser, R.E.: The Rod Pull Out Problem, Theory and Experiment. *J. Mech. Phys. Solids.* 30, 97–120 (1982)
114. Hutchinson, J.W., Mear, M.E., Rice, J.R.: Crack Paralleling an Interface Between Dissimilar Materials. *J. Appl. Mech.* 54, 9 (1987)
115. Hutchinson, J.W., Jensen, H.M.: Models of fiber debonding and pullout in brittle composites with friction. *Mech. Mater.* 9, 139–163 (1990).

REFERENCES

- doi:10.1016/0167-6636(90)90037-G
116. Wriggers P, Zavarise G, Zohdi T I: A computational study of interfacial debonding damage in brous composite materials. *Comput. Mater. Sci.* 12, 39–56 (1998)
117. Vu, V.D., Mir, A., Nguyen, G.D., Sheikh, A.H.: A thermodynamics-based formulation for constitutive modelling using damage mechanics and plasticity theory. *Eng. Struct.* 143, 22–39 (2017)
118. Davidson, P., Davis, R.: Mechanical Behavior of 6061 — T651 Aluminum. *AIAA J.* 13, 1547–1548 (1975)
119. Ghorbel, E.: A viscoplastic constitutive model for polymeric materials. *Int. J. Plast.* 24, 2032–2058 (2008). doi:10.1016/j.ijplas.2008.01.003
120. Wood, D.: Soil Behaviour and Critical State Soil Mechanics, http://books.google.pt/books/about/Soil_Behaviour_and_Critical_State_Soil_M.html?id=CBVVG1zzjjEC&redir_esc=y, (1990)
121. Asp, L.E., Berglund, L.A., Gudmundson, P.: Effects of a composite-like stress state on the fracture of epoxies. *Compos. Sci. Technol.* 53, 27–37 (1995). doi:10.1016/0266-3538(94)00075-1
122. Puck, A.: Calculating The Strength of Glass Fibre/Plastic Laminates Under Combined Load. *Kunststoffe, Gennan Plast.* 55, 18–19 [German] (1969)
123. Crisfield, M.A.: Non-linear finite element analysis of solids and structures. Volume 1: Essentials. John Wiley & Sons Ltd, Chichester (1991)
124. Vu, V.: A MICROMECHANICS BASED FINITE ELEMENT MODEL FOR PROGRESSIVE DAMAGE ANALYSIS OF COMPOSITE PLATE / SHELL. , Adelaide (2015)
125. Hill, R.: Self-Consistent Mechanics of Composite Materials. *J. Mech. Phys. Solids.* 13, 213–222 (1965)

APPENDICES

Conference Paper 1

Vu V.D., Nguyen G.D., Sheikh A.H., A Micromechanics Based Constitutive Model for Progressive Failure of Unidirectional Composites, 20th International Conference on Composite Materials, 19–24 July 2015, Copenhagen, Denmark.

A MICROMECHANICS BASED CONSTITUTIVE MODEL FOR PROGRESSIVE FAILURE OF UNIDIRECTIONAL COMPOSITES

Van D. Vu¹, Abdul H. Sheikh² and Giang Nguyen³

School of Civil, Environmental and Mining Engineering, the University of Adelaide

North Terrace Campus, Adelaide, South Australia, web page:

<http://www.adelaide.edu.au/>

¹Email: van.vu@adelaide.edu.au.

²Email: abdul.sheikh@adelaide.edu.au

³Email: g.nguyen@adelaide.edu.au

Keywords: Constitutive modelling, Micromechanics, unidirectional Composite, inelastic deformation

ABSTRACT

In this paper, a new micromechanics-based constitutive model is developed for fibre reinforced polymer matrix composites having unidirectional fibre orientations which can incorporate elastic and inelastic responses of both fibres and matrix. The composite material is idealised by a representative volume element consisting of four material blocks where one of them is for fibre and the others for matrix. Kinematic enrichments of different strain components for the different material blocks are used to accommodate the responses of different material blocks. The model is first used to evaluate orthotropic material properties of composites in the elastic range using isotropic material properties of the constituents. After a

successful validation of these predicted material properties using existing theoretical as well as experimental results, the model is applied to inelastic material response to assess its performance in the nonlinear range.

1 INTRODUCTION

The use of composite materials is becoming popular in many engineering disciplines over the last few decades due to their high specific strength and stiffness, exceptional durability and some other attractive features. The composite structures can be subjected to complex loading conditions such as extreme temperature, dynamic loads, impact, corrosion and some other loading scenarios which will induce complex loading paths on the materials. Moreover, the composite nature of these materials consisting of different dissimilar phases leads to additional complexities. Thus the analysis of composite structures requires a good model that can predict the behaviour of the material properly. This in turn needs an advanced constitutive model which will accurately capture the deformation of the matrix and fibres along with their interactions.

In the literature, a large number of models have been developed by different researchers attempting to capture the responses of these materials correctly. Most of the existing models can be categorised into two distinct branches: macro-mechanical and micro-mechanical models. The initial developments of some popular macro-mechanical models are due to Hoffman, Puck, Hashin and Rotem [1-3] and few others. Tsai [45] also attempted to develop a failure criterion, popularly known as Tsai-Hill theory, for “weak” anisotropic materials. Although these models are easy to use, they are of phenomenological nature that needs a large set of experimental data for their development. As a consequence these models may not be reliable when applied outside the range of these data sets. Macro-mechanical models actually treat the composite material as a single homogeneous material and do not follow the actual deformations and correct failure mechanisms of the constituents and their interactions.

On the other hand, some researchers such as Christensen and Lo, Mori and Tanaka, and Aboudi [5-7] have proposed micromechanics-based models, in which the overall properties of the composites are determined by using a Representative Volume Element (RVE) consist of their constituents. Despite the fact that more

realistic results could be obtained by using these micromechanics-based models, most of the earlier ones are not applicable in inelastic range where the constituents will have plastic deformations, damage and their coupling. Besides, thanks to the advances of computing power, full micromechanical analyses of composite materials, where all constituents can be modelled explicitly, are gradually applicable. This provides us with useful tools for the analysis of composite failure in the inelastic range and can produce results with high levels of accuracy, which seems quite attractive for furthering the understanding of failure mechanisms. However, the computational demand of a full micromechanical model is so high that the use of such model is not feasible for the analysis of a real structure.

In this study, a micromechanics-based constitutive model for unidirectional fibre composite is developed that can be used within a framework of a macro-mechanical analysis. The model inherits the computational efficiency of a macro-mechanical model and at the same time the important physical behaviours and interactions of matrix and fibre are embraced. First, a mathematical derivation of the current model is introduced following by the validation of the model in the elastic range with some existing classical theories as well as experimental results available in literature. The validation of these results covering a wide range of elastic material properties shows a promising performance of the proposed model. The model is then applied in the inelastic range taking nonlinear material response of the constituents and their interactions. The trend of the nonlinear results indicates a good future potential of the model.

2 A MICROMECHANICS BASED CONSTITUTIVE MODEL

Figure 1 shows a representative volume element (RVE) which is conceptualised for modelling the behaviours of unidirectional composites aiming to retain essential mechanisms of fibres, matrix and their interactions whilst being simple enough to accommodate inelastic behaviours of different phases. The central idea of this model is to have sufficient lower scale (fibre scale) details for the prediction at higher scales, while minimising the computational demand. In this sense, the deformation of the matrix and the fibre will be modelled distinctly and they will be combined together utilising their interaction to predict the deformation of the composite material. Denoting f as the matrix volume fraction, the corresponding

volume fractions of the three matrix blocks (M-1, M-2, M-3), defined as f_1, f_2 and f_3 respectively, can easily be expressed in terms of f (Figure 1). The homogenised or macro strain rate of the volume element or the composite can be written in matrix-vector form as:

$$\{\dot{\epsilon}\} = f_1\{\dot{\epsilon}_{m1}\} + f_2\{\dot{\epsilon}_{m2}\} + f_3\{\dot{\epsilon}_{m3}\} + (1 - f)\{\dot{\epsilon}_f\} \quad (1)$$

The strain rates (or increments) of the different matrix blocks can be defined in terms of fibre block strain rates with the enhancement of their transverse strain increments as:

$$\{\dot{\epsilon}_{m1}\} = \{\dot{\epsilon}_f\} + [N_2]\{\dot{\epsilon}_2\} + [N_3]\{\dot{\epsilon}_3\} \quad (2)$$

$$\{\dot{\epsilon}_{m2}\} = \{\dot{\epsilon}_f\} + [N_2]\{\dot{\epsilon}_2\} \quad (3)$$

$$\{\dot{\epsilon}_{m3}\} = \{\dot{\epsilon}_f\} + [N_3]\{\dot{\epsilon}_3\} \quad (4)$$

where the enhancement terms ($\{\dot{\epsilon}_2\} = \{\dot{\gamma}_{2xy} \dot{\epsilon}_{2yy} \dot{\gamma}_{2yz}\}^T$ and $\{\dot{\epsilon}_3\} = \{\dot{\gamma}_{3xz} \dot{\gamma}_{3yz} \dot{\epsilon}_{3zz}\}^T$) appear only in the appropriate positions of the strain vectors which are accommodated with the help of two matrices $[N_2]$ and $[N_3]$ corresponding to the directions (y and z respectively) of the two interfaces (see Appendix for details).

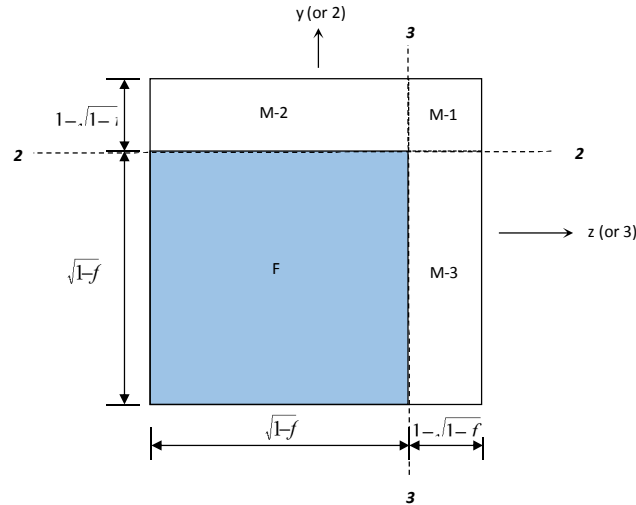


Figure 1: A Representative Volume Element for unidirectional composites (F: Fibre block; M-1, M-2, M-3: Matrix blocks).

From Equations (1) to (4), we can express the matrix and fibre strain rates in term of the homogenised strain rate and enhanced strain rates as:

$$\{\dot{\varepsilon}_f\} = \{\dot{\varepsilon}\} - (f_1 + f_2)[N_2]\{\dot{\varepsilon}_2\} - (f_1 + f_3)[N_3]\{\dot{\varepsilon}_3\} \quad (5)$$

$$\{\dot{\varepsilon}_{m1}\} = \{\dot{\varepsilon}\} + (1 - (f_1 + f_2))[N_2]\{\dot{\varepsilon}_2\} + (1 - (f_1 + f_3))[N_3]\{\dot{\varepsilon}_3\} \quad (6)$$

$$\{\dot{\varepsilon}_{m2}\} = \{\dot{\varepsilon}\} + (1 - (f_1 + f_2))[N_2]\{\dot{\varepsilon}_2\} - (f_1 + f_3)[N_3]\{\dot{\varepsilon}_3\} \quad (7)$$

$$\{\dot{\varepsilon}_{m3}\} = \{\dot{\varepsilon}\} - (f_1 + f_2)[N_2]\{\dot{\varepsilon}_2\} + (1 - (f_1 + f_3))[N_3]\{\dot{\varepsilon}_3\} \quad (8)$$

The enhanced strain rates can be eliminated from the above equations which will help to express the matrix and fibre strain rates in term of homogenised strain rates and volume fractions. Now the Hill-Mandel condition of virtual work [87] can be used as:

$$\begin{aligned} \{\sigma\}^T \{\dot{\varepsilon}\} &= f_1 \{\sigma_{m1}\}^T \{\dot{\varepsilon}_{m1}\} + f_2 \{\sigma_{m2}\}^T \{\dot{\varepsilon}_{m2}\} + f_3 \{\sigma_{m3}\}^T \{\dot{\varepsilon}_{m3}\} \\ &\quad + (1 - f) \{\sigma_f\}^T \{\dot{\varepsilon}_f\} \end{aligned} \quad (9)$$

Substitution of the segmental strain rates as expressed in Equations (5) to (8) into the above equation (9), it can be rewritten as:

$$\begin{aligned} \{\sigma\}^T \{\dot{\varepsilon}\} &= f_1 \{\sigma_{m1}\}^T (\{\dot{\varepsilon}\} + (1 - (f_1 + f_2))[N_2]\{\dot{\varepsilon}_2\} \\ &\quad + (1 - (f_1 + f_3))[N_3]\{\dot{\varepsilon}_3\}) \\ &\quad + f_2 \{\sigma_{m2}\}^T (\{\dot{\varepsilon}\} + (1 - (f_1 + f_2))[N_2]\{\dot{\varepsilon}_2\} \\ &\quad - (f_1 + f_3)[N_3]\{\dot{\varepsilon}_3\}) \\ &\quad + f_3 \{\sigma_{m3}\}^T (\{\dot{\varepsilon}\} - (f_1 + f_2)[N_2]\{\dot{\varepsilon}_2\} \\ &\quad + (1 - (f_1 + f_3))[N_3]\{\dot{\varepsilon}_3\}) \\ &\quad + (1 - f) \{\sigma_f\}^T (\{\dot{\varepsilon}\} - (f_1 + f_2)[N_2]\{\dot{\varepsilon}_2\} \\ &\quad - (f_1 + f_3)[N_3]\{\dot{\varepsilon}_3\}) \end{aligned} \quad (10)$$

The above equation will be valid for any arbitrary values of these strain rates $\{\dot{\varepsilon}_f\}$, $\{\dot{\varepsilon}_2\}$, and $\{\dot{\varepsilon}_3\}$ if the following conditions are satisfied:

$$\{\sigma\} = f_1 \{\sigma_{m1}\} + f_2 \{\sigma_{m2}\} + f_3 \{\sigma_{m3}\} + (1 - f) \{\sigma_f\} \quad (11)$$

$$f_1(1 - (f_1 + f_2))\{\sigma_{m1}\}^T[N_2] + f_2(1 - (f_1 + f_2))\{\sigma_{m2}\}^T[N_2] - f_3(f_1 + f_2)\{\sigma_{m3}\}^T[N_2] - (1 - f)(f_1 + f_2)\{\sigma_f\}^T[N_2] = 0 \quad (12)$$

$$f_1(1 - (f_1 + f_3))\{\sigma_{m1}\}^T[N_3] - f_2(f_1 + f_3)\{\sigma_{m2}\}^T[N_3] + f_3(1 - (f_1 + f_3))\{\sigma_{m3}\}^T[N_3] - (1 - f)(f_1 + f_3)\{\sigma_f\}^T[N_3] = 0 \quad (13)$$

Equation (11) gives the homogenised stresses of the whole RVE expressed in terms of stresses of the matrix and fibre and their volume fractions. Equations (12) and (13) enforce average traction continuity across the interfaces 2-2 and 3-3 (Figure 1).

Now denoting $[F]$ and $[M]$ as the tangent stiffness matrix of the fibre and matrix respectively, the stresses rates in the fibre and matrix blocks can be written in generic forms as:

$$\{\dot{\sigma}_f\} = [F]\{\dot{\epsilon}_f\} \quad (14)$$

$$\{\dot{\sigma}_{m1}\} = [M_1]\{\dot{\epsilon}_{m1}\} \quad (15)$$

$$\{\dot{\sigma}_{m2}\} = [M_2]\{\dot{\epsilon}_{m2}\} \quad (16)$$

$$\{\dot{\sigma}_{m3}\} = [M_3]\{\dot{\epsilon}_{m3}\} \quad (17)$$

Using Equation (11), the relationship between the homogenised or macro stress rates can be expressed in terms of stress rates of all the material blocks as:

$$\{\dot{\sigma}\} = f_1\{\dot{\sigma}_{m1}\} + f_2\{\dot{\sigma}_{m2}\} + f_3\{\dot{\sigma}_{m3}\} + (1 - f)\{\dot{\sigma}_f\} \quad (18)$$

Moreover, the stress rates in all material blocks are connected through the continuity of traction rates at the interfaces between the fibre and matrix blocks which can be obtained using Equations (12) and (13) as:

$$f_1(1 - (f_1 + f_2))\{\dot{\sigma}_{m1}\}^T[N_2] + f_2(1 - (f_1 + f_2))\{\dot{\sigma}_{m2}\}^T[N_2] - f_3(f_1 + f_2)\{\dot{\sigma}_{m3}\}^T[N_2] - (1 - f)(f_1 + f_2)\{\dot{\sigma}_f\}^T[N_2] = 0 \quad (19)$$

$$f_1(1 - (f_1 + f_3))\{\dot{\sigma}_{m1}\}^T[N_3] - f_2(f_1 + f_3)\{\dot{\sigma}_{m2}\}^T[N_3] + f_3(1 - (f_1 + f_3))\{\dot{\sigma}_{m3}\}^T[N_3] - (1 - f)(f_1 + f_3)\{\dot{\sigma}_f\}^T[N_3] = 0 \quad (20)$$

Substitution of Equations (5) - (8) and (14) - (17) into Equations (19) and (20), we can obtain:

$$\begin{bmatrix} A_{11} & A_{12} \\ A_{21} & A_{22} \end{bmatrix} \begin{Bmatrix} \{\dot{\varepsilon}_2\} \\ \{\dot{\varepsilon}_3\} \end{Bmatrix} = \begin{bmatrix} B_1 \\ B_2 \end{bmatrix} \{\dot{\varepsilon}\} \quad (21)$$

which shows that the homogenised strain rates can be determined with the strain enhancements, and the matrices $[A_{11}]$, $[A_{12}]$, $[A_{21}]$, $[A_{22}]$, $[B_1]$ & $[B_2]$ which are dependent on material properties and volume fractions of the matrix and fibres (refer to the Appendix for more details). Now the strain enhancement terms can be expressed in terms of the homogenised strain terms from the above equation as:

$$\begin{Bmatrix} \{\dot{\varepsilon}_2\} \\ \{\dot{\varepsilon}_3\} \end{Bmatrix} = \begin{bmatrix} A_{11} & A_{12} \\ A_{21} & A_{22} \end{bmatrix}^{-1} \begin{bmatrix} B_1 \\ B_2 \end{bmatrix} \{\dot{\varepsilon}\} = \begin{bmatrix} P_1 \\ P_2 \end{bmatrix} \{\dot{\varepsilon}\} \quad (22)$$

Using Equations (5) to (8) and (22), the strain rates in the matrix and fibre blocks can be completely defined by the homogenised strain rate as:

$$\{\dot{\varepsilon}_{m1}\} = \{\dot{\varepsilon}\} + (1 - (f_1 + f_2))[N_2][P_1]\{\dot{\varepsilon}\} + (1 - (f_1 + f_3))[N_3][P_2]\{\dot{\varepsilon}\} \quad (23)$$

$$\{\dot{\varepsilon}_{m2}\} = \{\dot{\varepsilon}\} + (1 - (f_1 + f_2))[N_2][P_1]\{\dot{\varepsilon}\} - (f_1 + f_3)[N_3][P_2]\{\dot{\varepsilon}\} \quad (24)$$

$$\{\dot{\varepsilon}_{m3}\} = \{\dot{\varepsilon}\} + (f_1 + f_2)[N_2][P_1]\{\dot{\varepsilon}\} - (1 - (f_1 + f_3))[N_3][P_2]\{\dot{\varepsilon}\} \quad (25)$$

$$\{\dot{\varepsilon}_f\} = \{\dot{\varepsilon}\} - (f_1 + f_2)[N_2][P_1]\{\dot{\varepsilon}\} - (f_1 + f_3)[N_3][P_2]\{\dot{\varepsilon}\} \quad (26)$$

Substituting these strain rate expressions (23-26) into the volume averaged stress rate relationship (18), the constitutive relationship for the homogenised/macro stress and strain can finally be obtained in rate form as:

$$\{\dot{\sigma}\} = [C]\{\dot{\varepsilon}\} \quad (27)$$

where

$$\begin{aligned} [C] = & f_1[M_1] + f_2[M_2] + f_3[M_3] + (1 - f)[F] + (f_1 - f_1(f_1 + \\ & f_2))[M_1][N_2][P_1] + (f_1 - f_1(f_1 + f_3))[M_1][N_3][P_2] + (f_2 - f_2(f_1 + \\ & f_2))[M_2][N_2][P_1] - f_2(f_1 + f_3)[M_2][N_3][P_2] - f_3(f_1 + \\ & f_2)[M_3][N_2][P_1] + (f_3 - f_3(f_1 + f_3))[M_3][N_3][P_2] - (1 - f)(f_1 + \\ & f_2)[F][N_2][P_1] - (1 - f)(f_1 + f_3)[F][N_3][P_2] \end{aligned} \quad (28)$$

The above equation shows that the rate form of the constitutive matrix of the homogenised composite material is explicitly defined in terms of constitutive matrices (in rate form) of the constituents and their volume fractions. Thus the model does not have any restriction in its application in the elastic as well as inelastic ranges. In principle, the macro-mechanical strain rates at an integration point of an element within a structure can be resolved into strain rates of the fibre and matrix blocks (Fig. 1). With these strain rates, the stresses in each block can be calculated following standard stress return algorithms (see [123]). The homogenised stress can then be obtained from Equation (11). Further details can be found in [124].

3 INELASTIC ANALYSIS

As mentioned in the previous section, the formulation can be readily extended to inelastic/nonlinear range. To test the ability of the model in predicting constitutive behaviours of metal matrix composite, the material blocks in this study are assumed to follow Von Mises plasticity model. The stress-strain relationship can be described as:

$$\sigma_{ij} = C_{ijkl}(\varepsilon_{ij} - \varepsilon_{ij}^p) \quad (29)$$

where C_{ijkl} is the elastic tangent stiffness tensor, ε_{ij}^p represents the plastic strain tensor and ε_{ij} is the total strain tensor comprising elastic and plastic strains.

According to von Mises plasticity theory, the yield function may be written as:

$$y = f(\varepsilon_p) = \sigma_e - k \quad (30)$$

with associated flow rule:

$$\varepsilon_{ij}^p = \lambda \frac{\partial y}{\partial \sigma_{ij}} \quad (31)$$

The effective stress σ_e and effective plastic strain ε_p used in the above equations can be defined as:

$$\sigma_e = \sqrt{3J_2} = \sqrt{\frac{3}{2} s_{ij} s_{ij}} \quad (32)$$

$$\dot{\varepsilon}_p = \sqrt{\frac{2}{3} \dot{\varepsilon}_{ij}^p \dot{\varepsilon}_{ij}^p} = d\lambda \sqrt{\frac{2}{3} \frac{\partial y}{\partial \sigma_{ij}} \frac{\partial y}{\partial \sigma_{ij}}} \quad (33)$$

The term k used in Equation (30) corresponds to instantaneous yield stress for an uniaxially loaded member which represents hardening or softening process and it is a function of effective plastic strain ε_p . This yield stress for a linear hardening/softening case may be expressed as:

$$k = \sigma_y + H\varepsilon_p \quad (34)$$

For nonlinear hardening/softening case, it can be expressed as:

$$k = \sigma_y + Q(1 - e^{-b\varepsilon_p}) \quad (35)$$

where H is the hardening or softening rate with respect to plastic strain; Q is the difference between initial yielding stress and ultimate stress; and b is another material property that controls the hardening or softening for the nonlinear case. The choice of these material constants dictates the behaviours of the material blocks of interest.

4 RESULTS AND DISCUSSIONS

This section is dedicated to the verification of the proposed micromechanics based model in both elastic and inelastic range. Initially the elastic stiffness parameters of unidirectional FRC are predicted by the proposed model and these results are validated with existing theoretical and experimental results for various fibre volume fractions. The proposed model is then examined for its ability to capture the inelastic responses of unidirectional FRC with both hardening and softening behaviours.

4.1 Elastic Properties

4.1.1 Longitudinal Elastic Modulus:

Figure shows the prediction of longitudinal modulus E_l of a composite material (refer to Table 2 for materials properties of the constituents) with respect to fibre volume fractions. The model predictions follow the upper bound solution according to rule of mix or Voigt model. This corresponds to the condition of equal strains within the constituents and it is nicely simulated by the proposed model as it does

not have strain enhancement in the longitudinal direction. This behaviour is commonly considered appropriate in the literature.

Engineering constant		Matrix	Fibre
E	[GPa]	5.35	113.4
ν	–	0.22	0.35

Table 1: Material Properties obtained from [2].

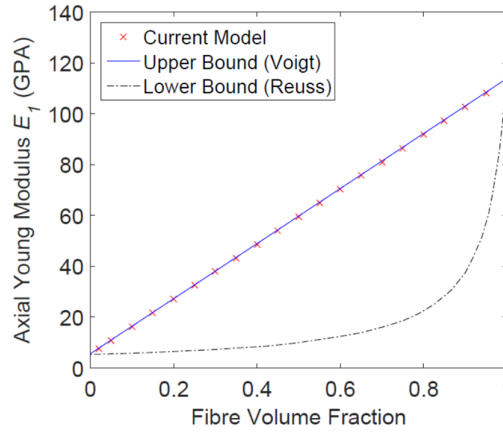


Figure 2: Longitudinal Young modulus E_1 – (other results obtained from [2]).

4.1.2 Transverse Elastic Modulus (E_2 and E_3):

In a similar manner, the variation of transverse modulus predicted by the proposed model is presented in Figure 3 which is found to deviate from the lower bound solution (Reuss model). According to the rule of mixture, the transverse modulus should follow the lower bound solution which corresponds to the condition of equal stress within the constituents. However, the real test data indicates that the value of transverse modulus should be higher than the lower bound solution and definitely lower than the upper bound solution. Actually, the lower bound solution is based on an assumption that the transverse normal stress within the entire volume of the matrix in the RVE is equal to that of the fibre which follows the concept of springs-in-series. However, this assumption is not valid in reality as only a portion of the matrix volume behaves according to this concept.

The current model is based on more realistic assumptions and according to these, the loading in a transverse direction, e.g., direction 2 will allow only matrix blocks M-1 and M-2 to have same transverse normal stresses (σ_{22}^{m1} and σ_{22}^{m2}) as that of fibre block (σ_{22}^f). On the other hand, the transverse normal strain of M-3 (ϵ_{22}^{m3}) will be equal to that of fibre (ϵ_{22}^f) that will produce different stress within these two blocks as they are having different stiffness of material properties. The present results are also found to closely follows the trend of other theoretical models such as Mori-Tanaka[88], upper bound of Concentric Cylinder Assemblage (CCA+)[90] or Self-Consistent[125] (Figure 3). A similar behaviour is also found for loading in transverse direction 3 and in-plane shearing.

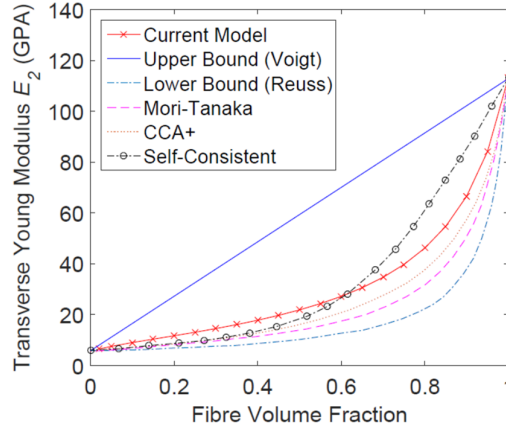


Figure 3: Transverse modulus E_2 – (other results obtained from [2]). Material properties are given in Table 2.

The transverse modulus E_2 or E_3 predicted by the current model for different fibre volume fractions are found to be marginally higher than the upper bound solution of [90](Figure 4). It should be noted that the concept of Hashin’s upper bound solution is different from that of rule of mixture. Actually, Hashin’s model is based on two hypotheses: (i) maximum potential energy and (ii) maximum elastic compliance energy, which results in two distinct bounds for a single material parameter such as transverse modulus. This is a little confusing as this model does not provide a unique value of a modulus. In that sense, the present model is consistent as it predicts a single solution.

The transverse modulus predicted by the current model is also validated against experimental results, as shown in Figure 4 where the material properties used for the constituents are given in Table 3.

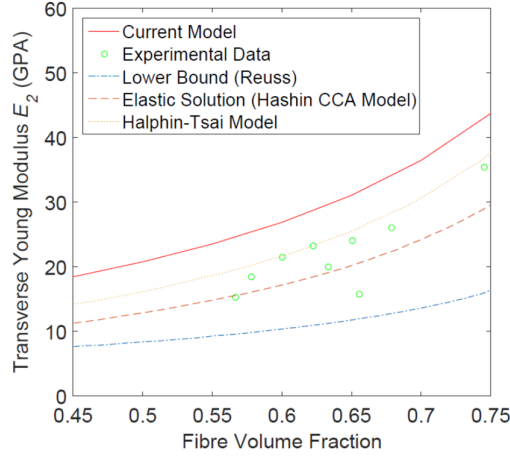


Figure 4: Transverse modulus E_2 and in-plane shear modulus G_{12} and G_{23} (other results and experimental data obtained from [1]) – Material properties are given in Table 3.

Engineering constant		Matrix	Fibre
E	[GPa]	4.14	414
ν	–	0.35	0.2

Table 3: Material Properties obtained from [1].

4.1.3 In-plane Shear Modulus

The variation of in-plane shear modulus G_{12} and G_{13} predicted by the proposed model is plotted in Figure 5 along with that obtained by other theories such as Mori-Tanaka[88], Method of Cells (MOCTI)[94] and Self-Consistent[125]. The results in Figure 5 show good correlation with those predicted by most of existing theories. The present results are also validated against the experimental data in Figure 6 which show good agreement between them. In this case, the properties of fibre and matrix are given in Table 4.

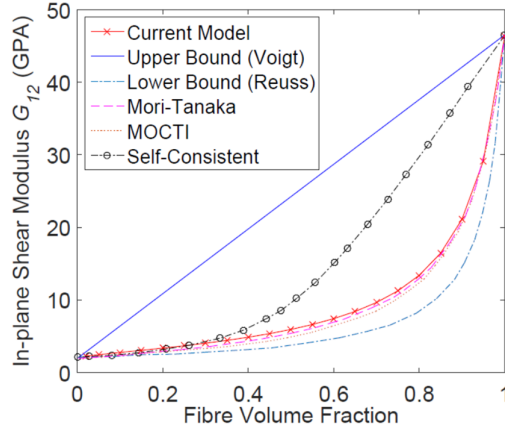


Figure 5: In-plane Shear modulus G_{12} & G_{23} - (other results obtained from [2]). Material properties are given in Table 2.

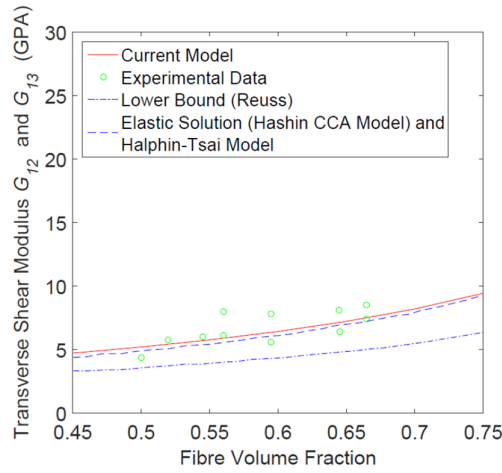


Figure 6: In-plane shear modulus G_{12} and G_{23} for fibre volume fraction from 0.45 to 0.75 (other results obtained from [1]) - Material properties are given in Table 4.

Engineering constant		Matrix	Fibre
G	[GPa]	1.83	30.19
E (Calculated)	[GPa]	5.35	113.4
ν (Calculated)	–	0.22	0.35

Table 2: Material Properties obtained from [1].

4.1.4 Transverse Shear Modulus

The transverse shear modulus G_{23} predicted by the current model is presented in Figure 7 along with that obtained from other theories. The values of G_{23} are less than in-plane shear modulus and closer to the lower bound solution of rule of mix

(Figure 7). The predicted values of G_{23} are consistent with the typical properties of unidirectional lamina having isotropic constituents according to [2] i.e., the transverse shear modulus are slightly less than the in-plan shear modulus for the same fibre volume fraction.

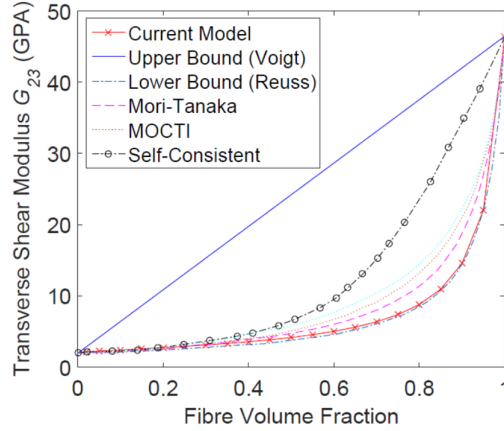


Figure 7: Shear modulus G_{12} & G_{23} - other results obtained from [2]. Material properties are given in Table 2.

4.2 Inelastic Response

Examples of plastic behaviours at constitutive level are given in this section. Table 5 & 6 below provide the model parameters used for the four materials behaviours in the study. In all four cases simulations were carried out under uniaxial tension along fibre direction for matrix volume fraction of 0.38. Different softening behaviours of the constituents are employed. We note that this is only a preliminary analysis to demonstrate the behaviour of the proposed composite model in inelastic range. More advanced constitutive models for the constituents are being developed and further analyses will be carried out and presented in the future.

Engineering constant		Matrix	Fibre
E	[GPa]	4.14	414
ν	-	0.35	0.2
σ_y	[GPa]	0.03	0.8

Table 3: Material Properties in both hardening and softening cases.

As illustrated in Figure 8 & 9 the proposed constitutive model has the ability to capture stress-strain curve of the homogenised RVE while keeping track of the

APPENDICES

behaviours in the material constituents. In other words, the constituent behaviours are homogenised in every step of calculation to obtain the macro behaviour, following the steps described above. This allows both elastic and inelastic behaviours for the constituents.

The responses of all four material blocks (refer to previous sections) are governed by parameters of the Von Mises model. They in turn control the overall constitutive behaviour of the homogenised composite model. As anticipated, under uniaxial loading in the fibre direction the overall behaviours of the composite is substantially influenced by the responses of fibres which are expected to have major impacts to the overall material stiffness in this loading condition (Figs. 8 & 9). On the other hands, in this uniaxial condition, due to significantly low stiffness of matrix compared to fibres, the contribution of matrix to the overall stiffness of the material is negligible. The softening behaviour in this case is encountered in all constituents. While the fibre behaviour is distinguished, all three matrix blocks behave only slightly differently in this case. These blocks in general response differently due to difference in their input strain rates [10].

Case	Engineering constant		Matrix	Fibre
Linear Hardening	H	–	5	20
Linear Softening	H	–	-0.5	-5
Non-linear Hardening	Q	[GPa]	0.08	1
	b	–	40	100
Non-linear Softening	Q	[GPa]	-0.08	-1
	b	–	20	50

Table 4: Model parameters.

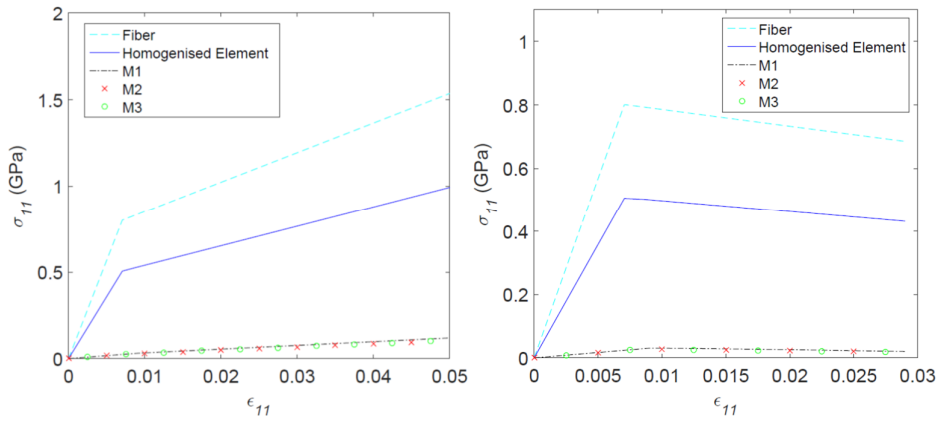


Figure 1: Stress-strain curve for linear strain hardening and softening materials.

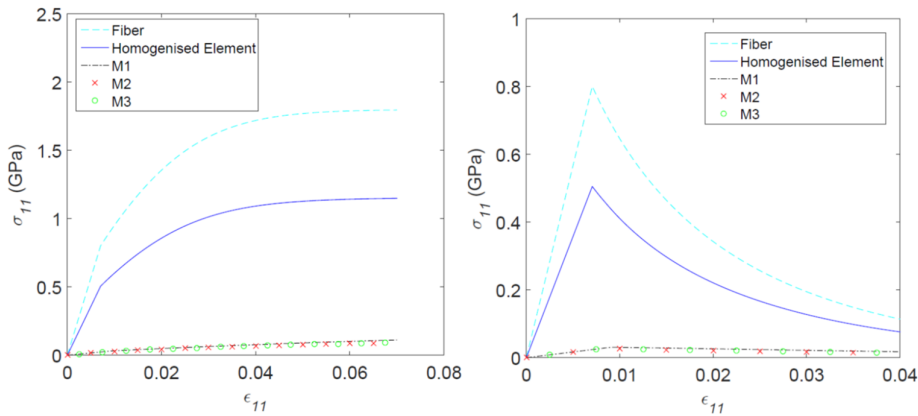


Figure 2: Stress-strain curve for nonlinear strain hardening and softening materials.

5 CONCLUSION

The current micromechanics based model has shown very good potentials through their predictions of elastic properties comparable to those by classical theories and experimental results, while possessing capability to handle material nonlinearity. In particular, the enhancements through kinematic terms in this case lead to a mix upper-lower bound solution that in turn result in effective properties close to classical predictions. The embedded fibre and matrix phases are interacting with each other and together control the response of the composite material model. Thanks to the rate form of the whole formulation, any constitutive behaviour can be used for the matrix and fibre. This is the key advantages in further extending the model capability to nonlinear cases with the development and incorporating more capable constitutive behaviour for fibre and matrix.

REFERENCES

- [1] O. Hoffman, The brittle strength of orthotropic materials, *Journal of Composite Materials*, 1967, **1**, pp. 200-206.
- [2] A. Puck, Calculating the strength of glass fibre/plastic laminates under combined load, *Kunststoffe Gennan Plastic*, 1969, **55**, pp. 18-19.
- [3] Z. Hashin, A. Rotem, A fatigue failure criterion for fiber reinforced materials, *Journal of Composite Materials*, 1973, **7**, pp. 448-464.
- [4] S.W. Tsai, *Strength of Theories of Filamentary Structures. Fundamental Aspects of Fiber Reinforced Plastic Composites*, John Wiley & Sons, USA, 1968.
- [5] M.R. Christensen, K.H. Lo, Solutions for effective shear properties in three phase sphere and cylinder models, *Journal of the Mechanics and Physics of Solids*, 1979, **27**, pp. 315-330.
- [6] T. Mori, K. Tanaka, Average stress in matrix and average elastic energy of materials with misfitting inclusions, *ACTA Metallurgica*, 1974, **21**, pp. 571-574.
- [7] J. Aboudi, Micromechanical Analysis of Composites by the Method of Cells, *American Society of Mechanical Engineers*, 1989, **42**, pp. 193-221.
- [8] R. Hill, Elastic properties of reinforced solids: some theoretical principles, *Journal of Mechanics and Physics of Solids*, 1963, **11**, pp.357-372.
- [9] M.A. Crisfield, *Non-Linear Finite Element Analysis of Solids and Structures. Volume 1: Essentials*, John Wiley & Sons Ltd, Chichester, 1991.
- [10] V. Vu, *A micromechanics based finite element model for progressive damage analysis of composite plate / shell*, Adelaide, 2015 [Progress Report].
- [11] C.T. Herakovich, *Mechanics of Fibrous Composites*, John Wiley & Sons Inc, New York, 1998.
- [12] Z. Hashin, B. Rosen, The elastic moduli of fiber-reinforced materials, *Journal of Applied Mechanics*, 1964, pp. 223-232.
- [13] R. Hill, Self-Consistent Mechanics of Composite Materials, *Journal of Mechanics and Physics of Solids*, 1965, pp. 213-222.

[14] A.K. Kaw, *Mechanics of Composite Materials*, Taylors & Francis Group, New York, 2006.

APPENDIX

Detailed expressions of enhanced strains and normal matrix $[N_2]$ and $[N_3]$

$$\{\dot{\epsilon}_{m2}\} = \begin{Bmatrix} \dot{\epsilon}_{xx}^f \\ \dot{\epsilon}_{yy}^f \\ \dot{\epsilon}_{zz}^f \\ \dot{\gamma}_{xy}^f \\ \dot{\gamma}_{yz}^f \\ \dot{\gamma}_{xz}^f \end{Bmatrix} + \begin{Bmatrix} 0 \\ \dot{\epsilon}_{2yy} \\ 0 \\ \dot{\gamma}_{2xy} \\ 0 \\ \dot{\gamma}_{2xz} \end{Bmatrix} = \begin{Bmatrix} \dot{\epsilon}_{xx}^f \\ \dot{\epsilon}_{yy}^f \\ \dot{\epsilon}_{zz}^f \\ \dot{\gamma}_{xy}^f \\ \dot{\gamma}_{yz}^f \\ \dot{\gamma}_{xz}^f \end{Bmatrix} + \begin{bmatrix} 0 & 0 & 0 \\ 0 & 1 & 0 \\ 0 & 0 & 0 \\ 1 & 0 & 0 \\ 0 & 0 & 1 \\ 0 & 0 & 0 \end{bmatrix} \begin{Bmatrix} \dot{\gamma}_{2xy} \\ \dot{\epsilon}_{2yy} \\ \dot{\gamma}_{2yz} \end{Bmatrix} = \{\dot{\epsilon}_f\} + [N_2]\{\dot{\epsilon}_2\}$$

$$\{\dot{\epsilon}_{m3}\} = \begin{Bmatrix} \dot{\epsilon}_{xx}^f \\ \dot{\epsilon}_{yy}^f \\ \dot{\epsilon}_{zz}^f \\ \dot{\gamma}_{xy}^f \\ \dot{\gamma}_{yz}^f \\ \dot{\gamma}_{xz}^f \end{Bmatrix} + \begin{Bmatrix} 0 \\ 0 \\ \dot{\epsilon}_{3zz} \\ 0 \\ \dot{\gamma}_{3yz} \\ \dot{\gamma}_{3xz} \end{Bmatrix} = \begin{Bmatrix} \dot{\epsilon}_{xx}^f \\ \dot{\epsilon}_{yy}^f \\ \dot{\epsilon}_{zz}^f \\ \dot{\gamma}_{xy}^f \\ \dot{\gamma}_{yz}^f \\ \dot{\gamma}_{xz}^f \end{Bmatrix} + \begin{bmatrix} 0 & 0 & 0 \\ 0 & 0 & 0 \\ 0 & 0 & 1 \\ 0 & 0 & 0 \\ 0 & 1 & 0 \\ 1 & 0 & 0 \end{bmatrix} \begin{Bmatrix} \dot{\gamma}_{3xz} \\ \dot{\gamma}_{3yz} \\ \dot{\epsilon}_{3zz} \end{Bmatrix} = \{\dot{\epsilon}_f\} + [N_3]\{\dot{\epsilon}_3\}$$

$$\{\dot{\epsilon}_{m1}\} = \{\dot{\epsilon}_f\} + [N_2]\{\dot{\epsilon}_2\} + [N_3]\{\dot{\epsilon}_3\}$$

Detailed expressions of matrices in equation (21):

$$[A_{11}] = f_1(1 - (f_1 + f_2))^2 [N_2]^T [M_1] [N_2] + f_2(1 - (f_1 + f_2))^2 [N_2]^T [M_2] [N_2] + f_3(f_1 + f_2)^2 [N_2]^T [M_3] [N_2] + (1 - f)(f_1 + f_2)^2 [N_2]^T [F] [N_2]$$

$$[A_{12}] = f_1(1 - (f_1 + f_2))(1 - (f_1 + f_3)) [N_2]^T [M_1] [N_3] - f_2(1 - (f_1 + f_2))(f_1 + f_3) [N_2]^T [M_2] [N_3] - f_3(f_1 + f_2)(1 - (f_1 + f_3)) [N_2]^T [M_3] [N_3] + (1 - f)(f_1 +$$

$$f_2)(f_1 + f_3)[N_2]^T [F][N_3]$$

$$\begin{aligned} [A_{21}] = & f_1(1 - (f_1 + f_3))(1 - (f_1 + f_2))[N_3]^T [M_1][N_2] - f_2(f_1 + f_3)(1 - \\ & (f_1 + f_2))[N_3]^T [M_2][N_2] - f_3(1 - (f_1 + f_3))(f_1 + f_2)[N_3]^T [M_3][N_2] + \\ & (1 - f)(f_1 + f_3)(f_1 + f_2)[N_3]^T [F][N_2] \end{aligned}$$

$$\begin{aligned} [A_{22}] = & f_1(1 - (f_1 + f_3))^2 [N_3]^T [M_1][N_3] + f_2(f_1 + f_3)^2 [N_3]^T [M_2][N_3] + \\ & f_3(1 - (f_1 + f_3))^2 [N_3]^T [M_3][N_3] + (1 - f)(f_1 + f_3)^2 [N_3]^T [F][N_3] \end{aligned}$$

$$\begin{aligned} [B_1] = & (1 - f)(f_1 + f_2)[N_2]^T [F] - f_1(1 - (f_1 + f_2))[N_2]^T [M_1] - f_2(1 - \\ & (f_1 + f_2))[N_2]^T [M_2] + f_3(f_1 + f_2)[N_2]^T [M_3] \end{aligned}$$

$$\begin{aligned} [B_2] = & (1 - f)(f_1 + f_3)[N_3]^T [F] - f_1(1 - (f_1 + f_3))[N_3]^T [M_1] + f_2(f_1 + \\ & f_3)[N_3]^T [M_2] - f_3(1 - (f_1 + f_3))[N_3]^T [M_3] \end{aligned}$$

Conference Paper 2

Mir A., Vu V.D., Nguyen G.D., Sheikh A.H., Coupling Damage with Plasticity in Thermodynamics Based Constitutive Models, 10th International Conference on Structural Integrity and Failure (SIF-2016): Advances in Materials and Structures, 12–15 July 2016, Adelaide, Australia.

Coupling Damage with Plasticity in Thermodynamics Based Constitutive Models

Arash Mir^{1,a}, Van D. Vu^{2,b}, Giang D. Nguyen^{3,c*}, Abdul Hamid Sheikh^{4,d}

^{1,2,3,4} School of Civil, Environmental and Mining Engineering, The University of Adelaide, Australia

^aarash.mirahmadizoghi@adelaide.edu.au, ^bvan.vu@adelaide.edu.au,
^cg.nguyen@adelaide.edu.au, ^dabdul.sheikh@adelaide.edu.au

Keywords: Coupled damage-plasticity, constitutive modelling, thermodynamics

Abstract. The focus of this work is on specifying the coupling between damage and plasticity, which are commonly recognised as two underlying dissipative mechanisms in deformation of engineering materials. The features of the proposed framework allow for the existence of a single generalised yield potential, which controls the evolution of all internal variables. Developments of the proposed framework are presented and its applications to modelling different behaviours of materials, particularly, the inelastic dilative/contractive behaviours with non-associated flow rules are discussed.

Introduction

Theories of plasticity and continuum damage mechanics (CDM) have been widely used in order to develop constitutive models for engineering materials, such as steel, concrete, composites, polymers, etc. and geomaterials such as soils and rocks. Within the framework of thermodynamics with internal variables (TIV), inelastic deformation at macro scale can be described by capturing the fundamental mechanisms of deformation and energy dissipation at micro scale by expressing them as functions of internal variables that encapsulate the history of deformation,

e.g. [1-9]. In constitutive modelling, the effect of all underlying mechanisms that give rise to the macroscopic residual strains (e.g. frictional sliding, dislocation of defects, etc.) is represented by plastic strains while mechanisms responsible for strength and stiffness degradation (e.g. void nucleations and growths, void coalescence, microcrack openings, etc.) are represented by a damage variable. During the course of inelastic deformation damage and plasticity can occur together and they influence the evolution of each other. Therefore it is essential for a constitutive model to address the interaction and coupling between these dissipative mechanisms through a unified yield/failure function.

In this study, a generic framework for constitutive modelling of engineering materials is developed based on the principles of TIV. Within this framework the entire constitutive relations are derived through introducing two scalar functions, one describing the energy stored within a material and the other describing the energy dissipated during the course of inelastic deformation of the material. The coupling between damage and plasticity is controlled through introducing a coupling parameter. It is also shown that the features of the proposed framework allow for addressing the modelling issues in problems involving inelastic volumetric deformations and non-associated flow rules. A brief presentation of the general formulation, described in detail in [10], is given in the subsequent section, followed by illustrations of coupling effects between damage and plasticity for both pressure-independent and pressure-dependent materials.

Coupling damage with plasticity in a thermodynamics based formulation

For rate independent materials under isothermal deformation, the Helmholtz free energy function is:

$$f = (1 - D) \left[\frac{1}{2} K (\varepsilon_V - \alpha_V)^2 + \frac{3}{2} G (\varepsilon_S - \alpha_S)^2 \right]. \quad (36)$$

In the above expression, $\varepsilon_V = \varepsilon_{ii}$ and $\varepsilon_S = \sqrt{2e_{ij}e_{ij}/3}$ are total volumetric and effective shear strains (with ε_{ij} being the strain tensor and $\varepsilon_S = \sqrt{2/3 e_{ij}e_{ij}}$ the deviatoric strain tensor), while α_V and α_S represent plastic volumetric and effective plastic shear strains, the bulk and shear moduli are denoted as K and G , respectively, and D is a scalar damage variable representing the effects of micro-

defects which is assumed to be uniformly distributed within the material. Following the procedures in Houlsby and Puzrin [2], the true triaxial stresses (p , q), generalised stresses ($\bar{\chi}_V$ and $\bar{\chi}_S$), and conjugate damage energy $\bar{\chi}_D$ can be deduced as:

$$\bar{\chi}_V = p = \frac{\partial f}{\partial \varepsilon_V} = (1-D)K(\varepsilon_V - \alpha_V), \quad \text{and} \quad \bar{\chi}_S = \quad (37)$$

$$q = \frac{\partial f}{\partial \varepsilon_S} = (1-D)3G(\varepsilon_S - \alpha_S).$$

$$\bar{\chi}_D = -\frac{\partial f}{\partial D} = \frac{1}{2}K(\varepsilon_V - \alpha_V)^2 + \frac{3}{2}G(\varepsilon_S - \alpha_S)^2. \quad (38)$$

The dissipation rate function is proposed in the following form [10]:

$$\Phi = \sqrt{\varphi_V^2 + \varphi_S^2 + \varphi_D^2} + r_V \varphi_V + r_S \varphi_S \geq 0. \quad (39)$$

In the above expression, φ_V , φ_S and φ_D are homogeneous first order functions in terms of the rates of internal variables, representing the contribution of the three individual dissipative mechanisms (volumetric plastic deformation, plastic deformation in shear and damage), and the dimensionless parameters r_V and r_S are functions of stresses. These functions can be defined as [10]:

$$\varphi_V = F(p, q, D, \varepsilon_p) \dot{\alpha}_V, \quad \text{and} \quad \varphi_S = F(p, q, D, \varepsilon_p) \dot{\alpha}_S. \quad (40)$$

$$r_V = \frac{p - a\sqrt{E(p, q)}}{F(p, q, D, \varepsilon_p)}, \quad \text{and} \quad r_S = \frac{q - b\sqrt{E(p, q)}}{F(p, q, D, \varepsilon_p)}. \quad (41)$$

$$\varphi_D = \frac{F(p, q, D, \varepsilon_p) \bar{\chi}_D}{\cos \omega \sqrt{E(p, q)}} \dot{D}. \quad (42)$$

where E and F are functions of stresses and internal variables with specific forms depending on the type of material behaviour [10], and ε_p is the accumulative plastic strain, the rate of which is defined as $\dot{\varepsilon}_p = \sqrt{2/3 \dot{\alpha}_{ij} \dot{\alpha}_{ij}}$ where α_{ij} is plastic strain tensor. The parameters a and b meeting the condition $a^2 + b^2 = \sin^2 \omega$ are responsible for capturing the dilatant and contractive behaviour, commonly observed in pressure dependent materials [10]. The auxiliary angle ω , which appears in Eqs. (7), is employed in order to quantify the contribution of damage processes and plastic deformations in the total dissipated energy, during the course

of inelastic deformation. In this sense, $\omega=0^\circ$ implies that damage is the only active dissipative mechanism with no occurrence of plastic deformation and the reverse is true when $\omega=90^\circ$. Full details on the formulation can be found in [10]. The Legendre transformation of the dissipation potential leads to the following yield function in generalised stress space [10]:

$$y^* = \left(\frac{\chi_V}{\partial\phi_V/\partial\dot{\alpha}_V} - r_V \right)^2 + \left(\frac{\chi_S}{\partial\phi_S/\partial\dot{\alpha}_S} - r_S \right)^2 + \frac{\chi_D^2}{\frac{\partial\phi_D}{\partial\dot{D}} \frac{\partial\phi_D}{\partial\dot{D}}} - 1 \leq 0. \quad (43)$$

with the following evolution rules for plastic strains and damage:

$$\begin{aligned} \dot{\alpha}_V &= \lambda \frac{\partial y^*}{\partial \chi_V} = 2\lambda \left(\frac{a\sqrt{E}}{F^2} \right), \quad \dot{\alpha}_S = \lambda \frac{\partial y^*}{\partial \chi_S} = 2\lambda \left(\frac{b\sqrt{E}}{F^2} \right), \quad \text{and} \\ \dot{D} &= \lambda \frac{\partial y^*}{\partial \chi_D} = 2\lambda \frac{\cos^2 \omega E}{F^2 \chi_D}. \end{aligned} \quad (44)$$

It can be seen in (9) that the magnitudes of volumetric and shear plastic deformation is governed by the ratio between parameters a and b . In this sense, in order to control the dilatant and contractive behaviours through controlling the direction of the plastic flow vector [10] a parameter c is also introduced so that:

$$\frac{\dot{\alpha}_V}{\dot{\alpha}_S} = \frac{a}{b} = \frac{\partial y^* / \partial \chi_V}{\partial y^* / \partial \chi_S} = c \frac{\partial y / \partial p}{\partial y / \partial q}. \quad (45)$$

By substituting Eqs. (5) – (7) into Eq. (8) the generic form of the yield function in true stress space is given as:

$$y = E - F^2 = 0. \quad (46)$$

Applications

In this section, the coupling features of the proposed framework is demonstrated by coupling damage with Von Mises plasticity, which is widely used for modelling the behaviour of pressure independent materials. The capability of the proposed framework in producing the non-associated flow rules by controlling the plastic flow direction is also investigated through constructing a coupled damage plasticity model for pressure dependent materials based on the Drucker-Prager model.

Von Mises type model. Using $E = q$ and $F = \sqrt{k}$, the yield function of the classical Von Mises model can be obtained as:

$$y = \sqrt{3J_2} - k(D, \varepsilon_p) = q - k(D, \varepsilon_p) = 0. \quad (47)$$

The function $k = k(D, \varepsilon_p)$ governing the yielding and failure process may take the following form:

$$k = (1 - D)(f_y + Q(1 - e^{-b\varepsilon_p})). \quad (48)$$

Figure 1 shows the effect of the coupling parameter ω on stress-strain curves of steel with the model parameters: $E = 200GPa$, $\nu = 0.3$, $f_y = 250MPa$, $Q = 50MPa$ and $b_t = 1000$. Since there are no volumetric plastic strains for Von Mises type materials, associated flow rules are used in this case by setting $a = c = 0$, which in turn results in $b = \sin\omega$. For cases when plastic deformations and damage processes evolve together ($0^\circ < \omega < 90^\circ$), the effect of damage is manifested by lower ultimate stresses, compared to purely plastic deformation ($\omega = 90^\circ$).

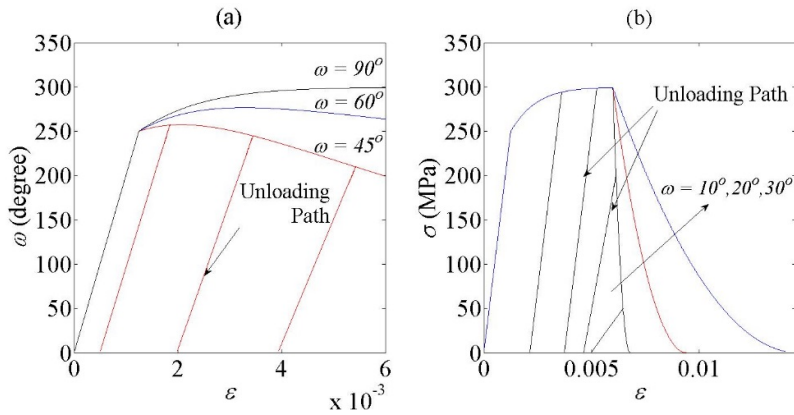


Figure 1: (a) Stress strain response under uniaxial stress condition with associated flow rules; (b) Typical Stress-strain response of steel generated by the model, using different values of ω

Experimental observations have revealed that metals exhibit a ductile behaviour which can be described as strain hardening with negligible reduction in stiffness, immediately after the initial yield stress. In tensile loading, once a critical strain is reached, softening behaviour is observed followed by complete disintegration of the material. This type of behaviour can be captured by the model through varying the coupling angle ω to mimic the real behaviour of the material Figure 1 (a). For instance, effects of damage can be switched off during the strain hardening process,

assuming a purely plastic deformation, by setting $\omega=90^\circ$, $a = 0$ and $b = \sin\omega = 1$. As can be seen from the unloading paths in the hardening region in Fig 1(b) no stiffness reduction occurs due to deactivation of damage. On the other hand, softening behaviour can be modelled through activating damage processes by switching ω to values less than 90° , once the critical strain is reached (Figure 1b).

Drucker-Prager type model. The Drucker-Prager yield function can be generated by taking $F = \sqrt{\kappa}$ and $E = q + \beta p$:

$$y = q + \beta p - \kappa(\varepsilon_p, D). \quad (49)$$

In the above expression $\kappa = 2f_{cy}f_{ty}/(f_{cy} + f_{ty})$ and $\beta = 3(f_{cy} - f_{ty})/(f_{cy} + f_{ty})$, where f_{cy} and f_{ty} are yield stresses under uniaxial compression and tension, respectively. Also the hardening rules may be defined as:

$$f_{cy} = (1 - D)(f_{c0} + Q_c(1 - e^{-b_c \varepsilon_p})), \text{ and } f_{ty} = (1 - D)(f_{t0} + Q_t(1 - e^{-b_t \varepsilon_p})). \quad (50)$$

where Q_t , Q_c , b_t and b_c are material constants, representing the ultimate stress and rate of expansion of the yield surface in compression (subscript c) and tension (subscript t), respectively. As illustrated in Figure 2(a) the model behaviour transforms from a more brittle response towards a more ductile response as the plasticity is set to be the dominant mechanism of energy dissipation by setting values of ω closer to 90° . The model behaviour under triaxial compression is also demonstrated in Figure 2(b) for three different confining pressures. Increase in nominal strength and more ductile behaviour is predicted by the model for higher confining pressures, as expected for pressure dependent materials.

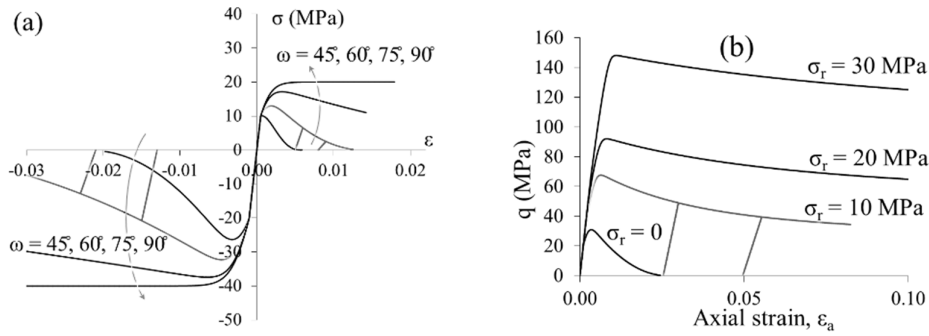


Figure 2: (a) The effect of ω on the model behaviour under uniaxial loading and (b) pressure dependent behaviour under triaxial loading; $f_{cy} = Q_c = 20 \text{ MPa}$, $f_{ty} = Q_t = 10 \text{ MPa}$, $b_t = 1500$ and $b_c = 500$.

Figure 3 (a) shows how the dilatant behaviour of the material can be controlled by varying the parameter c . Also, as shown in Figure 3 (b), if a larger volumetric plastic strain increment than that calculated by the associate flow is assumed ($c > 1$), the model behaviour is more brittle whereas for $c < 1$ more ductile behaviour is exhibited by the model.

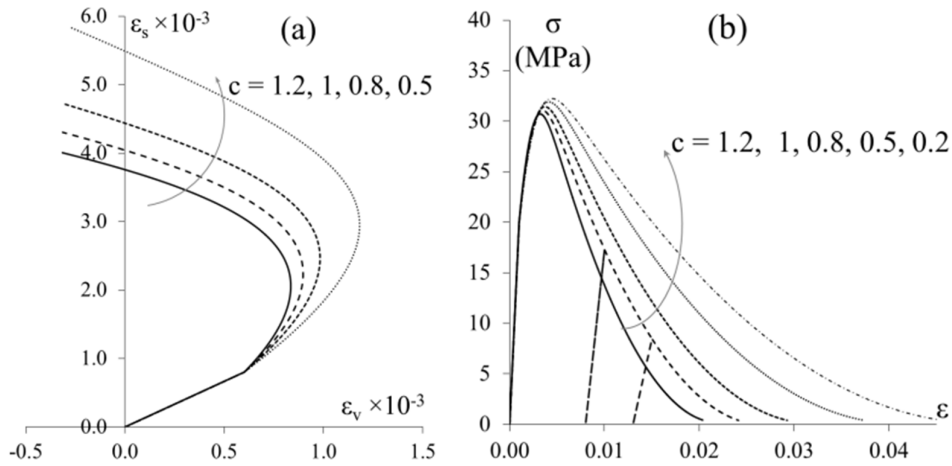


Figure 3: The effect of c and non-associated flow rule (a) on stress strain response and (b) on dilative behaviour, under uniaxial compression ($\omega = 60^\circ$).

4 Conclusion

We proposed a general approach to couple damage with plasticity to appropriately describe the behaviour of engineering materials. The whole formulation is casted in the TIV framework, ensuring consistency and rigour in both the behaviour and energy aspects of the model. A brief presentation with some examples are given in this short paper, while more details and examples involving the application of the proposed approach to both enhancing existing models and developing new and better constitutive models are described in detail in [10]. Future applications will include more underlying micro-mechanisms to enhance the predictive capability of constitutive models.

5 Acknowledgements

This work was supported by the Australian Research Council through Discovery Projects FT140100408 and DP140100945.

References

1. Ziegler, H., *An Introduction to Thermomechanics*,(1977). 1983, North-Holland Pub. Co.
2. Houlsby, G. and A. Puzrin, *A thermomechanical framework for constitutive models for rate-independent dissipative materials*. International Journal of Plasticity, 2000. **16**(9): p. 1017-1047.
3. Collins, I. and P. Kelly, *A thermomechanical analysis of a family of soil models*. Geotechnique, 2002. **52**(7): p. 507-518.
4. Collins, I.F. and T. Hilder, *A theoretical framework for constructing elastic/plastic constitutive models of triaxial tests*. International Journal for Numerical and Analytical Methods in Geomechanics, 2002. **26**(13): p. 1313-1347.
5. Einav, I., *Breakage mechanics—part I: theory*. Journal of the Mechanics and Physics of Solids, 2007. **55**(6): p. 1274-1297.
6. Einav, I., *Breakage mechanics—Part II: Modelling granular materials*. Journal of the Mechanics and Physics of Solids, 2007. **55**(6): p. 1298-1320.

7. Nguyen, G.D., A.M. Korsunsky, and J. Belnoue. *Coupled damage-plasticity modelling of ductile failure in an aluminium alloy*. in *Applied Mechanics and Materials*. 2015. Trans Tech Publications.
8. Nguyen, G.D., A.M. Korsunsky, and J.P.-H. Belnoue, *A nonlocal coupled damage-plasticity model for the analysis of ductile failure*. *International Journal of Plasticity*, 2015. **64**: p. 56-75.
9. Houlsby, G.T. and A.M. Puzrin, *Principles of hyperplasticity: an approach to plasticity theory based on thermodynamic principles*. 2007: Springer Science & Business Media.
10. Vu, V., A. Mir, G.D. Nguyen, A.H. Sheikh, *A Generic Thermodynamic-based Framework for Constitutive Modelling using Damage Mechanics and Plasticity Theory*. 2016 (to be submitted).

Conference Paper 3

Mir A., Nguyen G.D., Sheikh A.H., **Vu V.D.**, Modelling Dilatant and Contractive Behaviour in Soft Rocks, International Conference on Geomechanics, Geo-energy and Geo-resources IC3G 2016, Melbourne Australia

Modelling Dilatant and Contractive Behaviour in Soft Rocks

A. Mir^{a*}, G. D. Nguyen^b, A. H. Sheikh^c, V. Vu^d

^{a,b,c,d} The University of Adelaide, Adelaide, Australia

[*arash.mir@adelaide.edu.au](mailto:arash.mir@adelaide.edu.au)

Abstract

The importance of inelastic volumetric strains as well as frictional processes or the pressure sensitivity has long been recognised in the study of geomaterials. In this paper, a systematic derivation of the constitutive relations within the framework of thermodynamics with internal variables (TIV) is presented. Within this framework the entire constitutive description is given through introducing two scalar functions, namely the energy function and the dissipation rate function, and the thermodynamic admissibility of the model is guaranteed. In addition, non-associated plastic flow is defined as normal to the yield surface in generalised dissipative stress space, rather than through introducing a plastic potential in true stress space. The dilatant or contractive behaviour is also controlled through introducing two parameters in the dissipation rate function which eventually gives rise to a single-surface loading function which controls the simultaneous evolution of damage and plasticity. The single-surface yield function exhibits a smooth and closed shape in true stress space, thus it is capable of reflecting the primary yielding condition at significantly high confining pressures. The evolution of the loading function from an initial yield surface to a final failure surface is governed by the evolution of the damage variable as it grows from zero to unity. The model, therefore, profits from using one single loading function for the description of initial yielding, softening (or hardening) and failure. Finally, the model behaviour is assessed against experimental data on sandstone available in the literature.

Keywords: Thermodynamics, Damage and plasticity, Porous rocks, Dilation, Compaction

Introduction

Stability analysis of any excavation in relatively soft geological formations requires the knowledge and understanding of deformation and failure of materials comprising these formations. Laboratory and field observations testify that changes in effective pressure, at different excavation depths or under different loading configuration in experiments, lead to variations in failure mode (e.g. Baud et al., 2004; Baud et al., 2006; Klein et al., 2001; Lyakhovsky et al., 2015; Sheldon et al., 2006; Sheldon and Ord, 2005; Vajdova et al., 2004a, b; Wong and Baud, 1999; Zhu and Wong, 1997). At shallower depths and under low effective pressures soft rocks display dilatancy and fail by strain softening and brittle faulting. Under significantly high effective pressures at deeper depths the failure of soft rocks can be described as compaction with homogeneous distribution of damage within the material. The transition from localised shear dilation to homogeneous compaction involves localised compaction or formation of compaction bands under medium effective pressures. These behaviours observable at macro-scale are, however, mainly governed by deformation and energy dissipative processes at micro-scale.

At micro-scale, inelastic deformation of soft rocks involves a series of micro-mechanical processes which lead to degradation of micro-structure of the material. These processes usually begin with initiation of micro-cracks followed by frictional sliding between the two surfaces of pervasive micro-cracks. Micro-cracks then localise within a band of certain thickness where they finally coalesce and form the macroscopic fracture. The initiation and development of micro-cracks or damage is observed as stiffness and strength reduction at macro-scale. Furthermore, residual or plastic strains observed as dilation and/or compaction at macro-scale can be ascribed to phenomena such as frictional sliding and asperity interlocking. A common practice in constitutive modelling is to describe all the mechanisms that cause stiffness and strength reduction as damage and all the phenomena that give rise to residual strains as plastic deformations. Furthermore, during the course of inelastic deformations damage and plastic deformations occur together and one affects the evolution of the other. Therefore, specification of coupling between

damage and plasticity in the model formulation is of necessity for the model to follow the experimental observations closely.

Constitutive modelling within the framework of TIV (Houlsby and Puzrin, 2007; Ziegler, 1983) requires the explicit definition of two scalar functions. These functions include the free energy potential and the dissipation rate function. Once the explicit expression of the dissipation rate function is given, the formulation of the yield function in dissipative stress space can be derived by performing a degenerate Legendre transformation. Flow rules are also defined as normal to the yield surface in dissipative stress space rather than true stress space. Constitutive models developed within the TIV framework are guaranteed to be thermodynamically admissible. In this paper, following the coupling scheme developed by (Vu et al., 2016) within the framework of TIV, coupling between damage and plasticity is specified in the formulation of the dissipation rate function. This method of coupling allows for the existence of a single yield function which controls the evolution of both damage and plasticity processes. The yield function, which has a closed tear drop-shaped envelope in true stress space, evolves as damage grows within the material until it is transformed to a linear frictional Coulomb type failure envelope when the material is fully damaged. This evolution of yield behaviour is also observed in laboratory experiments on sandstones (Baud et al., 2006; Tembe et al., 2008; Wong and Baud, 2012). Furthermore, following the standard procedures of TIV, non-associated flow rules are defined using the yield function in dissipative stress space. It is also shown that controllable flow rules allow for describing the dilatant and contractive behaviours in accordance with softening and hardening responses. Throughout this paper, notations appropriate for triaxial tests, namely, mean pressure, $p = -\sigma_{ii}/3$, deviatoric stress, $q = \sqrt{3J_2}$, volumetric strain, $\varepsilon_v = \varepsilon_{ii}$ and effective shear strain, $\varepsilon_s = \sqrt{2e_{ij}e_{ij}/3}$, with $e_{ij} = \varepsilon_{ij} - \varepsilon_v/3$ are used.

Methodology; Thermomechanical Formulation

In this section, following the principles of TIV the entire constitutive relations are derived through explicitly defining two scalar functions, namely the free energy potential and the dissipation rate function.

Free Energy Potential, Dissipation Rate Function and Yield Function

In the case of isothermal problems, an appropriate choice for the free energy potential is the Helmholtz free energy, which can be given, for triaxial tests, as follows:

$$\Psi = (1 - D) \left[\frac{1}{2} K (\varepsilon_v - \varepsilon_v^p)^2 + \frac{3}{2} G (\varepsilon_s - \varepsilon_s^p)^2 \right] \quad [1]$$

In the above expression K and G are bulk and shear moduli, respectively and D is the scalar damage variable. Based on the above definition for free energy potential, following the standard procedures, mean pressure, p, and deviatoric stress, q, are given as follows:

$$p = \frac{\partial \Psi}{\partial \varepsilon_v} = (1 - D) K (\varepsilon_v - \varepsilon_v^p); \text{ and } q = \frac{\partial \Psi}{\partial \varepsilon_s} = 3(1 - D) G (\varepsilon_s - \varepsilon_s^p) \quad [2]$$

Also, generalised stresses (see Houlsby and Puzrin, 2007), $\bar{\chi}_v$ and $\bar{\chi}_s$, and the conjugate damage energy, $\bar{\chi}_D$, are derived as:

$$\bar{\chi}_v = -\frac{\partial \Psi}{\partial \varepsilon_v^p} = (1 - D) K (\varepsilon_v - \varepsilon_v^p) = p; \text{ and} \quad [3]$$

$$\bar{\chi}_s = -\frac{\partial \Psi}{\partial \varepsilon_s^p} = 3(1 - D) G (\varepsilon_s - \varepsilon_s^p) = q$$

$$\bar{\chi}_D = -\frac{\partial \Psi}{\partial D} = \left[\frac{1}{2} K (\varepsilon_v - \varepsilon_v^p)^2 + \frac{3}{2} G (\varepsilon_s - \varepsilon_s^p)^2 \right] = \frac{p^2}{2K(1-D)^2} + \frac{q^2}{6G(1-D)^2} \quad [4]$$

The dissipation rate function for rate independent behaviour of material is a homogeneous first order function in the rates of internal variables ($\dot{\varepsilon}_v^p$, $\dot{\varepsilon}_s^p$ and \dot{D}). Following the coupling scheme developed by (Vu et al., 2016), the following form of the dissipation rate function is assumed:

$$\Phi = \sqrt{\varphi_v^2 + \varphi_s^2 + \varphi_D^2} + f_v \varphi_v + f_s \varphi_s \geq 0 \quad [5]$$

In the above expression, φ_v , φ_s and φ_D are homogeneous first order functions in terms of the rates of internal variables, representing the contribution of each individual dissipative mechanism in the total dissipation rate and the dimensionless

parameters f_v and f_s are functions of stresses. The specific definitions of these functions depend on the problem in hand. For the purpose of constitutive modelling for soft rocks these functions are defined as follows:

$$\varphi_i = (p - \alpha(p - \rho))\dot{\varepsilon}_i^p = F \dot{\varepsilon}_i^p; \quad i = v, s \quad [6]$$

$$\varphi_D = \frac{F \bar{\chi}_D}{c \sqrt{\left[\left[\frac{(1-D)(p-\rho)F}{A} \right]^2 + \left[\frac{q}{M} \right]^2 \right]}} \dot{D} = \frac{F \bar{\chi}_D}{c \sqrt{E}} \dot{D} \quad [7]$$

$$f_v = (p - a\sqrt{E})/F; \text{ and } f_s = (q - b\sqrt{E})/F \quad [8]$$

with parameters ρ and α in Eq. [6] being defined as:

$$\rho = \frac{(4-\gamma)p_c p_t + \gamma p_c^2}{2(p_c + p_t)}; \text{ and } \alpha = \sqrt{1-D} \left[\alpha_0 + \frac{(1-D)^2 \sqrt{D}}{2} \right] \quad [9]$$

where α_0 and γ are material parameters and p_t and p_c are pressures at yield under isotropic compression and expansion, respectively. Also, parameters A and M appearing in Eq. [7] are given as:

$$A = \left[\frac{(1-\gamma)p_c - p_t}{p_c + p_t} \right] p + \frac{1}{2}(1-D)\gamma p_c; \text{ and } M = M_0 + \frac{(1-D)^2 \sqrt{D}}{2} \quad [10]$$

where M_0 is the slope of the final failure envelope in p - q space. Parameters a , b and c in Eqs. [7] and [8] determine the level to which each dissipation mechanism is active. In particular, parameters a and b control the share of volumetric and shear plastic deformations in the total plastic dissipation rate at each step of inelastic loading and, therefore, control the direction of plastic flow vector in true stress space. Furthermore, inelastic dilation in soft rocks can be attributed to damage and volumetric plastic strain due to asperity interlocking of micro-cracks. Hence, energy dissipation due to damage and volumetric plastic strain is termed here as volumetric dissipation and its contribution to the total dissipation rate is represented by a ratio r_v defined as; $r_v = a^2 + c^2$. Another source of energy dissipation is shear sliding between the two faces of micro- and macro-cracks. The share of frictional sliding in total dissipation rate is, thus, termed as shear dissipation and it is denoted by a ratio $r_s = b^2$. Ratios, r_v and r_s are fractions of a unit energy budget that has been dissipated and thereby they are bound through the condition; $r_v + r_s = 1$. Within the framework of TIV, the yield function in generalised dissipative stress space can

be derived by performing a Legendre transformation on the dissipation rate function. Performing Legendre transform on a first-order function of rates of internal variables, $\Phi = \Phi(\dot{\epsilon}_v^p, \dot{\epsilon}_s^p, \dot{D})$, results in a function of the conjugate variables, $y^* = y^*(\chi_v, \chi_s, \chi_D)$. Using Eq. [5] these conjugate variables are defined as follows:

$$\chi_v = \frac{\partial \Phi}{\partial \dot{\epsilon}_v^p} = \frac{\partial \Phi}{\partial \varphi_v} \frac{\partial \varphi_v}{\partial \dot{\epsilon}_v^p} = \left(\frac{\varphi_v}{\sqrt{\varphi_v^2 + \varphi_s^2 + \varphi_D^2}} + f_v \right) \frac{\partial \varphi_v}{\partial \dot{\epsilon}_v^p} \quad [11]$$

$$\chi_s = \frac{\partial \Phi}{\partial \dot{\epsilon}_s^p} = \frac{\partial \Phi}{\partial \varphi_s} \frac{\partial \varphi_s}{\partial \dot{\epsilon}_s^p} = \left(\frac{\varphi_s}{\sqrt{\varphi_v^2 + \varphi_s^2 + \varphi_D^2}} + f_s \right) \frac{\partial \varphi_s}{\partial \dot{\epsilon}_s^p} \quad [12]$$

$$\chi_D = \frac{\partial \Phi}{\partial \dot{D}} = \frac{\partial \Phi}{\partial \varphi_D} \frac{\partial \varphi_D}{\partial \dot{D}} = \left(\frac{\varphi_D}{\sqrt{\varphi_v^2 + \varphi_s^2 + \varphi_D^2}} \right) \frac{\partial \varphi_D}{\partial \dot{D}} \quad [13]$$

As can be seen in Eqs. [11]-[13] each conjugate variable is linked to the rates of all internal variables. Accordingly, specification of coupling between internal variables in the expression of the dissipation rate function gives rise to the existence of a single yield function which controls the simultaneous evolution of damage and plasticity and it is obtained as:

$$y^* = \left(\frac{\chi_v}{\partial \varphi_v / \partial \dot{\epsilon}_v^p} - f_v \right)^2 + \left(\frac{\chi_s}{\partial \varphi_s / \partial \dot{\epsilon}_s^p} - f_s \right)^2 + \left(\frac{\chi_D}{\partial \varphi_D / \partial \dot{D}} \right)^2 - 1 \leq 0 \quad [14]$$

In addition, using Eqs. [6]-[8] along with Eq. [14], the yield function in true stress space, $y = y(p, q, D)$, is given as:

$$y = \left[\frac{(1-D)(p-\rho)}{A} \right]^2 + \left[\frac{q}{MF} \right]^2 - 1 \leq 0 \quad [15]$$

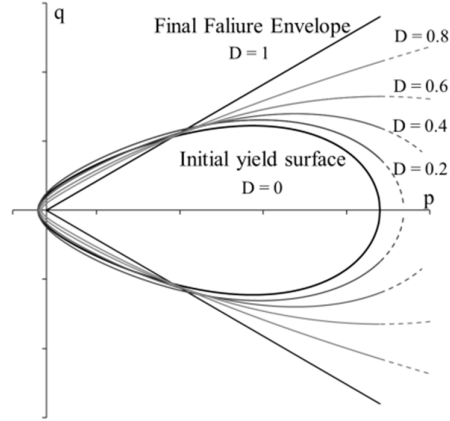


Figure 1: Yield function in true stress space

As illustrated in Figure 1, the yield function of Eq. [14] possesses a tear-drop shape in true stress space, $p - q$, similar to that developed by (Collins and Hilder, 2002) for sand. Furthermore, incorporation of damage in the formulation of yield function allows for transformation of the initial yield surface to a linear frictional Coulomb type failure envelope as the damage variable grows from zero to unity.

Non-associated Flow Rules

Within the framework of TIV flow rules are defined using the yield function in generalised dissipative stress space. By use of Eqs. [3] and [4] and by invoking Ziegler's orthogonality condition, evolution rules for plastic strains and damage variable are given as:

$$\dot{\varepsilon}_v^p = \dot{\lambda} \partial y^* / \partial \chi_v = 2\dot{\lambda} (a\sqrt{E}/F^2); \text{ and } \dot{\varepsilon}_s^p = \dot{\lambda} \partial y^* / \partial \chi_s = 2\dot{\lambda} (b\sqrt{E}/F^2) \quad [16]$$

$$\dot{D} = \dot{\lambda} \partial y^* / \partial \chi_D = 2\dot{\lambda} c^2 E / F^2 \bar{\chi}_D \quad [17]$$

From the plastic flow rules, given by "Eq. [16]", the ratio between the volumetric and shear components of the plastic flow vector is:

$$\dot{\varepsilon}_v^p / \dot{\varepsilon}_s^p = a/b \quad [18]$$

Furthermore, parameter a is defined in terms of stresses as follows:

$$a = \frac{p - \rho}{|p - \rho| - p_t} \quad [19]$$

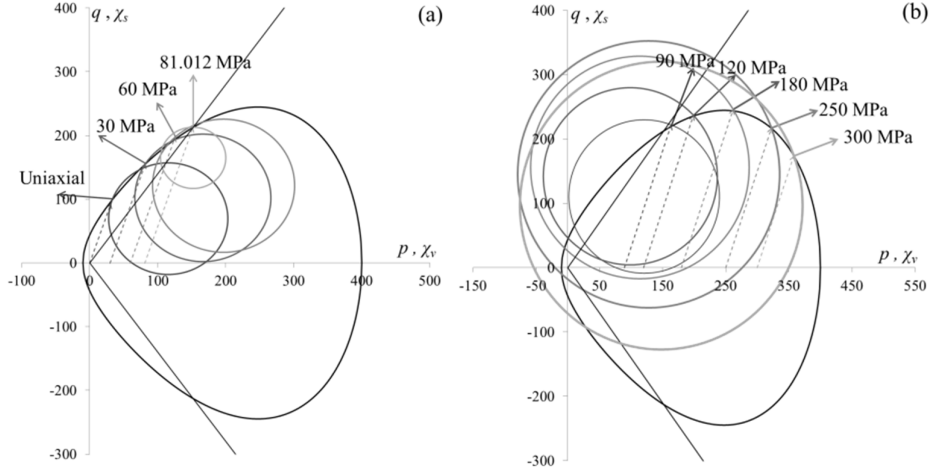


Figure 2: Non-associated flow for Bentheim sandstone with model parameters as; $\gamma = 0.82$, $\alpha_0 = 0.55$, $M_0 = 1.4$, $p_c = 400$ MPa, $p_t = -10$ MPa, $r_v = 0.8$, and $r_s = 0.2$
 (a) dilation and (b) compaction

Direction of Plastic flow vectors is now controlled merely by determining the contribution of the volumetric and shear dissipation rates in the total dissipation rate, that is, by determining r_v and r_s . The plastic flow vectors are defined as normal to the yield surface in dissipative stress space. However, they are not always normal to the yield surface in true stress space except for non-frictional materials for which the flow rules are associated. Corresponding to any yield point on the initial yield surface in true stress space $(p_y - q_y)$, there exist an ellipsoidal yield potential in generalised dissipative stress space (χ_v, χ_s, χ_D) which can be obtained, from Eq. [14], as:

$$y^* = \left[\chi_v - (p_y - a\sqrt{E}) \right]^2 + \left[\chi_s - (q_y - b\sqrt{E}) \right]^2 + \left[c\sqrt{E} \chi_D / \bar{\chi}_D \right]^2 = F^2 \quad [20]$$

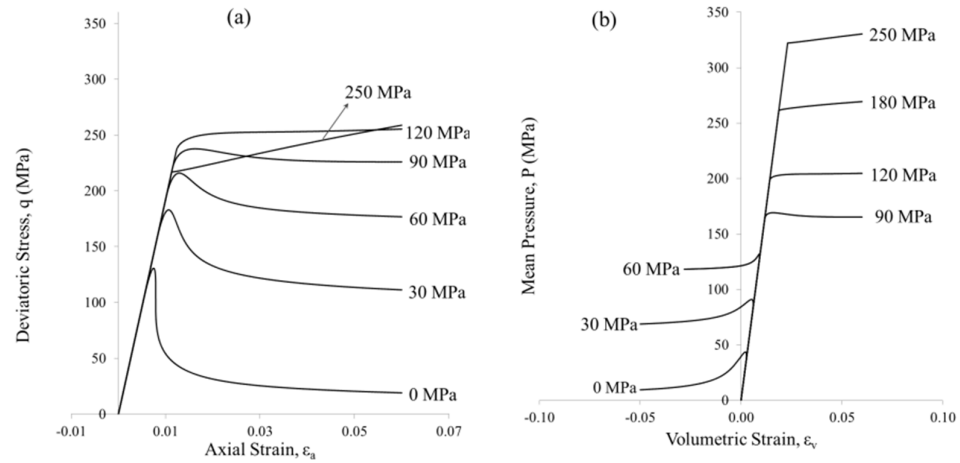
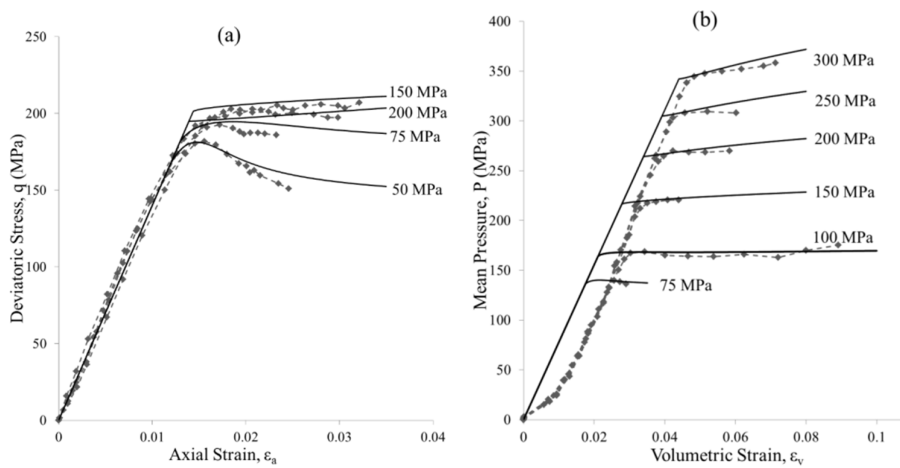


Figure 3: Model behaviour (a) softening and hardening responses and (b) dilative and contractive behaviours

These yield loci in dissipative stress space are analogous to the concept of plastic potential in conventional plasticity. The projection of the ellipsoidal yield potential on the plane $\chi_D = 0$, corresponding to a number of yield points ($p_y - q_y$), is illustrated in Figure 2. As can be seen in Figure 2, for the present formulation the planes $\chi_D = 0$ and $p - q$ coincide, however, this is not always the case (see Collins and Hilder, 2002). In accordance with the direction of plastic flow vector in Fig. 2, dilative/softening and contractive/hardening behaviour of the model is demonstrated in Figure 3. Model input parameters were taken from tests on Bentheim sandstone (Wong et al., 2001).

Results and Discussion

In this section the predictive capability of the model is assessed against experimental data from Berea sandstone (Baud et al., 2006). The model parameters are calibrated using the initial yield point for one or two sets of data. As illustrated in Figure 4 the proposed model predicts the inelastic deformation of these sandstones reasonable well. Although the calibration of the model parameters is relatively straightforward, it is desirable for the two model parameters r_v and r_s (representing the share of volumetric and shear dissipation, respectively) to be determined in a more systematic manner.



Berea sandstone (a) Mean stress-volumetric strain (b) deviatoric stress-axial strain with model parameters; $M_0 = 1.35$, $\gamma = 0.75$, $\alpha_0 = 0.65$, $p_c = 387$ MPa, $p_t = -10$ MPa, *Young's modulus* = 14.125 GPa, *Poisson's ratio* = 0.2

Conclusion

A thermodynamically consistent coupled damage-plasticity model is developed to describe the mechanical behaviour of soft rocks. The whole formulation is casted in the framework of thermodynamics with internal variables, ensuring the consistency and rigour both the behaviour and energy aspects of the model. A brief presentation with some examples are given in this short paper, while further improvements and generalisations will be given in Vu et al (2016). Future improvements will focus mainly on further generalisation of the dissipation rate function and on a detailed analysis of different failure modes as well as modes of energy dissipation.

Acknowledgements

Giang Nguyen would like to thank the Australian Research Council for support through Discovery Projects FT140100408 and DP140100945.

References

- Baud, P., Klein, E., Wong, T.-f., 2004. Compaction localization in porous sandstones: spatial evolution of damage and acoustic emission activity. *Journal of Structural Geology* 26, 603-624.
- Baud, P., Vajdova, V., Wong, T.f., 2006. Shear-enhanced compaction and strain localization: Inelastic deformation and constitutive modeling of four porous sandstones. *Journal of Geophysical Research: Solid Earth* 111.
- Collins, I.F., Hilder, T., 2002. A theoretical framework for constructing elastic/plastic constitutive models of triaxial tests. *International Journal for Numerical and Analytical Methods in Geomechanics* 26, 1313-1347.
- Houlsby, G.T., Puzrin, A.M., 2007. *Principles of hyperplasticity: an approach to plasticity theory based on thermodynamic principles*. Springer Science & Business Media.
- Klein, E., Baud, P., Reuschlé, T., Wong, T., 2001. Mechanical behaviour and failure mode of Bentheim sandstone under triaxial compression. *Physics and Chemistry of the Earth, Part A: Solid Earth and Geodesy* 26, 21-25.
- Lyakhovskiy, V., Zhu, W., Shalev, E., 2015. Visco-poroelastic damage model for brittle-ductile failure of porous rocks. *Journal of Geophysical Research: Solid Earth* 120, 2179-2199.
- Sheldon, H., Barnicoat, A., Ord, A., 2006. Numerical modelling of faulting and fluid flow in porous rocks: an approach based on critical state soil mechanics. *Journal of structural geology* 28, 1468-1482.
- Sheldon, H., Ord, A., 2005. Evolution of porosity, permeability and fluid pressure in dilatant faults post-failure: implications for fluid flow and mineralization. *Geofluids* 5, 272-288.
- Tembe, S., Baud, P., Wong, T.f., 2008. Stress conditions for the propagation of discrete compaction bands in porous sandstone. *Journal of Geophysical Research: Solid Earth* 113.

APPENDICES

- Vajdova, V., Baud, P., Wong, T.f., 2004a. Compaction, dilatancy, and failure in porous carbonate rocks. *Journal of Geophysical Research: Solid Earth* 109.
- Vajdova, V., Baud, P., Wong, T.f., 2004b. Permeability evolution during localized deformation in Bentheim sandstone. *Journal of Geophysical Research: Solid Earth* 109.
- Vu, V., Mir, A., Sheikh, A.H., Nguyen, G.D., 2016. A Thermodynamics-based Formulation for Constitutive Modelling using Damage Mechanics and Plasticity Theory (to be submitted).
- Wong, T.-f., Baud, P., 2012. The brittle-ductile transition in porous rock: A review. *Journal of Structural Geology* 44, 25-53.
- Wong, T., Baud, P., 1999. Mechanical compaction of porous sandstone. *Oil & Gas Science and Technology* 54, 715-727.
- Wong, T.f., Baud, P., Klein, E., 2001. Localized failure modes in a compactant porous rock. *Geophysical Research Letters* 28, 2521-2524.
- Zhu, W., Wong, T.-f., 1997. Shear-enhanced compaction in sandstone under nominally dry and water-saturated conditions. *International Journal of Rock Mechanics and Mining Sciences* 34, 364. e361-364. e312.
- Ziegler, H., 1983. *An Introduction to Thermomechanics*,(1977). North-Holland Pub. Co.